Reactivity Studies of the 2-phosphaethynolate Anion: A Pathway to Phosphinecarboxamides

Erica Neves de Faria

St Hugh's College

University of Oxford

A thesis submitted for the degree of

Doctor of Philosophy in Inorganic Chemistry

Michaelmas 2019

Acknowledgments

I would like to thank all the amazing people I had the opportunity to meet throughout my DPhil. Firstly, I want to thank my supervisor, Dr. Jose Goicoechea, for all the guidance, enthusiasm, for being such a nice person to be around and work with. For all the support not only in Chemistry but in my personal life. I consider myself very lucky in that respect as I could not have asked for a better supervisor. I am very grateful for the opportunity that he gave me.

I also need to thank all the people that I worked closely in the lab. Dr. Thomas Robinson for teaching me how to use a Schlenk line. Dr. Andy Jupp for being so special and for being the light in the lab. Dr. Jordan Waters for introducing me to momo's. It is still my choice when I go to the market. Dr. Alex Hinz, the German that likes to pretend to be grumpy but is, in fact, very sweet. For being such a good friend at all times but especially when I really needed and, of course, for introducing me to what is now my favourite drink, gin. Dr. David Lo for giving me a map to UniClub on my first day. When I realised it was just around the corner, I knew he had to be a nice person and that we would become very good friends. Dan Wilson, for being such a nice person, for all the nice chats shared and for all the help with calculations. Geve, my part II, who gave me the opportunity to learn how to supervise someone and who contributed to this project. Fabian, the very happy summer student that I had the opportunity to supervise. Gabi, a brilliant exchange student that I was lucky to meet and become good friends. Zumba class was never the same after she left. Dr. Sebastian Bestgen, a lovely postdoc with the longest eye lashes I have ever seen, with whom I shared a lot of fun moments. Dr. Roy Schreiber, for the friendship, for all the nice Israeli dishes he used to make us in the holidays and for all the help with my thesis. Doruk, for being such a good person, for all the conversations and glasses of wine shared and for keeping inviting me to his

college a few times for the “first time”. Steven, for being the sweetest person I know. For being such a thoughtful friend, for all the snacks he always provides to the lab and for always telling me I am beautiful. You are my sunshine! Dr. Meera Mehta, for all the amazing and fun moments together but also for all the serious moments and for correcting my thesis. Dr. Nick Rees for all the assistance with NMR spectroscopy and for all the fighting tricks I learned while waiting for an experiment to run.

Dr. Ivo for encouraging me to come to Oxford in the first place and for all the support provided while applying for it. For making sure we all had lunch together every day, keeping the group always together. Dr. Pri, an amazing person who I admire for so many things that I couldn’t even list here. Dr. Ari, for all the amazing moments and conversations over meals and wine that we shared in our kitchen. One of my favourite places in Oxford. Dr. Henrique, for changing the weekend menu when he found out I didn’t really like risotto and also for sharing the kitchen with us. You four were like my family here. Ana, Carol, Ricardo and Dom, awesome people with whom I didn’t share as many moments as I wish. They are amazing. My London friends, Arthur, João, Hannah and Felipe with whom I had so much fun. For always being so nice to me and for taking me in. I would also like to thank my good friends Tay, Erico and Carol who, even with all the distance, are always present, never letting the friendship die.

Dr. Chris Kennell for all the fun moments shared in the last years of this process. For all the friendship and love and for picking me up in the moments of desperation. For making me calm. For feeding me when I get nervous because I am hungry and don’t even notice. For giving me a place to live for the last few months and for being incredibly supportive, specially while writing my thesis. And of course, thank you for teaching me how to ride a bike!

Finally, I would like to thank my family, especially my mum, dad and sister, for the endless support I had from the beginning. I don’t tell them enough, but they are the most special people in my life. They are everything to me. Thank you for always being there no matter what.

Thank you all for being part of this chapter of my life. You are all very important to me!

Abstract

Reactivity Studies of the 2-phosphaethynolate Anion:

A Pathway to Phosphinecarboxamides

Erica Faria — St Hugh's College

DPhil in Inorganic Chemistry — Michaelmas Term 2019

This thesis summarises the research carried out during my PhD on the phosphinecarboxamide family. Inspired by Wöhler's seminal synthesis of urea, the phosphinecarboxamides are obtained by the reaction of the 2-phosphaethynolate anion, PCO^-, a heavier congener of the cyanate anion, with ammonium salts. These species are phosphorus-containing analogues of urea, RHPC(O)NHR'. These compounds are prime examples of primary phosphines that exhibit remarkably air- and moisture stability. Several examples of these compounds were obtained by the reaction of the 2-phosphaethynolate anion with a variety of amines such as amino acids, leading to *N*-functionalised chiral products and bidentate amines. The reactivity of these compounds was explored by promoting deprotonation of the molecules, which allowed post functionalisation, affording new *P*-functionalised species. These phosphinecarboxamides were also shown to be able to act as Lewis bases, as they were able to use the phosphorus lone-pair to coordinate to transition metals centres. Finally, this thesis underlines the reactivity of the PCO^- anion with amines bearing a ferrocenyl group as well the reactivity of the resulting products.

List of Units, Symbols and Abbreviations

18-crown-6	1,4,7,10,13,16-hexaoxacyclooctadecane
Å	ångström
Ar	aryl group
au	atomic unit
av	average (mean)
Br	broad
Bz	benzyl
calc	calculated
cm^{-1}	wavenumber
COSY	correlation spectroscopy
Cp	cyclopentadienyl or cyclopentadienide
Cy	cyclohexyl
d	doublet
DCM	dichloromethane
Diox	1,4-dioxane
DFT	density functional theory
DME	1,2-dimethoxyethane
DMF	*N*,*N*-dimethylformamide
eV	electronvolt
ESI	electrospray ionisation
EXSY	exchange spectroscopy
g	gram
H_2O	water

HOMO	highest occupied molecular orbital
HMBC	correlation spectroscopy
HMDS	hexamethyldisilylamide, $N(SiMe_3)_2$
HSQC	correlation spectroscopy
Hz	Hertz
J	Joule
J	coupling constant
K	Kelvin
kcal	kilocalorie
KHMDS	potassium bis(trimethylsilyl)amide
kJ	kilojoule
LUMO	lowest unoccupied molecular orbital
m	multiplet
Me	methyl
MeCN	acetonitrile
Mes*	supermesityl (2,4,6-$^t Bu_3C_6H_2$)
mg	milligram
mL	millilitre
µL	microlitre
mol	mole
MS	mass spectrometry
NMR	nuclear magnetic resonance
OTf	triflate or trifluoromethanesulfonate (CF_3SO_3)
Ph	phenyl
ppm	parts per million

py	pyridine
s	singlet
SOMO	singly occupied molecular orbital
t	triplet
^{t}Bu	*tert*-butyl
THF	tetrahydrofuran
γ	gyromagnetic ratio
δ	chemical shift
µL	microlitre
v	vibrational frequency
°	degree
°C	degree Celsius

List of Compounds

Chapter 2

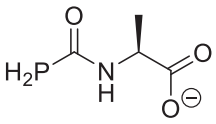

1

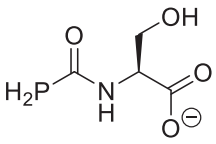

2

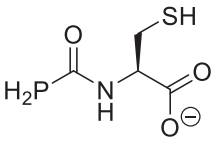

3

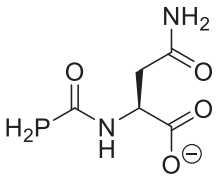

4

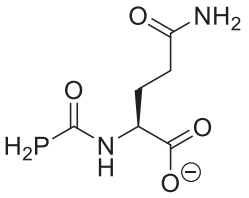

5

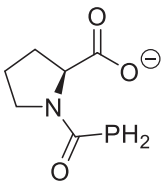

cis-**6**

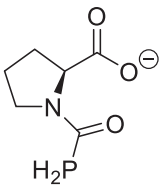

trans-**6**

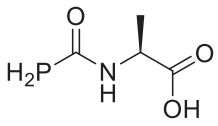

7

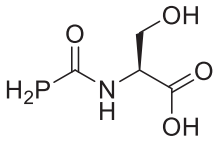

8

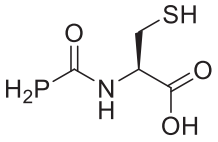

9

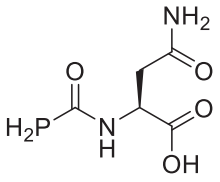

10

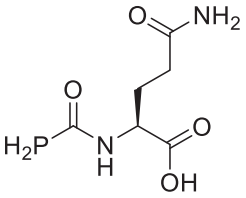

11

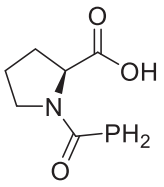

cis-**12**

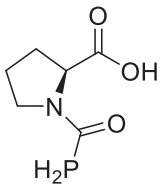

trans-**12**

Chapter 3

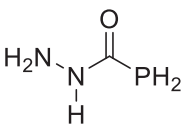

13a

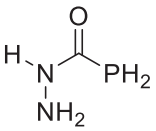

13b

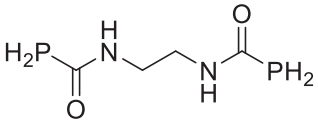

14

Chapter 4

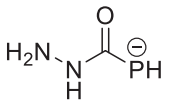

15a *cis*

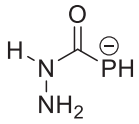

15a *trans*

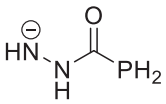

15b *cis*

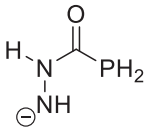

15b *trans*

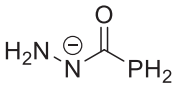

15c *cis*

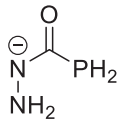

15c *trans*

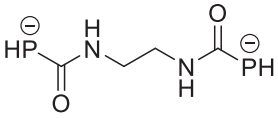

16

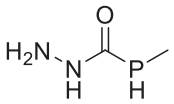

17a

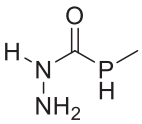

17b

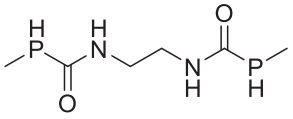

18a

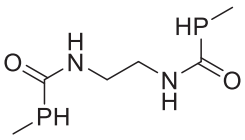

18b

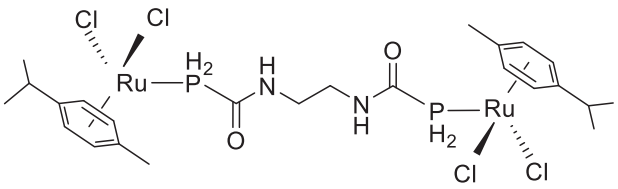

19

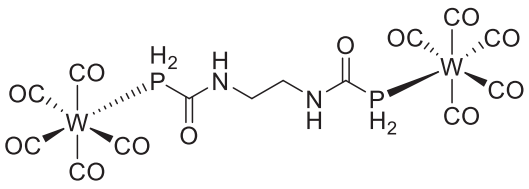

20

Chapter 5

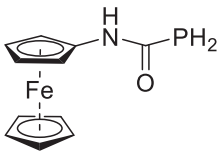

21

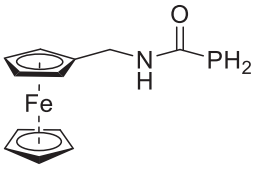

22

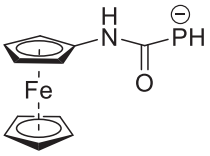

23a

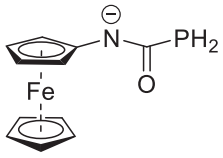

23b

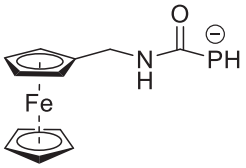

24

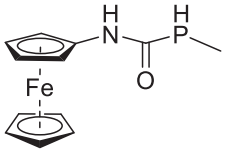

25

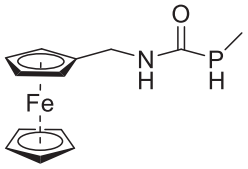

26

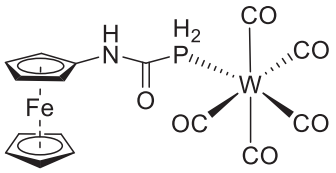

27

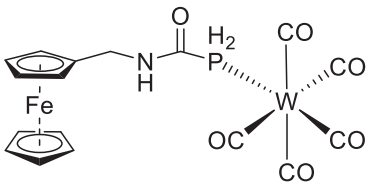

28

Table of Contents

Chapter 1: Introduction

1.1 Phosphorus and nitrogen

Phosphorus and nitrogen both belong to group 15 of the periodic table rendering them valence isoelectronic. Some similarities and general trends are observed between them; however, it is well known that there are some noteworthy differences between the elements of the first and second row of the p-block in the periodic table. This is evidenced by the different existing allotropes for each one of these elements. Elemental nitrogen, under standard conditions, exclusively forms dinitrogen, a gaseous dimer featuring a triple bond between the atoms with a short interatomic distance (109.76 pm). This triple bond is amongst the strongest element–element bonds and, consequently, N_2 has a very high bond dissociation energy (945.41 kJ mol^{-1}), making this gas highly inert.[1] By contrast, there are several known allotropes of phosphorus, all containing P–P single bonds.

White phosphorus, the simplest stable allotrope, consists of P_4 tetrahedral units where the atoms experience high angular strain (P–P–P angles of approximately 60°), making it also the most reactive and the least thermodynamically stable allotrope. Red phosphorus, obtained by heating of white phosphorus, is much less reactive and it is formed as an amorphous three-dimensional polymeric networks of P_4 units connected by P–P bonds. Violet (or Hittorf's) phosphorus is formed by heating of red phosphorus and consists of P_8 and P_9 groups linked alternately by pairs of P atoms to form a repeating unit of 21 atoms. Finally, black phosphorus is the most thermodynamically stable allotrope at room temperature and atmospheric pressure, formed by heating P_4 under high pressures. Its structure consists of layers of six-membered rings.[1]

The diatomic P_2 form of phosphorus does exist in the gas phase but only in equilibrium with P_4 at high temperatures and low pressures. The preference of phosphorus to form single bonds in all of its allotropes other than P_2 gas is the most

striking difference between these two elements and can be generally rationalized in terms of the relative strengths of the bonds formed.[1,2] The interatomic distance observed in the P_2 molecule is 189.5 pm, 80 pm longer than that of N_2,[1] with a bond strength of 490 kJ mol^{-1},[3] a value that is significantly smaller than that of dinitrogen gas.

Previously only observed under harsh conditions, Cummins and co-workers recently reported that the diphosphorus molecule can also be accessed using a novel organophosphorus species. The anthracene-based system was generated in solution using a niobium complex as a carrier of P_4. The diphosphorus compound formed is then trapped with an organic diene.[4] In the ensuing years, carbenes have also been used to stabilize the P_2 fragment.[5,6] Recently, the Cummins group also reported an anthracene-based source of P_2 shown in Scheme 1.1 that was found to eliminate anthracene and diphosphorus upon mild heating.[7] This compound can be further reacted with an azide to access an all-pnictogen planar heterocycle [$P_2N_3^-$].[8]

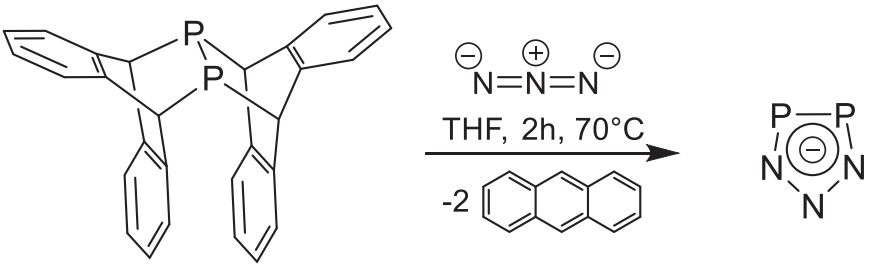

Scheme 1.1: Thermal generation of the P_2 fragment and further reaction with an azide to form the [$P_2N_3^-$] ring.

1.2 Air stable primary phosphines

In contrast to primary amines, primary phosphines (PH_2R) are known to be highly reactive, flammable and toxic species.[1,9] Nevertheless, phosphines are widely employed in polymer science,[10–12] asymmetric catalysis,[13–15] and biochemistry.[16] Therefore, access to more stable primary phosphines is of great importance.

Although the mechanism of phosphine oxidation by oxygen is not yet fully understood, it is attributed to the formation of a very strong P–O double bond when in the presence of oxygen. It is believed to go through a radical mechanism leading to the formation of phosphine oxide (Figure 1.1).[9]

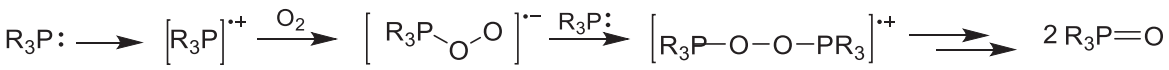

Figure 1.1: Postulated mechanism for oxidation of phosphines.

On account of this reactivity, the number of air-stable primary phosphines reported in the literature is scarce. Typically, the air stability of this family of compounds is rationalized either by the presence of bulky substituents or by delocalisation of the lone-pair of the phosphorus atom.[17] Unfortunately, these explanations do not apply to all cases, such as the primary phosphines (c) and (d) depicted in Figure 1.2. To try to address this issue, Higham has proposed a theory based on DFT calculations that rely on the SOMO energy of the radical cations obtained from the neutral species. If the energy of the SOMO is found to be above a threshold of –10 eV, that is, with higher energy values than that, the primary phosphine is predicted to be air stable.[9]

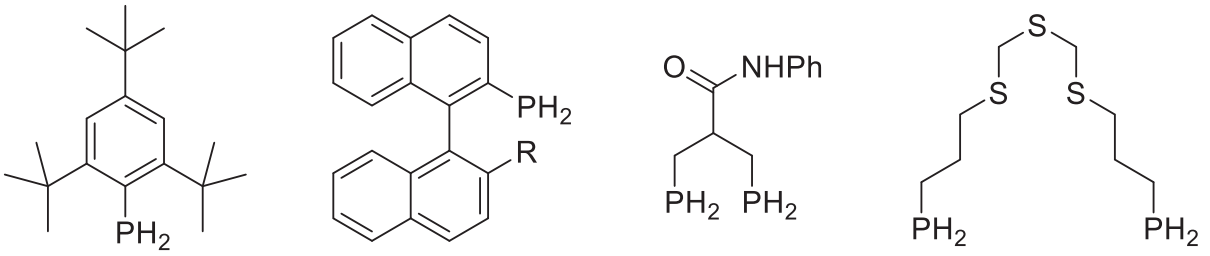

(a) (b) (c) (d)

Figure 1.2: Examples of air-stable primary phosphines.

1.3 Multiple bonds involving phosphorus

The thought of main group elements not belonging to the first row of the periodic table forming multiple bonds was previously inconceivable due to poor p_π-p_π orbital overlap. These heavier elements were assumed to favour the formation of multiple single bonds instead, as described in section 1.1. This concept, known as the "double bond rule" was, at the time, supported by the lack of experimental evidence for such compounds.[18–20] The rule states that elements with a principal quantum number higher than two should not be able to form p_π-p_π bond with themselves or with other elements and relies solely on bond strength.[21]

Following the formulation of this rule, several examples were reported featuring double or even triple bonds involving heavier p-block elements.[22–25] Bulky substituents are usually used to thermodynamically and kinetically stabilise multiple bonds in these compounds. Examples exist of molecules featuring elements from groups 13,[26–29] 14[30,31] and 16[32,33] that have multiple bonds between the same element as well as with atoms from neighbouring groups.[25] For this dissertation, examples incorporating group 15 elements, particularly phosphorus, are of importance.

The first stable phosphaalkene containing a P=C double bond was synthesised by Becker in 1976.[34] Soon after, in 1981, Yoshifuji and Inamoto reported the first

compound featuring a P=P double bond stabilised by supermesityl groups, Mes* (2,4,6-(^{t}Bu)$_3$C$_6$H$_2$).[35] In the same year, Becker reported the first isolable phosphaalkyne, featuring a P≡C triple bond (Figure 1.3).[36] Such species, as well as several others comprising multiple bonds with other heavier p-block elements, offer counterevidence to the “double bond rule”.

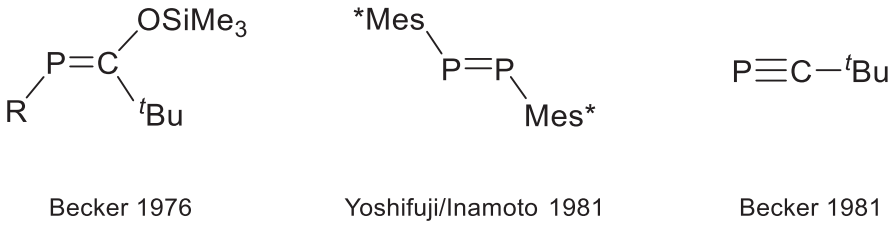

Figure 1.3: Early examples of compounds featuring multiple bonds to a pnictogen. (Mes* = 2,4,6-(^{t}Bu)$_3$C$_6$H$_2$).

1.4 Phospha-organic chemistry

Nobel laureate Roald Hoffmann described two fragments as “isolobal if the number, symmetry properties, approximate energy and shape of the frontier orbitals and the number of electrons in them are similar – not identical, but similar”.[37,38] This theory helps understanding the bonding and reactivity of more esoteric molecules by relating them to familiar compounds. Isolobal theory acts as a starting point to investigate these esoteric systems. It is worth noting, however, that there are many examples where the reactivity of isolobal compounds diverges.

Relevant to this work is the diagonal relationship between the phosphorus atom and the methine fragment (C–H) (Figure 1.4). It is often the interest of synthetic chemists to obtain phosphorus containing analogues of organic molecules. Noteworthy examples of such analogous molecules are the phosphaalkenes and phosphaalkynes that are valence isoelectronic with alkenes and alkynes, respectively. These compounds are often unstable due their weak π-bonds and require stabilization to

prevent polymerization. This can be accomplished either kinetically by introducing sterically protecting substituents[39] or thermodynamically by lowering the energy of the double bond via delocalization of the π electrons.[40] Because of its diagonal relationship with carbon, phosphorus is frequently regarded as a “carbon-copy”.[41]

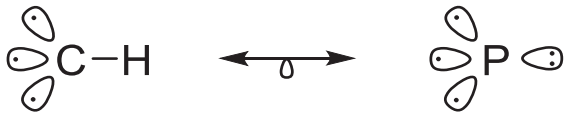

Figure 1.4: Isolobal relationship between the C–H and P fragments.

In light of the isolobal relationship between these two fragments, a parallel can be drawn between compounds containing a phosphorus-carbon bond, such as phosphaalkenes, phosphaalkynes and phosphaketenes and their organic counterparts (Figure 1.5).

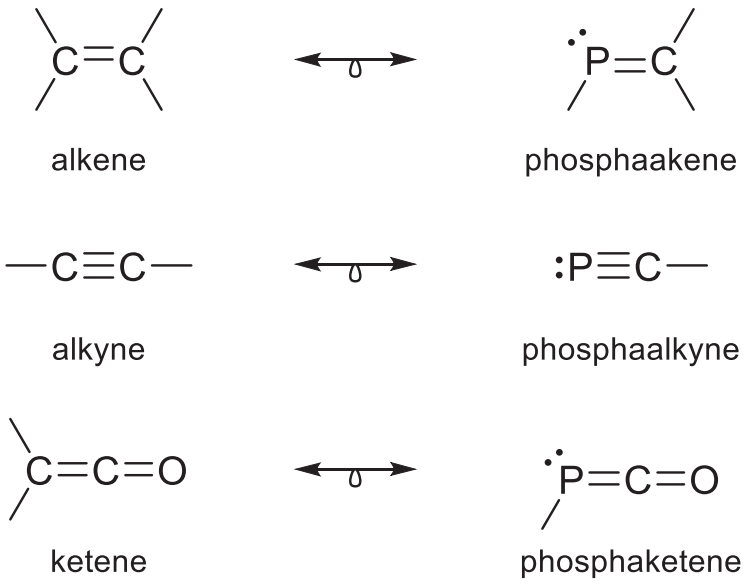

Figure 1.5: Multiple bond organic species and their phosphorus-containing equivalents.

1.4.1 Phosphaalkenes

Phosphaalkenes are phosphorus containing analogues of imines ($R^1R^2C{=}NR^3$). The electronegativity of phosphorus is lower compared to that of nitrogen, thus the phosphorus-carbon double bond would be expected to be less polar. This suggests that phosphaalkenes are more likely to exhibit reactivity in line with that of alkenes rather than imines.[42,43] Given the high reactivity of P=C double bonds, often added stabilization is necessary for these species to be observed.[44] The first stable phosphaalkene was reported by Becker in 1976 and relies on bulky siloxy and tert-butyl groups to stabilise the phosphorus-carbon double bond (Scheme 1.2).[34]

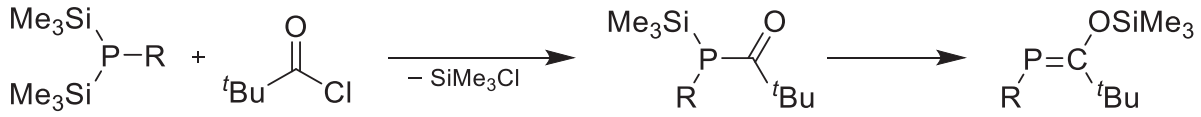

Scheme 1.2: Becker's synthesis of the first stable phosphaalkene.

UV photoelectron spectroscopy of phosphaethene ($CH_2{=}PH$), the parent compound of the phosphaalkene series, revealed that the HOMO of this species is located at the π bond (πCP), with an ionization energy of –10.3 eV, and not at the phosphorus lone pair (nP), which has an ionization energy of –10.7 eV.[45] This very small energy gap between the π manifold and the lone pair at the phosphorus orbitals suggests that electrophiles will not always be able to distinguish between the double bond and the lone pair.[44]

Typically, the electron density at the P–C double bond leans towards the carbon ($P^{\delta+}–C^{\delta-}$) due to the difference in electronegativity of carbon (2.5) and phosphorus (2.1).[46] However the nature of the substituents can cause polarity inversion of the π-electron distribution ($P^{\delta-}–C^{\delta+}$).[47,48] Despite the similar behaviour displayed by phosphaalkenes when compared to alkenes, the P=C π bond is weaker than the

corresponding C=C π bond in alkenes, calculated to be 43 kcal/mol and 65 kcal/mol, respectively.[49,50] These findings are in accordance with the “double bond rule”, as the P=C bond is highly reactive and needs to be kinetically stabilized.

1.4.2 Phosphaalkynes

The very first report of phosphaalkynes dates back to 1961, when Gier managed to detect the parent species of this family of compounds, HC≡P, by mass spectrometry and IR spectroscopy. This methinophosphide was obtained by decomposition of phosphine in an electric arc between graphite electrodes, but the product was a very reactive gas that could only be stored at very low temperatures.[44,51] A few years later, in 1976, Kroto and co-workers also identified the presence of HC≡P, this time by microwave spectroscopy, while trying to detect unstable phosphaalkenes such as CH_2=PCl. The compound was obtained by loss of two equivalents of hydrochloric acid from CH_3PCl_2,[52] which was one of the methods Gier used to independently support his claim of finding HC≡P. Even though the synthetic procedure became more accessible, the parent phosphaalkyne was still highly unstable, deterring further investigations.

A landmark contribution in organo-phosphorus chemistry was reported in 1981 by Becker who synthesised *t*Bu–C≡P (Scheme 1.3), the first isolable compound featuring a phosphorus-carbon triple bond that was stable at room temperature.[36] Subsequently, several studies have been conducted to explore the chemistry of these compounds. An array of other phosphaalkyne derivatives have also been synthesised since this finding.[2,53,54]

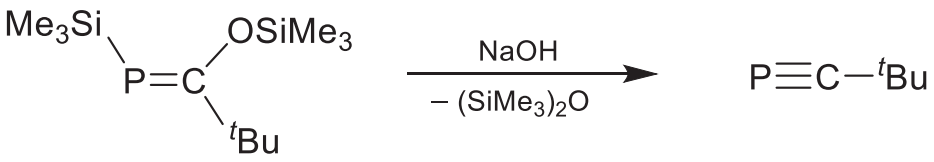

Scheme 1.3: Becker's synthesis of ^{t}Bu–C≡P.

Phosphaalkynes are heavier analogues of nitriles (R–C≡N), but their chemistry displays some striking differences. Interestingly, for nitriles the multiple bond is polarised in the direction of the pnictogen, whereas for phosphaalkynes the opposite is true.[24] Photoelectron spectroscopy studies conducted by Kroto and co-workers in the early 80s provided information about the electronic properties of phosphaalkynes that included Becker's first example, ^{t}Bu–C≡P. For this compound, the authors report the first ionization potential associated with the removal of the π(CP) electrons at 9.61 eV, those corresponding to the HOMO. The second ionization potential, associated with the removal of the n(P) electrons, is 11.44 eV. The significantly lower energy on the phosphorus lone pair is reflected in its diminished reactivity.[55] These findings are supported by experimental evidence that show exclusive protonation at the carbon involved in the triple bond while the phosphorus centre remains unreacted, even in the presence of super acids.[56]

All substituted examples of phosphaalkynes (R–C≡P) that have been structurally characterized exhibit R-C-P angles close to 180°. The solid state structure of the ^{t}Bu–C≡P molecule reveals a P–C distance of 1.548(1) Å, comparable to other phosphaalkynes, including the parent species.[24,25] Phosphaalkynes can undergo various types of cycloadditions, typically [2+3] reactions when reacted with 1,3-dipole compounds such as azides, to yield phosphorus containing heterocycles.[57] Furthermore, phosphaalkynes participate in a variety of oligomerization reactions to

form complex cage compounds.[58–60] However, in some cases more alkyne-like behaviour may also be observed.[44,61]

1.4.3 Phosphaketenes

Heavy analogues of isocyanates (R–N=C=O) containing phosphorus are called phosphaketenes. They are known to be very reactive species, so much so that, to date, only two examples of hydrocarbon-substituted phosphaketenes have been reported. The first example of this class of compounds, *t*-butylphosphaketene (^{t}Bu–P=C=O), was reported by Appel and Paulen but is only stable as a monomer below –60 °C. At higher temperatures it was found to quickly dimerize to form diphosphaketenedione (Scheme 1.4-above).[62] In the same year the same authors managed to synthesise the first room temperature stable phosphaketene by introducing the bulky supermesityl (Mes* = 2,4,6-(^{t}Bu)$_3$C$_6$H$_2$)) group (Scheme 1.4-below).[63] Both phosphaketenes were synthesised via the same synthetic route with minor changes to the reaction conditions.

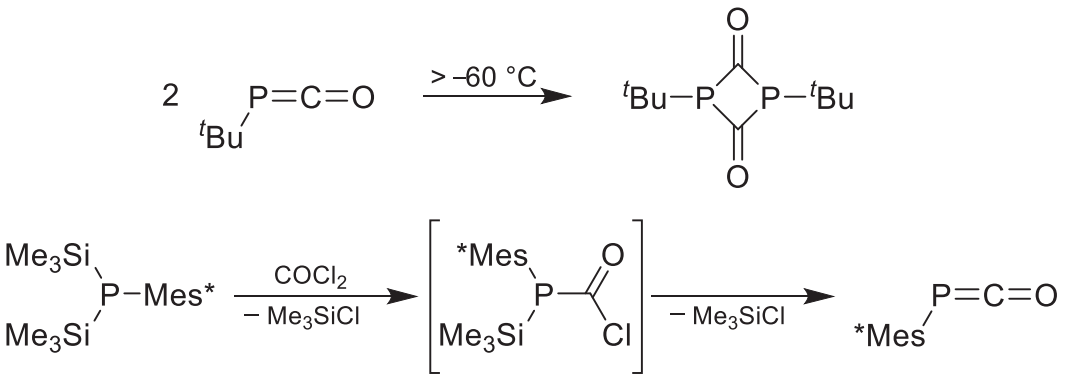

Scheme 1.4: Dimerization of ^{t}Bu–P=C=O at temperatures higher than –60 °C (above) and the synthesis of Mes*–P=C=O (below).

The parent phosphaketene, H–P=C=O, analogous to isocyanic acid (H–N=C=O), is more elusive with limited analytical data available. This molecule has been

the subject of several theoretical studies that show that the HPCO isomer is 98.7 kJ/mol more stable than HOCP,[64–67] inspiring efforts to obtain experimental characterization. Two experiments mimicking interstellar conditions, where HPCO is believed to exist, were able to generate the molecule in the gas phase and record the infrared and microwave spectra of this molecule confirming the presence of the HPCO isomer over HOCP.[68,69] More recently, Goicoechea reported the synthesis of HPCO using standard Schlenk line techniques by heating a solid mixture of stearic acid and [Na(dioxane)$_x$][PCO] under vacuum to yield the product as a gas that was subsequently condensed into an NMR tube containing solvent, allowing its full NMR spectroscopic characterization (Scheme 1.5).[70] The product was also found to be stable for a few hours in solution at low temperatures.

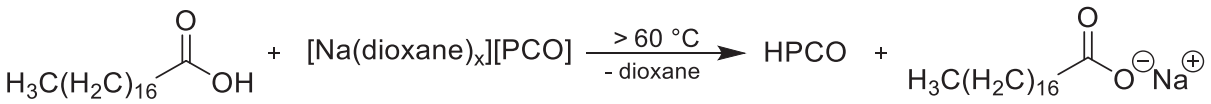

Scheme 1.5: Reaction between stearic acid and PCO^- to obtain HPCO.

The 2-phosphaethynolate anion (PCO^-), can also be regarded as an anionic phospheketene.[71] It has been demonstrated by the Grützmacher group that substitution of the phosphorus atom can also provide enough stabilization to make the monomeric form of the 2-phosphaethynolate anion isolable in the form of the heterophosphaketenes $R_3E–P=C=O$ (E = Si, Ge, Sn, Pb; R = Ph or ^{i}Pr) (Scheme 1.6).[72,73] The PCO^- anion was also found to be stable in the coordination sphere of transition metals such as rhenium and tungsten, in which case it is best described as a metallaphosphaketene, M–P=C=O.[74,75]

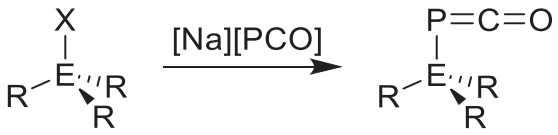

Scheme 1.6: Reaction of PCO^- with triorganyl tetrel compounds to yield stable phosphaketenes. E = Si, Ge, Sn, Pb; R = Ph or ^{i}Pr; X = Cl or OTf.

1.5 The 2-phosphaethynolate anion (PCO^-)

1.5.1 Synthesis of the PCO^- anion

The PCO^- anion was first reported in 1992 by Becker and co-workers as a lithium salt, $[Li(DME)_2][PCO]$ (DME = 1,2-dimethoxyethane), by reacting lithium bis(trimethylsilyl)phosphine and dimethyl carbonate as shown in Scheme 1.7. However, due to the inherent instability of this salt it remained largely underexplored for the next twenty years.[76]

Scheme 1.7: Becker's synthesis of $[Li(DME)_2][PCO]$.

In 2002 the scope of PCO^- anion salts was expanded with the preparation of a series of alkaline earth metal bis(2-phosphaethynolates) salts. However reactivity studies into these salts were also limited as the dimers were found to be as unstable as the lithium salt toward oligomerization.[77] A less conventional route to Na[PCO] was reported in 2012 by reaction of a terminal niobium phosphide ($[Na][\{(C_6F_5)_3B\}PNb(N[Np]Ar)_3]$ (Ar = 3,5-$C_6H_3Me_2$; Np = neopentyl) with carbon dioxide.[78]

In 2011, Grützmacher et. al., reported the synthesis of $[Na(DME)_2][PCO]$ and $[Na(dioxane)_{2.5}][PCO]$, noting that unlike the other s-block salts, the Na[PCO] salt was

remarkably stable even in air for short periods of time.[79] However, the reaction conditions employed were quite harsh, demanding high temperatures and a high pressure of CO gas (Scheme 1.8).

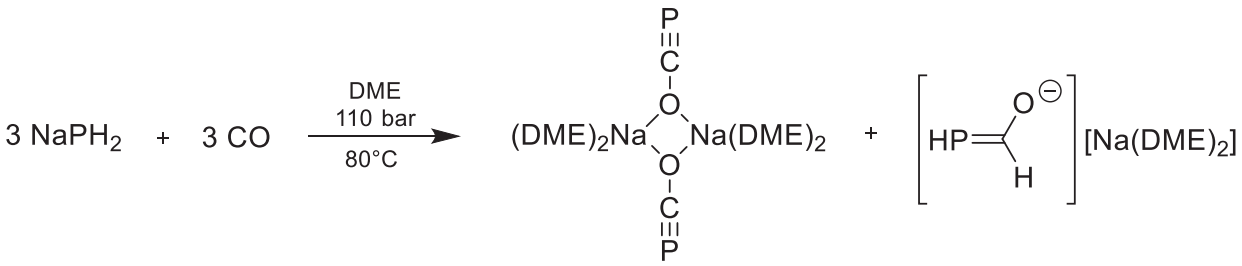

Scheme 1.8: Grützmacher's synthesis of $[Na(DME)_2][PCO]_2$.

In 2014, a state of the art synthesis of $[Na(dioxane)_x][PCO]$ was discussed by Grützmacher allowing access to this material on a multigram scale from inexpensive commercially available starting materials (Scheme 1.9).[71]

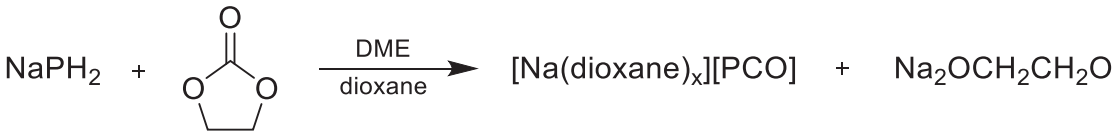

Scheme 1.9: Grützmacher's synthesis of $[Na(dioxane)_x][PCO]$.

In 2013, the Goicoechea group reported an alternative synthesis of PCO^- as a $[K(18\text{-crown-6})]^+$ salt by using the Zintl phase K_3P_7 as a phosphide source and DMF (*N,N*-dimethylformamide) as a CO source (Scheme 1.10). The potassium salt of PCO^- was also found to have comparable stability to the sodium salt.[80] With these new synthetic routes in hand, more reactivity studies into this small anion became possible.

Scheme 1.10: Goicoechea's synthesis of [K(18-crown-6)][PCO].

Although the current state of the art of the PCO^- synthesis is the one reported in 2014 by Grützmacher, other alternative routes have been reported. More recently, in 2016, the synthesis of ammonium and phosphonium salts of the 2-phosphaethynolate anion were described from the reaction of organic methylcarbonate salts with tris(trimethylsilyl)phosphine.[81] The last known synthetic route of the 2-phosphaethynolate anion was also reported by Grützmacher's group by exposure of a THF solution of NaO^tBu to phosphine gas, that is used as a phosphorus source.[82]

Over the years since its first report, the synthesis of the 2-phosphaethynolate anion has gone through several modifications and it can now be obtained as stable salts and in multigram scales. These findings made possible further studies of this anion, which proved it to be highly versatile, participating in various types of reactions.

1.5.2 Structure and bonding

The 2-phosphaethynolate anion is best described as the superposition of three resonances structures. By far the two greatest contributions are from the phosphaethynolate, comprising a formal triple bond between the phosphorus and the carbon with a negative charge on the oxygen (Figure 1.6-a) and the phosphaketene, which features a formal double bond between the phosphorus and the carbon with a negative charge on the phosphorus (Figure 1.6-b). A third resonance form is a carbonyl adduct of monoanionic phosphide (Figure 1.6-c), which contributes to a lesser extent to the overall structure, but should still be mentioned as PCO^- can undergo a number of reactions where it decarbonylates and transfers a monoanionic phosphide.[83,84]

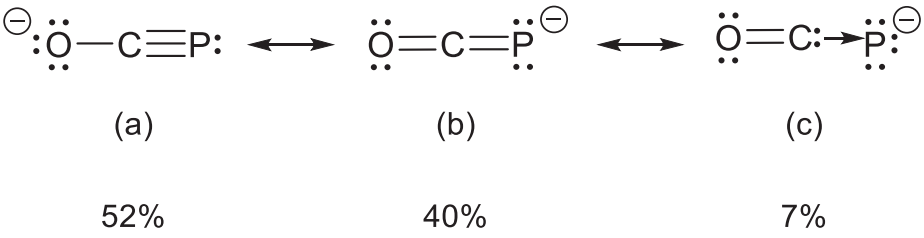

Figure 1.6: Resonance structures of PCO^- and their weights.

The PCO^- anion is a rare example of a main group compound where the phosphorus atom is engaged in a multiple bond that is not stabilized by bulky steric protecting groups. In this case, the P–C bond is stabilized by delocalization of the negative charge along the anion promoting electrostatic repulsion between monomers, thus precluding normal decomposition pathways, such as oligomerization.[75]

As discussed above, the 2-phosphaethynolate anion has been synthesised through various routes using different counter cations. For means of illustration and, as the data is consistent with other reported species, only the features found in [K(18-crown-6)][PCO] will be briefly highlighted here. The ^{31}P and $^{13}C\{^1H\}$ NMR spectra of this compound exhibit a singlet at –396.8 ppm and doublet at 170.3 ppm ($^1J_{P–C}$ = 62 Hz), respectively. The crystal structure shows that the atoms in the PCO^- anion are in a linear arrangement with a P–C–O angle of 178.9(3) Å (Figure 1.7). The potassium cation is located inside the 18-crown-6 pocket and it interacts electrostatically with both oxygen and phosphorus atoms of the anion giving rise to one-dimensional chains. The P–C and C–O distances are 1.579(3) Å and 1.212(4) Å, respectively, and are consistent with the aforementioned phosphaethynolate resonance form, with a triple bond between the phosphorus and the carbon and a negative charge on the oxygen.[80]

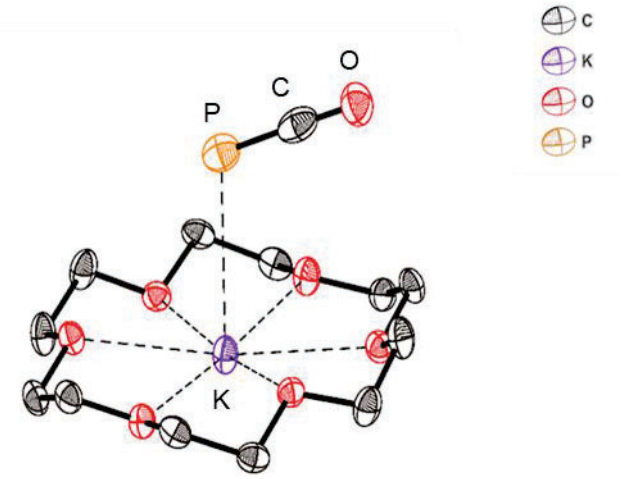

Figure 1.7: Crystal structure of the [K(18-crown-6)][PCO]. P–C and C–O bond lengths are 1.579(3) Å and 1.212(4) Å respectively.

1.5.3 Reactivity of the PCO^- anion

1.5.3.1 Coordination Chemistry

The 2-phosphaethynolate anion is an ambidentate nucleophile and, as such, can coordinate via the phosphorus or the oxygen atom. The first report of a transition metal complex of PCO^-, (triphos)Re(PCO)$(CO)_2$ (triphos = $MeC(CH_2PPh_2)_3$), resulted from the reaction of (triphos)Re(OTf)$(CO)_2$ (OTf = trifluoromethasulfonate) with [Na(dioxane)$_{2.5}$][PCO], detailed by Peruzzini and co-workers (Figure 1.8-a).[74] In this work, an analogous NCO^- complex was also synthesised and, despite both ligands binding through the pnictogen, their coordination behaviour was found to differ greatly. The NCO^- ligand binds in an approximately linear fashion, with a Re-N-C bond angle of 166.2°, whereas the PCO^- coordination mode is bent, with the Re-P-C angle of 92.6° indicating that the PCO complex is best described as a metallaphosphaketene while the NCO complex contains a C–N triple bond and a O–C single bond.

Following this work, a series of other examples have been reported of the 2-phosphaethynolate anion acting as a ligand. Interestingly, binding through the

phosphorus atom is far more common and, in doing so, the PCO^- anion adopts the phosphaketene form. As an example, the PCO^- anion can undergo ligand displacement reactions when reacted with compounds coordinated by relatively weak Lewis bases such as $W(CO)_5(MeCN)$, to afford the anionic coordination complex $[W(CO)_5(PCO)]^-$ (Figure 1.8-b). In this species, the phosphaketene is coordinated through the phosphorus centre in a bent geometry relative to the metal, in contrast with its lighter congener, the cyanate, which exhibits a linear arrangement.[75]

Only a few examples are known of coordination via the oxygen, the phosphaethynolate form, but they should still be mentioned as they highlight the ambident character of the PCO^- anion. This bonding mode has been structurally authenticated in the coordination sphere of uranium, thorium and scandium where it binds with a linear geometry to the metal. The P–C bond is shortened and the C–O bond is lengthened compared to values observed for the phosphorus-bonded species.[85–87] Only two structurally authenticated examples are known of a phosphaethynolate compound with a main-group element. The Goicoechea group reacted PCO^- with a bulky bromoborane (Figure 1.8-c). The boron has a strong oxophilic character that favours the formation of a phosphaethynolate-type compound.[88] In this compound, an enhancement of the reactivity of the P≡C triple bond is also observed and this species can be regarded as a phosphaalkyne analogue. In 2019, Grützmacher reported [Al]–OCP complexes ([Al] = salen(^{t}Bu)Al or salophen (^{t}Bu)Al) that are supported by sterically encumbering salen ligands.[89]

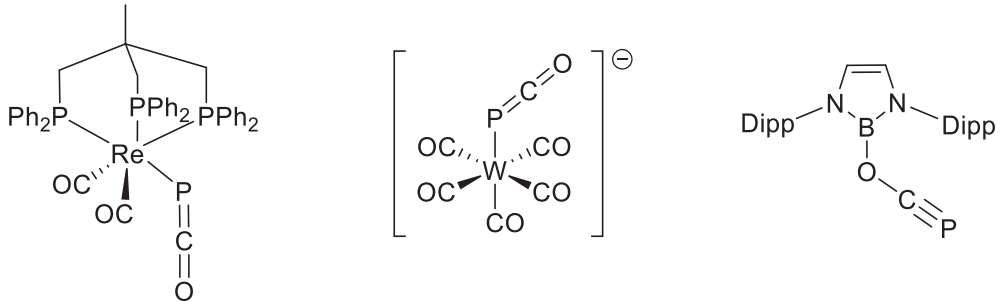

Figure 1.8: PCO^- coordination compounds. Dipp = 2,6-diisopropylphenyl.

1.5.3.2 Oligomerization

Two 2-phosphaethynolate anions are very unlikely to undergo spontaneous dimerization to form $(P_2C_2O)_2^{2-}$ due to electrostatic repulsion of the monomers.[71] In 1995, Becker reported the oxidative tetramerization of the PCO^- anion to give the heterobicyclic dianion $(P_4C_4O_4)^{2-}$ when $[Li(DME)_2][PCO]$ was allowed to react with sulphur dioxide (SO_2) or iodine, as shown in Scheme 1.11.[90]

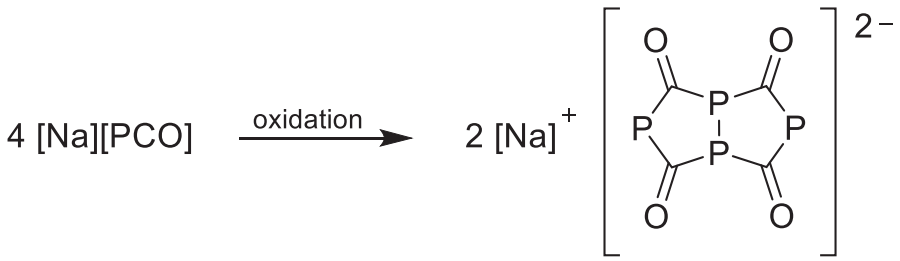

Scheme 1.11: Synthesis of $(P_4C_4O_4)_2^{2-}$ by oxidation of PCO^-.

In the following years, a handful of derivatives of $(P_2C_2O)_2^{2-}$ were reported. The carbon dioxide adduct of this theoretical dimer was synthesised by the Grützmacher group by reacting $[Na(dioxane)_x][PCO]$ with CO_2 to yield a dianionic four-membered ring with a carboxylate unit coordinated to one of the phosphorus atoms (Scheme 1.12). Computational studies revealed that the reaction mechanism differs from the classical concerted [2+2] cycloadditions, involving nucleophilic attack on the CO_2

carbon centre by the phosphorus centre of PCO^- to form $[O_2C–P=C=O]^-$ followed by attack by a second PCO^- anion to the carbon centre of the resulting species.[71]

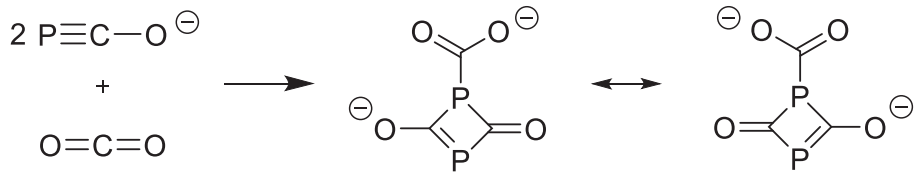

Scheme 1.12: Synthesis of $Na_2(P_2C_3O_4)$ by reaction of PCO^- and CO_2.

1.5.3.3 Cycloadditions

The 2-phosphaethynolate anion has been extensively studied in cycloaddition chemistry when in the presence of unsaturated systems. It has been shown that this species can act as a building block to afford a series of three-, four-, five- and six-membered phosphorus-containing heterocycles. A cycloaddition reaction involving the PCO^- anion was first proposed by Becker in 1994 when PCS^- was obtained by the reaction of PCO^- and CS_2 (Scheme 1.13). The four-membered ring formed through the cycloaddition of the P≡C triple bond and the C=S double bond was postulated as an intermediate for this reaction.[91]

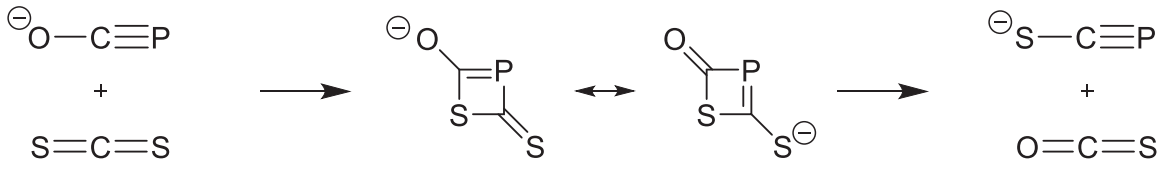

Scheme 1.13: Reaction of PCO^- and CS_2 to form PCS^-.

In light of this result, in 2013, the Goicoechea group reported the synthesis and characterization of anionic four-membered rings containing phosphorus by reaction of [K(18-crown-6)][PCO] with sterically bulky heteroallenes, like diphenylketene ($O=C=C(C_6H_5)_2$) and bis(2,6-diisopropylphenyl)carbodiimide (DippN=C=NDipp). The products resulted from the addition of P≡C triple bond of PCO^- across the C=C double

bond of the ketene and of the C=N double bond of the carbodiimide. In both cases, monoanionic four-membered heterocycles were isolated (Scheme 1.14).[80]

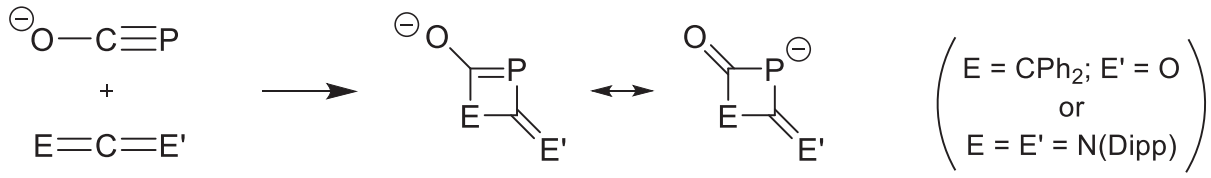

Scheme 1.14: [2+2] cycloaddition reaction of the PCO^- anion with heteroallenes.

1.5.3.4 Phosphinecarboxamides

Of the discussed reactivity of PCO^- no parallels can be drawn with the reactivity of its lighter congener, the cyanate anion. However, when in the presence of ammonium salts, PCO^- reacts similarly to NCO^- to yield the phosphorus containing analogue of urea, called phosphinecarboxamide. This molecule will be further discussed in section 1.6 of this introduction.[92]

1.5.3.5 PCO as a P^- donor

From the examples mentioned above it can be noted that 2-phosphaethynolate anion can be used as a versatile building block for the preparation of a library of organophosphorus compounds. However, thus far only examples involving the phosphaketene and phosphaethynolate resonance forms have been mentioned. The PCO^- anion can also be referred to as an adduct of carbon monoxide and P^- and, albeit a minor resonance contributor, this form is consistent with the rich decarbonylation chemistry observed with PCO^- .[93–95]

The first report of PCO^- acting as a P^- transfer agent was published by the Grützmacher group in 2014. These findings were a result of the reaction between $[Na(dioxane)_x][PCO]$ with an imidazolium salt that afforded a carbene-stabilized phosphanediyls (Scheme 1.15).[94]

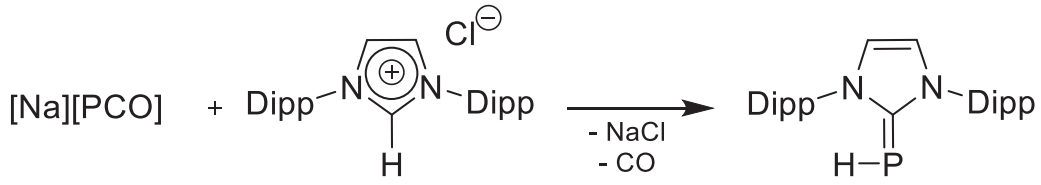

Scheme 1.15: Synthesis of NHC-stabilized phosphanediyls. Dipp = diisopropylphenyl.

Another interesting example of the 2-phosphaethynolate anion acting as a P^- source was reported by the Goicoechea group when PCO^- was reacted with unsaturated three-membered silicon rings. The P–C multiple bond of the 2-phosphaethynolate is cleaved and the PCO^- anion is added across the Si–Si double bond as a phosphide (P^-) and a carbonyl moiety (CO), yielding a bicyclic compound. Subsequent irradiation of the bicycle gave rise to a phosphorus-containing four-membered-ring, suggesting that the overall reaction of PCO^- with the three-membered silicon ring under photolytic conditions may be considered a direct incorporation of phosphide into an unsaturated ring system (Scheme 1.16).[96]

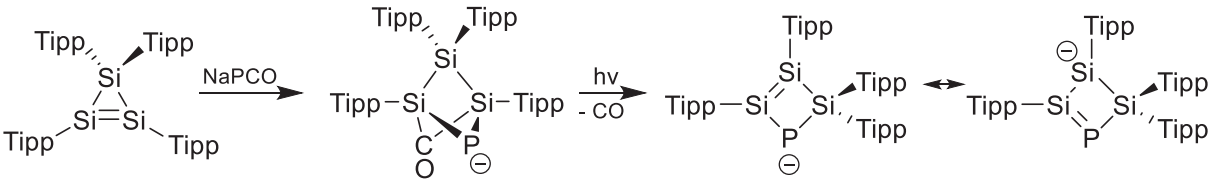

Scheme 1.16: Reaction of PCO^- with cyclotrisilene and consecutive decarbonylation. Tipp = triisopropylphenyl.

Seminal work in this field was reported by Bertrand and co-workers, where it was demonstrated that the photolysis of a phosphinophosphaketene led to a (phosphino)phosphinidene, a compound that exhibits a multiple bond between the two phosphorus centres, best described by the three resonance structures shown in Scheme 1.17.[97]

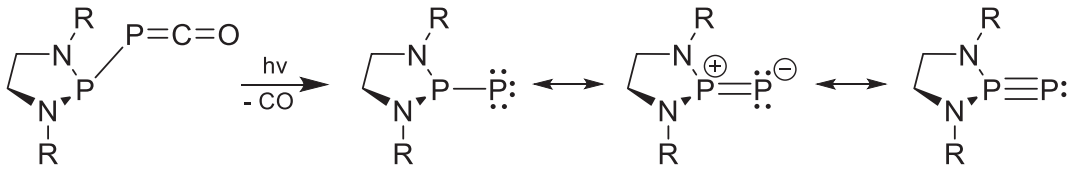

Scheme 1.17: Synthesis of (phosphino)phosphinidene.

1.6 Phosphinecarboxamide

1.6.1 Synthesis of urea

In 1828, Wöhler reported the synthesis of urea by reacting silver cyanate and ammonium chloride with the initial intent of producing ammonium cyanate.[98–100] This unexpected result represented a landmark in chemistry as it was the very first time that inorganic starting materials were used to obtain a naturally occurring molecule (Scheme 1.18). These findings offered counterevidence to the theory of vitalism that was believed at the time and can even be considered the birth of organic chemistry.[100]

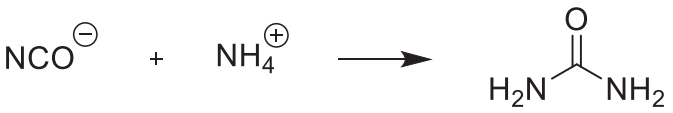

Scheme 1.18: Wöhler's synthesis of urea.

1.6.2 Synthesis of the parent phosphinecarboxamide ($H_2PC(O)NH_2$)

Inspired by Wöhler's serendipitous synthesis of urea, and considering that the 2-phosphaethynolate anion is a phosphorus-containing analogue of cyanate, the Goicoechea group sought to explore any similarities in their reactivity. The reaction of [K(18-crown-6)][PCO] with simple ammonium salts NH_4X (X = BPh_4, Cl) resulted in the formation of the parent phosphinecarboxamide (Scheme 1.19).[92]

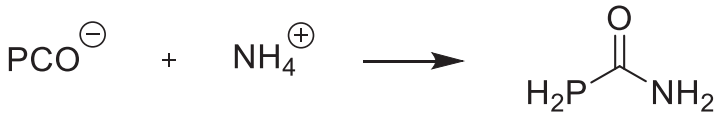

Scheme 1.19: Synthesis of the parent phosphinecarboxamide.

This compound is a heavier analogue of urea where one of the nitrogen atoms has been replaced by a phosphorus atom. This species, unlike most primary phosphines, exhibits remarkable air and moisture stability, to the extent of allowing synthesis in aqueous solutions. The species has a half-life of approximately nine days in a d_5-pyridine solution exposed to air.[92] Although the parent phosphinecarboxamide was not synthesised until 2013, derivatized *P*-functionalised and *N*-functionalised phosphinecarboxamides were previously known.[101–103]

1.6.2.1 Formation mechanism

The formation of the phosphinecarboxamide is believed to occur via initial protonation of the 2-phosphaethynolate anion to form the parent acid HPCO, followed by nucleophilic attack of the amine, going through a four-membered intermediate and final formation of the product (Figure 1.9). The mechanism is postulated as being the same as that proposed for urea.[104]

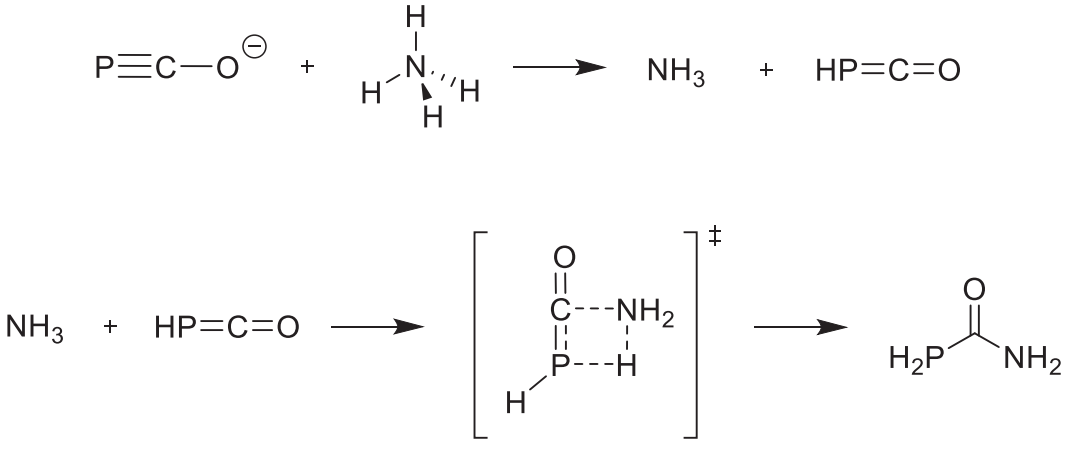

Figure 1.9: Postulated mechanism for the formation of the phosphinecarboxamide.

1.6.2.2 Structural analysis of $H_2PC(O)NH_2$

The phosphinecarboxamide moiety exhibits very characteristic NMR resonances. The ^{31}P NMR spectrum in d_5-pyridine shows a triplet of doublets centred at –134.4 ppm ($^1J_{P–H}$ = 209 Hz, $^2J_{P–H}$ = 12 Hz) which collapses to a singlet upon proton decoupling. The ^1H NMR reveals a doublet centred at 3.82 ppm, corresponding to the phosphine protons, with a coupling constant of $^1J_{P–H}$ = 209 Hz, that collapses to a singlet upon selective phosphorus decoupling, as well as two broad resonances at 8.57 and 9.05 ppm corresponding to the two inequivalent amide protons. The $^{13}C\{^1H\}$ NMR spectrum shows a doublet at 175.8 ppm ($^1J_{P–C}$ = 8 Hz) due to coupling with the phosphorus atom.[92]

X-ray crystallography studies of the parent phosphinecarboxamide revealed a trigonal pyramidal geometry at the phosphorus atom with a planar carboxamide moiety. The P–C bond distance is 1.865(1) Å, which is consistent with a single bond and the C–N bond distance is 1.329 (2) Å, suggesting some multiple bond character between these atoms (Figure 1.10).[92]

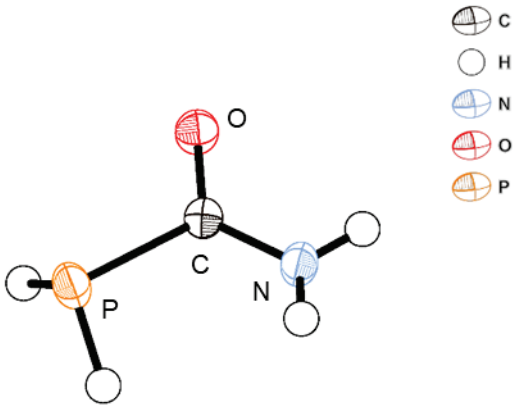

Figure 1.10: Crystal structure of $H_2NC(O)PH_2$. P–C and C–N bond lengths are 1.865(1) Å and 1.329(2) Å respectively.

Three resonances structures can be drawn for the parent phosphinecarboxamide. Even though the combination of the spectroscopic and crystallographic data implies that there is delocalisation of the π electron density over the amide group, there is no significant interaction between the lone pair of the phosphorus and the carbonyl. Thus, the most significant contributions to the final structure are thought to arise from (i) and (ii) shown in Figure 1.11.[92]

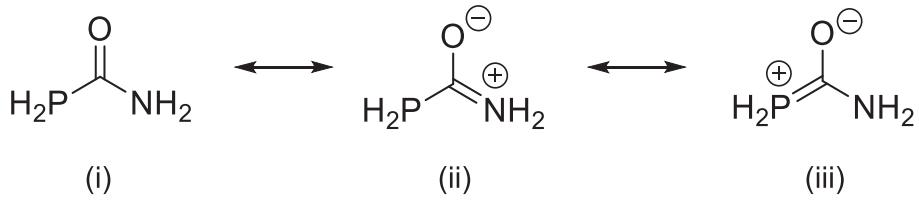

(i) (ii) (iii)

Figure 1.11: Resonance structures of the parent phosphinecarboxamide.

In spite of these findings, some attention should still be drawn to resonance structure (iii) as it helps to explain the remarkable air- and moisture stability of this compound, as some degree of stabilization to oxidation may result from delocalization of the phosphorus lone-pair into the amide functionality.[105]

1.6.3 Other routes to phosphinecarboxamides

Derivatized *P*-functionalised phosphinecarboxamides have been known since the late 1960s and were obtained by reaction of isocyanic acid with primary and secondary phosphines (Scheme 1.20).[101,102] *N*-functionalised phosphinecarboxamides could also be prepared by room temperature catalytic hydrophosphination of isocyanates with secondary phosphines, where the P–H bond is added across the C=N bond of the isocyanate (Scheme 1.20).[103]

More recently, the mechanochemical synthesis of *N*-aryl/alkyl phosphinecarboxamides has been reported as an alternative route to

carbamoylphosphines, solvent-free, by reacting Na[PCO] with aryl and alkyl primary amines.[106] The parent phosphinecarboxamide was alternatively obtained by this route in high yields by grinding the solids of the sodium salt of the 2-phosphaethynolate anion and ammonium chloride and the product was subsequently extracted with chloroform.

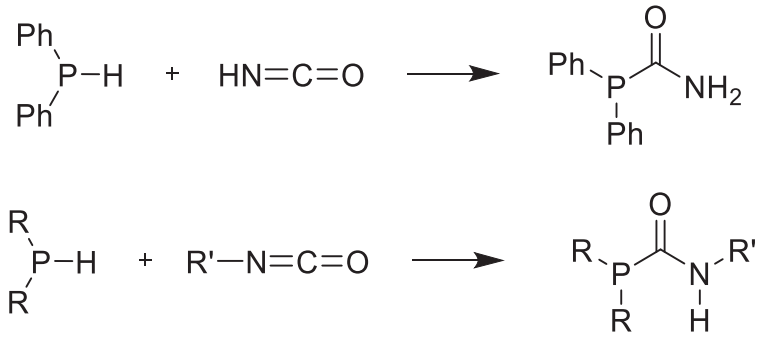

Scheme 1.20: *P*- and *N*-functionalized carbamoylphosphines.

1.7 Aims

The aim of this thesis is to summarize the research conducted throughout my PhD on the relatively small family of phosphinecarboxamides (or carbamoylphosphines), phosphorus containing analogues of urea. Recently, the Goicoechea group reported the synthesis and characterization of the parent phosphinecarboxamide, a prime example of a primary phosphine that displayed remarkable air- and moisture stability. We sought to expand the scope of these compounds by reacting the 2-phosphaethynolate anion with a variety of amines. Chapter 2 will focus on using amino acids, biologically relevant substrates, as the source of amine, to yield chiral products with potential applications in biochemistry. Chapter 3 will explore bidentate amines with the intention to produce bis-phosphinecarbaxamides that could be exploited as chelating ligands. Chapter 4 will pinpoint the possibility of deprotonation and further reactivity with electrophiles to yield *P*-functionalized phosphinecarboxamides as well as determine the ability of these

compounds to coordinate to transition metal centres. Finally, Chapter 5 will underline the reactivity of the PCO^- anion towards amines bearing a ferrocenyl group and the reactivity of the resulting products.

1.8 References

[1] A. Greenwood, N. N. Earnshaw, *Chemistry of the Elements*, Butterworth-Heinemann, **1997**.

[2] M. Regitz, *Chem. Rev.* **1990**, *90*, 191–213.

[3] Y.-R. Luo, Y.-R. Luo, *Comprehensive Handbook of Chemical Bond Energies*, CRC Press, **2007**.

[4] N. A. Piro, J. S. Figueroa, J. T. McKellar, C. C. Cummins, *Science (80-.).* **2006**, *313*, 1276–1279.

[5] Y. Wang, Y. Xie, P. Wei, R. B. King, H. F. Schaefer, P. V. R. Schleyer, G. H. Robinson, *J. Am. Chem. Soc.* **2008**, *130*, 14970–14971.

[6] O. Back, G. Kuchenbeiser, B. Donnadieu, G. Bertrand, *Angew. Chemie Int. Ed.* **2009**, *48*, 5530–5533.

[7] A. Velian, M. Nava, M. Temprado, Y. Zhou, R. W. Field, C. C. Cummins, *J. Am. Chem. Soc.* **2014**, *136*, 13586–13589.

[8] A. Velian, C. C. Cummins, *Science (80-.).* **2015**, *348*, 1001–1004.

[9] B. Stewart, A. Harriman, L. J. Higham, *Organometallics* **2011**, *30*, 5338–5343.

[10] T. N. Hooper, M. A. Huertos, T. Jurca, S. D. Pike, A. S. Weller, I. Manners, *Inorg. Chem.* **2014**, *53*, 3716–3729.

[11] H. Dorn, R. A. Singh, J. A. Massey, J. M. Nelson, C. A. Jaska, A. J. Lough, I. Manners, *J. Am. Chem. Soc.* **2000**, *122*, 6669–6678.

[12] H. Dorn, R. A. Singh, J. A. Massey, A. J. Lough, I. Manners, *Angew. Chemie Int. Ed.* **1999**, *38*, 3321–3323.

[13] T. Clark, C. Landis, *Tetrahedron: Asymmetry* **2004**, *15*, 2123–2137.

[14] G. Hoge, B. Samas, *Tetrahedron: Asymmetry* **2004**, *15*, 2155–2157.

[15] D. J. Brauer, K. W. Kottsieper, S. Roßenbach, O. Stelzer, *Eur. J. Inorg. Chem.* **2003**, *2003*, 1748–1755.

[16] K. V. Katti, H. Gali, C. J. Smith, D. E. Berning, *Acc. Chem. Res.* **1999**, *32*, 9–17.

[17] J. T. Fleming, L. J. Higham, *Coord. Chem. Rev.* **2015**, *297–298*, 127–145.

[18] R. S. Mulliken, *J. Am. Chem. Soc.* **1950**, *72*, 4493–4503.

[19] R. S. Mulliken, *J. Am. Chem. Soc.* **1955**, *77*, 884–887.

[20] K. S. Pitzer, *J. Am. Chem. Soc.* **1948**, *70*, 2140–2145.

[21] P. Jutzi, *Angew. Chemie Int. Ed. English* **1975**, *14*, 232–245.

[22] K. Dimroth, P. Hoffmann, *Angew. Chemie Int. Ed. English* **1964**, *3*, 384–384.

[23] E. Niecke, W. Flick, *Angew. Chemie Int. Ed. English* **1973**, *12*, 585–586.

[24] P. P. Power, *Chem. Rev.* **1999**, *99*, 3463–3503.

[25] R. C. Fischer, P. P. Power, *Chem. Rev.* **2010**, *110*, 3877–3923.

[26] R. J. Wright, A. D. Phillips, N. J. Hardman, P. P. Power, *J. Am. Chem. Soc.* **2002**, *124*, 8538–8539.

[27] M. S. Hill, P. B. Hitchcock, R. Pongtavornpinyo, *Angew. Chemie Int. Ed.* **2005**, *44*, 4231–4235.

[28] Y. Wang, B. Quillian, P. Wei, C. S. Wannere, Y. Xie, R. B. King, H. F. Schaefer, P. V. R. Schleyer, G. H. Robinson, *J. Am. Chem. Soc.* **2007**, *129*, 12412–12413.

[29] Y. Wang, B. Quillian, P. Wei, Y. Xie, C. S. Wannere, R. B. King, H. F. Schaefer, P. V. R. Schleyer, G. H. Robinson, *J. Am. Chem. Soc.* **2008**, *130*, 3298–3299.

[30] A. G. Brook, S. C. Nyburg, F. Abdesaken, B. Gutekunst, G. Gutekunst, R. Krishna, M. R. Kallury, Y. C. Poon, Y. M. Chang, W. N. Winnie, *J. Am. Chem. Soc.* **1982**, *104*, 5667–5672.

[31] G. Maier, G. Mihm, H. P. Reisenauer, *Angew. Chemie Int. Ed. English* **1981**, *20*, 597–598.

[32] O. Blacque, H. Brunner, M. M. Kubicki, F. Leis, D. Lucas, Y. Mugnier, B. Nuber, J. Wachter, *Chemistry (Easton).* **2001**, *7*, 1342–1349.

[33] L. Dostál, R. Jambor, A. Růžička, A. Lyčka, J. Brus, F. De Proft, *Organometallics* **2008**, *27*, 6059–6062.

[34] G. Becker, *ZAAC - Z. Anorg. Allg. Chem.* **1976**, *423*, 242–254.

[35] M. Yoshifuji, I. Shima, N. Inamoto, K. Hirotsu, T. Higuchi, *J. Am. Chem. Soc.* **1981**, *103*, 4587–4589.

[36] G. Becker, G. Gresser, W. Uhl, *Acyl- Und Alkylidenphosphane, XV [1] 2.2-Dimethylpropylidinphosphan, Eine Stabile Verbindung Mit Einem Phosphoratom Der Koordinationszahl 1*, **1981**.

[37] M. Elian, M. M. L. Chen, D. M. P. Mingos, R. Hoffmann, *Inorg. Chem.* **1976**, *15*, 1148–1155.

[38] R. Hoffmann, *Angew. Chemie Int. Ed. English* **1982**, *21*, 711–724.

[39] P. P. Power, *J. Organomet. Chem.* **2004**, *689*, 3904–3919.

[40] A. G. Sykes, *Advances in Inorganic Chemistry. Volume 33*, Academic Press, **1989**.

[41] K. B. Dillon, F. Mathey, J. F. Nixon, *Phosphorus : The Carbon Copy : From Organophosphorus to Phospha-Organic Chemistry*, Wiley, **1998**.

[42] W. W. Schoeller, *J. Chem. Soc. Chem. Commun.* **1985**, 334.

[43] F. Mathey, *Acc. Chem. Res.* **1992**, *25*, 90–96.

[44] F. Mathey, *Angew. Chemie Int. Ed.* **2003**, *42*, 1578–1604.

[45] S. Lacombe, D. Gonbeau, J. L. Cabioch, B. Pellerin, J. M. Denis, G. Pfister-Guillouzo, *J. Am. Chem. Soc.* **1988**, *110*, 6964–6967.

[46] L. Weber, *Eur. J. Inorg. Chem.* **2000**, *2000*, 2425–2441.

[47] E. P. O. Fuchs, H. Heydt, M. Regitz, W. W. Schoeller, T. Busch, *Tetrahedron Lett.* **1989**, *30*, 5111–5114.

[48] M. Cicač-Hudi, J. Bender, S. H. Schlindwein, M. Bispinghoff, M. Nieger, H. Grützmacher, D. Gudat, *Eur. J. Inorg. Chem.* **2016**, *2016*, 649–658.

[49] M. W. Schmidt, P. N. Truong, M. S. Gordon, *J. Am. Chem. Soc.* **1987**, *109*, 5217–5227.

[50] P. v. R. Schleyer, D. Kost, *J. Am. Chem. Soc.* **1988**, *110*, 2105–2109.

[51] T. E. Gier, *J. Am. Chem. Soc.* **1961**, *83*, 1769–1770.

[52] M. J. Hopkinson, H. W. Kroto, J. F. Nixon, N. P. C. Simmons, *J. Chem. Soc., Chem. Commun.* **1976**, 513–515.

[53] W. Rösch, U. Vogelbacher, T. Allspach, M. Regitz, *J. Organomet. Chem.* **1986**, *306*, 39–53.

[54] G. Markl, H. Sejpka, *Tetrahedron Lett.* **1985**, *26*, 5507–5510.

[55] J. C. T. R. B.-S. Laurent, M. A. King, H. W. Kroto, J. F. Nixon, R. J. Suffolk, *J. Chem. Soc., Dalt. Trans.* **1983**, *0*, 755–759.

[56] K. K. Laali, B. Geissler, M. Regitz, J. J. Houser, *J. Org. Chem.* **1995**, *60*, 6362–6367.

[57] F. Mathey, *Phosphorus-Carbon Heterocyclic Chemistry : The Rise of a New Domain*, Elsevier Science Ltd, **2001**.

[58] T. Wettling, J. Schneider, O. Wagner, C. G. Kreiter, M. Regitz, *Angew. Chemie Int. Ed. English* **1989**, *28*, 1013–1014.

[59] T. Wettling, B. Geissler, R. Schneider, S. Barth, P. Binger, M. Regitz, *Angew. Chemie Int. Ed. English* **1992**, *31*, 758–759.

[60] A. Chirila, R. Wolf, J. Chris Slootweg, K. Lammertsma, *Coord. Chem. Rev.* **2014**, *270–271*, 57–74.

[61] F. Tabellion, A. Nachbauer, S. Leininger, C. Peters, F. Preuss, M. Regitz, *Angew. Chemie Int. Ed.* **1998**, *37*, 1233–1235.

[62] R. Appel, W. Paulen, *Tetrahedron Lett.* **1983**, *24*, 2639–2642.

[63] R. Appel, W. Paulen, *Angew. Chemie Int. Ed. English* **1983**, *22*, 785–786.

[64] M. T. Nguyen, A. F. Hegarty, M. A. McGinn, P. Ruelle, *J. Chem. Soc. Perkin Trans. 2* **1985**, 1991–1997.

[65] C. Dimur, F. Pauzat, Y. Ellinger, G. Berthier, *Spectrochim. Acta Part A Mol. Biomol. Spectrosc.* **2001**, *57*, 859–873.

[66] M. Lattelais, F. Pauzat, J. Pilmé, Y. Ellinger, *Phys. Chem. Chem. Phys.* **2008**, *10*, 2089.

[67] X. Cheng, Y. Zhao, L. Li, X. Tao, *J. Mol. Struct. THEOCHEM* **2004**, *682*, 137–

143.

[68] Z. Mielke, L. Andrews, *Chem. Phys. Lett.* **1991**, *181*, 355–360.

[69] S. Thorwirth, V. Lattanzi, M. C. McCarthy, *J. Mol. Spectrosc.* **2015**, *310*, 119–125.

[70] A. Hinz, R. Labbow, C. Rennick, A. Schulz, J. M. Goicoechea, *Angew. Chemie Int. Ed.* **2017**, *56*, 3911–3915.

[71] D. Heift, Z. Benko, H. Grützmacher, *Dalt. Trans.* **2014**, *43*, 831–840.

[72] D. Heift, Z. Benko, H. Grützmacher, *Dalt. Trans.* **2014**, *43*, 5920–5928.

[73] D. Heift, Z. Benḱ, H. Grützmacher, *Chem. - A Eur. J.* **2014**, *20*, 11326–11330.

[74] S. Alidori, D. Heift, G. Santiso-Quinones, Z. Benkå, H. Grützmacher, M. Caporali, L. Gonsalvi, A. Rossin, M. Peruzzini, *Chem. - A Eur. J.* **2012**, *18*, 14805–14811.

[75] A. R. Jupp, M. B. Geeson, J. E. McGrady, J. M. Goicoechea, *Eur. J. Inorg. Chem.* **2016**, *2016*, 639–648.

[76] G. Becker, W. Schwarz, N. Seidler, M. Westerhausen, *Z. Anorg. Allg. Chem.* **1992**, *612*, 72–82.

[77] M. Westerhausen, S. Schneiderbauer, H. Piotrowski, M. Suter, H. Nöth, *J. Organometalic Chem.* **2002**, *643–644*, 189–193.

[78] I. Krummenacher, C. C. Cummins, *Polyhedron* **2012**, *32*, 10–13.

[79] F. F. Puschmann, D. Stein, D. Heift, C. Hendriksen, Z. A. Gal, H. F. Grützmacher, H. Grützmacher, *Angew. Chemie Int. Ed.* **2011**, *50*, 8420–8423.

[80] A. R. Jupp, J. M. Goicoechea, *Angew. Chemie Int. Ed.* **2013**, *52*, 10064–10067.

[81] M. Jost, L. H. Finger, J. Sundermeyer, C. Von Hänisch, *Chem. Commun.* **2016**, *52*, 11646–11648.

[82] R. Suter, Z. Benkő, M. Bispinghoff, H. Grützmacher, *Angew. Chemie* **2017**, *129*, 11378–11383.

[83] D. Heift, Z. Benk, R. Suter, R. Verel, H. Grützmacher, *Chem. Sci.* **2016**, *7*, 6125–6131.

[84] J. M. Goicoechea, H. Grützmacher, *Angew. Chemie Int. Ed.* **2018**, *57*, 16968–16994.

[85] C. Camp, N. Settineri, J. Lefèvre, A. R. Jupp, J. M. Goicoechea, L. Maron, J. Arnold, *Chem. Sci.* **2015**, *6*, 6379–6384.

[86] C. J. Hoerger, F. W. Heinemann, E. Louyriac, L. Maron, H. Grützmacher, K. Meyer, *Organometallics* **2017**, *36*, 4351–4354.

[87] L. N. Grant, B. Pinter, B. C. Manor, H. Grützmacher, D. J. Mindiola, *Angew. Chemie Int. Ed.* **2018**, *57*, 1049–1052.

[88] D. W. N. Wilson, A. Hinz, J. M. Goicoechea, *Angew. Chemie Int. Ed.* **2018**, *57*, 2188–2193.

[89] Y. Mei, J. E. Borger, D. J. Wu, H. Grützmacher, *Dalt. Trans.* **2019**, *48*, 4370–4374.

[90] G. Becker, G. Heckmann, K. Hübler, W. Schwarz, *ZAAC - Z. Anorg. Allg. Chem.* **1995**, *621*, 34–46.

[91] G. Becker, K. Hübler, *ZAAC - J. Inorg. Gen. Chem.* **1994**, *620*, 405–417.

[92] A. R. Jupp, J. M. Goicoechea, *J. Am. Chem. Soc.* **2013**, *135*, 19131–19134.

[93] D. Heift, Z. Benko, H. Grützmacher, A. R. Jupp, J. M. Goicoechea, *Chem. Sci.* **2015**, *6*, 4017–4024.

[94] A. M. Tondreau, Z. Benkő, J. R. Harmer, H. Grützmacher, *Chem. Sci.* **2014**, *5*, 1545–1554.

[95] Z. Li, X. Chen, M. Bergeler, M. Reiher, C.-Y. Y. Su, H. Grützmacher, *Dalt. Trans.* **2015**, *44*, 6431–6438.

[96] T. P. Robinson, M. J. Cowley, D. Scheschkewitz, J. M. Goicoechea, *Angew. Chemie Int. Ed.* **2015**, *54*, 683–686.

[97] L. Liu, D. A. Ruiz, D. Munz, G. Bertrand, *Chem* **2016**, *1*, 147–153.

[98] F. Wöhler, *Ann. der Phys. und Chemie* **1828**, *87*, 253–256.

[99] Royal Institution of Great Britain, **1822**, *Vol XII*, 492.

[100] P. S. Cohen, S. M. Cohen, *J. Chem. Educ.* **1996**, *73*, 883.

[101] G. P. Papp, S. A. Buckler, *Carbamoylphosphines*, American Chemical Society, **1966**.

[102] L. G. Vaughan, R. V. Lindsey, *J. Org. Chem.* **1968**, *33*, 3088–3089.

[103] A. C. Behrle, J. A. R. R. Schmidt, *Organometallics* **2013**, *32*, 1141–1149.

[104] C. A. Tsipis, P. A. Karipidis, *J. Am. Chem. Soc.* **2003**, *125*, 2307–2318.

[105] M. B. Geeson, A. R. Jupp, J. E. McGrady, J. M. Goicoechea, *Chem. Commun.* **2014**, *50*, 12281–12284.

[106] Y. H. Wu, Z. F. Li, W. P. Wang, X. C. Wang, Z. J. Quan, *European J. Org. Chem.* **2017**, *2017*, 5546–5553.

Chapter 2: Reactivity of the PCO^- anion with amino acids

2.1 Introduction

2.1.1 Amino Acids

Amino acids are a group of organic molecules that share the same basic structure consisting of a central carbon atom, often referred to as the α-carbon, that is bound to a hydrogen atom, a primary amine group (-NH_2), a carboxylic acid group (-COOH) and a side chain R. The nature of the R group is what differentiates each one of them.[1–3] Amino acids can be described by the general formula R–CH(NH_2)–COOH (Figure 2.1-a), with the exception of compounds with a cyclic core such as proline.[4,5] Due to its amphoteric character, amino acids are most likely to exist in their zwitterionic form in polar solutions and in physiological pH, where the amino group is protonated and the carboxylic group deprotonated, creating a positive and negative charge respectively, but maintaining an overall neutral charge (Figure 2.1-b).[1,3]

(a) (b)

Figure 2.1: General formula of an amino acid in its neutral (a) and zwitterionic (b) form.

The biological importance of these compounds cannot be overstated, amino acids are essential building blocks for proteins, playing a role in every biological function. Proteins are formed from covalently bonded groups, by a condensation reactions between the amino and carboxylic groups, called an amide or peptide bond (Scheme 2.1).[2,6] Once the polypeptide bonds are formed, the intramolecular interaction between the R side chains gives rise to the three-dimensional structures of

proteins. Multiple proteins can also participate in intermolecular interactions to form larger macrostructures.[1]

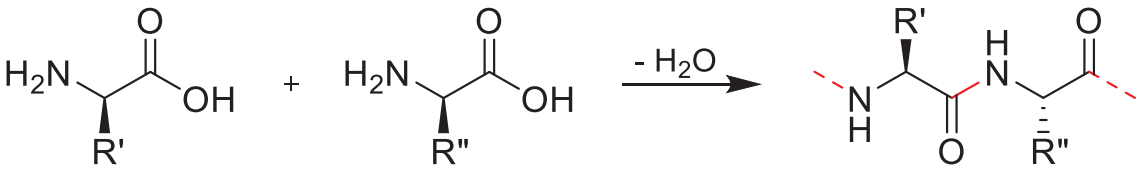

Scheme 2.1: Peptide bond formation.

The entire breadth of these complex macromolecules can be synthesised from a small group of twenty amino acids that are, therefore, referred to as proteinogenic amino acids.[7,8] From this group of twenty amino acids, the human body can only produce eleven that are classified as non-essential, the other nine being classified as essential because they are not produced by the body and have to be obtained from external sources.[1,9] With the exception of glycine, all amino acids have a chiral centre due to the presence of the chiral α-carbon. As such, the four different groups around the α-carbon can occupy two unique spatial arrangements that can form two possible enantiomeric stereoisomers, as they are nonsuperimposable mirror images of each other named L and D. Interestingly, proteinogenic amino acids are exclusively the L enantiomers.[3]

Amino acids can be further subdivided into five classes: 1) non-polar aliphatic, where the R groups are nonpolar and hydrophobic; 2) aromatic, that are relatively nonpolar and hydrophobic; 3) polar and uncharged, making these amino acids more soluble in water as they can form hydrogen bonds; 4) positively charged or basic, in which the R groups have significant positive charge at pH 7.0 due to the presence of a second amine group; and 5) the negatively charged or acidic, where the R group has a negative charge at pH 7.0 due to the presence of a second carboxyl group.[3]

2.1.2 Synthesis of Urea

In 1828, in an attempt to synthesise ammonium cyanate, Wöhler reacted silver cyanate with ammonium chloride. However this reaction afforded urea instead (Scheme 2.2).[10–12] His initial goal was achieved a few years later in collaboration with von Liebig,[13] although the solid state structure of ammonium cyanate was only elucidated over 100 years later in 2003.[14,15] This unexpected result is considered by many as the first time that a naturally occurring compound was prepared from inorganic starting materials, contradicting the theory of vitalism.[16] As such, this transformation represents an important milestone in the history of modern organic chemistry.[17–19]

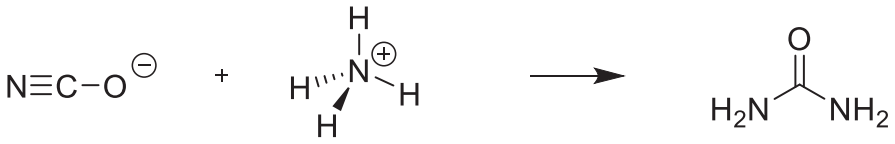

Scheme 2.2: Wöhler's synthesis of urea.

Despite extensive investigations into this transformation in the years following its initial report,[14] it was not possible to achieve consensus for a single mechanism for this reaction. Numerous reports offered evidence to support two possible routes for the transformation of ammonium cyanate to urea, namely the ionic and the molecular mechanisms. In the ionic mechanism, the reaction between $[NH_4]^+$ and $[NCO]^-$ would be the rate determining step, most likely involving a hydrogen-bonded intermediate complex (possibly $H_3N\cdots H\cdots NCO$). Whereas in the molecular mechanism, the reaction between NH_3 and HNCO would be the rate-determining step involving a nucleophilic attack of NH_3 on the carbon atom of HNCO, that can also be seen as the addition of H and NH_2 from NH_3 across the C=N double bond of HNCO (Scheme 2.3).[20,21]

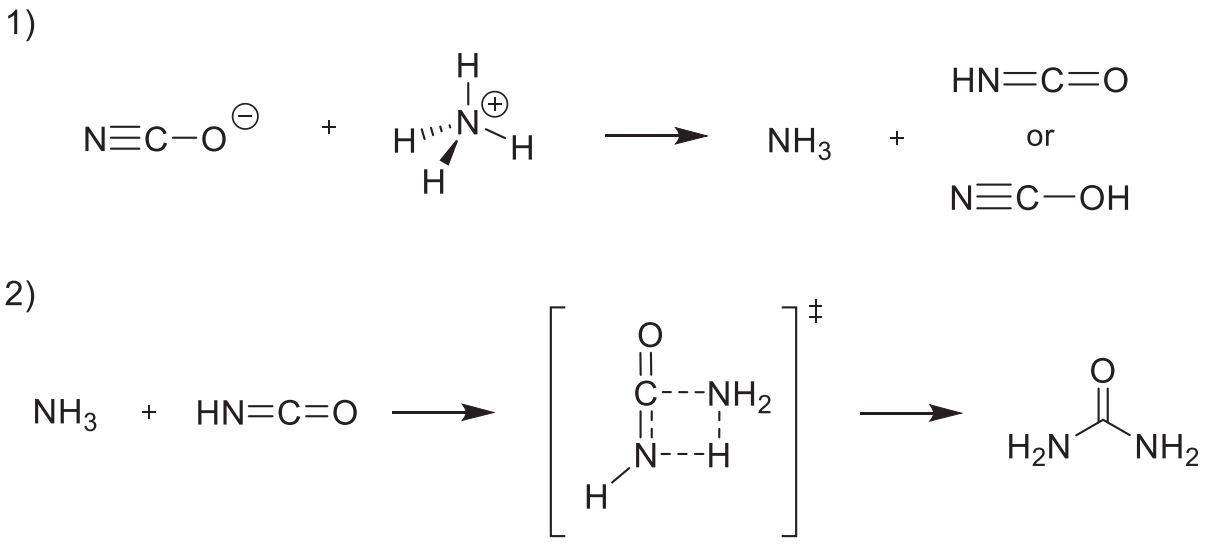

Scheme 2.3: Two steps of the molecular mechanism proposed for the formation of urea.

The mechanistic pathway remained unclear until 2003, when it was investigated via computational methods and it was shown to involve two steps, consistent with the molecular mechanism. The first step of this reaction, the protonation of the cyanate anion, can afford two isomers, isocyanic acid (HN=C=O) and cyanic acid (N≡C–OH), however HNCO was found to be 28.2 kcal/mol more stable than NCOH. Consequently, the former was chosen for the mechanistic investigation of Wöhler's reaction. The second step was shown to involve a nucleophilic attack of the ammonia to the carbon of HNCO followed by a proton rearrangement, going through a four-membered cyclic transition state, shown in Scheme 2.3, to yield the urea molecule. When the modelling of the same reaction was performed in aqueous solution, a water molecule was found to catalyse the addition of NH_3 to the C=N double bond of the H–N=C=O acid. This happens via a planar six-membered ring transition state formed through N–H···O and N···H–O bonds formed between the incoming water molecule and the interacting NH_3 and HNCO molecules.[22]

2.1.3 Phosphinecarboxamide

Recently, the Goicoechea group reported the synthesis of the parent phosphinecarboxamide, $H_2PC(O)NH_2$, a heavier analogue of urea, obtained from the reaction between PCO^- and simple ammonium salts NH_4X (X = BPh_4, Cl) (Scheme 2.4). As the 2-phosphaethynolate anion is a phosphorus-containing analogue of isocyanate, the mechanism of formation of phosphinecarboxamides was postulated to be similar to that of the formation of urea, as depicted in Scheme 2.4.[23] The first step of this reaction would involve the protonation of the PCO^- anion to form H–P=C=O, followed by nucleophilic attack of ammonia on the carbon of the parent phosphaketene forming a four-membered ring transition state which then continues to form the phosphinecarboxamide molecule. This is in good agreement with several theoretical studies that show that the HPCO isomer is more stable than HOCP,[24–27] as well as with infrared, microwave and NMR experimental data verifying the presence of HPCO over HOPC[28–30].

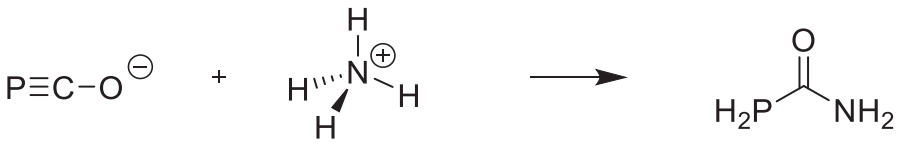

Scheme 2.4: Schematic representation of the synthesis of $H_2PC(O)NH_2$.

2.2 Aims

This chapter will describe the reactivity of the 2-phosphaethynolate anion towards a series of enantiomerically pure amino acids to yield novel anionic *N*-functionalised phosphinecarboxamides. These anionic species can be readily protonated to obtain a series of neutral phosphinecarboxamides containing both chiral and phosphine functionalities. The air stability of these primary phosphines will also be discussed.

2.3 (Phosphanyl)carbonyl-amino acids

Amino acids represent an interesting substrate scope to explore the synthesis of novel phosphinecarboxamides. Given their biological relevance, chiral functionality, and zwitterionic character, we suspected reactions of the PCO^- anion with amino acids would yield interesting enantiopure phosphinecarboxamides. Due to the amphoteric character of amino acids, their α-amino group is more likely to exist in the protonated form. Thus, the addition of a proton source is no longer necessary and, unlike with the preparation of the parent species, no by-products are expected to form in these reactions. The final phosphinecarboxamides obtained with this method, also known as (phosphanyl)carbonyl-amino acids, would be both chiral and anionic.[31] The enantiomerically pure α-amino acids used in this work were L-alanine (Ala), L-serine (Ser), L-cysteine (Cys), L-asparagine (Asn), L-glutamine (Gln), L-proline (Pro) and L-arginine (Arg) (Figure 2.2).

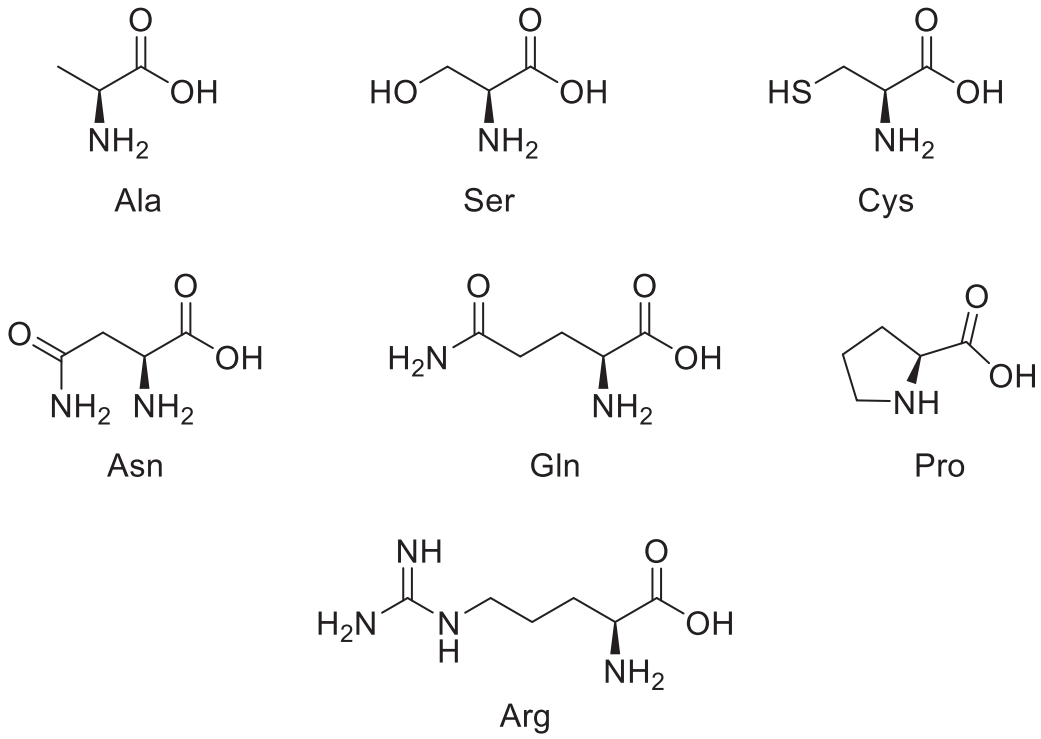

Figure 2.2: L-amino acids used in this work.

2.3.1 Synthesis of anionic (phosphanyl)carbonyl-amino acids

The anionic form of these phosphinecarboxamides was obtained by the reaction of one equivalent of the L-amino acid with one equivalent of [Na(dioxane)$_x$][PCO] using either pyridine or a mixture of pyridine and water when the solubility of the amino acid was too low (Scheme 2.5). Subsequent removal of volatiles under reduced pressure afforded the final products as microcrystalline materials in quantitative yields.[31]

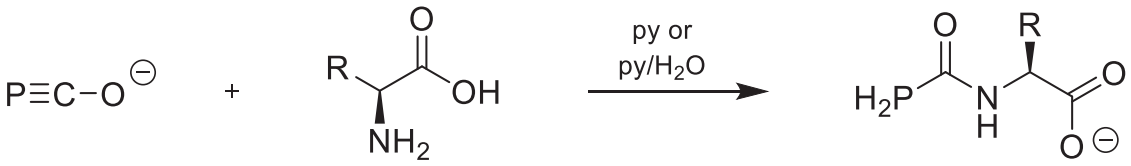

Scheme 2.5: Reaction of PCO^- with L-amino acids to afford the corresponding sodium salts of phosphinecarboxamides (R = CH_3 (**1**), CH_2OH (**2**), CH_2SH (**3**), $CH_2C(O)NH_2$ (**4**), $(CH_2)_2C(O)NH_2$ (**5**).

All of the reactions were monitored by ^1H, ^{13}C and ^{31}P NMR spectroscopy revealing the formation of the expected phosphinecarboxamides. The ^{31}P NMR spectra of **1**–**6** show a characteristic triplet that collapses to a singlet upon proton decoupling. These resonances appear between –130.6 and –131.4 ppm and have $^1J_{P–H}$ coupling constants between 210 and 211 Hz.

Due to the presence of a chiral centre in the backbone of the molecule, all the products (except for the one derived from cysteine) showed two diasterotopic phosphine protons in the ^1H NMR spectra. These resonances appear between 3.83 and 3.93 ppm with the same coupling constants observed in the corresponding ^{31}P NMR spectrum. As expected, $^1H\{^{31}P\}$ NMR investigations revealed that these signals collapsed to singlets upon selective phosphorus decoupling. These resonances are in line with the observations reported for the parent phosphinecarboxamide, $H_2PC(O)NH_2$.[23] Finally, a doublet appears in the $^{13}C\{^1H\}$ NMR spectra of the

compounds between 174.2 and 175.8 ppm and is attributed to the carbonyl carbon coupling to the phosphorus in the PH_2 fragment. Table 1 summarizes the most relevant NMR spectroscopic data for the sodium salts of **1**–**5** collected in d_5-pyridine or d_5-pyridine and a drop of distilled H_2O to aid solubility when necessary. Only ^{1}H and $^{13}C\{^{1}H\}$ resonances for the $PH_2C(O)^-$ functional groups are listed. In this table, AA refers to amino acid and PCA refers to phosphinecarboxamide.

Table 1: Selected NMR spectroscopic data for the sodium salts of **1**–**5** collected in d_5-pyridine. Chemical shifts are given in ppm and coupling constants in Hz.

AA	PCA	^{31}P	^{1}H	$^{1}J_{H-P}$	$^{2}J_{H-H}$	$^{13}C\{^{1}H\}$	$^{1}J_{C-P}$
L-Ala	**1**	–131.0	3.93, 3.90	211	12	175.0	8
L-Ser	**2**	–131.4	3.84, 3.83	210	12	174.2	8
L-Cys	**3**	–130.6	3.86	210	N.A.	174.6	8
L-Asn	**4**	–131.0	3.92, 3.91	211	12	175.8	9
L-Gln	**5**	–131.3	3.86, 3.85	210	12	174.5	8

It is worth mentioning that when PCO^- was allowed to react with L-proline, two triplets were observed in the ^{31}P NMR at –127.6 ppm ($^{1}J_{H-P}$ = 217 Hz) and –131.2 ppm ($^{1}J_{H-P}$ = 213 Hz) which collapsed to singlets upon proton decoupling. The two resonances suggest the presence of two isomers, which is unsurprising considering the presence of a five-membered ring in the backbone of the amino acid that prevents rotation. These integrate in a 1 : 0.35 ratio and correspond to the *cis* and *trans* isomers of the proline phosphinecarboxamide, **6**, respectively (Scheme 2.6).

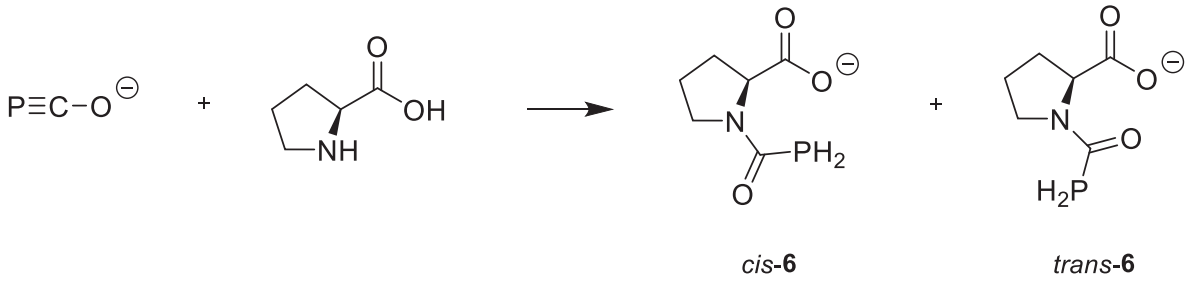

Scheme 2.6: Reaction scheme of PCO^- with L-proline to afford the two isomers of **6**.

Interestingly, when PCO^- was allowed to react with arginine, only a negligible conversion to the corresponding phosphinecarboxamide could be observed. This low reactivity can be attributed to the high pK_a value of its R group of 12.48 compared with the pK_a of its α-amino group of 9.04.[3] This means that an overall uncharged arginine molecule is most likely to exist with a protonated R group, with a local positive charge at the guanidine residue, a deprotonated α-carboxylic group, having a local negative charge and a neutrally charged α-amino group (Figure 2.3). This can also be rationalized by considering that the isoelectric point (pI) of arginine is 10.76, in-between the pK_a values for the α-amino and R groups. Nevertheless, the ^{31}P NMR shows approximately 10% of phosphinecarboxamide formed, implying that some of the amine group bound to the α-carbon is protonated. The low protonation of the α-amino group prevents rapid formation of the phosphinecarboxamide, as the first step of the reaction is proposed to be protonation of the PCO^- anion by the ammonium moiety.

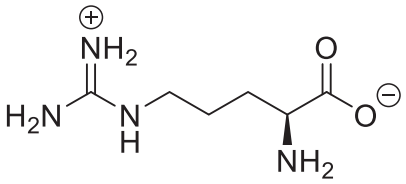

Figure 2.3: The most prevalent charge distribution in the L-arginine amino acid under the reaction conditions employed.

All the phosphinecarboxamide products were fully characterized by NMR spectroscopy and the complete data can be found in the experimental chapter. Herein only the results obtained with alanine and proline will be shown and discussed in significant detail as they are representative examples. Despite several attempts, no crystal structures were obtained for the compounds listed.

2.3.1.1 Characterization of 1

The alanine functionalized anionic (phosphanyl)carbonyl-amino acid was first identified by the presence of a characteristic triplet at –131.0 ppm ($^1J_{P–H}$ = 210.5 Hz) in the ^{31}P NMR spectrum as shown in Figure 2.4, that is within the expected region for this type of species.[23,32] The triplet collapses to a singlet upon proton decoupling (Figure 2.5). These resonances confirm the formation of the -PH_2 fragment in the phosphinecarboxamide moiety.

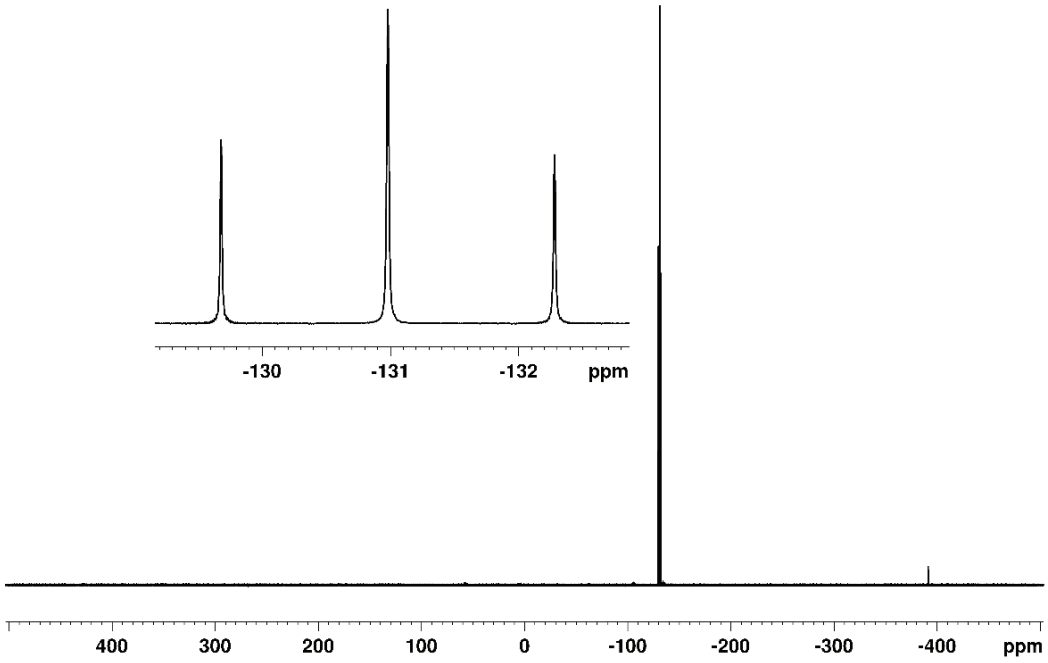

Figure 2.4: ^{31}P NMR spectrum of a d_5-pyridine solution of **1** with a drop of water to aid solubility.

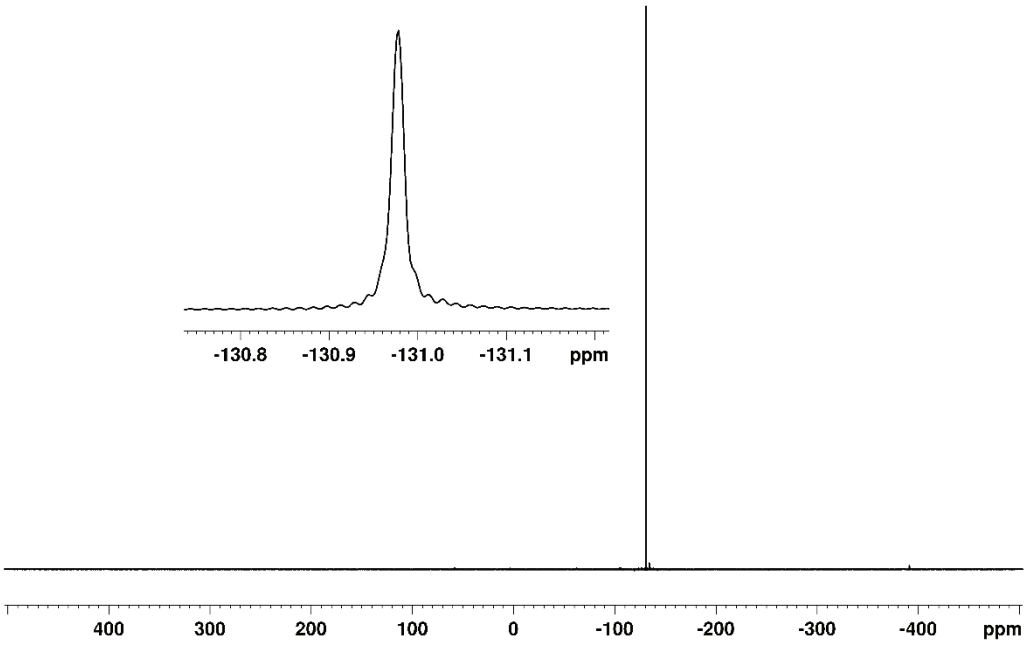

Figure 2.5: $^{31}P\{^{1}H\}$ NMR spectrum of a d_5-pyridine solution of **1** with a drop of water to aid solubility.

In the ^{1}H NMR spectrum of this compound it is important to highlight the two overlapping doublets centred at 3.93 and 3.90, with $^{1}J_{H-P}$ = 211 Hz and $^{2}J_{H-H}$ = 12 Hz that correspond to the two diastereotopic phosphine protons (Figure 2.6). These doublets collapse to singlets upon selective phosphorus decoupling as show in Figure 2.7 therefore confirming the *N*-functionalization of the amino acid with the desired phosphinecarboxamide. The other resonances correspond to the amino acid part of the molecule.

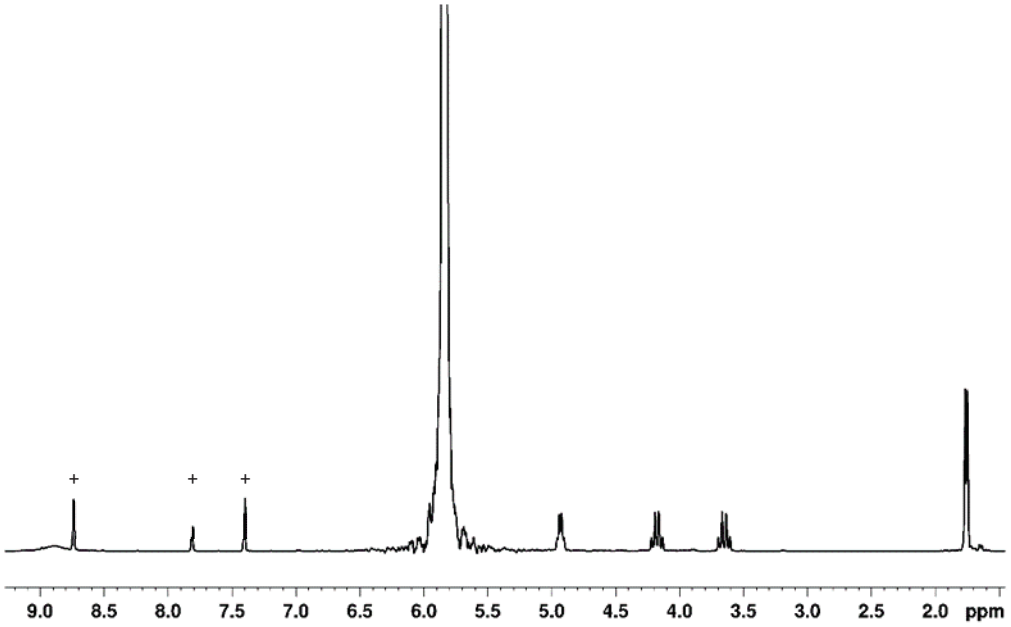

Figure 2.6: ^{1}H NMR spectrum of a d_5-pyridine solution of **1** with a drop of water to aid solubility. Solvent peaks are highlighted with +.

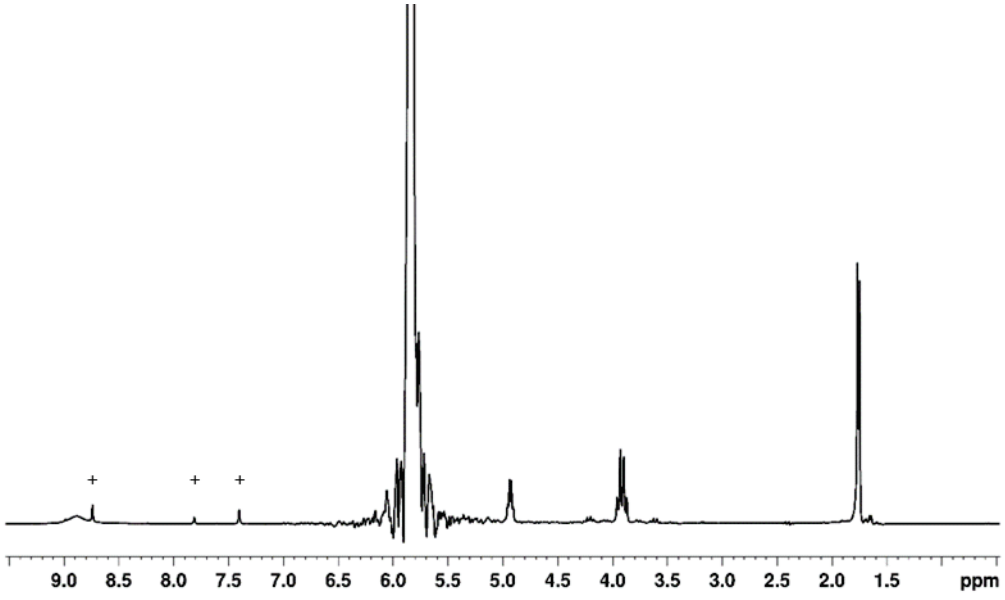

Figure 2.7: $^{1}H\{^{31}P\}$ NMR spectrum of a d_5-pyridine solution of **1** with a drop of water to aid solubility. Solvent peaks are highlighted with +.

In the $^{13}C\{^{1}H\}$ NMR spectrum of **1**, a doublet at 175.0 ppm ($^{1}J_{C-P}$ = 8 Hz) arises from the coupling between the phosphorus and the carbon of the carbonyl also corroborating the formation of the phosphinecarboxamide functionality (Figure 2.8).

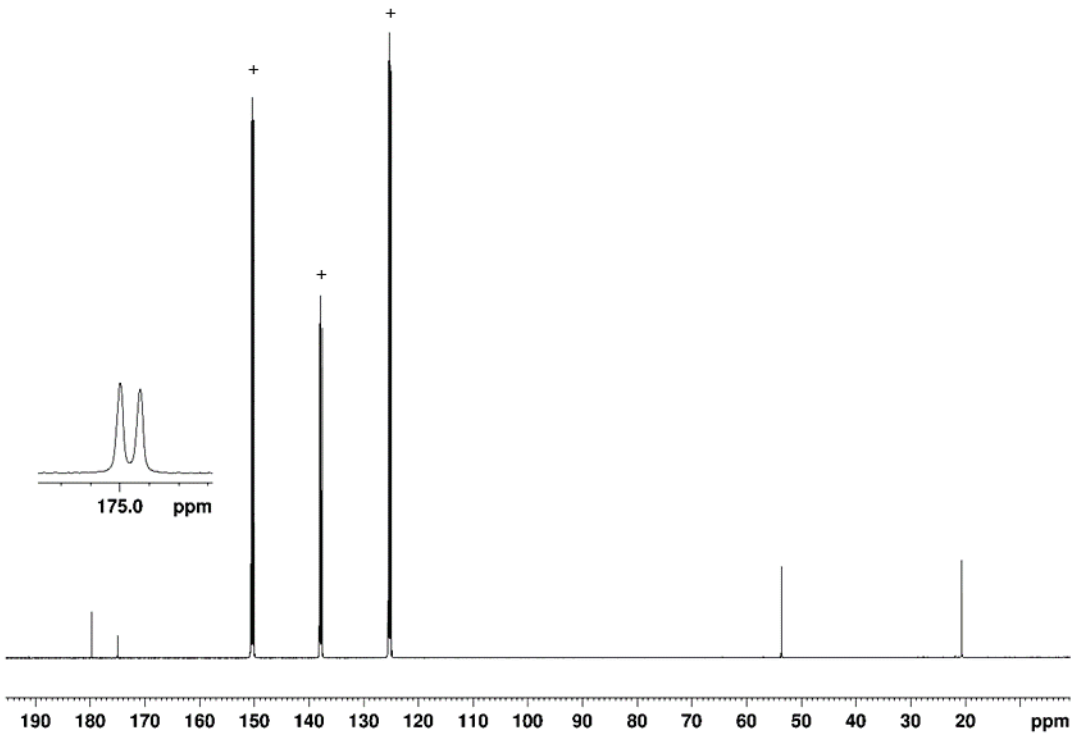

Figure 2.8: $^{13}C\{^{1}H\}$ NMR spectrum of a d_5-pyridine solution of **1** with a drop of water to aid solubility. Solvent peaks are highlighted with +.

Crystals suitable for single crystal X-ray diffraction were obtained by slow diffusion of hexane into a water/pyridine solution of the product (Figure 2.9). In this case, [K(18-crown-6)][PCO] was employed, affording [K(18-crown-6)][**1**]. The crystal structure contains four molecules in the asymmetric unit and, consequently, all the bond metric data will be discussed as average values. The resulting anionic phosphinecarboxamide is coordinated to the potassium through both oxygen centres of the carboxylate group. The P–C bond length is 1.862(av) Å, which is indicative of single bond, while the C–N bond (1.336(av) Å) has multiple bond character.

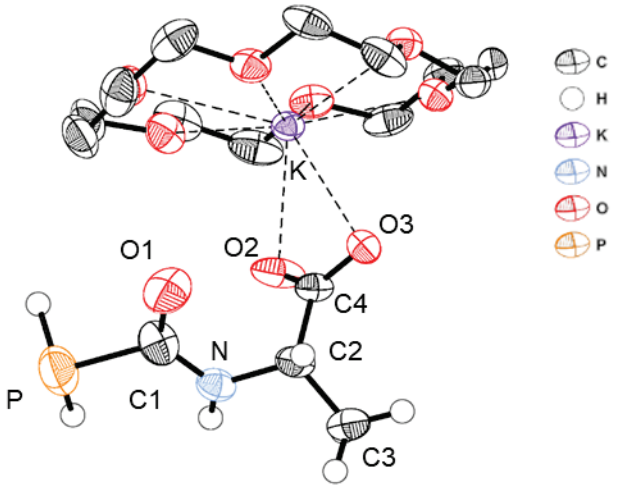

Figure 2.9: Crystal structure of [K(18-crown-6)][**1**]. P–C and C–N bond lengths are 1.862(av) Å and 1.336(av) Å respectively.

2.3.1.2 Characterization of 6

Due to the presence of a five-membered ring in the backbone of the amino acid L-proline, two isomers of the desired anionic phosphinecarboxamide product are possible (Figure 2.10). Because of that, the NMR spectra of **6** is more complicated when compared to the other linear amino acids used, hence it is worth discussing the NMR data of the isomers in greater detail.

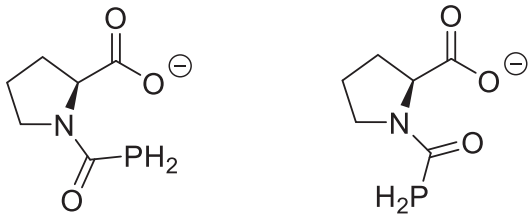

cis-**6** *trans*-**6**

Figure 2.10: *cis* and *trans* isomers of **6**.

The ^{31}P NMR spectrum of **6** shows two sets of triplets at –127.6 ($^{1}J_{H–P}$ = 217 Hz) and –131.2 ($^{1}J_{H–P}$ = 213 Hz) that integrate with a 1 : 0.35 ratio and correspond to the phosphinecarboxamide product formed in its *cis* and *trans* forms respectively (Figure

2.11). As expected, the triplets collapse to singlets upon proton decoupling (Figure 2.12) and correspond to the *cis* and *trans* isomers.

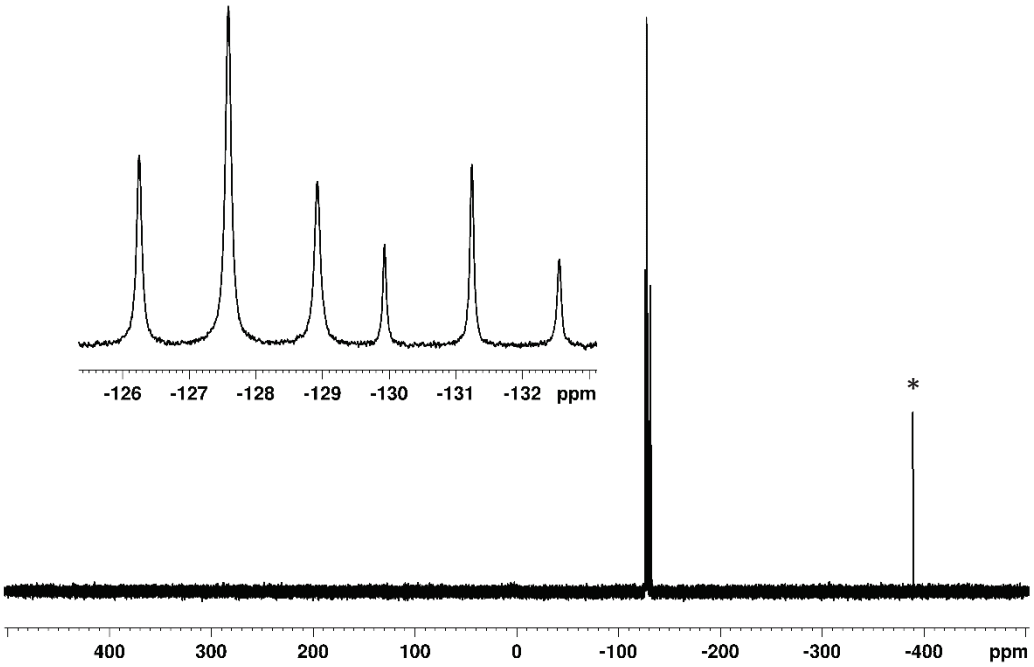

Figure 2.11: ^{31}P NMR spectrum of a d_5-pyridine solution of **6**. The resonance marked with * corresponds to unreacted PCO^-.

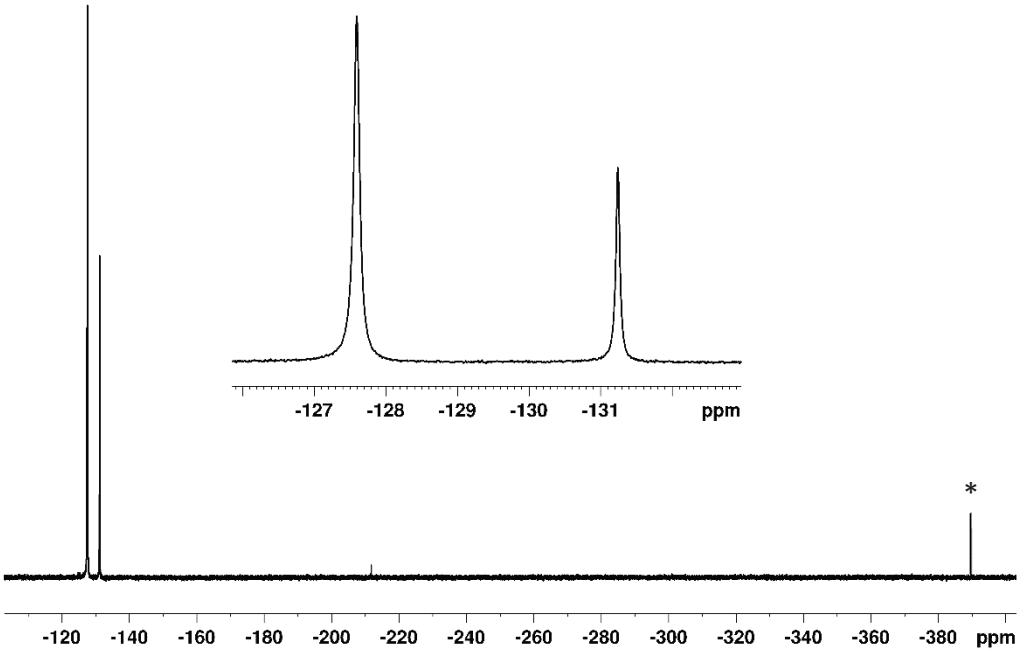

Figure 2.12: $^{31}P\{^1H\}$ NMR spectrum of a d_5-pyridine solution of **6**. The resonance marked with * corresponds to unreacted PCO^-.

The resonances in the ^{1}H NMR spectrum of this compound are broad and overlapping as shown in Figure 2.13. Correct assignment of peaks was made with the assistance of $^{1}H–^{13}C$ HMBC and $^{1}H–^{31}P$ HMBC 2D NMR experiments. The doublets corresponding to the formation of the *trans* and *cis* isomers, respectively, can be readily identified at 3.97 ppm ($^{1}J_{H–P}$ = 213 Hz) and 3.85 ppm ($^{1}J_{H–P}$ = 217 Hz) as well as the corresponding singlets in the ^{1}H {^{31}P} NMR spectrum after selective phosphorus decoupling (Figure 2.14).

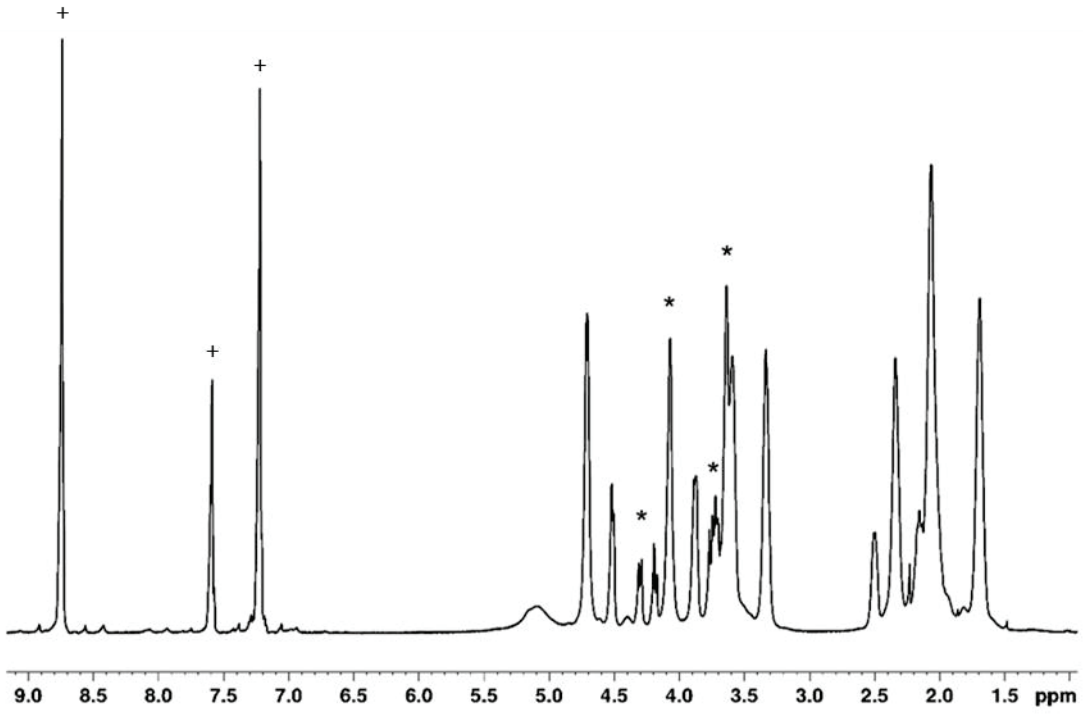

Figure 2.13: ^{1}H NMR spectrum of a d_5-pyridine solution of **6**. The resonances corresponding to the PH_2 protons are highlighted with * and solvent peaks with +.

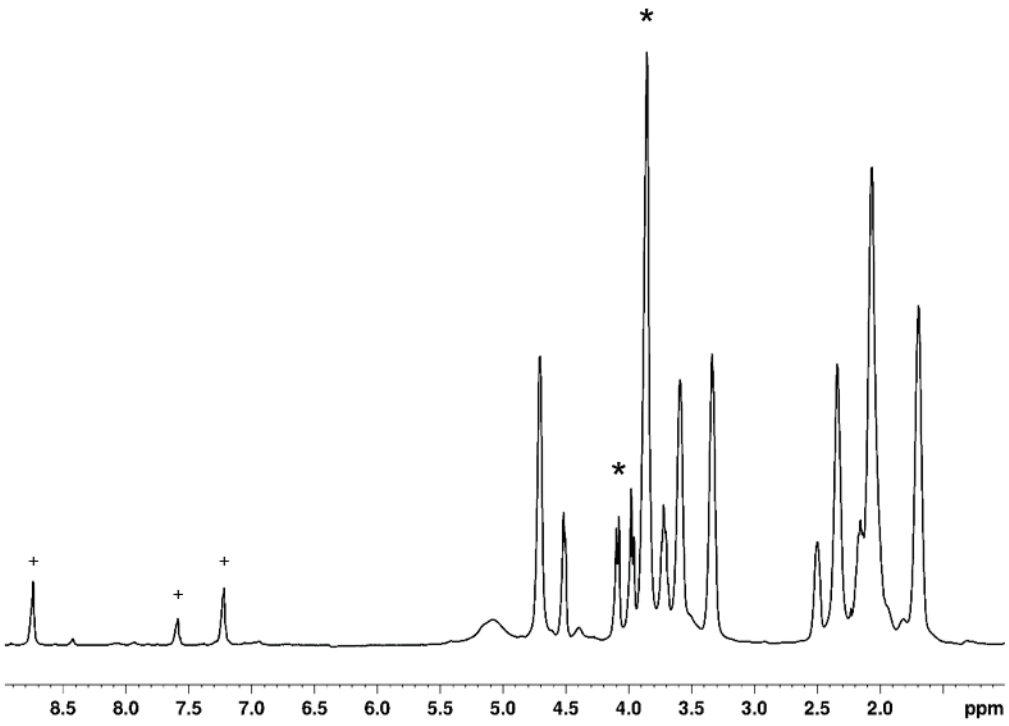

Figure 2.14: $^{1}H\{^{31}P\}$ NMR spectrum of a d_5-pyridine solution of **6**. The resonances corresponding to the PH_2 protons are highlighted with * and solvent peaks with +.

Consistent with the formation of two isomers, the $^{13}C\{^{1}H\}$ NMR spectrum of **6** also displays two resonances corresponding to the two isomers. Once again, the use of $^{1}H–^{13}C$ HSQC 2D NMR experiments allowed the correct assignment of the resonances, from which the most relevant are the two doublets at 174.2 ppm ($^{1}J_{C–P}$ = 7 Hz) and 173.6 ppm ($^{1}J_{C–P}$ = 6 Hz) that correspond to the coupling of the carbonyl carbon to the phosphorus of the phosphinecarboxamide moiety of the *cis* and *trans* isomers, respectively (Figure 2.15).

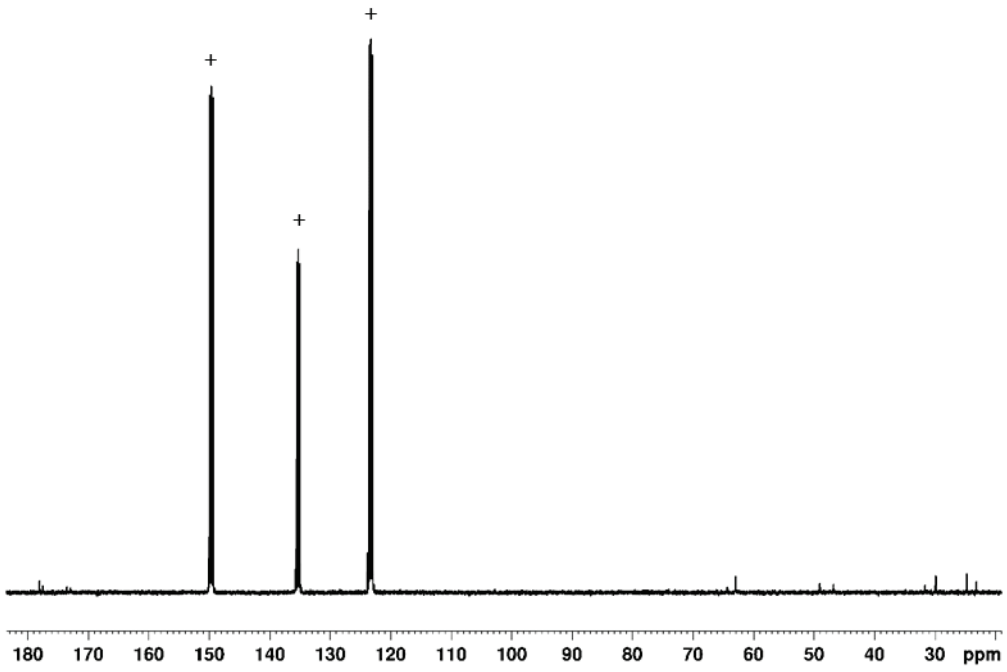

Figure 2.15: $^{13}C\{^{1}H\}$ NMR spectrum of a d_5-pyridine solution of **6**. Solvent peaks are highlighted with +.

2.3.2 Synthesis of neutral (phosphanyl)carbonyl-amino acids

The anionic species described previously can be readily protonated to yield the corresponding neutral (phosphanyl)carbonyl-amino acids (**7**–**12**) as shown in Scheme 2.7.

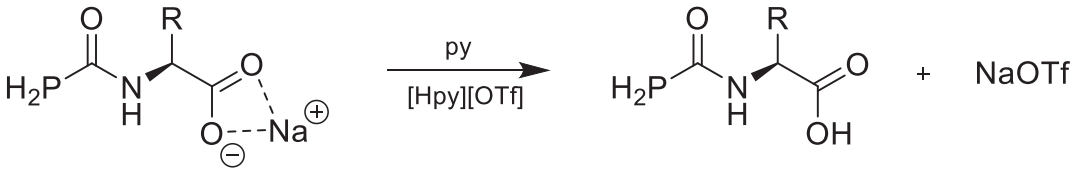

Scheme 2.7: Reaction of the sodium salts of (phosphanyl)carbonyl-amino acids with pyridinium trifluoromethanesulfonate ([HPy][OTf]) to afford the corresponding neutral compounds (R = CH_2 (**7**), CH_2OH (**8**), CH_2SH (**9**), $CH_2C(O)NH_2$ (**10**), $(CH_2)_2C(O)NH_2$ (**11**).

Upon addition of an acid, only a very small shift is observed in both ^{31}P and $^{31}P\{^{1}H\}$ NMR spectra as expected. The ^{1}H and $^{13}C\{^{1}H\}$ NMR spectra however, do present a significant change. The ^{1}H NMR of all neutral compounds exhibit a new

broad resonance between 12.26 and 16.27 ppm that correspond to the carboxylic proton (Figure 2.16). In the $^{13}C\{^{1}H\}$ NMR spectrum, the carboxyl doublet, is upfield shifted by approximately 3 ppm compared to the anionic species. The solubility of the neutral compounds obtained in non-aqueous media is increased significantly. While addition of water was always necessary for compounds **1**–**6** due to limited solubility, **7**–**12** are completely soluble in pyridine. Table 2 highlights these more relevant resonances that indicate protonation of the initial anionic compounds. In this table, AA is used as the abbreviation for amino acid and PCA is used as the abbreviation for phosphinecarboxamide.

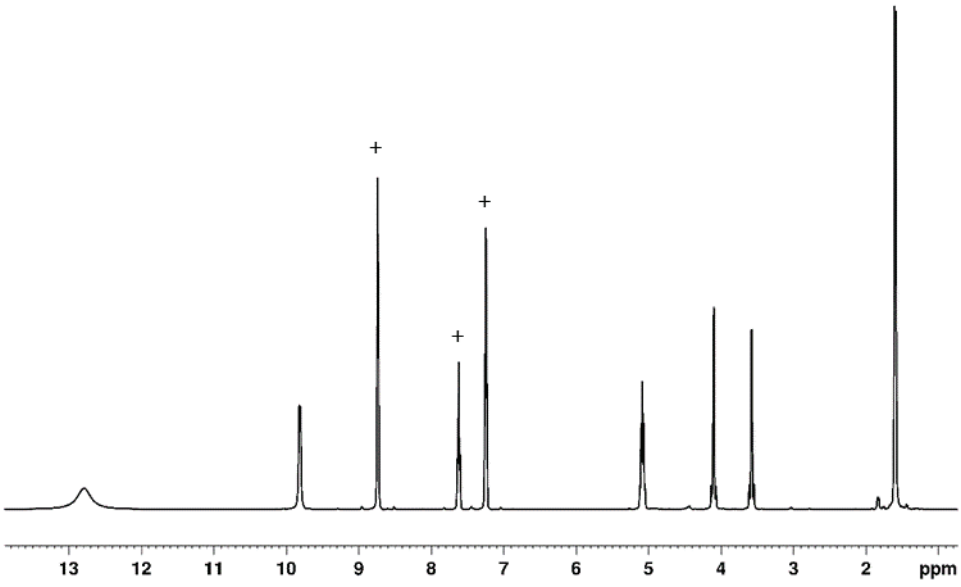

Figure 2.16: ^{1}H NMR spectrum of a d_5-pyridine solution of **7**. Solvent peaks are highlighted with +.

Table 2: NMR spectroscopic data for carboxyl functionalities of **1**–**6** and **7**–**12**. Chemical shifts given in ppm. NMR spectra collected in d_5-pyridine (or d_5-pyridine and a drop of water).

AA	Anionic PCA	^{13}C (COO^-)	Protonated PCA	$^{13}C\{^1H\}$ (COOH)	^1H (COOH)
L-Ala	**1**	179.7	**7**	176.5	12.79
L-Ser	**2**	177.2	**8**	174.3	12.26
L-Cys	**3**	176.8	**9**	174.0	16.03
L-Asn	**4**	177.7	**10**	175.1	16.27
L-Gln	**5**	178.6	**11**	175.9	12.42
L-Pro	**6**	178.7 (*cis*) 178.2 (*trans*)	**12**	175.6 (*cis*) 175.3 (*trans*)	16.15

2.4 Air Stability

To test the air stability of these compounds, the anionic phosphinecarboxamide functionalized with alanine, **1**, and the corresponding protonated species, **7**, were dissolved in d_5-pyridine (a drop of water was used in the first case to aid solubility) and the NMR tubes were opened to air overnight every day for a period of two weeks. The solutions were monitored by ^1H and $^{31}P\{^1H\}$ NMR.

Compound **1** was found to be a rather stable compound under atmospheric conditions where the ^1H NMR spectrum reveals only approximately 9% decomposition to free alanine after a period of two weeks (Figure 2.17). Furthermore, the $^{31}P\{^1H\}$ NMR spectrum revealed approximately 3% of PH_3 (resonance at –240.2 ppm) and no evidence of phosphine oxide (Figure 2.18).

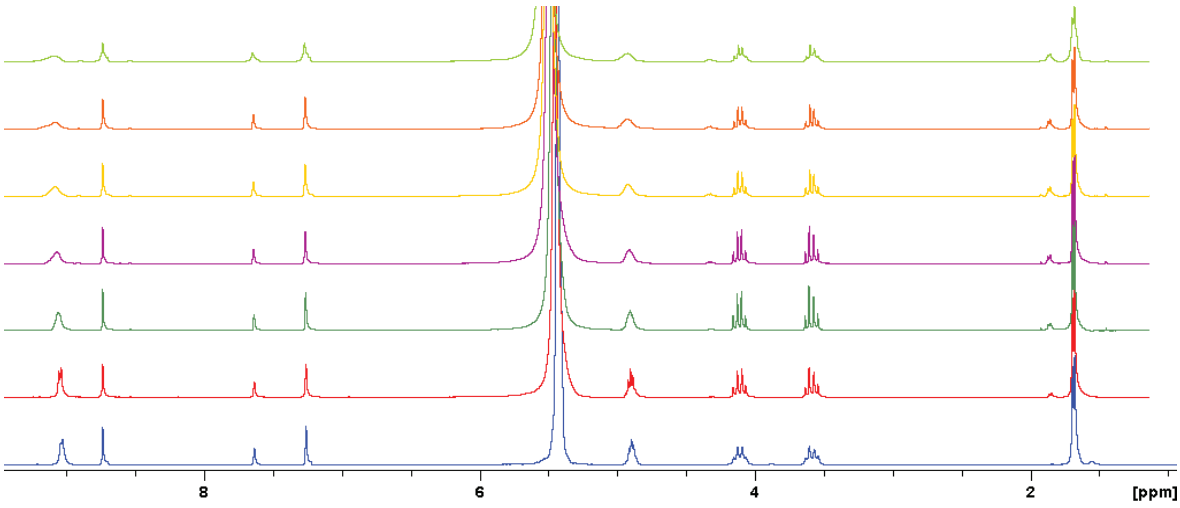

Figure 2.17: ^{1}H NMR spectra of a d_5-pyridine solution of **1** with a drop of H_2O that was exposed to air. From bottom to top: day 1, 3, 5, 8, 10, 12 and 15.

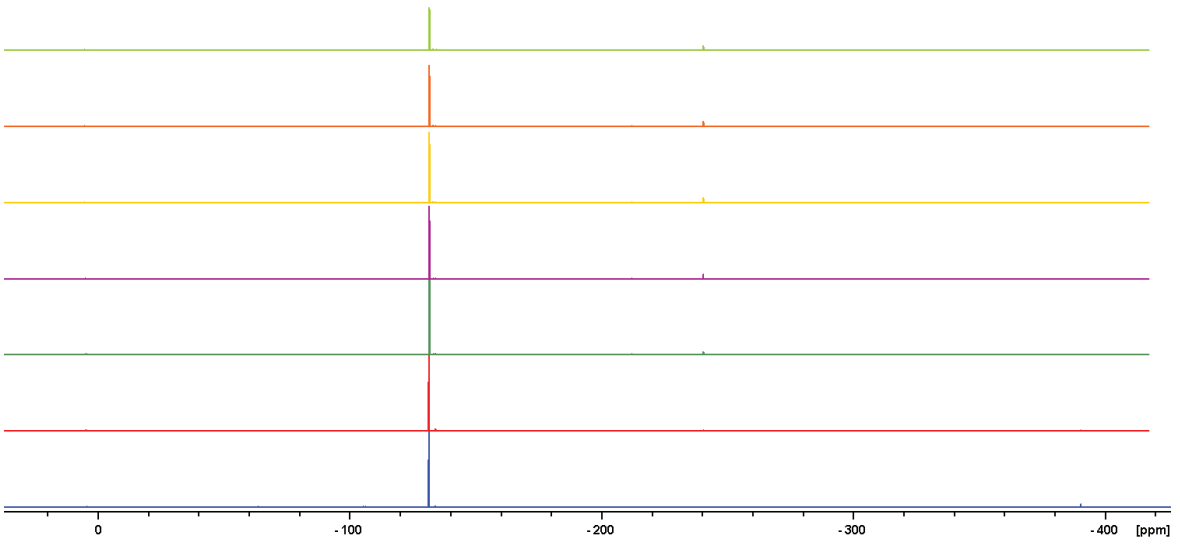

Figure 2.18: $^{31}P\{^{1}H\}$ NMR spectra of a d_5-pyridine solution of **1** with a drop of H_2O that was exposed to air. From bottom to top: day 1, 3, 5, 8, 10, 12 and 15.

By contrast, compound **7** showed significant decomposition after three days. After a fifteen day period there was no evidence of oxidation of the (phosphanyl)carbonyl-amino acid, although the ^{1}H NMR spectra that revealed about 40% of **7** had decomposed to L-alanine (Figure 2.19). The decomposition of these

phosphinecarboxamides is believed to involve loss of HPCO, a compound that is known to be unstable at room temperature.[30] This decomposition pathway is further corroborated by the of formation of precipitate in the NMR tube over time, consistent with the decomposition of HPCO into insoluble phosphorus containing species. This is also supported by the diminishing intensity of the phosphinecarboxamide peak shown in the $^{31}P\{^{1}H\}$ NMR (Figure 2.20).

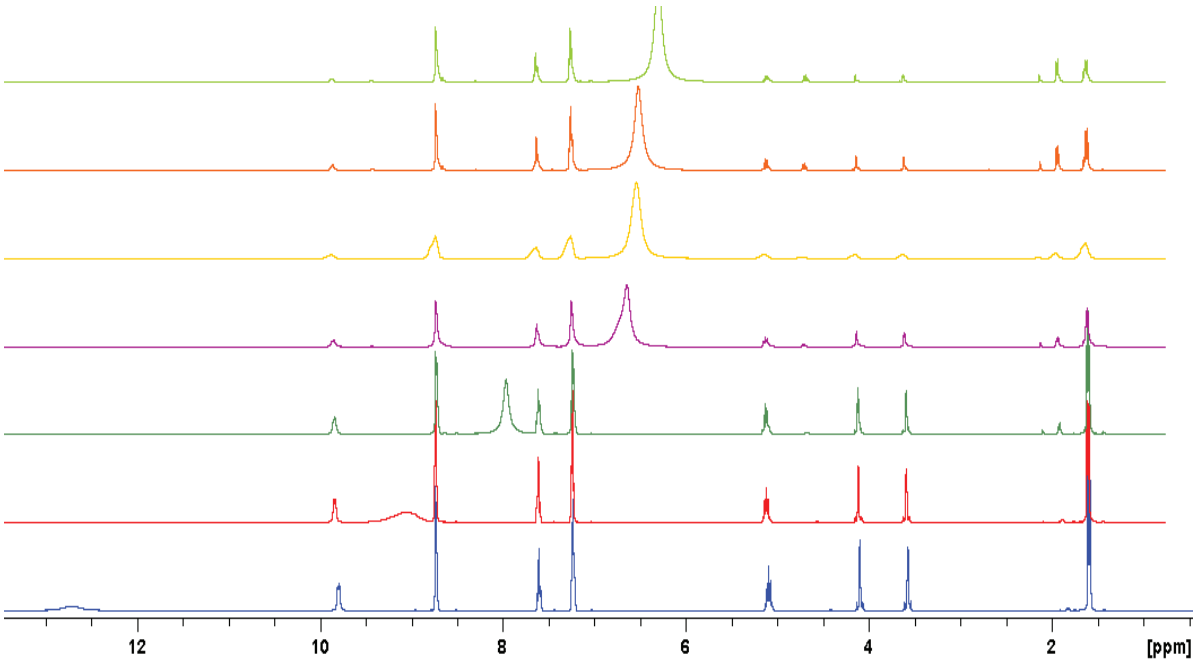

Figure 2.19: ^{1}H NMR spectra of a d_5-pyridine solution of **7** that was exposed to air. From bottom to top: day 1, 3, 5, 8, 10, 12 and 15.

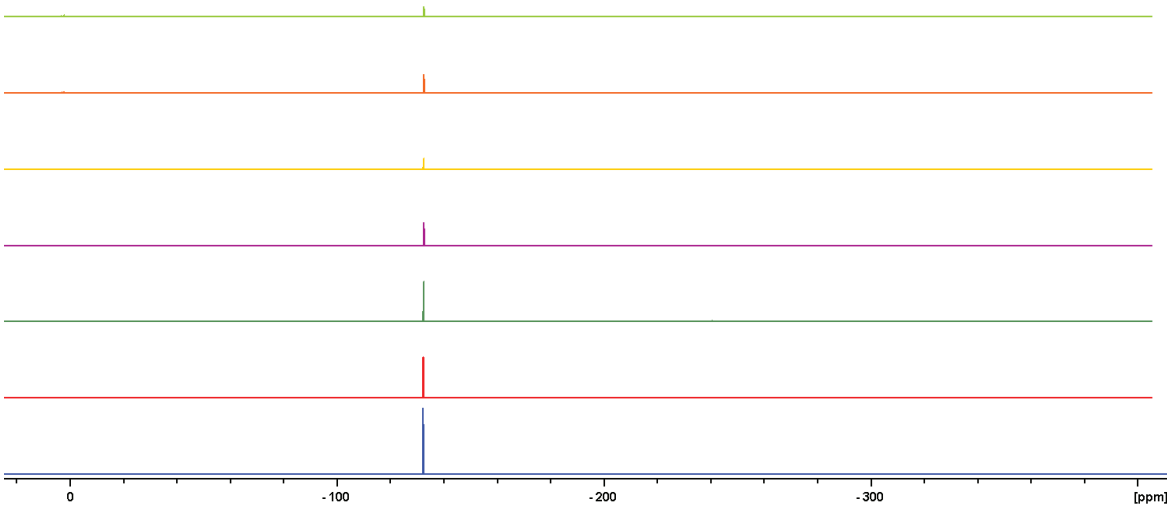

Figure 2.20: $^{31}P\{^{1}H\}$ NMR spectra of a d_5-pyridine solution of **7** that was exposed to air. From bottom to top: day 1, 3, 5, 8, 10, 12 and 15.

As mentioned previously, the air stability of primary phosphines is usually achieved either via stabilization by bulky substituents or by delocalization of the lone pair of the phosphorus atom into one or several substituents.[33] In our case however, the phosphine moiety is not particularly sterically encumbered and the lone pair is most likely isolated from the rest of the molecule. It has been shown for the parent phosphinecarboxamide that the HOMO has significant lone-pair character on the phosphorus atom (44.38%) and its crystal structure displays a pyramidalized geometry at the phosphorus with a planar carboxamide moiety, which is also consistent with delocalization of the π electron density between of the amide lone pair into the carbonyl group.[23] Therefore, even though delocalization of the phosphine lone-pair is not a major contributor to the overall stability of the molecule, it can still be invoked to partially explain the air and moisture stability of phosphinecarboxamides, although the main cause for the stability of (phosphanyl)carbonyl-amino acids still remains unclear.

2.5 H/D exchange

It was found that in deuterated solvents such as D_2O, the sodium salts of (phosphanyl)carbonyl-amino acids undergo proton exchange of the phosphine and amide protons. In the ^{31}P NMR spectrum a 1 : 2 : 3 : 2 : 1 quintet is observed in place of the diagnostic phosphinecarboxamide triplet. Therefore, NMR spectroscopy data for these compounds is reported in d_5-pyridine despite issues associated with their solubility.

Reactivity of **1** in D_2O is discussed below as a representative example. When compound **1** was allowed to dissolve in D_2O, a quintet was observed at –134.1 ppm in the ^{31}P NMR spectrum (Figure 2.21) with a coupling constant of $^1J_{D–P}$ of 33 Hz. This value is expected based on the different gyromagnetic ratios of ^2H and ^1H ($\gamma_H/\gamma_D \approx 6.5$) and is consistent with deuterium exchange in both amine and phosphine functionalities (Scheme 2.8). It is also possible to see two small triplets as minor products. The signal at –132.5 ppm, with a 1 : 1 : 1 intensity, corresponds to partial exchange of the phosphine group, where only one of the protons has been replaced by a deuterium. The 1 : 2 : 1 resonance at –137.9 ppm corresponds to the product of H/D exchange at the nitrogen atom instead of phosphorus (Figure 2.21).

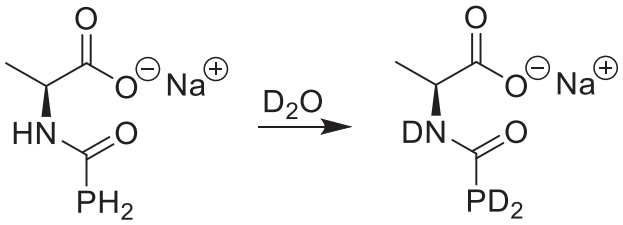

Scheme 2.8: Representation of the d_3-isotopologue H/D exchange product.

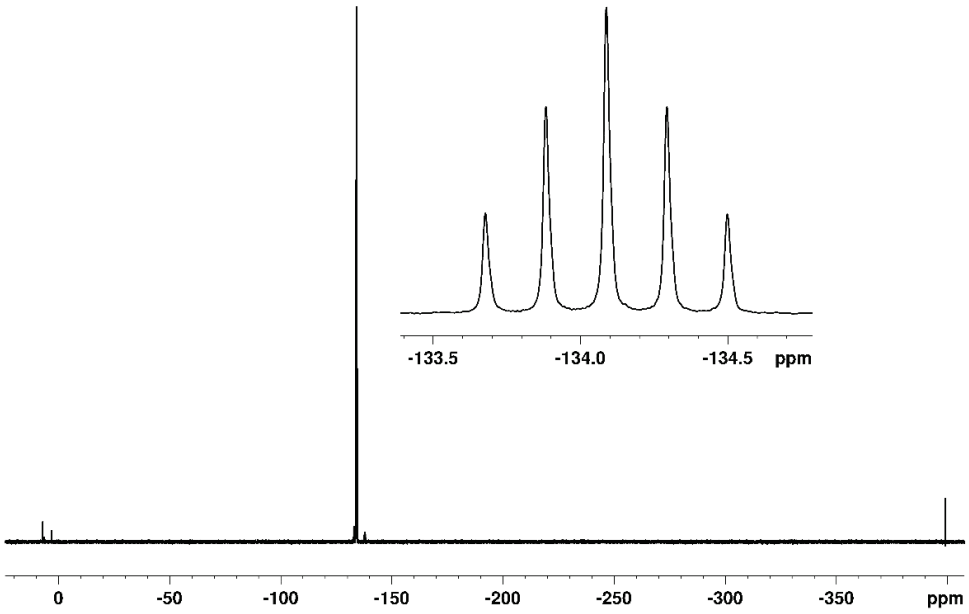

Figure 2.21: ^{31}P NMR spectrum of a D_2O solution of **1**.

The formation of the d_3-isotopologue is also confirmed by the loss of the resonances arising from the PH_2 and C(O)NH functionalities in the ^1H NMR spectra (Figure 2.22).

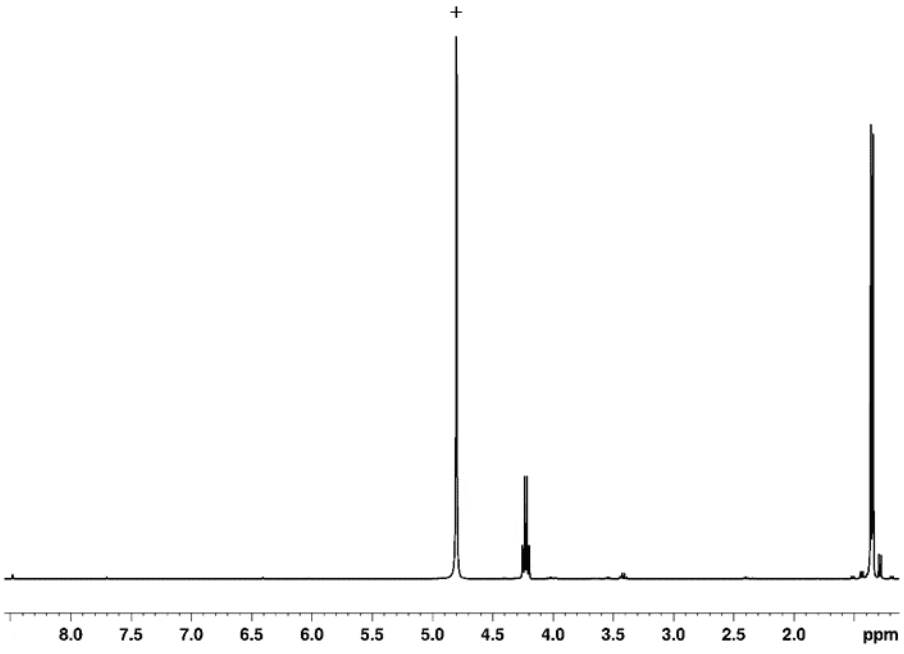

Figure 2.22: ^1H NMR spectrum of a D_2O solution of **1**. Solvent peak is highlighted with +.

2.6 Conclusions

The compounds described in this chapter are a novel group of amino acids bearing an *N*-carbamoyl phosphine residue. The transformations used to access such systems can be employed for the *N*-labelling of amino acids with an NMR active functional group that can potentially be used to incorporate phosphorus in peptides. Compared to the synthesis of the parent phosphinecarboxamide, the synthesis of the (phosphanyl)carbonyl-amino acid derivatives could be readily accessed as no side products were formed. Compounds **1**–**6** were found to display unusual air and moisture stability for primary phosphines when monitored over a period of two weeks. Furthermore, these compounds were shown to undergo deuterium exchange when in the presence of protic solvents.

2.7 References

[1] J. Clayden, N. Greeves, S. Warren, *Organic Chemistry*, Oxford University Press, **2001**.

[2] L. Berg, Jeremy M.; Tymoczko, John L.;Stryer, *Biochemistry*, New York: W H Freeman, **2002**.

[3] D. L. Nelson, M. M. Cox, *Lehninger Principles of Biochemistry*, Freeman, W. H. & Company, **2008**.

[4] H. B. Vickery, C. L. A. Schmidt, *Chem. Rev.* **1931**, *9*, 169–318.

[5] H. Bradford Vickery, *Adv. Protein Chem.* **1972**, *26*, 81–171.

[6] I.-I. J. C. on B. N. (JCBN), *Eur. J. Biochem.* **1984**, *138*, 9–37.

[7] D. P. Glavin, J. E. Elsila, A. S. Burton, M. P. Callahan, J. P. Dworkin, R. W. Hilts, C. D. K. Herd, *Meteorit. Planet. Sci.* **2012**, *47*, 1347–1364.

[8] J. M. Rogers, H. Suga, *Org. Biomol. Chem.* **2015**, *13*, 9353–9363.

[9] E. Volpi, H. Kobayashi, M. Sheffield-Moore, B. Mittendorfer, R. R. Wolfe, *Am. J. Clin. Nutr.* **2003**, *78*, 250–258.

[10] F. Wöhler, *Ann. Phys.* **1828**, *87*, 253–256.

[11] Royal Institution of Great Britain, **1822**, *Vol XII*, 492.

[12] P. S. Cohen, S. M. Cohen, *J. Chem. Educ.* **1996**, *73*, 883–886.

[13] J. Liebig, F. Wöhler, *Ann. Phys.* **1830**, *96*, 369–400.

[14] J. D. Dunitz, K. D. M. Harris, R. L. Johnston, B. M. Kariuki, E. J. MacLean, K. Psallidas, W. B. Schweizer, R. R. Tykwinski, *J. Am. Chem. Soc.* **1998**, *120*,

13274–13275.

[15] E. J. MacLean, K. D. M. Harris, B. M. Kariuki, S. J. Kitchin, R. R. Tykwinski, I. P. Swainson, J. D. Dunitz, *J. Am. Chem. Soc.* **2003**, *125*, 14449–14451.

[16] C. Zabel, *The History and Theory of Risk*, London, Macmillan, **2018**.

[17] P. J. Ramberg, *Ambix* **2000**, *47*, 170–195.

[18] T. O. Lipman, *J. Chem. Educ.* **1964**, *41*, 452–458.

[19] D. McKie, *Nature* **1944**, *153*, 608–610.

[20] J. Shorter, *Chem. Soc. Rev.* **1978**, *7*, 1–14.

[21] M. J. Ten Hoor, *J. Chem. Educ.* **1996**, *73*, 42–45.

[22] C. A. Tsipis, P. A. Karipidis, *J. Am. Chem. Soc.* **2003**, *125*, 2307–2318.

[23] A. R. Jupp, J. M. Goicoechea, *J. Am. Chem. Soc.* **2013**, *135*, 19131–19134.

[24] M. T. Nguyen, A. F. Hegarty, M. A. McGinn, P. Ruelle, *J. Chem. Soc. Perkin Trans. 2* **1985**, 1991–1997.

[25] C. Dimur, F. Pauzat, Y. Ellinger, G. Berthier, *Spectrochim. Acta - Part A Mol. Biomol. Spectrosc.* **2001**, *57*, 859–873.

[26] M. Lattelais, F. Pauzat, J. Pilmé, Y. Ellinger, *Phys. Chem. Chem. Phys.* **2008**, *10*, 2089–2097.

[27] X. Cheng, Y. Zhao, L. Li, X. Tao, *J. Mol. Struct. THEOCHEM* **2004**, *682*, 137–143.

[28] Z. Mielke, L. Andrews, *Chem. Phys. Lett.* **1991**, *181*, 355–360.

[29] S. Thorwirth, V. Lattanzi, M. C. McCarthy, *J. Mol. Spectrosc.* **2015**, *310*, 119–

125.

[30] A. Hinz, R. Labbow, C. Rennick, A. Schulz, J. M. Goicoechea, *Angew. Chemie Int. Ed.* **2017**, *56*, 3911–3915.

[31] E. N. Faria, A. R. Jupp, J. M. Goicoechea, *Chem. Commun.* **2017**, *53*, 7092–7095.

[32] A. R. Jupp, G. Trott, É. Payen De La Garanderie, J. D. G. Holl, D. Carmichael, J. M. Goicoechea, *Chem. - A Eur. J.* **2015**, *21*, 8015–8018.

[33] B. Stewart, A. Harriman, L. J. Higham, *Organometallics* **2011**, *30*, 5338–5343.

3. Reactivity of the PCO^- anion with bidentate amines

3.1 Introduction

3.1.1 Phosphine Ligands

Phosphine ligands (PR_3) have been extensively explored as supporting ligands in organometallic chemistry. It has been shown that their steric and electronic properties can be exploited to tailor reactivity at the metal centre by varying the R groups[1,2]. Moreover, the presence of an NMR active nucleus (^{31}P) allows access to a versatile characterisation technique (NMR spectroscopy) to aid in the investigation of the bonding and structure of coordination compounds.[3]

These ligands can act both as σ-donors, via the lone pair at the phosphorus (Figure 3.1-a), and as π-acceptors, due the availability of empty antibonding orbitals of suitable symmetry in the ligand from the P–R bonds (Figure 3.1-b). It was initially thought that the ability to act as a π-acceptor was due to the presence of 3d vacant orbitals present in second row elements.[4,5] However it was later shown that the phosphine LUMOs are a doubly degenerate pair of orbitals of π symmetry that possess P–R σ* character. These form hybridized orbitals with π* symmetry that will then interact with the appropriate orbitals on the metal as shown in Figure 3.1-b.[1,5–8]

Figure 3.1: Schematic representation of the molecular orbitals involved in metal–phosphine bonding interactions: (a) R_3P to M σ-donation and (b) M to R_3P π back-donation.

3.1.2 The Tolman Electronic Parameter

Phosphine-metal interactions have been the subject of much interest as compounds featuring these interactions find applications in various areas, most notably catalysis. The properties of a complex can be altered and controlled via the phosphine ligands by carefully choosing its substituents. For that reason, it is fundamental to understand the phosphine-metal interactions. Such interactions are usually rationalized in terms of electronic and steric effects. Tolman proposed quantitative measures for such electronic[9] and steric[10] effects. In order to do so, he introduced the concepts of electronic parameter (ν), based on carbonyl stretching frequencies in $[Ni(CO)_3L]$ complexes and the cone angle (θ) as a method of classifying phosphine ligands.

The electronic parameter ν was defined using infrared spectroscopy as the A_1 carbonyl stretching mode of $[Ni(CO)_3L]$ in CH_2Cl_2, where L represents a coordinated phosphine ligand.[9] When compared to CO, phosphines are worse π-acceptors, therefore the nickel centre is more electron rich in $[Ni(CO)_3(PR_3)]$ than in $[Ni(CO)_4]$. This phenomenon would translate into an increase of electron density donation from the nickel to the C–O π* antibonding orbitals and a consequent lowering of the ν(CO) stretch. In contrast, phosphines with more electronegative substituents are better π-acceptors via their σ* orbitals and compete for π back-donation with the carbon monoxide, therefore possess a higher electronic parameter value. These observations can be illustrated by the increasing series of electronic parameter displayed by $P(^tBu)_3$ (2056 cm^{-1}), PMe_3 (2064 cm^{-1}), PPh_3 (2068 cm^{-1}), and PF_3 (2111 cm^{-1}).[2]

The ligand cone angle concept was introduced to help rationalize steric effects in phosphorus-transition metal complexes based on ligand exchange experiments on Ni(0). It has been shown that steric effects are often more relevant than electronic

effects in determining the exchange equilibria among phosphorus ligands on Ni(0) and to determine the degree of substitution of CO in $Ni(CO)_4$ by these ligands.[10] Unsurprisingly, the degree of ligand displacement decreases as the size of the ligand increases.

3.1.3 Primary phosphines

Primary phosphines are commonly highly reactive, volatile, flammable and toxic compounds and are therefore often difficult to handle.[11–14] Despite these undesirable characteristics, primary phosphines have been demonstrated to have application in several fields such as asymmetric catalysis,[15–17] biochemistry[18] and polymer science[19–21]. Reports on this kind of species are still somewhat scarce, but they have been attracting increased attention as it has been shown that aerobic oxidation can be overcome by the insertion of sterically hindering substituents, by adding an appropriate degree of π conjugation to their backbone or by sufficient presence of heteroatoms, subsequently inhibiting the reaction with dioxygen.[11,13] Due to the presence of two P–H bonds, the *s* character of the phosphorus lone pair is increased in primary phosphines compared to that of tertiary phosphines. As such, primary phosphines are expected to be weaker donors.[22]

3.2 Aims

The aim of this chapter is to synthesise di-substituted phosphinecarboxamides that can ultimately be used as chelating ligands. For this purpose, hydrazine, methylenediamine and ethylenediamine were used as diamine source and were reacted with PCO^- to access these compounds. The formation of the phosphinecarboxamide moiety was observed in every case but only in the latter was the initial goal fully achieved. This chapter will discuss the different results obtained and propose a rational explanation for these findings.

3.3 Phosphinecarboxamides from bidentate amines

Previously, our group reported the synthesis of the parent phosphinecarboxamide ($H_2PC(O)NH_2$)[23] as well as some coordination studies showing that it can act as a ligand when in the presence of metal compounds such as $W(CO)_5(THF)$ and $Mo(CO)_4(COD)$.[24] Those findings prompted us to investigate the accessibility of di-substituted phosphinecarboxamides by using diamines as starting materials. With the intent to elucidate a trend in reactivity, the diamines hydrazine, methylenediamine and ethylenediamine were used. In principle, the 2-phosphaethynolate anion can react with any primary amine to yield the corresponding phosphinecarboxamide. Unlike with the preparation of the amino acid derivatives, addition of a stoichiometric excess of protons was found to be necessary for the phosphinecarboxides discussed in this chapter (Scheme 3.1).

Scheme 3.1: Schematic representation of the synthesis of bis-phophinecarboxamides from diamines, with n = 0,1,2.

3.3.1 Reactivity of PCO^- anion with hydrazine salts

With the intention of using less dangerous and harmful reagents and taking into consideration the previous examples of phosphinecarboxamides described in this thesis, we turned our attention to the hydrochloride salts of hydrazine, that intrinsically provides the proton source required for these reactions to proceed. The hydrochloride and dihydrochloride forms are commercially available, less explosive and much easier to handle in a day-to-day laboratory manipulations as they are solids.

3.3.1.1 Hydrazine hydrochloride ($NH_2NH_2 \cdot 1HCl$)

The aim of the reaction between hydrazine hydrochloride and the 2-phosphaethynolate anion is to obtain a monosubstituted hydrazine phosphinecarboxamide as shown in Scheme 3.2.

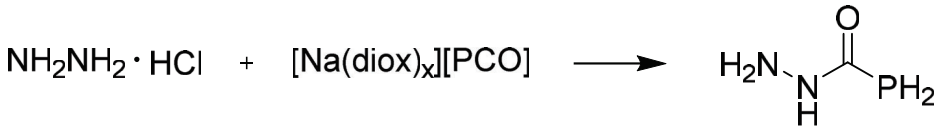

Scheme 3.2: Synthesis of the monosubstituted hydrazine phosphinecarboxamide.

The reaction of $NH_2NH_2 \cdot 1HCl$ and one equivalent of $[Na(dioxane)_x][PCO]$ gives rise to two sets of resonances in the ^{31}P NMR spectrum, a triplet at –139.9 ppm ($^1J_{P-H}$ = 206 Hz) and triplet of doublets at –128.2 ppm ($^1J_{P-H}$ = 218 Hz, $^3J_{P-H}$ = 4.6 Hz) when the deuterated solvent used is d_5-pyridine (Figure 3.2). Despite having two signals instead of one, both are characteristic for phosphinecarboxamides in terms of chemical shifts and *J* couplings. Both triplets collapse to singlets upon proton decoupling, suggesting the formation of two isomers of the product (Figure 3.3).

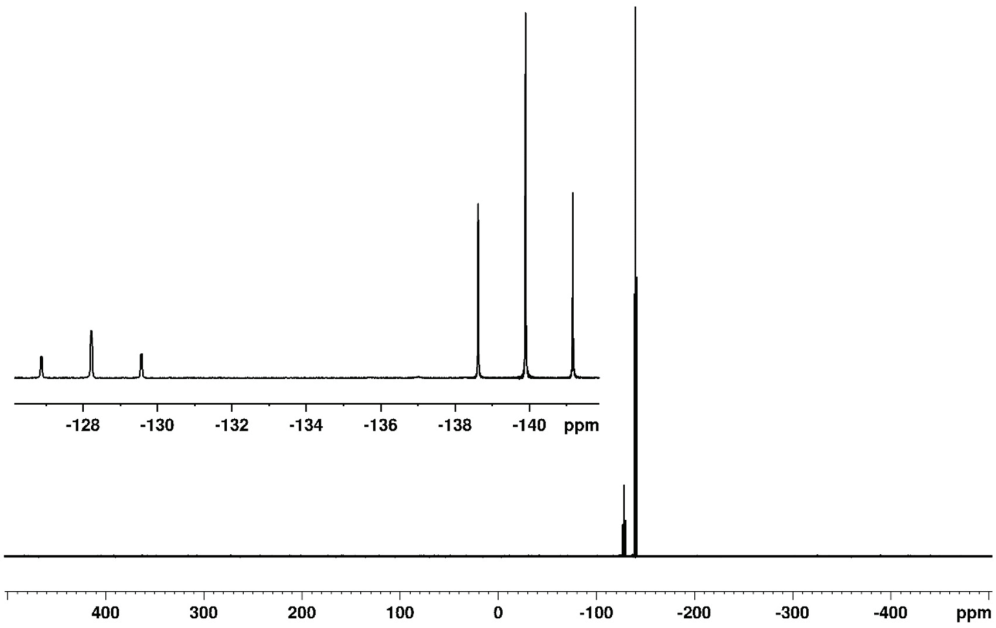

Figure 3.2: ^{31}P NMR spectrum of a d_5-pyridine solution of **13**.

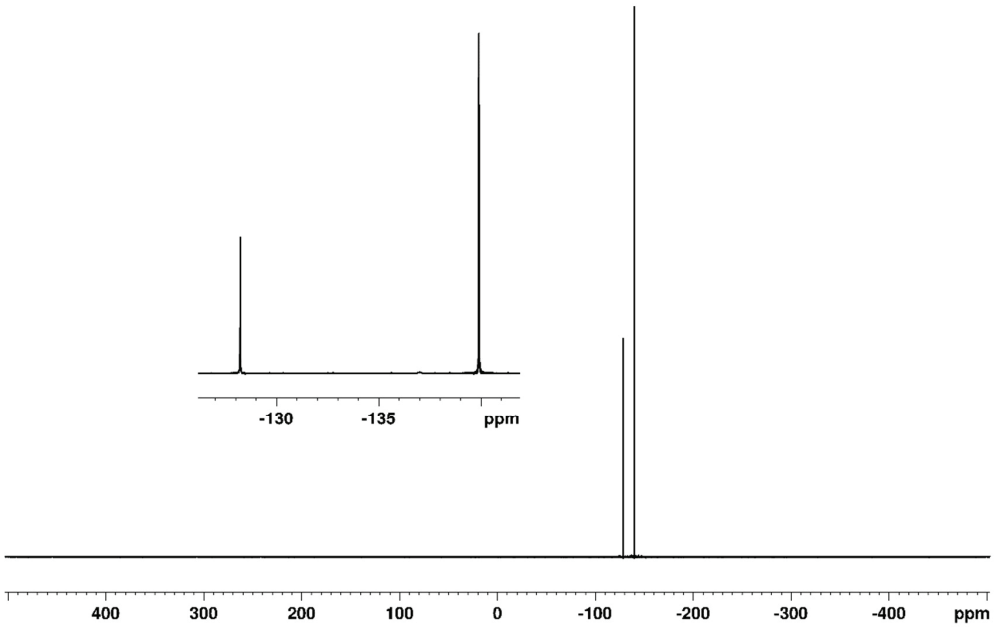

Figure 3.3: $^{31}P\{^1H\}$ NMR spectrum of a d_5-pyridine solution of **13**.

The peak at –139.9 ppm, the major product of this reaction, is attributed to the *cis* isomer of the monosubstituted hydrazine phosphinecarboxamide and the peak at –128.2 ppm, the minor product, is attributed to the *trans* isomer of the aforementioned compound. This assignment is based on the previous report of the parent species that show that the coupling between the phosphine and the amide proton can only be resolved for the *trans* species.[23] The terms *cis* and *trans* are used in this case to refer to the position of the proton attached to the nitrogen and the phosphine group relative to the C–N bond as highlighted in Figure 3.4.

13a **13b**

Figure 3.4: Representation of the *cis* (**13a**) and *trans* (**13b**) isomers of the hydrazine mono-phosphinecarboxamide.

As expected, the ^{1}H NMR spectrum of this compound also shows two sets of doublets centered at 3.72 ppm ($^{1}J_{H-P}$ = 206 Hz) and 4.02 ppm ($^{1}J_{H-P}$ = 218 Hz) corresponding to the protons attached to the phosphorus atom in the *cis* and *trans* isomers, respectively (Figure 3.5). These doublets have the same coupling constant found in the ^{31}P NMR spectrum and they collapse to singlets upon selective phosphorus decoupling, consistent with the formation of the desired products (Figure 3.6).

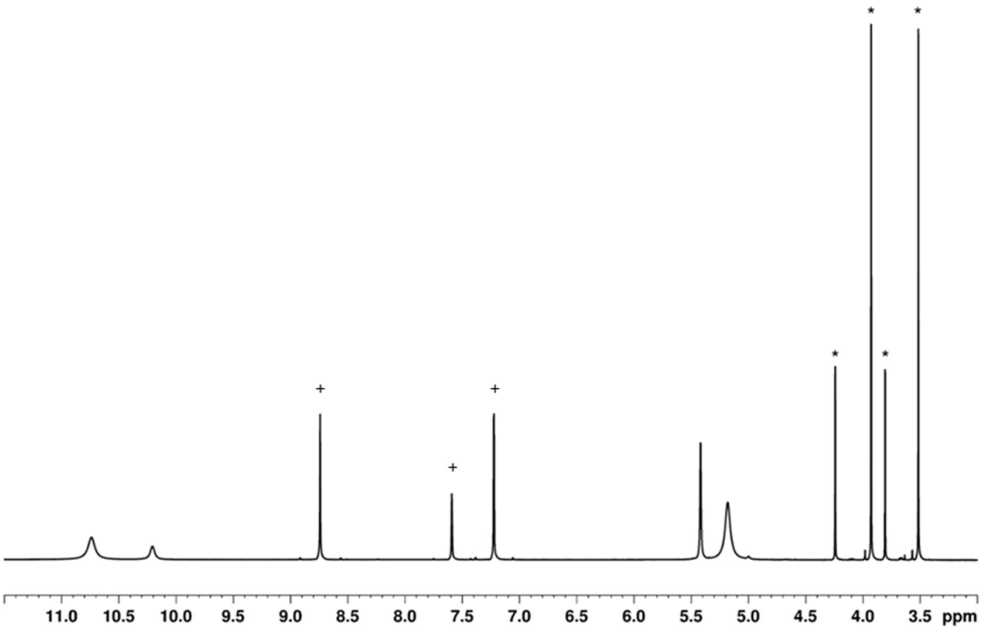

Figure 3.5: ^{1}H NMR spectrum of a d_5-pyridine solution of **13**. The resonances corresponding to the phosphine protons are highlighted with * and the solvent peaks with +.

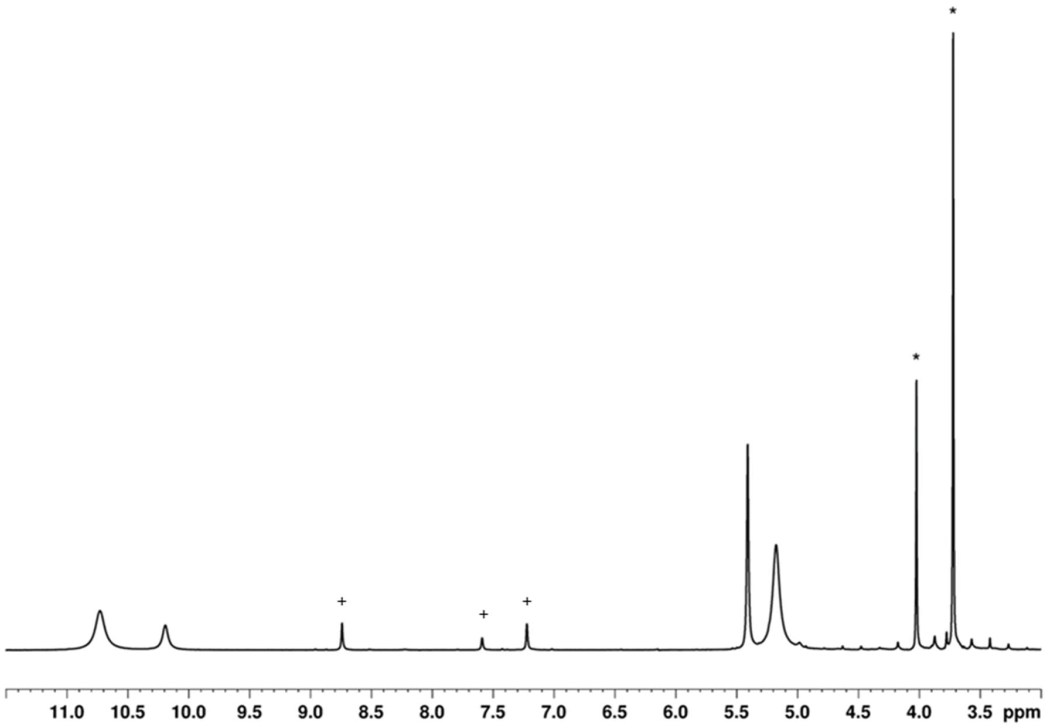

Figure 3.6: $^{1}H\{^{31}P\}$ NMR spectrum of a d_5-pyridine solution of **13**. The resonances corresponding to phosphine protons are highlighted with * and the solvent peaks with +.

The $^{13}C\{^{1}H\}$ NMR data is also consistent with the proposed structures. Two resonances can be observed in the downfield region of the spectrum, a doublet at 172.6 ppm ($^{1}J_{C-P}$ = 9 Hz) and a singlet at 181.5 ppm that correspond to the carbonyl carbon in the *cis* and *trans* isomers, respectively. Interestingly, the coupling between carbon and phosphorus could not be resolved for the *trans* isomer (Figure 3.7). However, $^{1}H–^{13}C$ HSQC 2D NMR experiments were used to unambiguously assign the peaks confirming that the singlet does correspond to **13b** and not to an undesired side product.

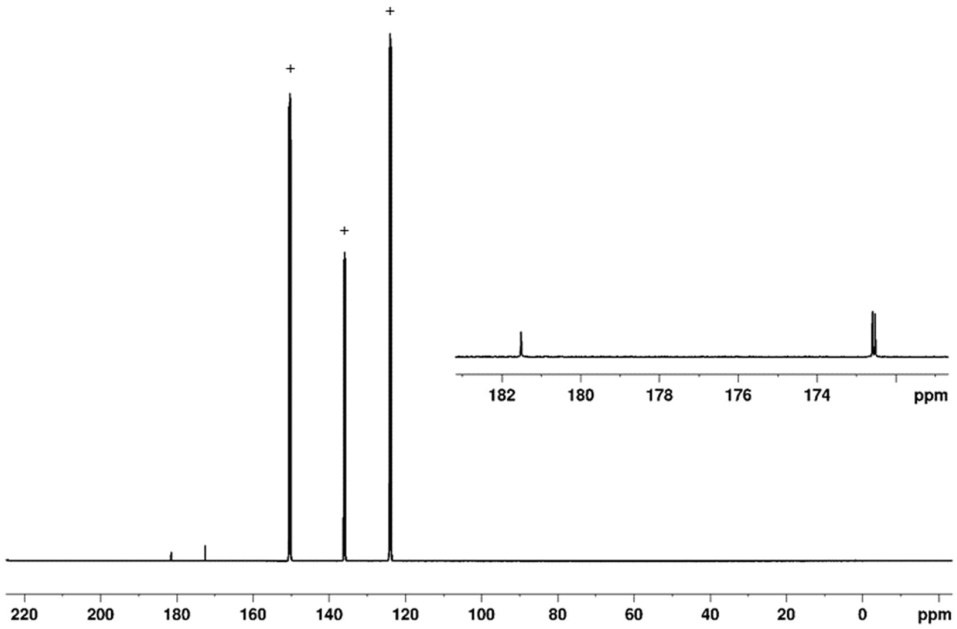

Figure 3.7: $^{13}C\{^{1}H\}$ NMR spectrum of a d_5-pyridine solution of **13**. The solvent peaks are highlighted with +.

Crystals were obtained from a toluene solution and confirm the solid-state structure of the major *cis* product (Figure 3.8). X-ray diffraction studies revealed that the proton attached to the α-nitrogen is *cis* to the phosphorus atom relative to the carbon-nitrogen bond. In the crystal structure, the phosphorus presents a

pyramidalized geometry, while the NH–CO fragment is planar. The crystal structure contains two molecules in the asymmetric unit and, consequently, all the bond metric data will be discussed as average values. Bond metric data show a C–P bond length of 1.864(av) Å which is consistent with a single bond between the carbon and the phosphorus atoms and the C–N bond length is 1.334(av) Å suggesting multiple bond character between the carbon and the nitrogen. These data show that there is little interaction between the phosphine lone pair and the amide fragment in the molecule, suggesting that this species should have the ability to act as a Lewis base. This reactivity will be further discussed in Chapter 4.

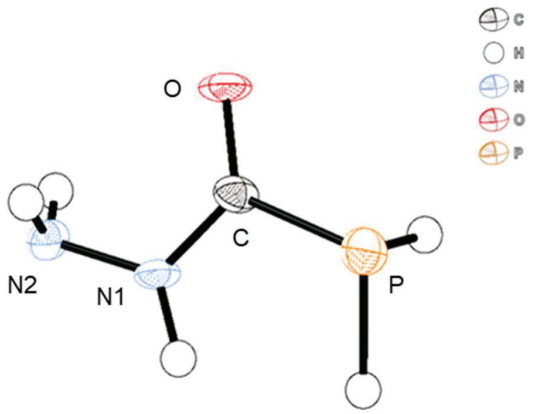

Figure 3.8: Crystal structure of the *cis* isomer of the hydrazine mono-phosphinecarboxamide **13a**. P–C and C–N bond lengths are 1.864(av) Å and 1.334(av) Å respectively.

The crystal structure as well as the spectroscopic data indicates that of the three conceivable resonance forms that can be drawn for this molecule (Figure 3.9), (i) and (ii) have a major contribution to the overall structure.

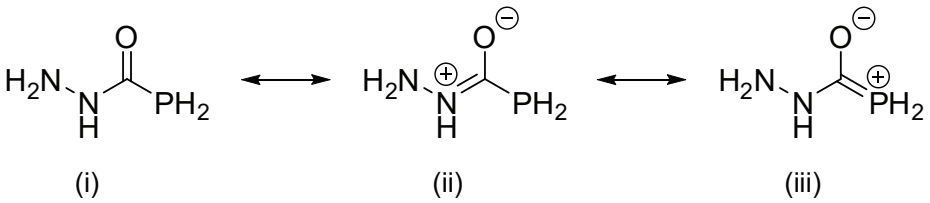

Figure 3.9: Resonance structures of the **13**.

Hoping to obtain more thermally stable crystals suitable for X-ray diffraction, one equivalent of 18-crown-6 was added to a THF solution of this compound and was layered with hexane. Surprisingly, crystals of the *trans* isomer were obtained this time (Figure 3.10). The bond metric data of the *trans* isomer **13b** is similar to those found for the *cis* isomer **13a**, with a C–P bond length of 1.871(av) Å which is consistent with a single bond between the carbon and the phosphorus atoms and the C–N bond length is 1.338(av) Å suggesting a multiple bond character between the carbon and the nitrogen. This data also implies that the phosphine lone pair is reasonably isolated from the amide fragment in the molecule.

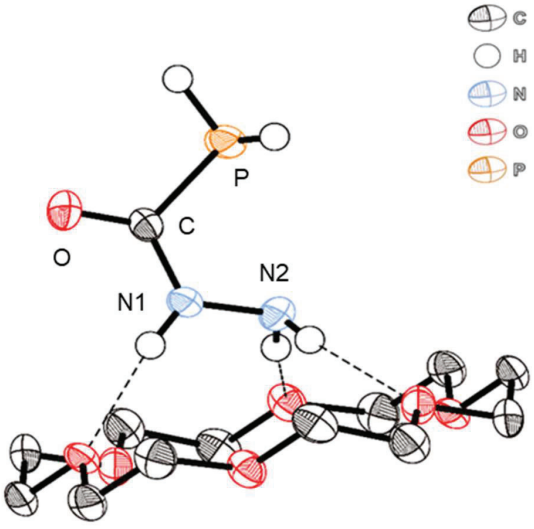

Figure 3.10: Crystal structure of the *trans* isomer of the hydrazine mono-phosphinecarboxamide **13b** in the presence of 18-crown-6. P–C and C–N bond lengths are 1.864(av) Å and 1.334(av) Å respectively.

The two isomers of the hydrazine mono-phosphinecarboxamide are always obtained as an oil when they are not in the crystalline form. Several attempts to obtain the product as a solid were made, including sublimation and trap-to-trap distillation, but unfortunately no success was achieved in this respect. The exception is the *trans* isomer, which co-crystalizes with 18-crown-6, that is stable at room temperature and can be stored under inert atmosphere for prolonged periods of time. The *cis* isomer crystals on the other hand dissolve back when brought to room temperature.

Compound **13** can adopt two different isomeric forms, *cis* and *trans*, **13a** and **13b**, respectively. NMR spectroscopy shows that both isomers can be observed at room temperature and both of their structures have been authenticated by single X-ray diffraction. From a mixture of the two, **13a** crystalizes exclusively when no sequestering agent is present, while **13b** crystalizes exclusively when 18-crown-6 is added to the mixture. These data imply that the two isomers should be close in energy and that the amide bond rotation should be high enough for both to be observed.

In order to confirm this hypothesis, the barrier to internal rotation around the C–N bond was calculated using Density Functional Theory and the results are summarized in Figure 3.11. The transition state was obtained by applying a rotation around the C–N bond and it was found to be 92 kJ mol^{-1} higher in energy than the more stable isomer. The *cis* isomer **13a** is more stable than the *trans* **13b** but only by 11 kJ mol^{-1}. This value is in good agreement with the ^{31}P NMR spectrum of these and with the fact that **13a** is the major product of the reaction between hydrazine hydrochloride and the 2-phosphaethynolate anion. A barrier of 92 kJ mol^{-1} is relatively high and interconversion between isomers is not possible due to thermal instability of phosphinecarboxamides.

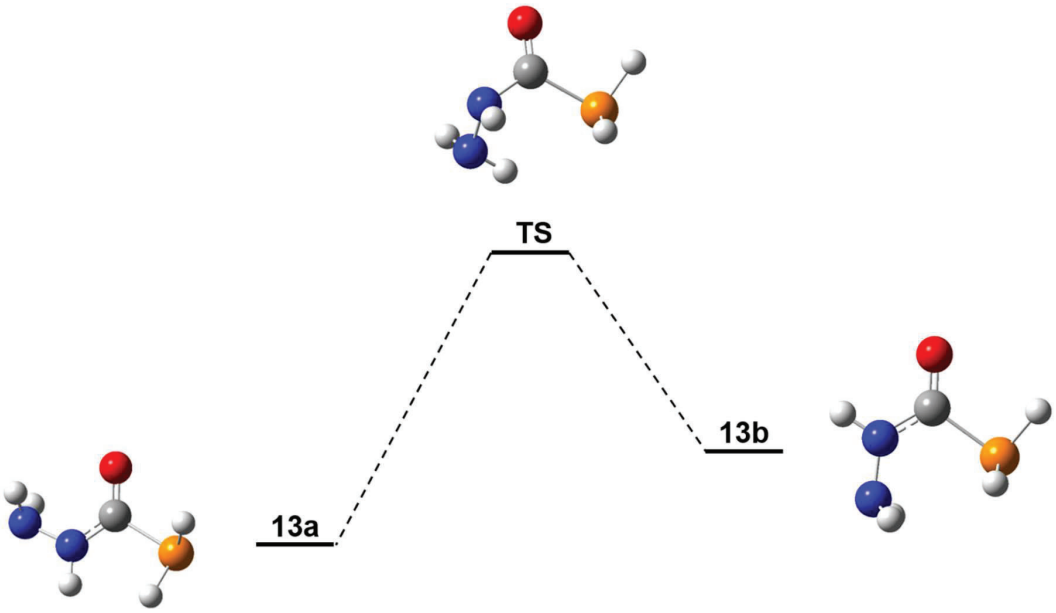

Figure 3.11: Schematic representation of the potential energy surface for C–N bond rotation. ΔG is given in kJ mol^{-1}: **13a** = 0; **TS** = 92; **13b** = 11.

The hindered rotation in amides can be explained based on resonance structures. The delocalization of electrons from the amide nitrogen into the carbonyl oxygen has significant contribution to the stabilization of amides. It results in a partial double bond between the carbon and nitrogen atoms, therefore hindering the rotation around this bond (resonance form II shown in Figure 3.9).

3.3.1.2 Hydrazine dihydrochloride ($NH_2NH_2 \cdot 2HCl$)

One of the goals of reacting hydrazine dihydrochloride and the 2-phosphaethynolate anion is to obtain a disubstituted hydrazine phosphinecarboxamide as shown in Scheme 3.3.

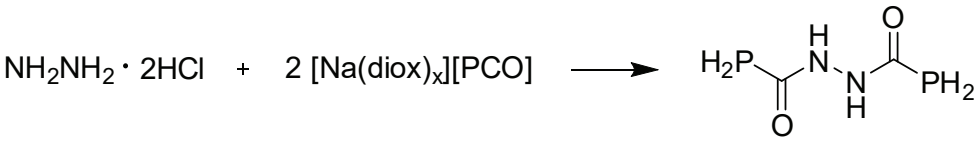

Scheme 3.3: Synthesis of the disubstituted hydrazine phosphinecarboxamide.

The hydrazine dihydrochloride salt has limited solubility in most common solvents. To address this issue, DMF was used for these reactions as it was the solvent which was found to dissolve most of the reactant. The reaction of $NH_2NH_2 \cdot 2HCl$ and two equivalents of [Na(dioxane)$_x$][PCO] gave rise to two major products in the ^{31}P and $^{31}P\{^1H\}$ NMR spectra in the expected region for this species at –129.3 ppm and –141.1 ppm (Figure 3.12). Unfortunately, these chemical shifts are the same as the ones found when $NH_2NH_2 \cdot 1HCl$ is reacted with one equivalent of PCO^- when DMF was used as a solvent.

Several attempts were made to try and push this reaction to completion, but unreacted PCO^- was always left in the reaction mixture (resonance at –387.5 ppm in Figure 3.12) suggesting that the hydrazine mono-phosphinecarboxamide formed was not incorporating a second phosphinecarboxamide moiety. Furthermore, with longer reaction times, the presence of phosphine (PH_3) and diphosphine (P_2H_4) could also be observed in the spectra, which is indicative of decomposition.

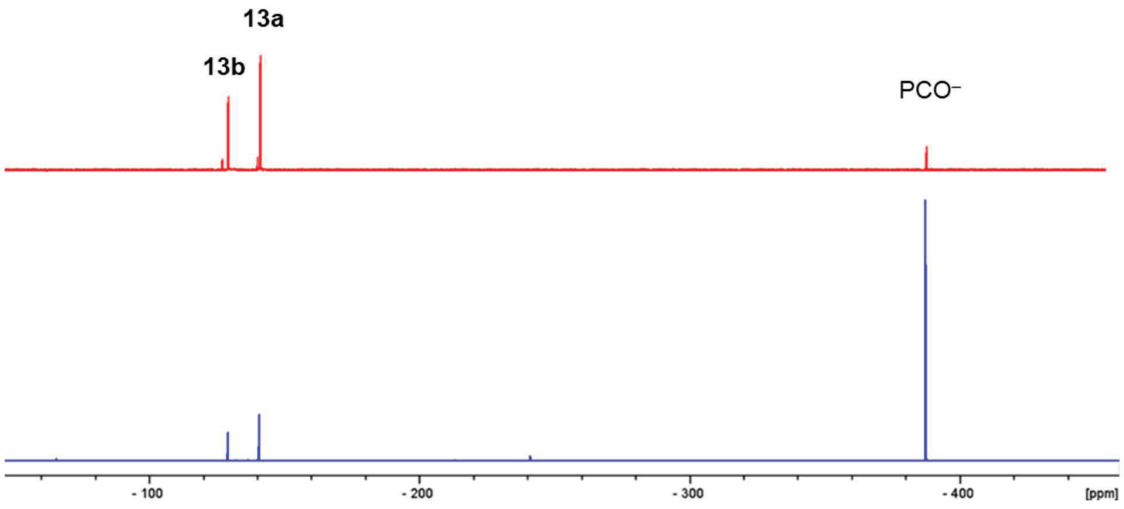

Figure 3.12: $^{31}P\{^1H\}$ NMR spectrum of the crude reaction between $NH_2NH_2 \cdot 2HCl$ and 4 equivalents of [Na(dioxane)$_x$][PCO] (bottom) and between $NH_2NH_2 \cdot 1HCl$ and 1 equivalent of [Na(dioxane)$_x$][PCO] (top), both reactions performed in DMF.

The disubstituted species was also not obtained when one equivalent of acid and one equivalent of PCO^- were added to the monosubstituted phosphinecarboxamide. Most likely, the desired compound could not be obtained due to steric hindrance provided by the presence of one phosphinecarboxamide moiety in the molecule. Consequently, nucleophilic attack from the β-nitrogen of the mono-phosphinecarboxamide species to the carbon in a second HPCO is prevented, therefore hindering the formation of the desired product.

3.3.2 Reactivity of PCO^- anion with methylenediamine ($NH_2CH_2NH_2 \cdot 2HCl$)

Methylenediamine is commercially available as a dihydrochloride salt and it was used as such. At a first glance, this ammonium salt offers the possibility to obtain the corresponding di-substituted phosphinecarboxamide or possibly the mono-substituted species (Scheme 3.4).

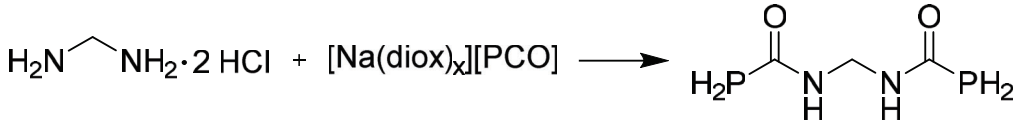

Scheme 3.4: Synthesis of the disubstituted methylenediamine phosphinecarboxamide.

In order to fulfill this goal, the diamine salt was reacted with one and two equivalents of [Na(dioxane)$_x$][PCO]. The formation of the phosphinecarboxamide moiety was achieved as evidenced by the ^{31}P and $^{31}P\{^1H\}$ NMR spectra, but the two results were identical (Figure 3.13).

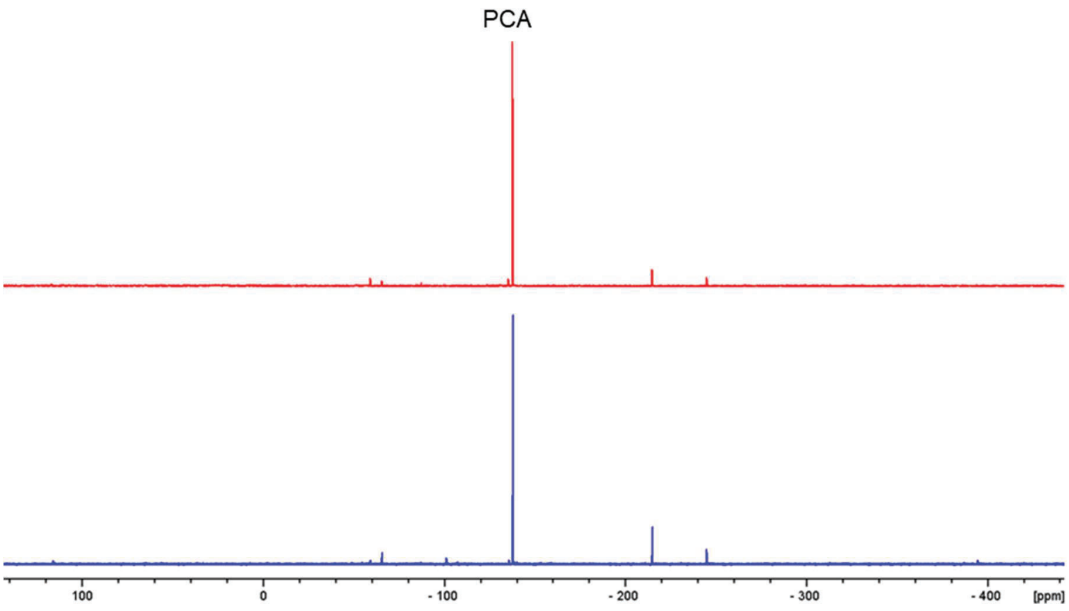

Figure 3.13: $^{31}P\{^{1}H\}$ NMR spectra of the reaction of MDA·2HCl with one (bottom) and two (top) equivalents of $[Na(dioxane)_x][PCO]$.

Even though no appreciable amount of unreacted PCO^- could be observed in the $^{31}P\{^{1}H\}$ NMR spectrum of the reaction of MDA·2HCl with two equivalents of $[Na(dioxane)_x][PCO]$, we propose that the product formed is the mono-substituted phosphinecarboxamide based on the results obtained with the hydrazine dihydrochloride salt. This was later confirmed when the spectrum obtained from the reaction of MDA·2HCl, one equivalent of $[Na(dioxane)_x][PCO]$ and one equivalent of sodium hydroxide was shown to have the same chemical shift as the previous experiment. For that reason, from then on, only one equivalent of PCO^- was used with this diamine.

Accordingly, when MDA·2HCl was allowed to react with one equivalent of $[Na(dioxane)_x][PCO]$, a white solid was obtained and characterized by NMR spectroscopy. Unfortunately, the product obtained was demonstrated to be the parent phosphinecarboxamide species ($H_2PC(O)NH_2$). This was discovered when attempting

to isolate the product as a solid by sublimation. The nature of the recovered solid in this process was confirmed by NMR spectroscopy, specially ^{1}H NMR, due to the absence of the methylene protons. At the end of the sublimation the sticky pale yellow/brown solid left at the bottom of the Schlenk tube was also investigated by NMR spectroscopy. The ^{1}H NMR in $CDCl_3$ showed a mixture of the parent species and a peak at 4.71 ppm that was identified as hexamethylenetetramine, also known as urotropine, an adamantane-like structure. This tetramer is most likely formed from the oligomerization of methylene imine that is assumed to be produced in the process.

Given the results obtained when methylenediamine is used as starting material, we propose that the desired phosphinecarboxamide product is initially formed but methylene imine is quickly eliminated to form the parent species and that the imine, in turn, oligomerises to yield the urotropine and ammonia as shown in Scheme 3.5.

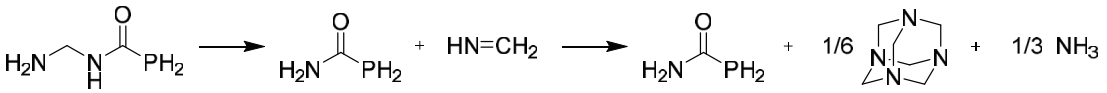

Scheme 3.5: Proposed decomposition pathway of the methylenediamine mono-phosphinecarboxamide derivative.

The relative energies of the three proposed stages of this decomposition reaction have been calculated using DFT and the data obtained are summarized in Figure 3.14. The final step is 53 kJ mol^{-1} more stable than if the reaction were to stop at **B**, which explains why the urotropine is observed in the ^{1}H NMR spectrum. This pathway is also supported by the presence of a small peak at 0.05 ppm that corresponds to the ammonia formed.[25]

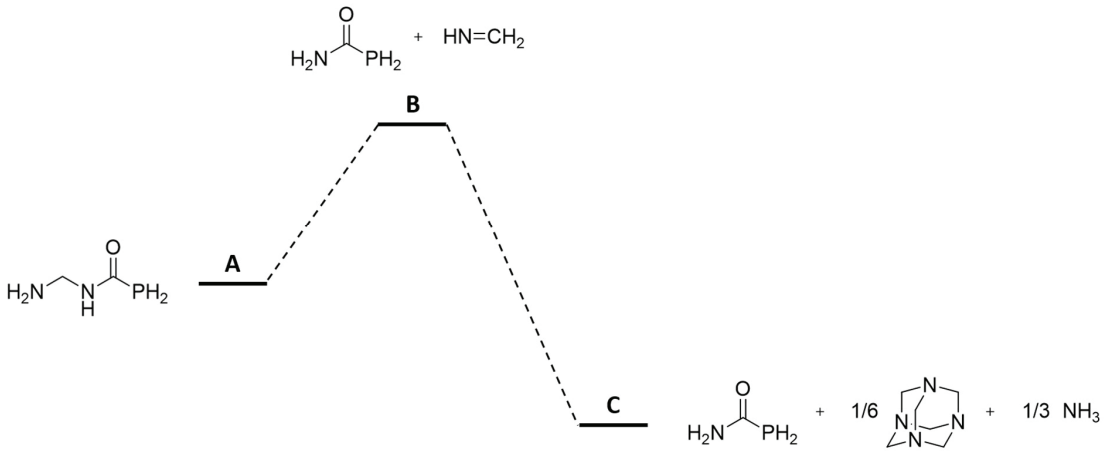

Figure 3.14: Schematic representation of the energy of the three proposed stages of decomposition of the methylenediamine mono-phosphinecarboxamide derivative. ΔG is given in kJ mol^{-1}: **A** = 0; **B** = 34; **C** = –19.

3.3.3 Reactivity of PCO^- anion with ethylenediamine

When $NH_2CH_2CH_2NH_2 \cdot 2HCl$ and two equivalents of $[Na(dioxane)_x][PCO]$ were allowed to react, the di-substituted phosphinecarboxamide **14** was obtained (Scheme 3.6). This compound was fully characterized by NMR spectroscopy.

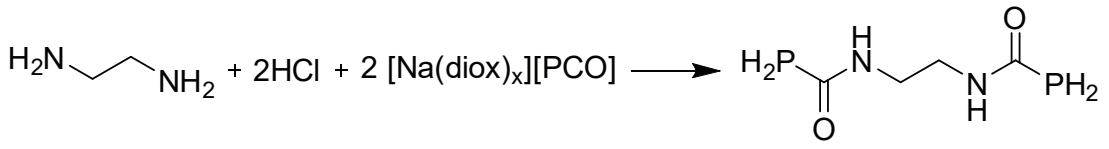

Scheme 3.6: Synthesis of the ethylediamine bis-phosphinecarboxamide **14**.

The ^{31}P NMR spectrum exhibits a triplet at –132.9 ppm ($^1J_{P-H}$ = 208 Hz) (Figure 3.15) characteristic of phosphinecarboxamides that collapses to a singlet on proton decoupling (Figure 3.16), indicating the formation of the phosphinecarboxamide moiety.

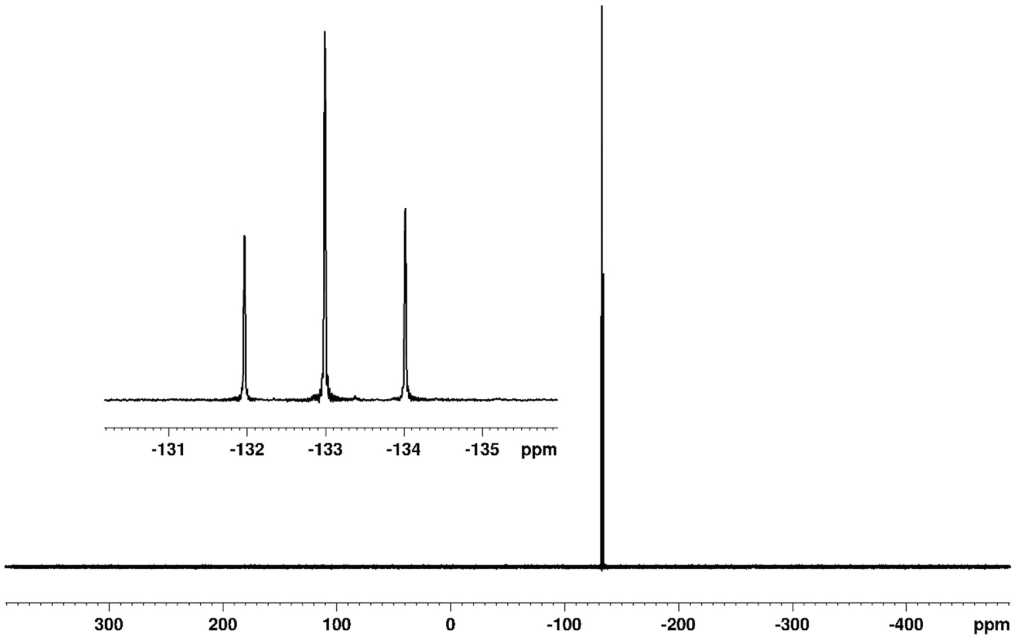

Figure 3.15: ^{31}P NMR spectrum of a d_5-pyridine solution of **14**.

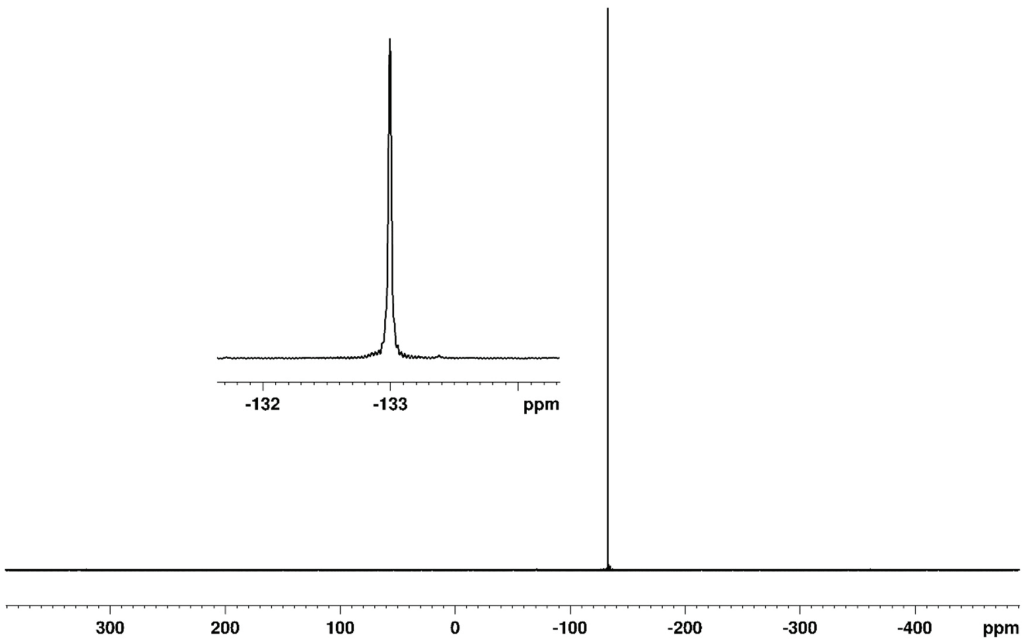

Figure 3.16: $^{31}P\{^1H\}$ NMR spectrum of a d_5-pyridine solution of **14**.

The ^{1}H NMR spectrum shows a doublet centered at 3.72 ppm ($^{1}J_{H-P}$ = 208 Hz) (Figure 3.17). This doublet collapses to a singlet upon selective phosphorus decoupling, corroborating the formation of the desired product (Figure 3.18). The ^{1}H NMR spectra also suggest that the compound is symmetrical, as there is only one chemical environment present.

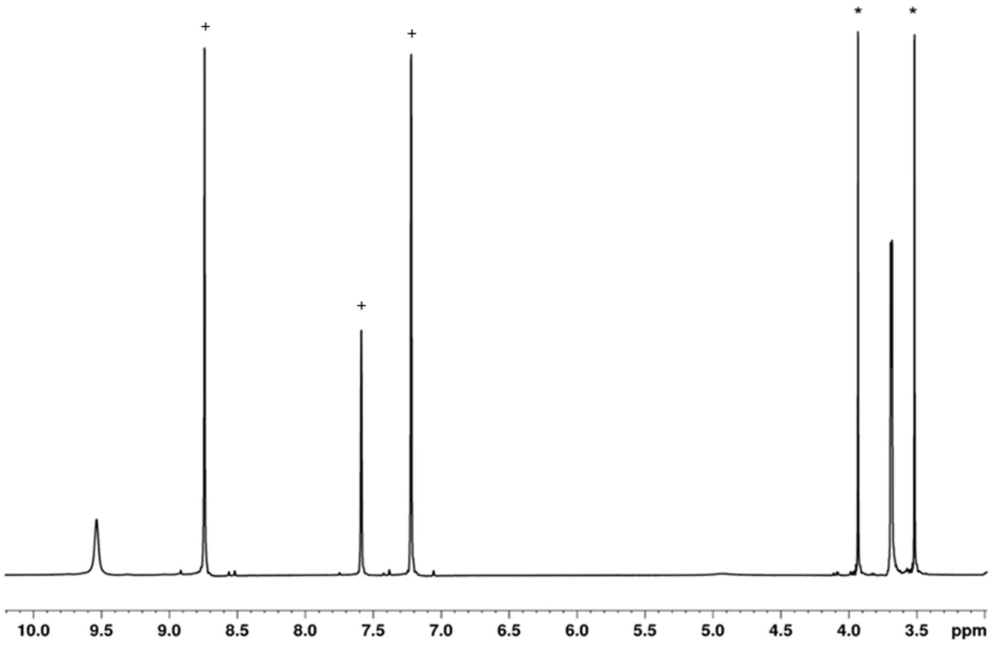

Figure 3.17: ^{1}H NMR spectrum of a d_5-pyridine solution of **14**. The resonances corresponding to the phosphine protons are highlighted with * and the solvent peaks with +.

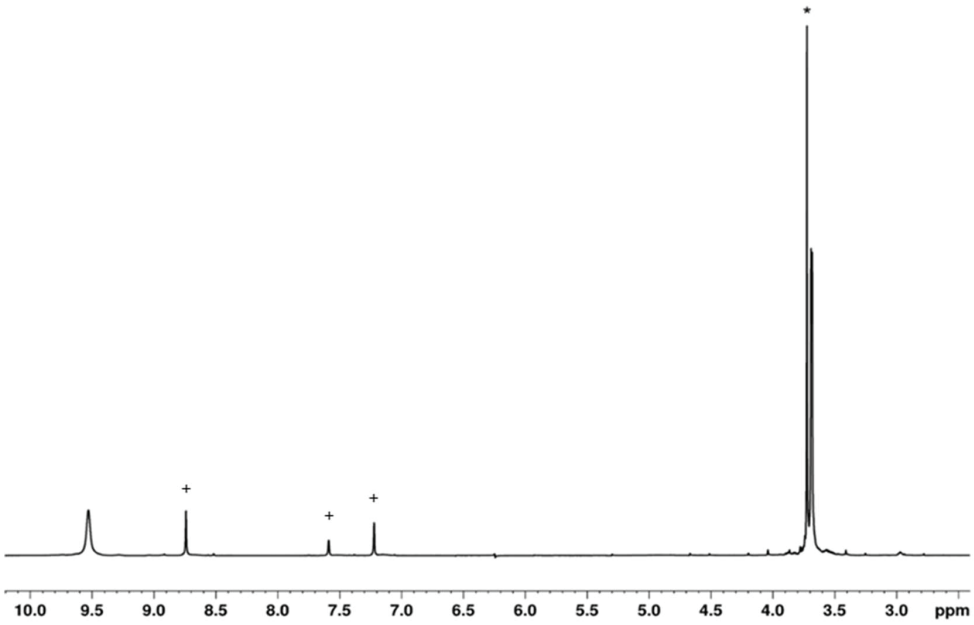

Figure 3.18: $^{1}H\{^{31}P\}$ NMR spectrum of a d_5-pyridine solution of **14**. The resonance corresponding to the phosphine protons are highlighted with * and the solvent peaks with +.

The $^{13}C\{^{1}H\}$ NMR spectrum shows a doublet at 172.8 ppm ($^{1}J_{C-H}$ = 7 Hz) that corresponds to the carbonyl carbons of the two phosphinecarboxamide moieties coupling to the phosphorus atoms (Figure 3.19).

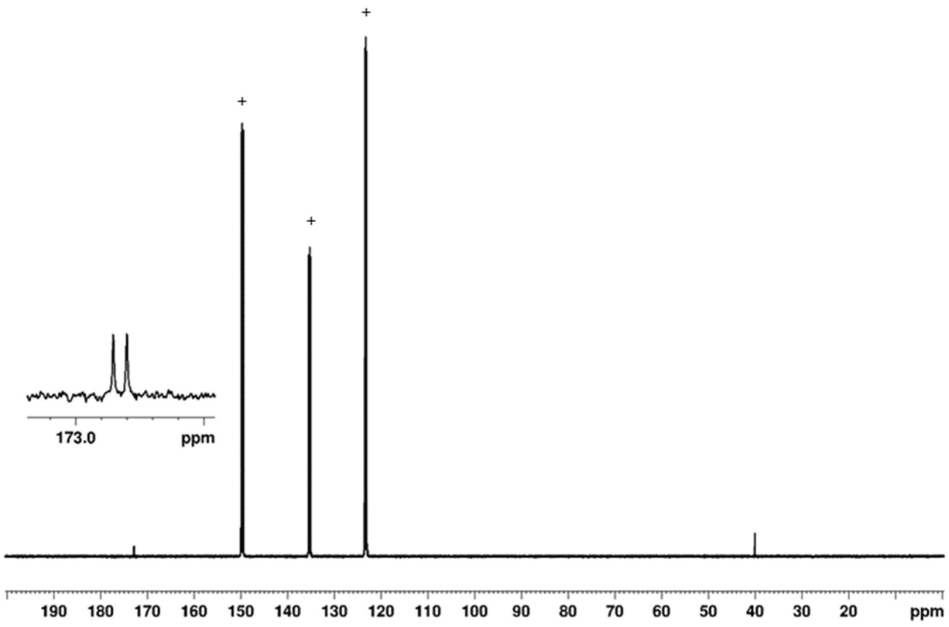

Figure 3.19: $^{13}C\{^{1}H\}$ NMR spectrum of a d_5-pyridine solution of **14**. Solvent peaks are highlighted with +.

Crystals obtained by slow diffusion of hexane into a THF solution of the product confirm the incorporation of two phosphinecarboxamide units to the ethylenediamine (Figure 3.20). Bond metric data show a C–P bond length of 1.863(2) Å, consistent with a single bond between the carbon and the phosphorus atoms and the C–N bond length is 1.326(2) Å suggesting a multiple bond character between these atoms. The amide portions of the molecule are planar suggesting isolation of the phosphine lone-pair from the rest of the molecule. This interesting feature prompted us to explore this compound as a ligand, possibly a chelating ligand. This feature will be discussed in greater depth in Chapter 4.

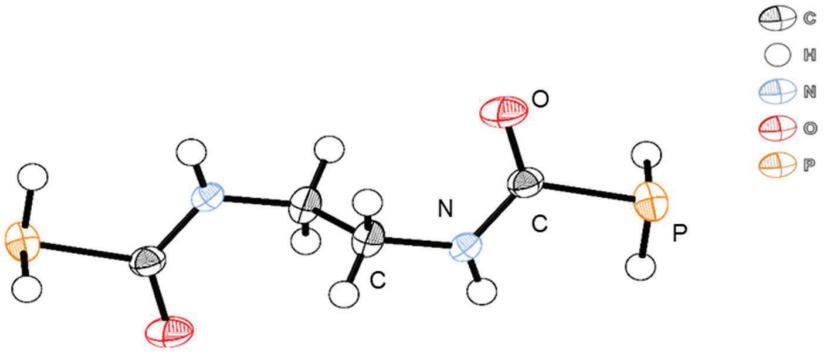

Figure 3.20: Crystal structure of the ethylenediamine bis-phosphinecarboxamide **14**. P–C and C–N bond lengths are 1.863(2) Å and 1.326(2) Å.

The fact that the bis-phosphinecarboxamide was obtained with this diamine implies that when the number of methylene spacers is two or more, the two amine groups start acting as two independent reaction sites.

3.4 Secondary amines

Next, we investigated cyclic amines as they can accommodate metals in their binding cavity. The idea was to incorporate as many phosphinecarboxamide moieties to the molecule as possible and use the phosphine fragments as auxiliary ligands to metal centres. In this work, 1,4,8,11-tetraazacyclotetradecane, abbreviated as TACTD, was used (Scheme 3.7).

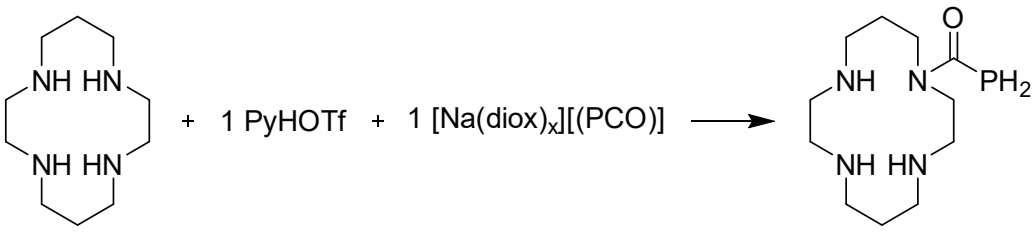

Scheme 3.7: Reaction of TACTD with an acid and [Na(dioxane)$_x$][PCO] to obtain the corresponding phosphinecarboxamide.

TACTD was initially reacted with one, two, three and four equivalents of [Na(dioxane)$_x$][PCO]. The ^{31}P NMR spectra of these reactions show several overlapping resonances. However on close inspection of the NMR spectra, it became apparent that they are very similar. Hence we focused on the reaction of one equivalent of TACTD, one of acid and one of PCO^- (Figure 3.21).

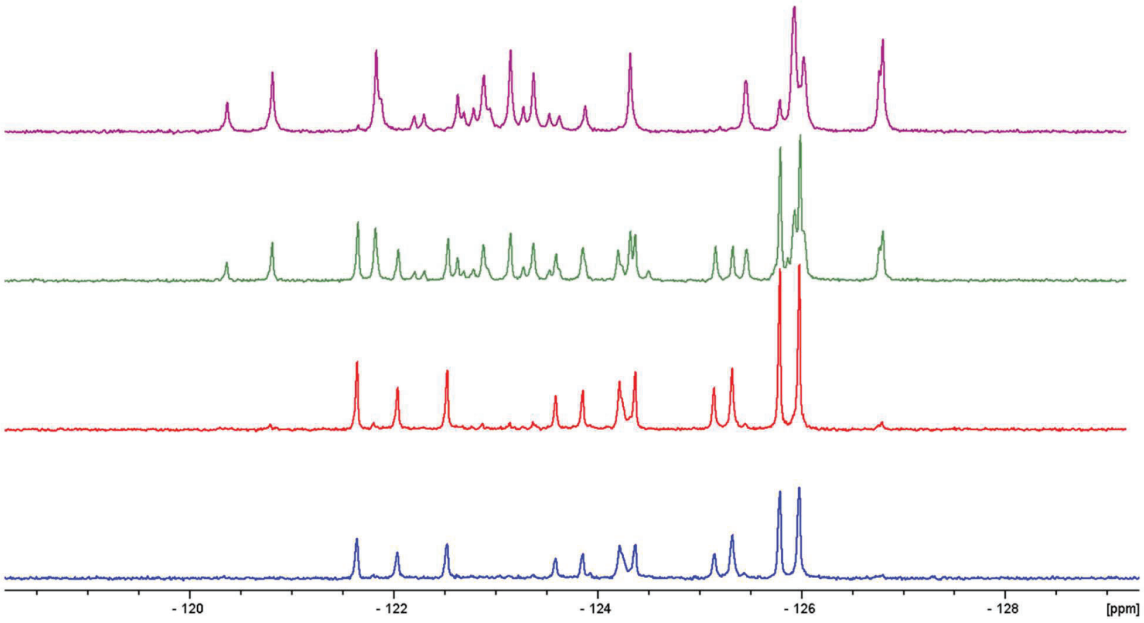

Figure 3.21: $^{31}P\{^1H\}$ NMR stacked plots of the reaction between one equivalent of TACTD and 1, 2, 3 and 4 equivalents of [Na(dioxane)$_x$][PCO], from the bottom to the top.

It is possible to identify a series of triplets in the ^{31}P NMR in the expected range for phosphinecarboxamides and with expected coupling constant values (Figure 3.22 (below)). These results are encouraging, however a closer analysis of the $^{31}P\{^1H\}$ NMR spectrum suggest the presence of at least eleven species, making it difficult to determine the number of substitutions, allowing the possibility of several different arrangements of the phosphinecarboxamide arms relative to the cycle (Figure 3.22 (above)). Additionally, the reactivity of secondary amines is usually lower compared to primary amines.

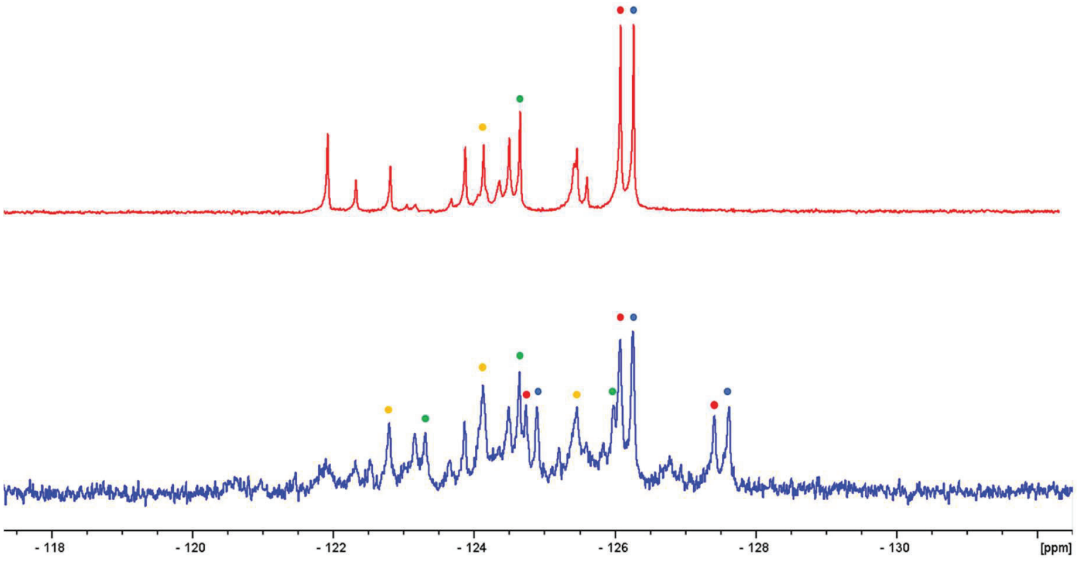

Figure 3.22: ^{31}P (below) and $^{31}P\{^{1}H\}$ NMR spectrum (above) of the reaction of TACTD, PyHOTf and [Na(dioxane)$_x$][PCO] in a 1 : 1 : 1 ratio.

It was possible to obtain a preliminary solid-state structure that confirmed the connectivity of one phosphinecarboxamide moiety. However, due to the high degree of disorder, no bond metric data could be inferred from the structure. Difficulties with isolation of pure sample unfortunately prevented further work with this cyclic amine.

In contrast to what is observed with primary amines, the reaction between a secondary amine and PCO^- in the presence of an acid does not proceed as readily. As the first step of formation of phosphinecarboxamides from ammonium salts is believed to be the protonation of the PCO^- anion by the ammonium salt to form HPCO followed by a nucleophilic attack of the amine on the acid to form the product. However, HPCO is known to be very unstable at room temperature and, with secondary amines, the subsequent nucleophilic attack of the amine on the HPCO carbon atom is retarded, resulting in significant decomposition of the acid, therefore hampering the formation of the desired phophinecarboxamide product. In this specific case, even more constraints are imposed by the presence of a macrocycle.

3.5 Conclusions

This chapter described the synthesis and characterization of the *cis* and *trans* isomers of the hydrazine mono-phosphinecarboxamide and the ethylenediamine bis-phosphinecarboxamide compounds using the corresponding diamines as starting materials. The goal was to start from the smallest diamine possible, hydrazine, and work our way to diamines with methylene spacers between the two nitrogen atoms. However not all the reactions proceeded as planned. Despite several attempts, the di-substituted hydrazine derivative could not be obtained, always leading to the incorporation of only one equivalent of the 2-phosphaethynolate anion. When methylenediamine was used, we propose that the mono-phosphinecarboxamide was formed initially but rapidly eliminates methylene imine to form the parent species. The phosphinecarboxamides **13** and **14** can, in theory, be used as ligands and their further reactivity will be discussed in Chapter 4.

3.6 References

[1] A. G. Orpen, N. G. Connelly, *Organometallics* **1990**, *9*, 1206–1210.

[2] C. A. Tolman, *Chem. Rev.* **1977**, *77*, 313–348.

[3] S. O. Grim, D. A. Wheatland, W. McFarlane, *J. Am. Chem. Soc.* **1967**, *89*, 5573–5577.

[4] K. A. R. Mitchell, *Chem. Rev.* **1969**, *69*, 157–178.

[5] D. G. Gilheany, *Chem. Rev.* **2002**, *94*, 1339–1374.

[6] B. J. Dunne, R. B. Morris, A. G. Orpen, *J. Chem. Soc. Dalt. Trans.* **1991**, 653.

[7] S. Xiao, W. C. Trogler, D. E. Ellis, Z. Berkovitch-Yellin, *J. Am. Chem. Soc.* **1983**, *105*, 7033–7037.

[8] D. S. Marynick, *J. Am. Chem. Soc.* **1984**, *106*, 4064–4065.

[9] C. A. Tolman, *J. Am. Chem. Soc.* **1970**, *92*, 2953–2956.

[10] C. A. Tolman, *J. Am. Chem. Soc.* **1970**, *92*, 2956–2965.

[11] B. Stewart, A. Harriman, L. J. Higham, *Organometallics* **2011**, *30*, 5338–5343.

[12] L. H. Davies, B. Stewart, R. W. Harrington, W. Clegg, L. J. Higham, *Angew. Chemie Int. Ed.* **2012**, *51*, 4921–4924.

[13] J. T. Fleming, L. J. Higham, *Coord. Chem. Rev.* **2015**, *297–298*, 127–145.

[14] L. H. Davies, J. F. Wallis, R. W. Harrington, P. G. Waddell, L. J. Higham, *J. Coord. Chem.* **2016**, *69*, 2069–2080.

[15] T. Clark, C. Landis, *Tetrahedron: Asymmetry* **2004**, *15*, 2123–2137.

[16] G. Hoge, B. Samas, *Tetrahedron: Asymmetry* **2004**, *15*, 2155–2157.

[17] D. J. Brauer, K. W. Kottsieper, S. Roßenbach, O. Stelzer, *Eur. J. Inorg. Chem.* **2003**, *2003*, 1748–1755.

[18] K. V. Katti, H. Gali, C. J. Smith, D. E. Berning, *Acc. Chem. Res.* **1999**, *32*, 9–17.

[19] T. N. Hooper, M. A. Huertos, T. Jurca, S. D. Pike, A. S. Weller, I. Manners, *Inorg. Chem.* **2014**, *53*, 3716–3729.

[20] H. Dorn, R. A. Singh, J. A. Massey, J. M. Nelson, C. A. Jaska, A. J. Lough, I. Manners, *J. Am. Chem. Soc.* **2000**, *122*, 6669–6678.

[21] H. Dorn, R. A. Singh, J. A. Massey, A. J. Lough, I. Manners, *Angew. Chemie Int. Ed.* **1999**, *38*, 3321–3323.

[22] M. Brynda, *Coord. Chem. Rev.* **2005**, *249*, 2013–2034.

[23] A. R. Jupp, J. M. Goicoechea, *J. Am. Chem. Soc.* **2013**, *135*, 19131–19134.

[24] M. B. Geeson, A. R. Jupp, J. E. McGrady, J. M. Goicoechea, *Chem. Commun.* **2014**, *50*, 12281–12284.

[25] F. Haase, J. Sauer, *J. Phys. Chem.* **1994**, *98*, 3083–3085.

4. Deprotonation, Alkylation and Coordination Chemistry of Phosphinecarboxamides

4.1 Introduction

Among the numerous known phosphorus-containing compounds, primary phosphines are of particular interest. Even though they are perceived as difficult to work with (due to air and moisture sensitivity as well as a very strong and unpleasant odour), they have found applications in several branches of chemistry.[1–5] The properties of phosphines can be altered by carefully choosing their substituents.[6] Primary phosphines are especially interesting as they possess two P–H bonds that are very reactive. The number of reported air stable primary phosphines has increased over the past few years, but the reasons for such stability are not always clear.[7,8]

Phosphines have been widely explored as ligands in coordination chemistry. Several complexes have been reported in the literature involving a range of metals from most groups across the periodic table.[8] As an example, Katti and co-workers reported the solid state structure of a chelating primary diphosphine, *cis*-[$W(CO)_4(H_2PCH_2)_2CHCOCHPh$], where the authors suggest that σ-donation is the dominant electronic factor in the complex (Figure 4.1).[9] Similarly, the Goicoechea group has reported a complex of molybdenum with the parent phosphinecarboxamide ($H_2NC(O)PH_2$), *cis*-[$Mo(CO)_4(H_2PC(O)NH_2)$]. This metal complex was used to determine the σ-donor and π-acceptor properties of phosphinecarboxamides and their results indicate very similar electronic properties to those of phosphine (PH_3) (Figure 4.1).[10]

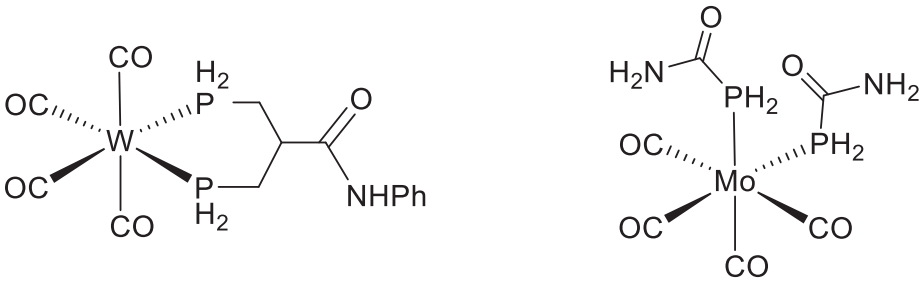

Figure 4.1: Selected examples of primary phosphine coordination complexes; *cis*-$[W(CO)_4(H_2PCH_2)_2CHCOCHPh]$ (left) and *cis*-$[Mo(CO)_4(H_2PC(O)NH_2)]$ (right).

4.2 Aims

This chapter will explore the potential of phosphinecarboxamides as chemical building blocks for a variety of compounds. First, deprotonation of the compounds described previously and formation of their corresponding phosphides will be described. The resulting species can be post-functionalised at the phosphorus centre as will be demonstrated by the reaction with simple electrophiles. Finally, this chapter will outline the ability of such species to act as ligands by presenting some of the coordination chemistry of the phosphinecarboxamides synthesised thus far.

4.3 Deprotonation

Phosphinecarboxamides have two possible nucleophilic sites, the phosphorus and nitrogen atoms. One way to identify whether this class of molecules behaves preferentially as a phosphine or as an amide is by observing its deprotonation chemistry. To investigate this matter, either benzyl potassium (BzK) or potassium bis(trimethylsilyl)amide (KHMDS) were selected as strong non-nucleophilic bases to deprotonate compounds **13** and **14** (described in the previous chapter).

4.3.1 Deprotonation of the hydrazine mono-phosphinecarboxamide

The addition of one equivalent of benzyl potassium (BzK) to unsequestered **13** in THF resulted in instant decomposition. In order to overcome this issue, one

equivalent of the sequestering agent 18-crown-6 was added, now giving rise to new resonances in the ^{31}P NMR spectrum (Figure 4.2).

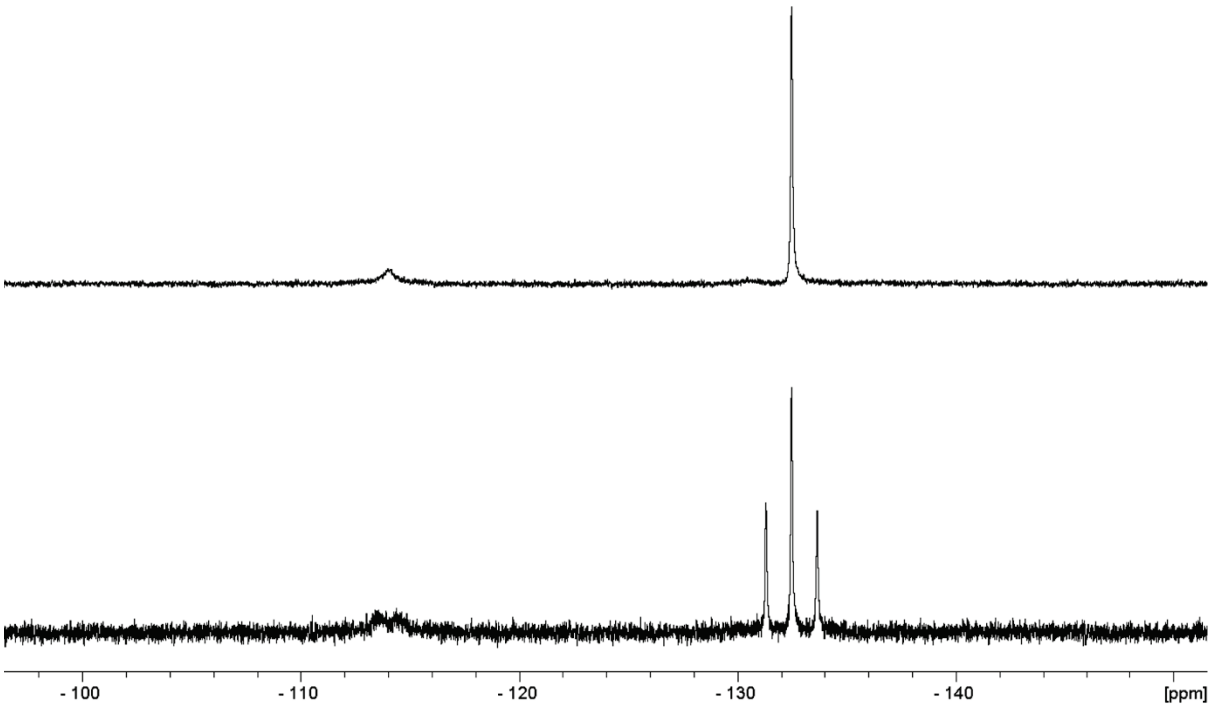

Figure 4.2: ^{31}P (bottom) and $^{31}P\{^{1}H\}$ (top) NMR spectrum of the reaction between **13** and BzK in the presence of 18-crown-6.

Interestingly, deprotonation at both nitrogen and phosphorus sites of the molecule was observed (**15**). This is apparent by the ^{31}P NMR spectrum taken in d_8-THF, that exhibits a broad doublet at –114.0 ppm ($^{1}J_{P–H}$ = 150 Hz) and a triplet at –132.5 ppm ($^{1}J_{P–H}$ = 190 Hz) (Figure 4.2). These resonances collapse into singlets upon proton decoupling and have an integration ratio of 0.3 : 1 respectively. The doublet is approximately 30 ppm downfield shifted relative to the neutral hydrazine phosphinecarboxamide isomers and presents a smaller coupling constant. This result indicates deprotonation at the phosphorus atom. The decrease in the $^{1}J_{P–H}$ coupling is explained by the increase in the electron density at the phosphorus on deprotonation.[11] The chemical shifts and coupling constants for **13** and **15**, the resulting deprotonated products, are summarized in Table 4.1.

Table 4.1: ^{31}P NMR chemical shifts and corresponding $^{1}J_{P–H}$ couplings of **13** and **15**.

	δ (ppm)	$^{1}J_{P–H}$ (Hz)
13a (*cis*)	–139.9 (t)	206
13b (*trans*)	–128.2 (t)	218
15	–114.0 (bd)	150
	–132.5 (t)	190

The triplet is approximately 7 ppm downfield-shifted from the neutral *cis*-hydrazine phosphinecarboxamide isomer, **13a**, and approximately 2 ppm shifted upfield from the *trans* isomer, **13b** (Table 4.1). The very small shift relative to **13** and the fact that it remained a triplet suggest that deprotonation is occurring at one of the nitrogen atoms in this case (Scheme 4.1).

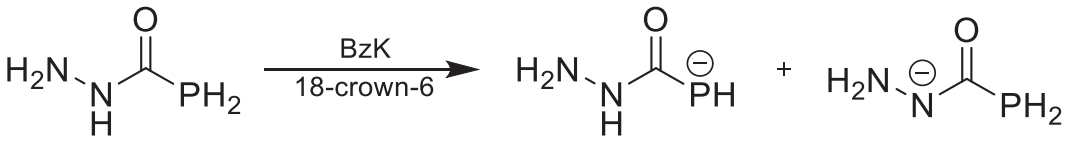

Scheme 4.1: Reaction of **13** with BzK in the presence of 18-crown-6 to yield **15**.

In the ^{1}H NMR spectrum run in d_8-THF, the P–H doublets corresponding to the products are broad and somewhat difficult to assign due to overlap with the 18-crown-6 peak. To overcome this issue, the spectra were recollected in d_5-pyridine. Under these conditions it is now possible to observe the presence of two well defined doublets, one centred at 2.95 ppm ($^{1}J_{P–H}$ = 150 Hz) corresponding to the phosphide product and the other at 4.08 ppm ($^{1}J_{P–H}$ = 190 Hz) that corresponds to the amide product resulting from deprotonation at the α-nitrogen atom (Figure 4.3).

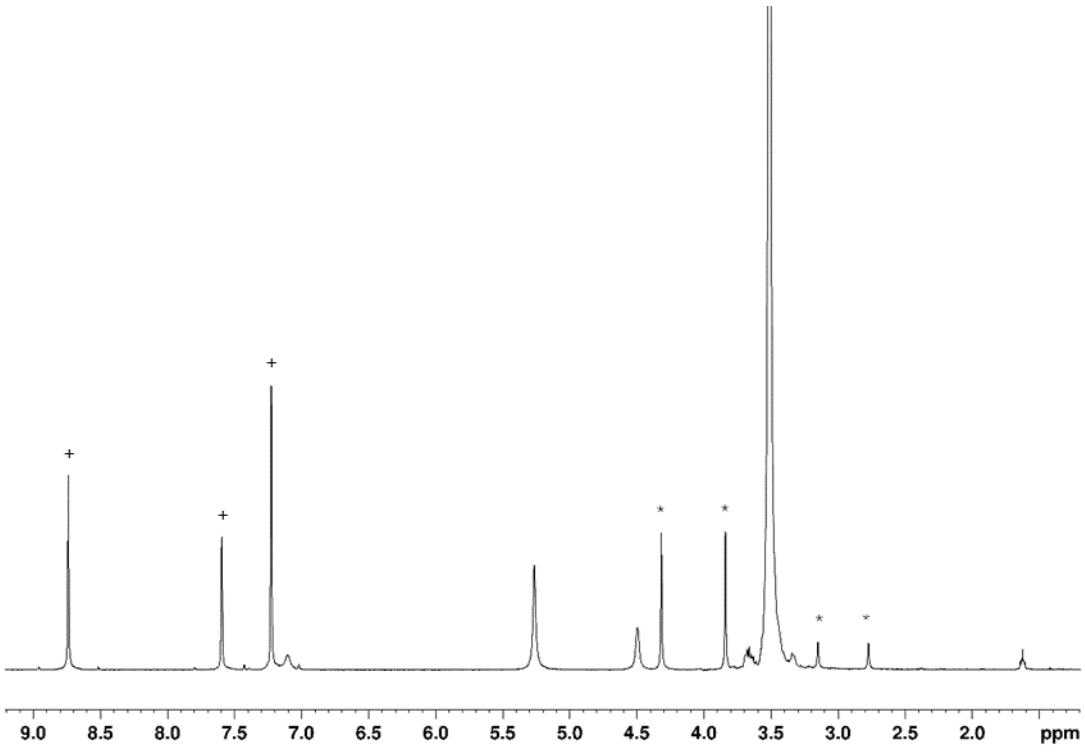

Figure 4.3: ^{1}H NMR spectrum of a d_5-pyridine solution of the crystals obtained from a reaction between **13** and BzK in the presence of 18-crown-6. The phosphine and phosphide doublets are highlighted with * and the solvent peaks with +.

These resonances collapse to singlets upon phosphorus decoupling. The other resonances belong to the two amines and one amide in the isomers as well as a large peak corresponding to 18-crown-6. The $^{13}C\{^{1}H\}$ NMR spectrum revealed a broad peak at 162.2 ppm. Due to the broadness, it was not possible to determine the P–C coupling constant. This resonance has been assigned to the carbonyl carbon of the nitrogen deprotonated product.

Compound **13** possess three possible deprotonation sites that can yield six possible isomers of **15** either in their *cis* or *trans* forms relative to the C–N bond as depicted in Figure 4.4.

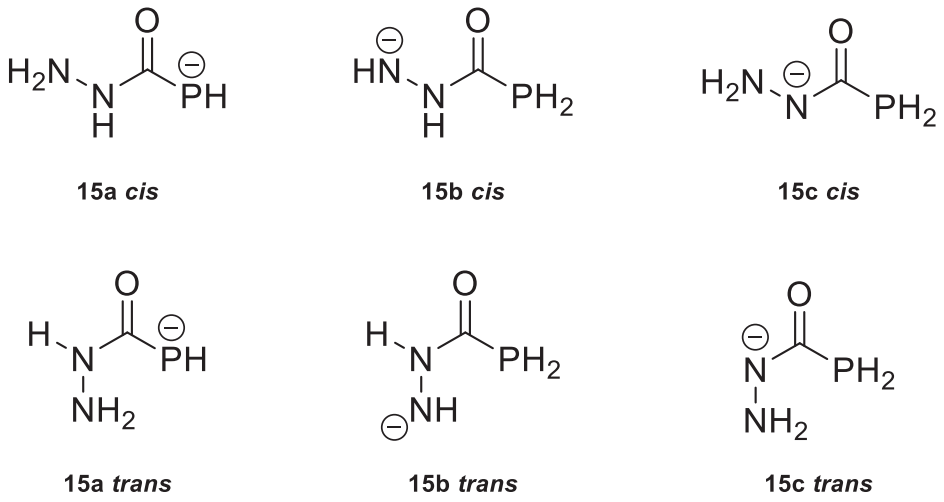

Figure 4.4: Possible deprotonation products of **15**.

The energy of both *cis* and *trans* isomers of **15a**–**15c** were calculated using density functional theory (DFT) and the results are presented in Table 4.2. The total bonding energies of the possible computed structures of **15** revealed that the phosphide **15a *cis*** is the most stable isomer. For that reason, its energy has been set as zero to ease comparison with the other possible products.

Table 4.2: Calculated total bonding energies of the possible deprotonation products of **15** given in kJ mol^{-1}, with ΔG relative to **15a *cis*** given in brackets.

	15a	**15b**	**15c**
cis	– 1486494.5 (0)	– 1486324.8 (169.7)	– 1486436.5 (58.0)
trans	– 1486415.4 (79.0)	– 1486437.2 (57.2)	– 1486411.5 (82.9)

Based on the results obtained from the calculations, we can assign the broad doublet in the ^{31}P NMR spectrum as being **15a *cis***, as this is the most stable phosphide isomer. Even though **15b *trans*** presents the lowest energy among the four possible

nitrogen deprotonated species, it is not possible to observe coupling to the proton attached to the α nitrogen atom. As it has been shown in Chapter 3, this coupling can be resolved in the case of *trans* phosphinecarboxamide, the triplet has, therefore, been assigned as **15c *cis***.

In the search for a better understanding of the dynamics of this reaction, a variable temperature NMR experiment was performed for the reaction mixture of **13**, KHMDS and 18-crown-6 in d_8-THF over the range of –80°C to +60°C taking 20°C increments up to 20°C and 10°C increments between 20°C and 60°C (Figure 4.5).

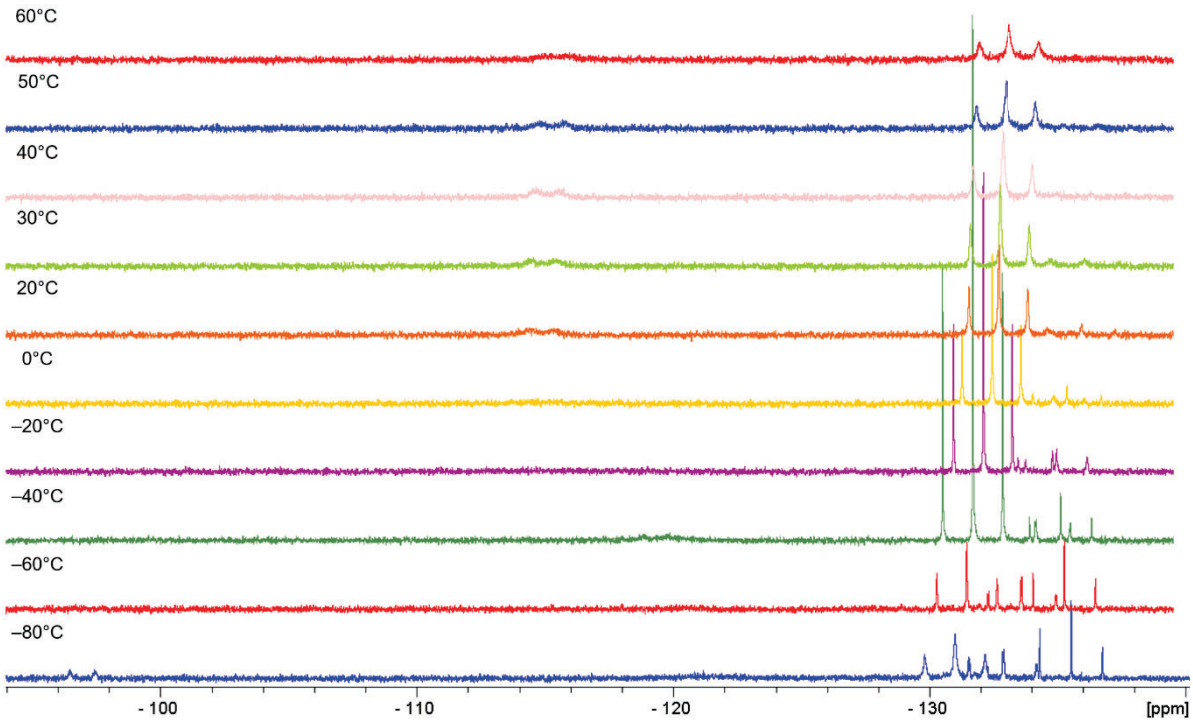

Figure 4.5: Plots of the variable temperature ^{31}P NMR experiment for the reaction of **13**, KHMDS and 18-crown-6 in d_8-THF from –80°C to +60°C.

At –80°C, it is possible to observe a broad doublet at –97 ppm ($^1J_{P–H}$ = 157 Hz), a triplet at –130.1 ppm ($^1J_{P–H}$ = 190 Hz), a triplet of doublets at –132.9 ppm ($^1J_{P–H}$ = 217 Hz, $^3J_{P–H}$ = 8 Hz) and another triplet –135.6 ppm ($^1J_{P–H}$ = 197 Hz). The broad doublet shifts from –97 ppm to –114 ppm as the temperature increases and two of the triplets disappear over time leaving only one broad triplet at +60°C (Figure 4.6).

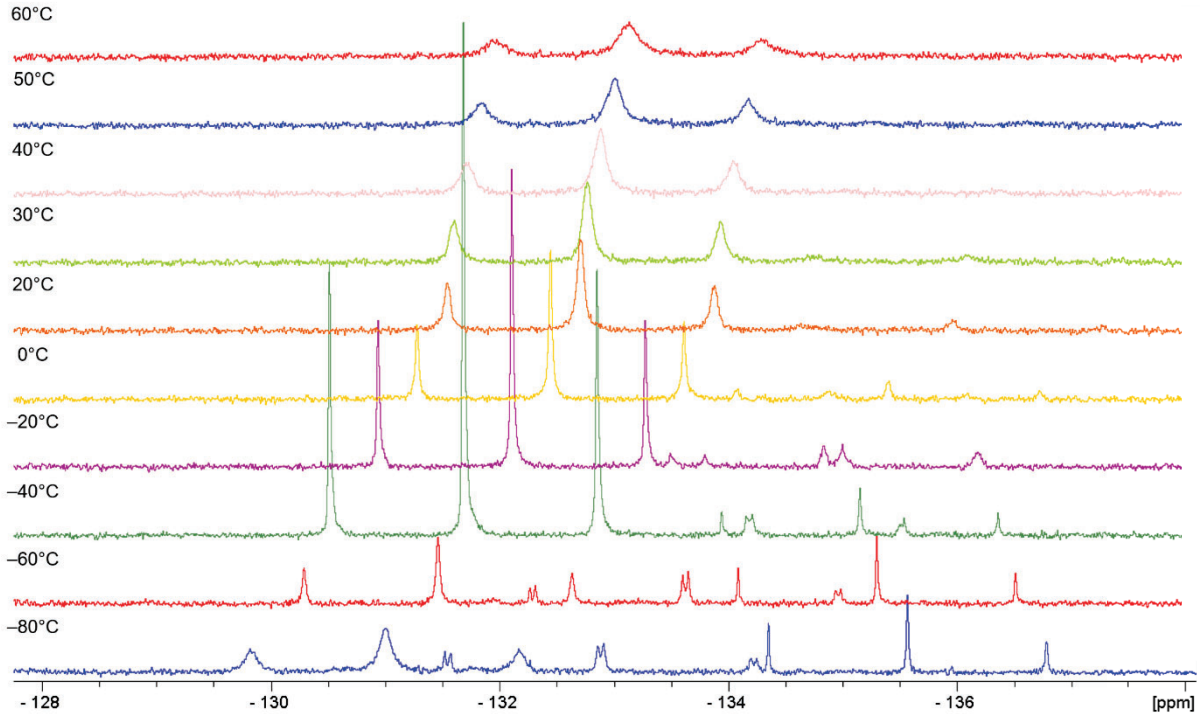

Figure 4.6: Enlarged section of the variable temperature ^{31}P NMR experiment for the reaction of **13**, KHMDS and 18-crown-6 in d_8-THF from –80°C to +60°C.

Based on the results obtained from the calculations and based on the findings described in Chapter 3, we can assign the triplet resonances at –130.1, –132.9 and –135.6 ppm at –80°C as corresponding to **15c *cis***, **15b *trans*** and **15c *trans***, respectively. Interestingly, even though the broad doublet shifted 18 ppm upfield, no coalescence between the doublet and the triplet could be observed as the temperature was increased from –80°C to room temperature. Instead, it is possible to notice that the triplets assigned to **15b *trans*** and **15c *trans*** have disappeared and that only the resonance assigned as **15c *cis*** remains. This it suggests that at room temperature, a rapid equilibrium between all these three species might be occurring. Moreover, as the

sample is heated above room temperature, the remaining triplet starts to broaden as well, indicating that an exchange process is most likely taking place.

The inability to observe coalescence in this system indicates that if exchange is taking place, it is slow on the NMR timescale. To further investigate the behaviour of the products formed in this reaction, a $^{31}P\{^{1}H\}$ 1D-EXSY exchange spectroscopy NMR experiment was conducted. This experiment provides information about dynamic processes and was performed at room temperature. The spectra obtained are shown in Figure 4.7.

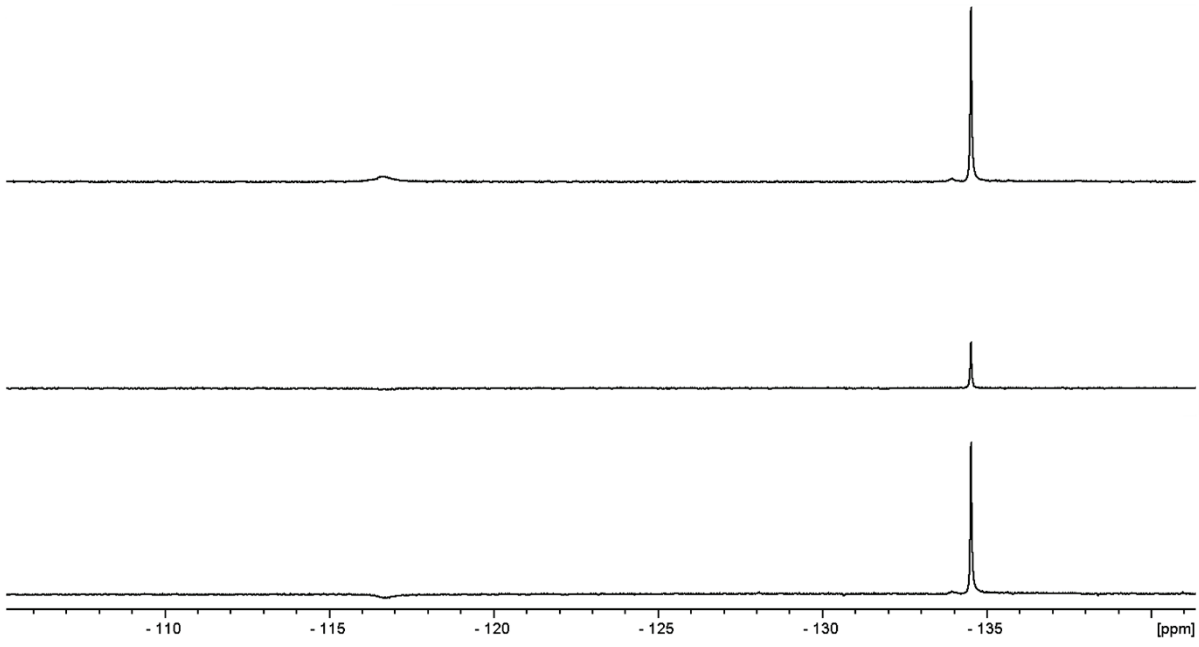

Figure 4.7: $^{31}P\{^{1}H\}$ selective inversion 1D-EXSY spectra of **15** at room temperature with initial inversion of the phosphide signal (bottom) followed by relaxation over time until the equilibrium (top).

In this experiment, the phosphide peak, on the left, was inverted while the signal of the phosphine, on the right, is monitored as a function of time as the inverted signal relaxes back to equilibrium. As the first peak relaxes, the intensity of the non-inverted signal is observed to decrease, with time, the phosphide resonance regains its initial

intensity while the phosphine increases its intensity, which suggests exchange between the two species at room temperature.

Single crystals suitable of X-ray diffraction were obtained from slow diffusion of hexane into a pyridine solution of the solid obtained. Interestingly, only compound **15a *trans***, one of the possible phosphides, crystalized from the solution (Figure 4.8). As expected, the potassium cation is accommodated by the 18-crown-6 pocket and interacts with the oxygen atom of the phosphinecarboxamide.

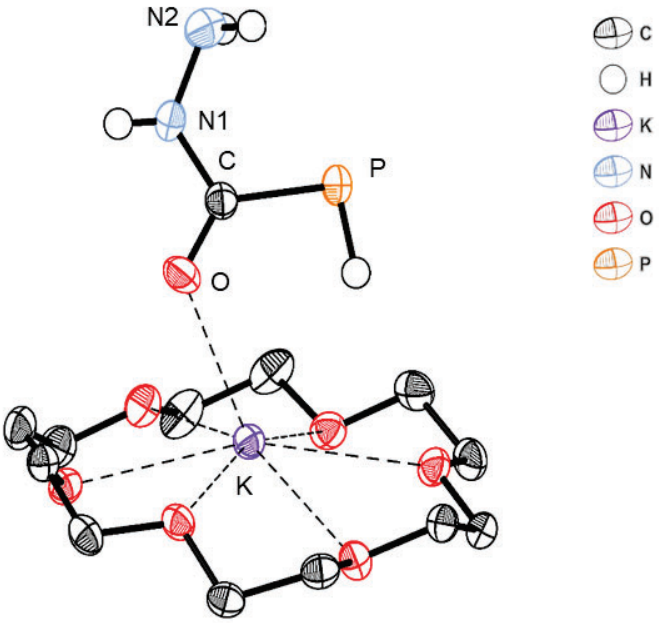

Figure 4.8: Crystal structure of **15a *trans***. P–C, C–N and C–O bond lengths are 1.793(3) Å, 1.383(3) Å and 1.248(3) Å respectively.

Bond metric data indicates that the P–C bond length is 1.793(3) Å, the C–N bond length is 1.383(3) Å and the C–O bond length is 1.248(3). In compound **15a *trans***, the P–C bond length is significantly shorter when compared to **13a** (1.864(av) Å) while both C–N and C–O bonds are elongated (C–N bond of 1.334(av) and C–O bond of 1.224(av) in **13a**). Selected bond lengths are presented in Table 4.3 to ease comparison with the **13a**.

Table 4.3: Selected bond lengths for **15a *trans*** and **13a** given in Å.

	P–C	C–N	C–O
15a *trans*	1.793(3)	1.384(3)	1.248(3)
13a	1.864(av)	1.334(av)	1.224(av)

These data suggest that upon deprotonation at the phosphorus atom, the degree of multiple bond character between phosphorus and carbon increases, while there is a decrease in the multiple bond character between the carbon and the α nitrogen. It should also be noted that the phosphide moiety and the proton attached to the α nitrogen exhibit a *trans* conformation relative to the C–N bond. Even though **15a *trans*** is 79 kJ mol^{-1} less stable than **15a *cis***, the fact that it crystalizes preferentially can be explained by the presence of hydrogen bonds with the neighbouring molecules that favours crystal packing. It should also be mentioned that the calculations done do not take into consideration the presence of the cation or the sequestering agent.

4.3.2 Deprotonation of the ethylenediamine bis-phosphinecarboxamide

Addition of two equivalents of KHMDS to **14** in pyridine in the presence of one or two equivalents of 18-crown-6 has been shown to promote exclusive deprotonation at the phosphorus atoms in this molecule, affording compound **16** (Scheme 4.2).

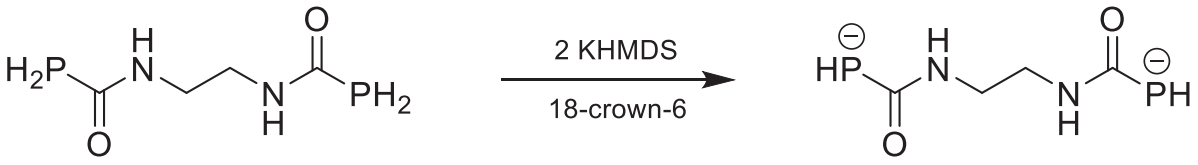

Scheme 4.2: Reaction of **14** with two equivalents of KHMDS in the presence of 18-crown-6 to yield **16**.

This selectivity is evident in the ^{31}P NMR spectrum, which exhibits a broad doublet centred at –98.8 ppm ($^{1}J_{P–H}$ = 150 Hz) (Figure 4.9). It is also possible to observe the presence of a broad triplet at –256.5 ppm ($^{1}J_{P–H}$ = 134 Hz) that corresponds to KPH_2, a decomposition product. These resonances collapse to singlets upon proton decoupling. Compound **16** is 34 ppm downfield-shifted relative to compound **14** (–132.9 ppm, $^{1}J_{P–H}$ = 208 Hz). As with **15**, the decrease in $^{1}J_{P–H}$ compared to the neutral species is attributed to the increase in electron density at the phosphorus atom.

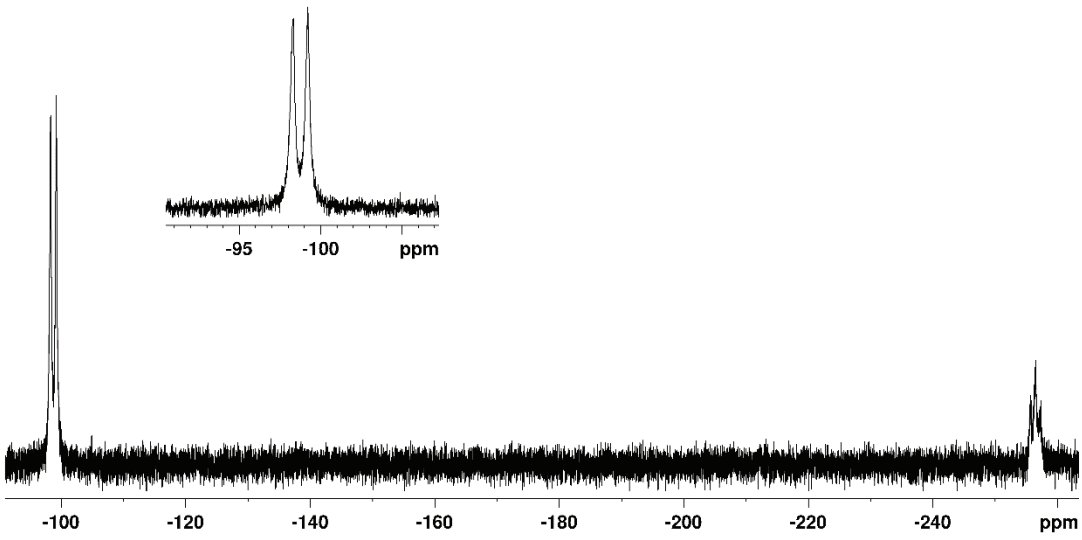

Figure 4.9: ^{31}P NMR spectrum of the reaction of **14** with two equivalents of KHMDS in the presence of 18-crown-6.

The ^{1}H NMR spectrum shows a doublet centred at 2.78 ppm ($^{1}J_{P–H}$ = 150 Hz) that corresponds to the phosphide moiety. The $^{13}C\{^{1}H\}$ NMR spectrum reveals a doublet at 203.8 ppm ($^{1}J_{C–P}$ = 59 Hz). The $^{1}J_{C–P}$ coupling constant found for this anion is significantly larger than that of the parent neutral species **14** ($^{1}J_{C–P}$ = 7 Hz) and is consistent with an increase in the s character of the P–C bond with the loss of a proton.

Other resonances present correspond to the bridging ethylene, amides, 18-crown-6 and HMDS.

The reaction of one equivalent of **14**, four equivalents of KHMDS and four equivalents of 18-crown-6 in pyridine gave rise to the same broad doublet and a triplet (in a 6 : 1 ratio) observed in the reaction of **14** with two equivalents of KHMDS. After four days, the major product was the triplet at –256.5 ppm shown in Figure 4.10. Therefore, we conclude that an excess of base causes decomposition of **16** over a short period of time to KPH_2. It is also possible to observe the presence of a doublet of triplets of equal intensities at –259.8 ppm that correspond to partial deuterium exchange at the phosphorus atoms of KPH_2, KPDH. These results suggest that even using more forceful conditions, it is not possible to access the product resulting from deprotonation at the nitrogen atoms.

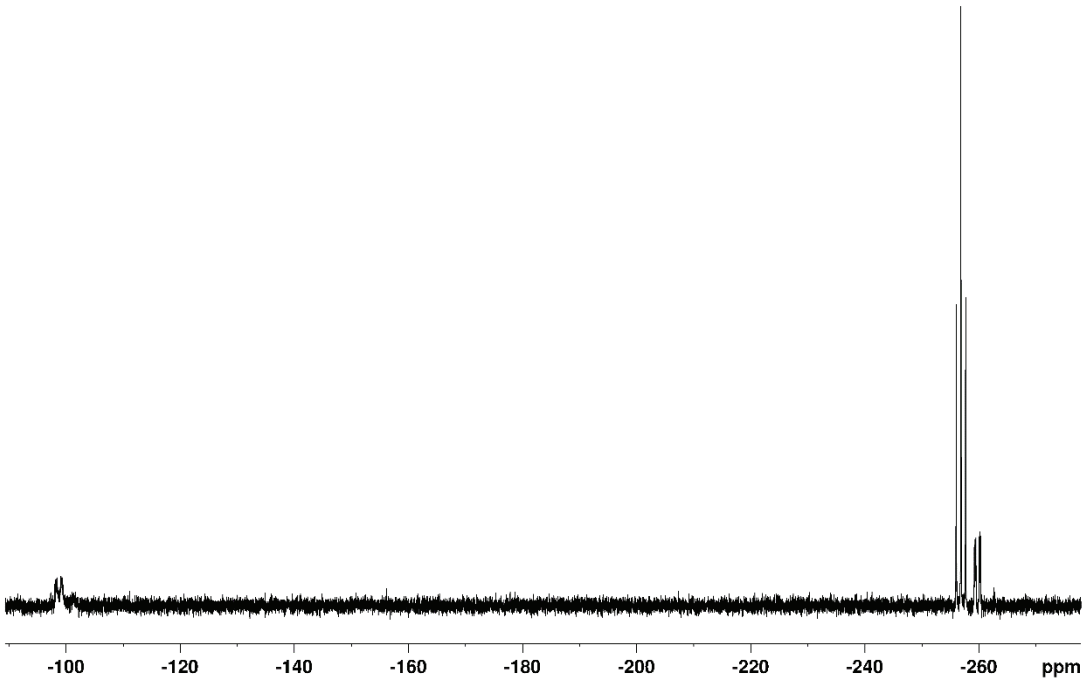

Figure 4.10: ^{31}P NMR spectrum of the reaction of **14** with four equivalents of KHMDS in the presence of 18-crown-6.

The energies of the two possible products of deprotonation at the phosphorus and nitrogen atoms were calculated using density functional theory (DFT). The results showed that deprotonation at the phosphorus is 81.6 kJ mol^{-1} more favorable than deprotonation at the nitrogen, corroborating the findings discussed previously.

4.4 Alkylation

The deprotonated species could be used as precursors to form secondary phosphines. In order to probe this, iodo methane (MeI) was chosen as a simple electrophile to generate *P*-functionalised phosphinecarboxamides.

4.4.1 Alkylation of 13

Iodomethane was added to compound **15** formed *in situ* by the reaction of **13** with KHMDS to yield the corresponding methylated species **17** (Scheme 4.3). It is worth keeping in mind that **13** was obtained as a mixture of the *cis* and *trans* isomers and, therefore both *cis* and *trans* isomers of the methylated products were obtained in solution, **17a** and **17b**, respectively.

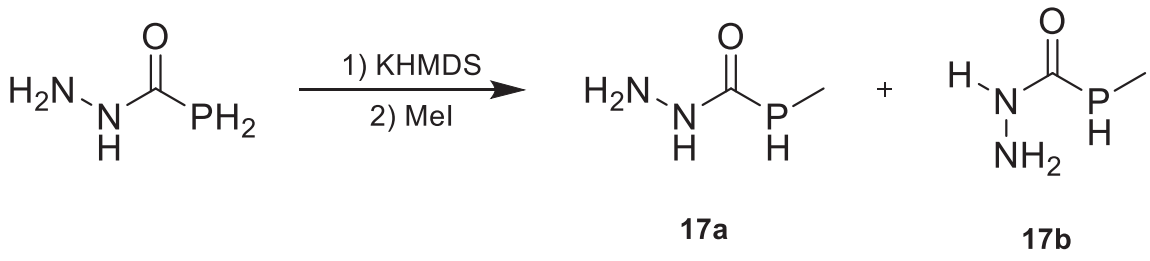

Scheme 4.3: Reaction of **13**, KHMDS and MeI to yield **17a** and **17b**.

The ^{31}P NMR spectrum revealed one major doublet of quartets at –85.3 ppm ($^{1}J_{P–H}$ = 207 Hz, $^{2}J_{P–H}$ = 3 Hz), as well as two other broad doublet of quartets at –86.6 ppm ($^{1}J_{P–H}$ = 113 Hz) and –84.2 ppm ($^{1}J_{P–H}$ = 106) (Figure 4.11). These resonances collapse to singlets upon phosphorus decoupling. The doublet and triplet resonances

of the two isomers of **15** are instead giving rise to doublets of quartets that are approximately 55 ppm downfield-shifted relative to **15**. These two findings suggest that methylation has taken place at the phosphorus centre upon addition of base.

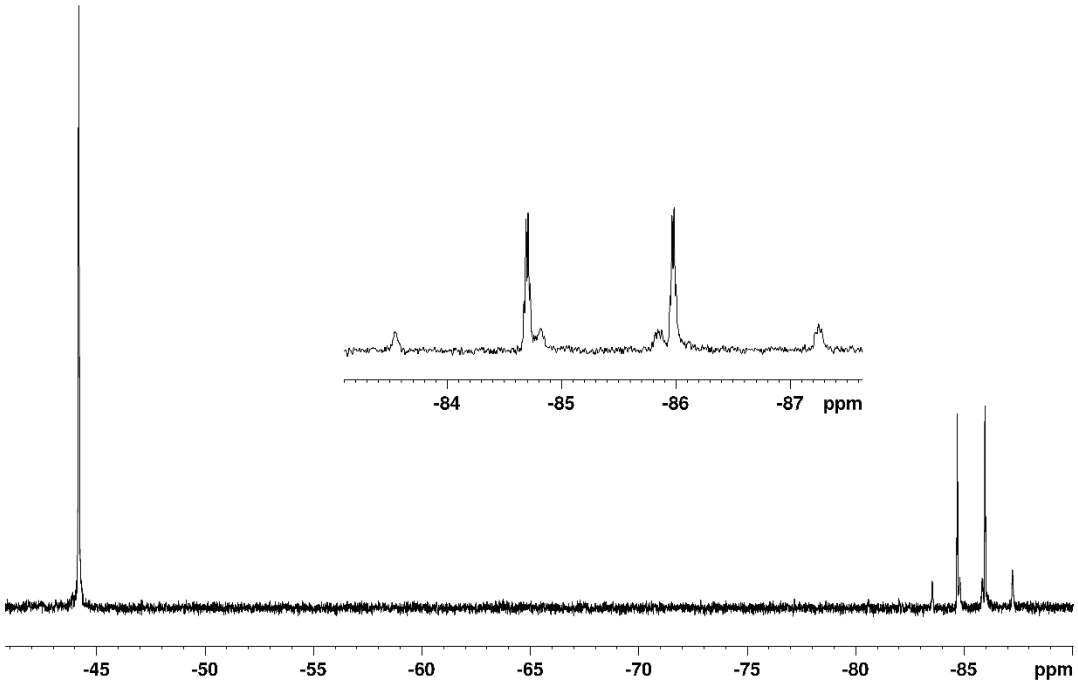

Figure 4.11: ^{31}P NMR spectrum of the reaction of **15**, KHMDS and MeI to yield **17**.

In the ^{1}H NMR spectrum it is possible to observe two clear sets of doublets of quartets centred at 4.04 ppm ($^{1}J_{P-H}$ = 207 Hz, $^{3}J_{H-H}$ = 8 Hz) and 4.58 ppm ($^{1}J_{P-H}$ = 227 Hz, $^{3}J_{H-H}$ = 7 Hz). These correspond to the *cis* and *trans* isomers of methylation at the phosphorus atom, compounds **17a** (*cis*) and **17b** (*trans*). Another very small doublet of quartets can also be observed at 4.11 ppm ($^{1}J_{P-H}$ = 206 Hz, $^{3}J_{H-H}$ = 7 Hz). Based on the results from calculations obtained in the previous section, this resonance was attributed either to the *cis* or *trans* isomer resulting from the methylation of **15b *trans*** or **15c *cis***. As the corresponding resonance for this compound in the ^{31}P NMR spectrum is broad, it is not possible to assign it unambiguously as the *cis* or *trans* isomer by NMR spectroscopy. Furthermore, the calculated energies for these isomers

are very close (57.2 and 58.0 kJ mol^{-1} respectively). As expected, these resonances collapse to quartets upon phosphorus decoupling.

It is important to note the presence of three doublets at 1.35 ppm ($^{2}J_{P-H}$ = 3 Hz), 1.38 ppm ($^{2}J_{P-H}$ = 3 Hz) and 1.46 ppm ($^{2}J_{P-H}$ = 3 Hz) that correspond to the methyl protons in the ^{1}H NMR spectrum. With the help an ^{1}H–^{31}P HSQC experiment, these doublets have been assigned as belonging to **17a *cis***, ***trans*** and to the nitrogen methylated product, respectively. The ^{13}C{^{1}H} NMR spectrum reveals doublets from the methyl carbons at 1.54 ppm ($^{1}J_{C-P}$ = 9 Hz) and 11.5 ppm ($^{1}J_{C-P}$ = 12 Hz) that, with the help of ^{1}H–^{13}C HSQC, have been attributed to **17a *cis*** and ***trans***, respectively. It was not possible to observe the corresponding resonance for the product formed by methylation at one of the nitrogen atoms. The carbonyl carbons could also be observed as doublets at 181.4 ppm ($^{1}J_{C-P}$ = 18 Hz) and 177.8 ppm ($^{1}J_{C-P}$ = 13 Hz). These resonances have been assigned with the help of ^{1}H–^{13}C HMBC as corresponding to **17a *cis*** and ***trans***, respectively.

The ^{31}P NMR spectrum also displays a septet at –44.2 ppm that corresponds to the product of double methylation of the phosphorus atom (Figure 4.11). This happens when there is an excess of KHMDS and MeI in solution. Initially the monoanionic species is formed and methylated. Excess base promotes a second deprotonation at the phosphorus that is then attacked by a second equivalent of electrophile.

4.4.2 Alkylation of 14

Iodomethane was added to compound **16** formed *in situ* by the reaction of **14** with two equivalents of KHMDS to yield the corresponding methylated product (Scheme 4.4). To our surprise, both *cis* and *trans* isomers were formed.

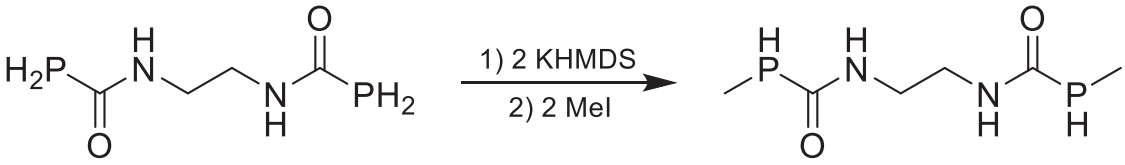

Scheme 4.4: Reaction of **16**, KHMDS and MeI to yield **18**.

The formation of the *cis* and *trans* methylated products are apparent in the ^{31}P NMR spectrum as two overlapping doublet of quartets centred at –81.2 and –81.1 ppm ($^{1}J_{P–H}$ = 208 Hz, $^{3}J_{H–H}$ = 3 Hz) (Figure 4.12). These resonances collapse to singlets upon proton decoupling and are approximately 51.5 ppm downfield-shifted relative to the protonated species and 17.6 ppm downfield-shifted relative to **16**.

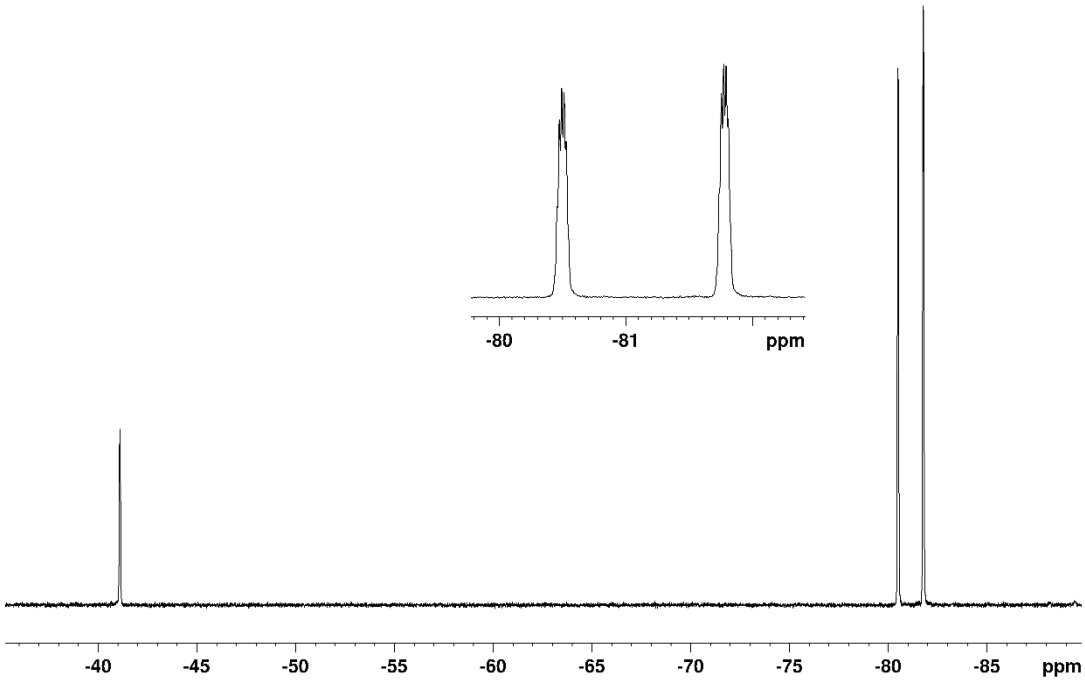

Figure 4.12: ^{31}P NMR spectrum of the reaction of **14**, two equivalents of KHMDS and two equivalents of MeI.

The ^{31}P NMR spectrum suggests that even though **14** is exclusively obtained as the *cis* isomer, both *cis* and *trans* isomers, **18a** and **18b**, are obtained from the methylation reaction (Figure 4.13). Other than the desired products obtained, it is also

possible to observe the presence of 10% of two overlapping septets at –41.0 ppm and –41.1 ppm correspond to the product of double methylation of the phosphorus atom and another 10% of unreacted starting material. The formation of this side product is due to the presence of an excess of both base and electrophile in solution.

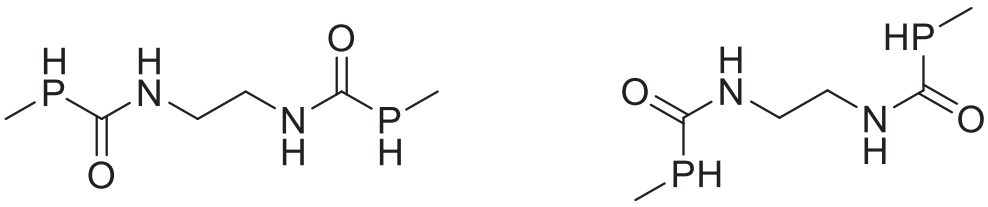

18a **18b**

Figure 4.13: *Cis* (**18a**) and *trans* (**18b**) isomers of **18**.

In the ^{1}H NMR spectrum the doublets originating from the PH_2 moiety have now been replaced by two overlapping doublets of quartets centred at 4.00 ppm ($^{1}J_{P–H}$ = 207 Hz, $^{3}J_{H–H}$ = 3 Hz) and 4.04 ppm ($^{1}J_{P–H}$ = 207 Hz, $^{3}J_{H–H}$ = 3 Hz) that correspond to the P–H proton in **18**. These resonances also overlap with the two methylene units from each isomer, but they become very clear in the $^{1}H\{^{31}P\}$ NMR spectrum where they collapse to quartets upon phosphorus decoupling. More importantly, the presence of two doublets at 1.32 ppm ($^{2}J_{H–H}$ = 3 Hz) and 1.34 ppm ($^{2}J_{H–H}$ = 3 Hz) that correspond to the methyl protons was noted. The $^{13}C\{^{1}H\}$ NMR spectrum reveals doublets from the methyl carbons at 1.72 ppm ($^{1}J_{C–P}$ = 8 Hz) and these appear to have the same chemical shift for the two isomers. The carbonyl carbons could also be observed as two overlapping doublets at 178.81 ppm ($^{1}J_{C–P}$ = 11 Hz) and 178.79 ppm ($^{1}J_{C–P}$ = 11 Hz). The other resonances present correspond to the two $–CH_2–$ spacers and the doubly methylated side product.

4.5 Coordination Chemistry

After the synthesis and characterization of the phosphinecarboxamides described thus far, we were interested in exploring the coordination chemistry of these compounds. Spectroscopic and crystallographic evidence discussed in the previous chapters suggest that the lone pair at the phosphorus atom of the phosphinecarboxamide moiety is mostly electronically isolated from the rest of the molecule. These findings suggest that phosphinecarboxamides can act as Lewis bases and coordinate through the phosphorus atom to metal centres.

4.5.1 Ruthenium complexes

4.5.1.1 Reaction of [Ru(*p*-cymene)Cl_2]$_2$ with 13

The reaction of one equivalent of [Ru(*p*-cymene)Cl_2]$_2$ dimer, where *p*-cymene = 4-isopropyltoluene, with two equivalents of **13**, the hydrazine mono-phosphinecarboxamide, in CH_2Cl_2 or THF at room temperature produced a bright red solution that was NMR silent. Difluorobenzene was alternatively used as a polar non-coordinating solvent, but the NMR remained silent. Finally, **13** was synthesised *in situ* in THF and [Ru(*p*-cymene)Cl_2]$_2$ was added to it. The volatiles were removed under vacuum leaving an orange solid behind which was further redissolved in d_6-dmso. The resulting bright red solution gave rise to two very weak and broad doublets in the ^{31}P NMR spectrum at 8.5 ppm ($^1J_{P-H}$ = 320 Hz) and 17.8 ppm ($^1J_{P-H}$ = 350 Hz) (Figure 4.14). These doublets collapse to singlets upon proton decoupling.

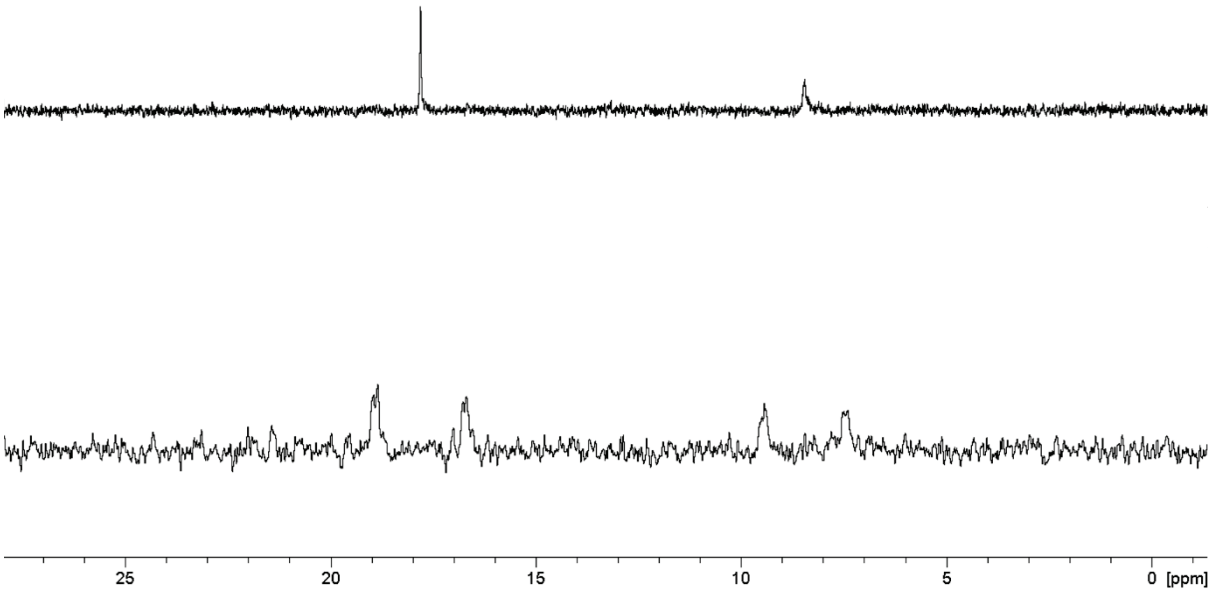

Figure 4.14: ^{31}P (bottom) and $^{31}P\{^{1}H\}$ (top) NMR spectra of the reaction of **13** and $[Ru(p\text{-cymene})Cl_2]_2$ in d_6-dmso.

The ^{31}P NMR spectrum suggests that the phosphorus atom has lost one of its protons and is bound to the ruthenium centre as a phosphide. Unfortunately, the products formed were very insoluble and prevented further solution state characterization. Furthermore, no crystals suitable for X-ray diffraction were obtained to confirm their nature. Nevertheless, we propose a possible structure for the product shown in Figure 4.15.

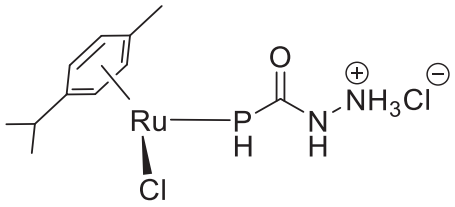

Figure 4.15: Proposed structure for the compound formed in the reaction of **13** and $[Ru(p\text{-cymene})Cl_2]_2$.

4.5.1.2 Reaction of [Ru(*p*-cymene)Cl_2]$_2$ with 14

The reaction of one equivalent of [Ru(*p*-cymene)Cl_2]$_2$ with one equivalent of **14**, the ethylenediamine bis-phosphinecarboxamide, in CH_2Cl_2 at room temperature gives to the primary phosphine complex [Ru(*p*-cymene)Cl_2]$_2$[$H_2PC(O)NH(CH_2)_2NHC(O)PH_2$] (**19**) as depicted in Scheme 4.5.

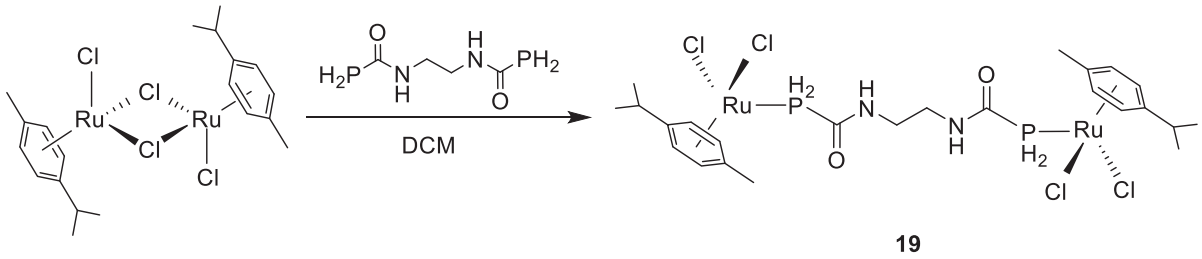

19

Scheme 4.5: Reaction of one equivalent of [Ru(*p*-cymene)Cl_2]$_2$ with two equivalents of **14** to yield **19**.

The ^{31}P NMR spectrum of **19** in CD_2Cl_2 reveals a triplet at –38.9 ppm ($^1J_{P–H}$ = 377 Hz) that collapses to a singlet upon proton decoupling (Figure 4.16). The new compound possess a downfield shift of 94 ppm when compared to the free ligand **14** (–132.9 ppm, $^1J_{P–H}$ = 208 Hz). The fact that the resonance remains a triplet in the ^{31}P NMR spectrum suggests that the PH_2 functionality is maintained upon coordination. Coordination is corroborated by the significant increase in the coupling constant value.

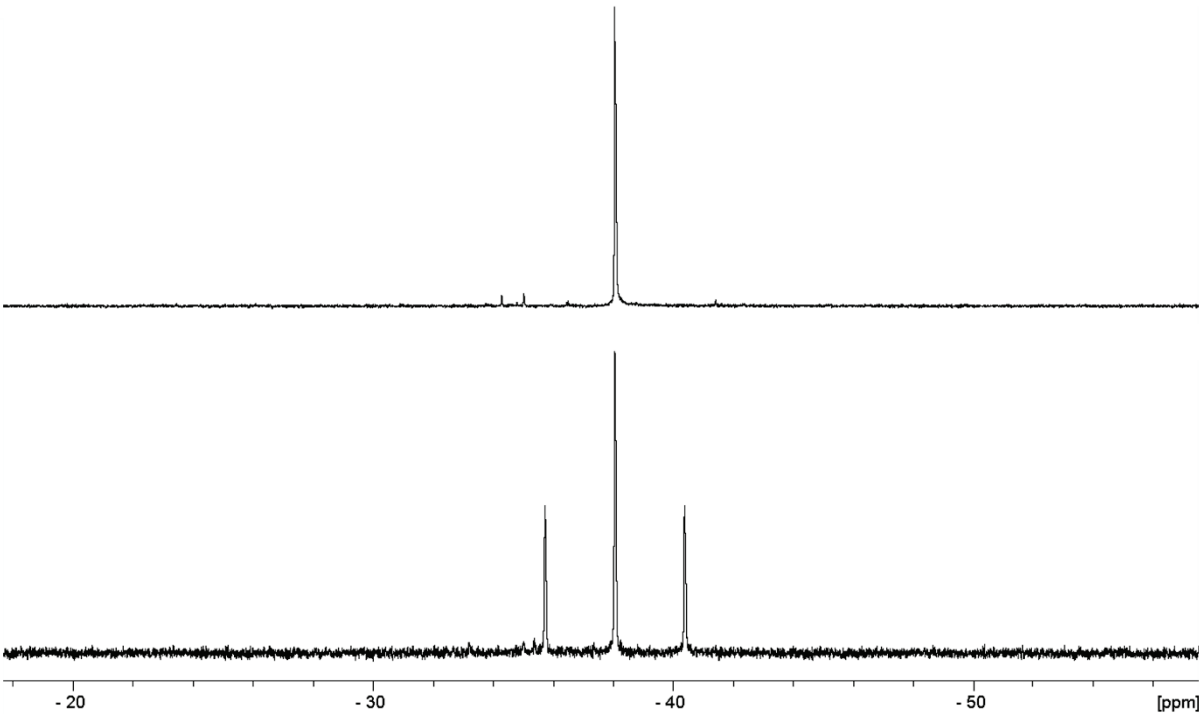

Figure 4.16: ^{31}P (below) and $^{31}P\{^{1}H\}$ NMR spectrum of **19** on CD_2Cl_2.

In the ^{1}H NMR spectrum of **19**, the doublet corresponding to the phosphine protons was shifted from 3.72 ppm ($^{1}J_{H-P}$ = 208 Hz) in the free ligand to 5.38 ppm and has the same coupling constant found in the ^{31}P NMR spectrum (Figure 4.17 (below)). The doublet collapses to a singlet upon selective phosphorus decoupling (Figure 4.17 (above)). The spectrum reveals only one chemical environment, suggesting that the complex formed is symmetrical.

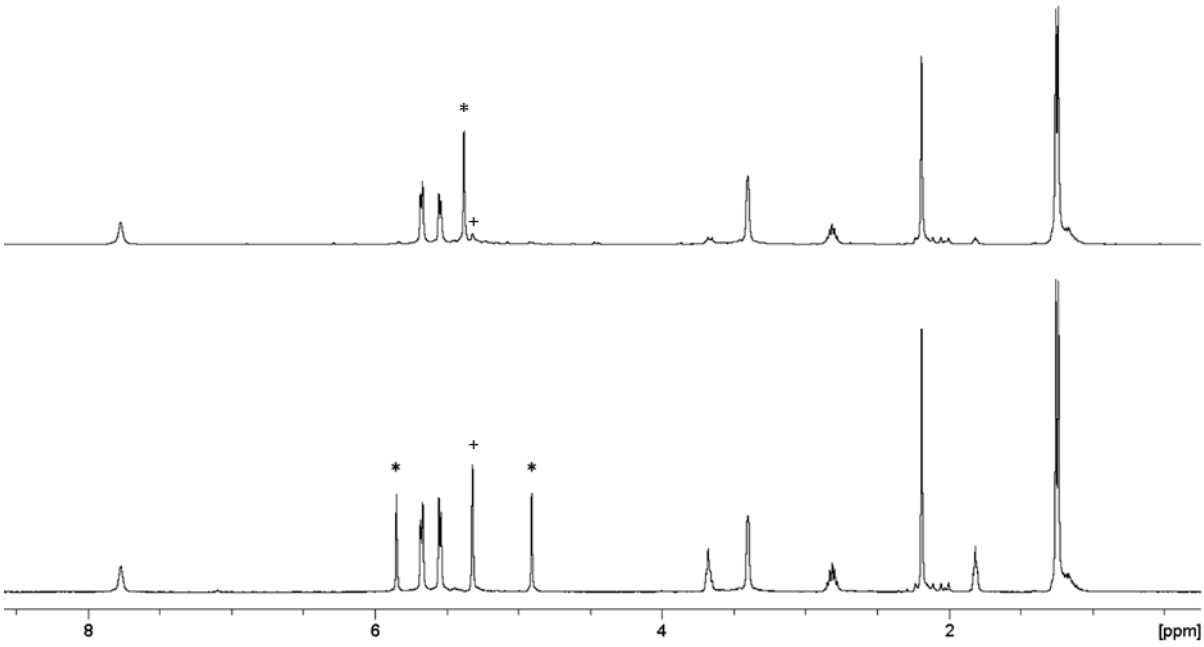

Figure 4.17: ^{1}H (below) and $^{1}H\{^{31}P\}$ (above) spectra of a CD_2Cl_2 solution of **19**. The resonances corresponding to the phosphine fragment are marked with * and the solvent peak with +.

The $^{13}C\{^{1}H\}$ NMR spectrum of **19** is consistent with the proposed product, with the most indicative resonance being a doublet at 166.3 ppm ($^{1}J_{C-P}$ = 54 Hz) corresponding to the carbonyl carbon of the phosphinecarboxamide moiety. Compared to the free ligand, where this resonance was found at 172.8 ppm ($^{1}J_{C-P}$ = 7 Hz), the significant increase in the coupling constant observed is also indicative of coordination.

The large downfield shift in the ^{31}P NMR signal as well as the increase in the coupling constants observed in all NMR spectra recorded relative to the free ligand **14** is consistent with coordination. This can be explained by the fact that phosphines are good σ-donors, thus the PH_2 moiety donates electron density to the ruthenium centres, therefore decreasing the electron density at the phosphorus atom.

Despite several attempts, no crystals suitable for X-ray diffraction experiments were obtained, with the product either forming an oil or micro crystalline solids. However, the results found are in good agreement with previously reported Ru(II) complexes of the ferrocenyl primary phosphines that exhibit similar spectroscopic data such as [(*p*-cymene)$RuCl_2(PH_2CH_2Fc)$] (δ = –27.7 ppm; *t*, $^1J_{P–H}$ = 359 Hz),[12] [(*p*-cymene)$RuCl_2(PH_2Mes^*)$] (Mes* = 2,4,6-$^t Bu_3C_6H_2$) (δ = –22.1 ppm; *t*, $^1J_{P–H}$ = 392 Hz),[13] and [(*p*-cymene)$RuCl_2(PH_2Fc)$] (δ = –27.6 ppm; *t*, $^1J_{P–H}$ = 394 Hz).[14]

4.5.2 Tungsten complexes

4.5.2.1 Reaction of $W(CO)_5$(NCMe) with 13

The reaction of **13** with one equivalent of $W(CO)_5$(NCMe) in THF at room temperature produced very broad peaks in the ^{31}P NMR spectrum between –80 ppm and –102 ppm. These peaks are approximately 35 ppm downfield-shifted relative to the ligand alone and are an indication that coordination via the phosphorus lone-pair might have happened, as –80 ppm to –102 ppm is within the expected region for this type of compound. However, these resonances are extremely broad and can barely be distinguished from the base line. Additionally, it is also possible to observe the peaks corresponding to uncoordinated **13**.

To try to overcome this issue, the solution was heated for one hour at 40°C but no change was observed in the ^{31}P NMR spectrum except for the appearance of a quartet at –245.7 ppm that indicates the formation of phosphine, which is unsurprising as phosphinecarboxamides are known to decompose upon heating. Consequently, even though the spectra obtained in this case indicate coordination of some sort, they do not offer conclusive evidence of coordination of this phosphinecarboxamide to the tungsten centre.

4.5.2.2 Reaction of $W(CO)_5(NCMe)$ with 14

In a further effort to probe the ability of phosphinecarboxamides as ligands, one equivalent of **14** was reacted with two equivalents of $W(CO)_5(NCMe)$ in THF affording the phosphorus coordinated product, **20** (Scheme 4.6).

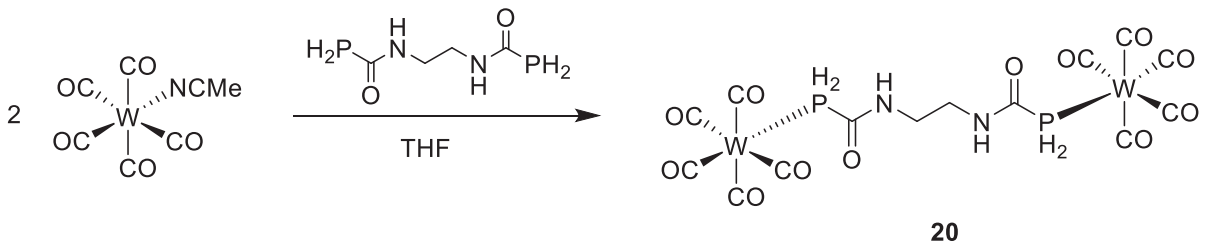

20

Scheme 4.6: Reaction of one equivalent of $W(CO)_5(NCMe)$ with two equivalents of **14** to yield **20**.

This reaction gave rise to two main resonances in the ^{31}P NMR spectrum. Two triplets centred at –91.2 ppm ($^1J_{P–H}$ = 349 Hz) and at –96.7 ppm ($^1J_{P–H}$ = 348 Hz) in a 1 : 1 ratio, which are shifted downfield by approximately 35 ppm relative to **14** (Figure 4.18). This shift is consistent with a reduction of electron density around the phosphorus atom upon coordination to the tungsten, leading to an increase in the coupling constant $^1J_{P–H}$.

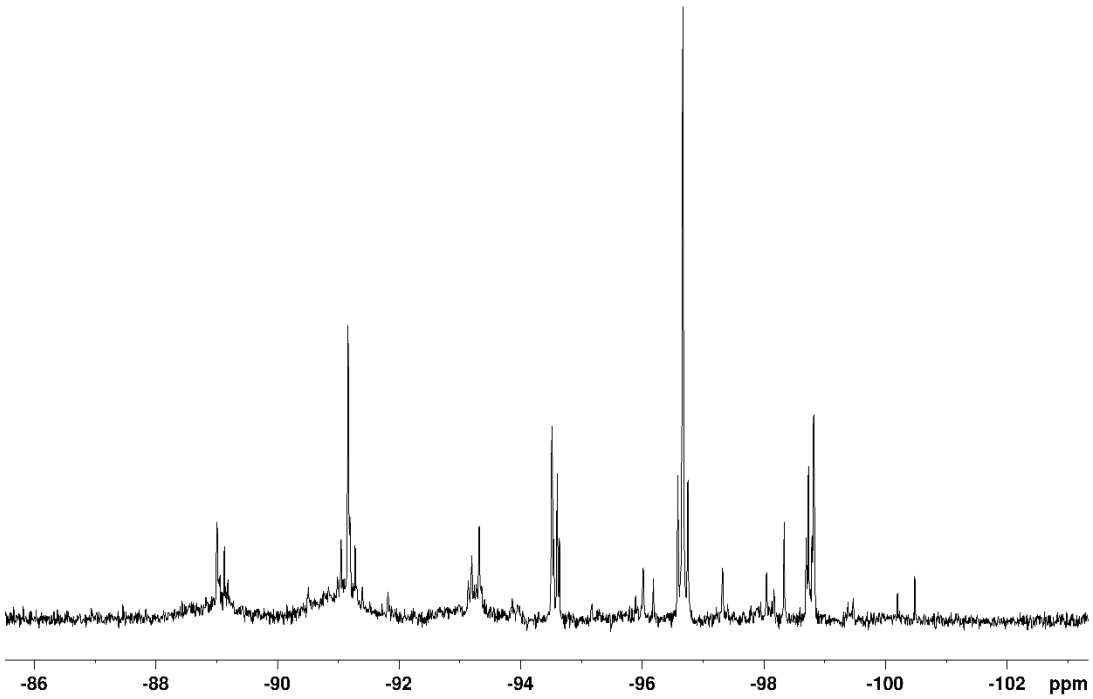

Figure 4.18: ^{31}P NMR spectrum of the reaction of two equivalents of $W(CO)_5(NCMe)$ with one equivalent of **14**.

These triplets collapse to singlets upon proton decoupling. In the $^{31}P\{^1H\}$ NMR spectrum it is also possible to observe coupling to the ^{183}W nucleus, noted by the presence of tungsten satellites with coupling constants of $^1J_{P-W}$ = 211 Hz (Figure 4.19), corroborating the phosphorus coordination to the tungsten centres.

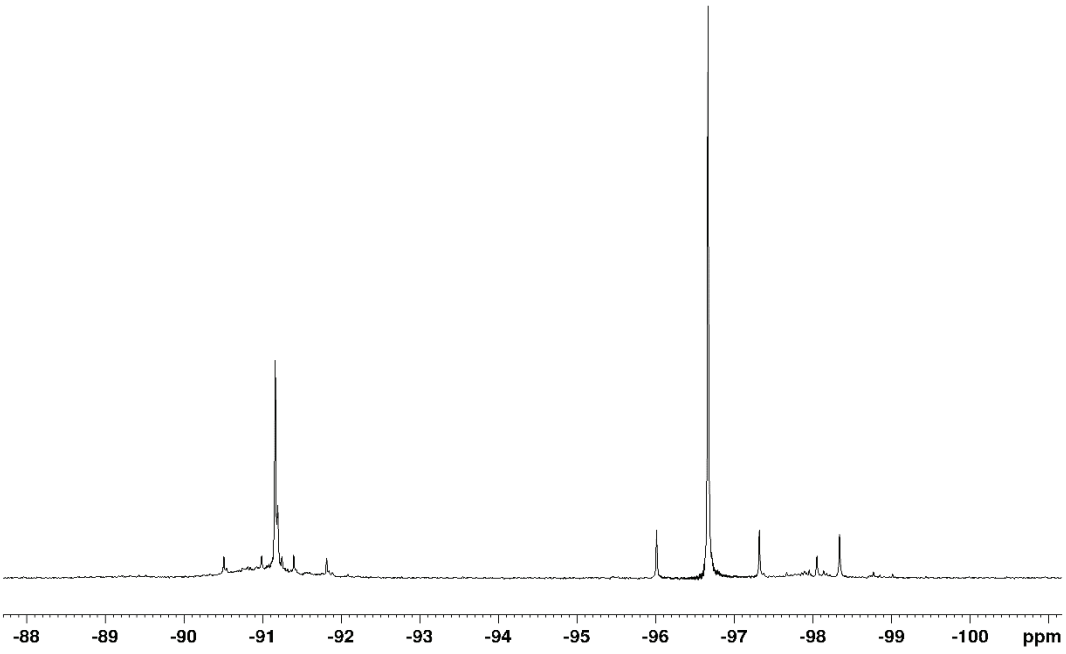

Figure 4.19: $^{31}P\{^{1}H\}$ NMR spectrum of the reaction of two equivalent of $W(CO)_5(NCMe)$ with one equivalent of **14**.

The ^{1}H NMR spectrum shows two main doublets centred at 5.19 ppm ($^{1}J_{P-H}$ = 348 Hz) and at 5.27 ppm ($^{1}J_{P-H}$ = 349 Hz) that collapse to singlets upon phosphorus decoupling. The downfield shift, the increase in the $^{1}J_{P-H}$ coupling constant, the presence of the tungsten satellites as well as the fact that the resonance remained a triplet in the ^{31}P NMR spectrum indicate that **14** has replaced the acetonitrile ligand in the coordination sphere of the tungsten and bonded through the lone-pair at the phosphorus atom.

These results suggest that one of the resonances observed in the ^{31}P NMR spectrum corresponds to the formation of the desired product **20**.[10] We propose that the second product formed is perhaps the one where **14** is acting as a chelating ligand through the phosphorus atoms to yield a nine membered metallacycle.[15,16] Numerous attempts to crystalize both products formed in this reaction in order to authenticate their structure were unsuccessful.

4.6 Conclusions

This chapter illustrated the versatility of phosphinecarboxamides as chemical reagents to produce an array of phosphorus containing compounds. It has been shown that, in general, despite having two possible deprotonation sites, the phosphorus-bound protons are more acidic than the amide protons and that phosphinecarboxamides are not able to tolerate very basic media, rapidly decomposing to KPH_2. The phosphides obtained can subsequently be functionalised and their reaction with simple electrophiles rendered *P*-functionalised phosphinecarboxamides. Furthermore, the reaction of the phosphinecarboxamides synthesised in the Chapter 3 with $[Ru(p\text{-cymene})Cl_2]_2$ and $W(CO)_5(NCMe)$ has shown that these compounds can also act as ligands through the phosphorus and coordinate to the metal centres either as a phosphine in the case of the ethylenediamine bis-phosphinecarboxamide or as a phosphide in the case of the hydrazine *mono*-phosphinecarboxamide with ruthenium metal.

4.7 References

[1] T. Clark, C. Landis, *Tetrahedron: Asymmetry* **2004**, *15*, 2123–2137.

[2] G. Hoge, B. Samas, *Tetrahedron: Asymmetry* **2004**, *15*, 2155–2157.

[3] K. V. Katti, H. Gali, C. J. Smith, D. E. Berning, *Acc. Chem. Res.* **1999**, *32*, 9–17.

[4] T. N. Hooper, M. A. Huertos, T. Jurca, S. D. Pike, A. S. Weller, I. Manners, *Inorg. Chem.* **2014**, *53*, 3716–3729.

[5] H. Dorn, R. A. Singh, J. A. Massey, A. J. Lough, I. Manners, *Angew. Chemie Int. Ed.* **1999**, *38*, 3321–3323.

[6] M. Brynda, *Coord. Chem. Rev.* **2005**, *249*, 2013–2034.

[7] B. Stewart, A. Harriman, L. J. Higham, *Organometallics* **2011**, *30*, 5338–5343.

[8] J. T. Fleming, L. J. Higham, *Coord. Chem. Rev.* **2015**, *297–298*, 127–145.

[9] N. Pillarsetty, K. Raghuraman, C. L. Barnes, K. V. Katti, *J. Am. Chem. Soc.* **2005**, *127*, 331–336.

[10] M. B. Geeson, A. R. Jupp, J. E. McGrady, J. M. Goicoechea, *Chem. Commun.* **2014**, *50*, 12281–12284.

[11] O. Kühl, *Phosphorus-31 NMR Spectroscopy: A Concise Introduction for the Synthetic Organic and Organometallic Chemist*, **2009**.

[12] N. J. Goodwin, W. Henderson, B. K. Nicholson, J. Fawcett, D. R. Russell, *J. Chem. Soc. Dalt. Trans.* **1999**, *0*, 1785–1794.

[13] A. T. Termaten, T. Nijbacker, M. Schakel, M. Lutz, A. L. Spek, K. Lammertsma, *Chem. - A Eur. J.* **2003**, *9*, 2200–2208.

[14] S. I. M. Paris, F. R. Lemke, R. Sommer, P. Lönnecke, E. Hey-Hawkins, *J. Organomet. Chem.* **2005**, *690*, 1807–1813.

[15] W. Malisch, C. Hahner, K. Grün, J. Reising, R. Goddard, C. Krüger, *Inorganica Chim. Acta* **1996**, *244*, 147–150.

[16] Z. Chen, H. W. Schmalle, T. Fox, O. Blacque, H. Berke, *J. Organomet. Chem.* **2007**, *692*, 4875–4885.

Chapter 5: Ferrocenyl Functionalised Phosphinecarboxamides

5.1 Introduction

5.1.1 Ferrocenyl Phosphines

Primary phosphines are usually highly reactive species and, therefore difficult to manipulate.[1] Nevertheless, they have been shown to be important starting materials for numerous reactions and have found various applications.[2–6] The introduction of sterically demanding substituents is the strategy most commonly employed to overcome their inherent reactivity and produce air-stable primary phosphines.[7,8]

There are several examples in the literature where a ferrocenyl backbone has been incorporated into primary phosphines. Initially it was expected that the ferrocenyl moiety would have a sterically demanding effect in the final compound, but it was observed that, from the series of ferrocenyl phosphines depicted in Figure 5.1, compounds A was air-sensitive and found to decompose within three days while B and C were indefinitely air-stable.[9–11] In fact, the solid state structure of B and C shows that the phosphine fragment is pointing away from the ferrocenyl group, preventing any interaction with the iron.[1] As a result, the stability of the latter compounds was then supposed to be more related to the existence of methylene and ethylene spacers than with the presence of the ferrocene backbone, but the reason underlying these findings is still not fully understood.[7]

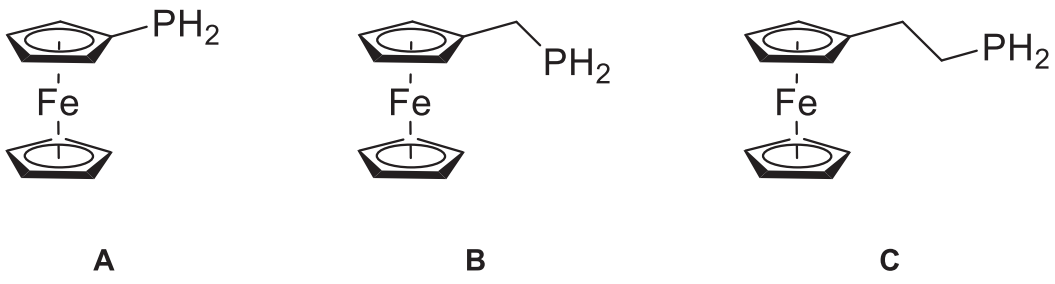

A B C

Figure 5.1: Examples of ferrocenyl phosphines described in the literature.

5.2 Aims

This chapter will extend the reactivity studies of the 2-phosphaethynolate anion to primary amines bearing a ferrocenyl group. The phosphinecarboxamides formed were fully characterized and their deprotonation, further functionalization and air stability were studied. Furthermore, their electronic properties were also investigated.

5.3 Ferrocenyl Phosphinecarboxamides

Two mono-substituted ferrocenyl amines were used, namely aminoferrocene and aminomethylferrocene. For the formation of phosphinecarboxamide, the later was reacted as the hydrochloride salt with [Na(dioxane)$_x$][PCO] whereas for the former, pyridinium triflate was used as a proton source for the former (Scheme 5.1).

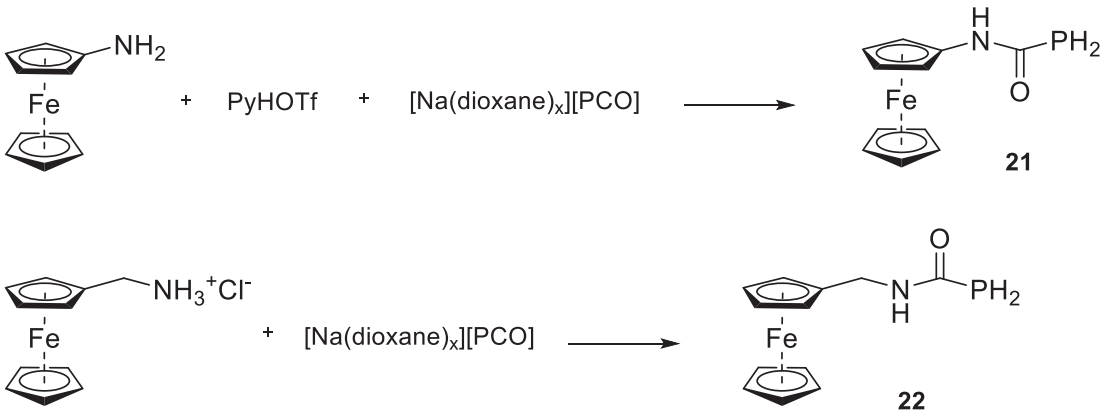

Scheme 5.1: Schematic representation of the synthesis of phosphinecarboxamides from aminoferrocene **21** (top) and aminomethylferrocene **22** (bottom).

The synthesis of **21** and **22** was performed in dichloromethane (DCM), a solvent in which [Na(dioxane)$_x$][PCO] is only sparingly soluble. Despite these solubility issues, the reactions proceed to yield the desired products, that are soluble in DCM. The by-products, NaOTf and NaCl, respectively, can be readily separated by filtration.

The ^{31}P NMR spectrum of **21** in d_5-pyridine exhibits a triplet at –129.9 ppm with a $^{1}J_{P–H}$ = 210 Hz coupling constant that collapses to a singlet upon proton decoupling, indicating the formation of the phosphinecarboxamide moiety (Figure 5.2).

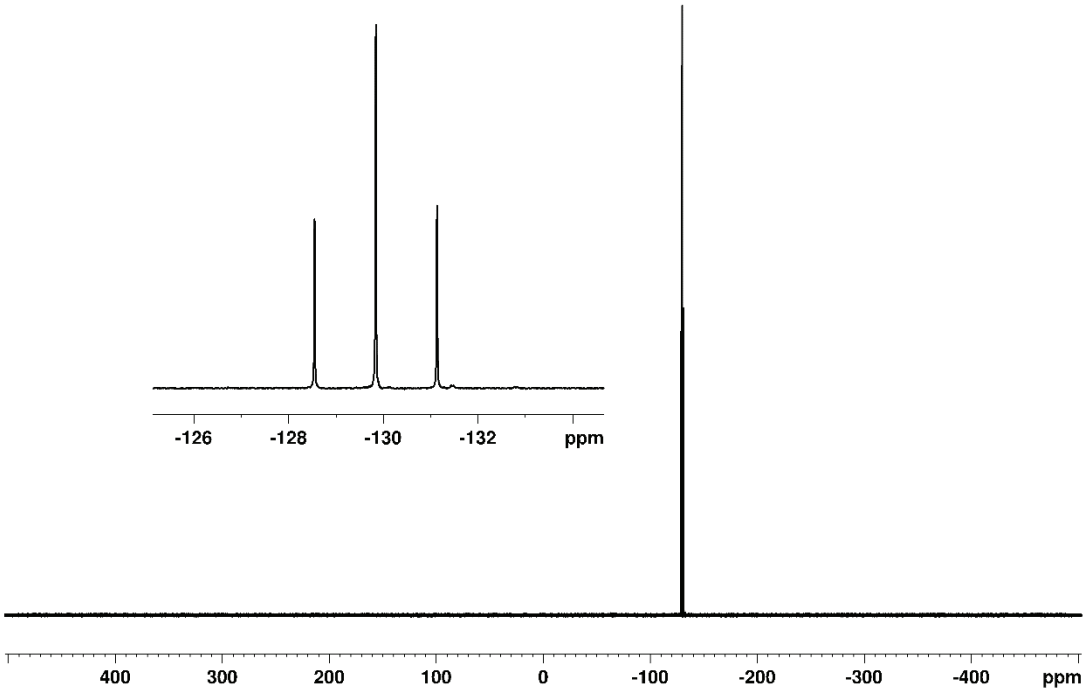

Figure 5.2: ^{31}P NMR spectrum of a d_5-pyridine solution of **21**.

The ^{1}H NMR spectrum shows a doublet centred at 3.87 ppm ($^{1}J_{H–P}$ = 210 Hz) that also collapses to a singlet upon selective ^{31}P decoupling, corroborating the formation of a phosphinecarboxamide (Figure 5.3). Additionally, the $^{13}C\{^{1}H\}$ NMR spectrum contained a doublet at 171.6 ppm ($^{1}J_{C–P}$ = 8 Hz) which corresponds to the carbonyl carbon (Figure 5.4).

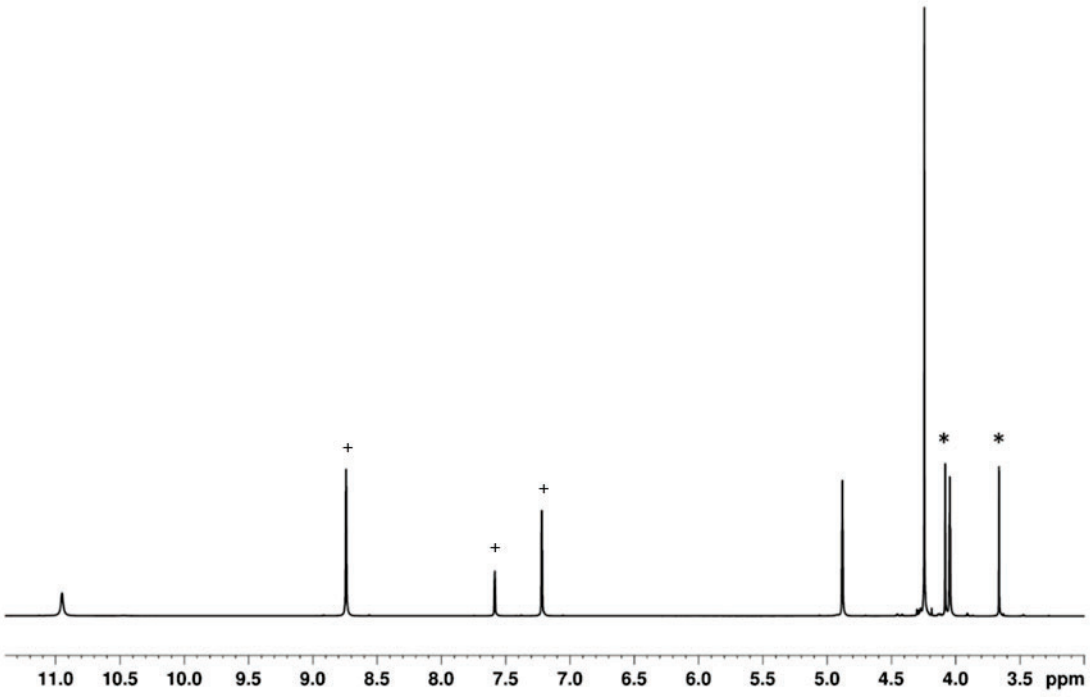

Figure 5.3: ^{1}H NMR spectrum of a d_5-pyridine solution **21**. The resonances corresponding to the phosphine fragment are marked with * and the solvent peaks with +.

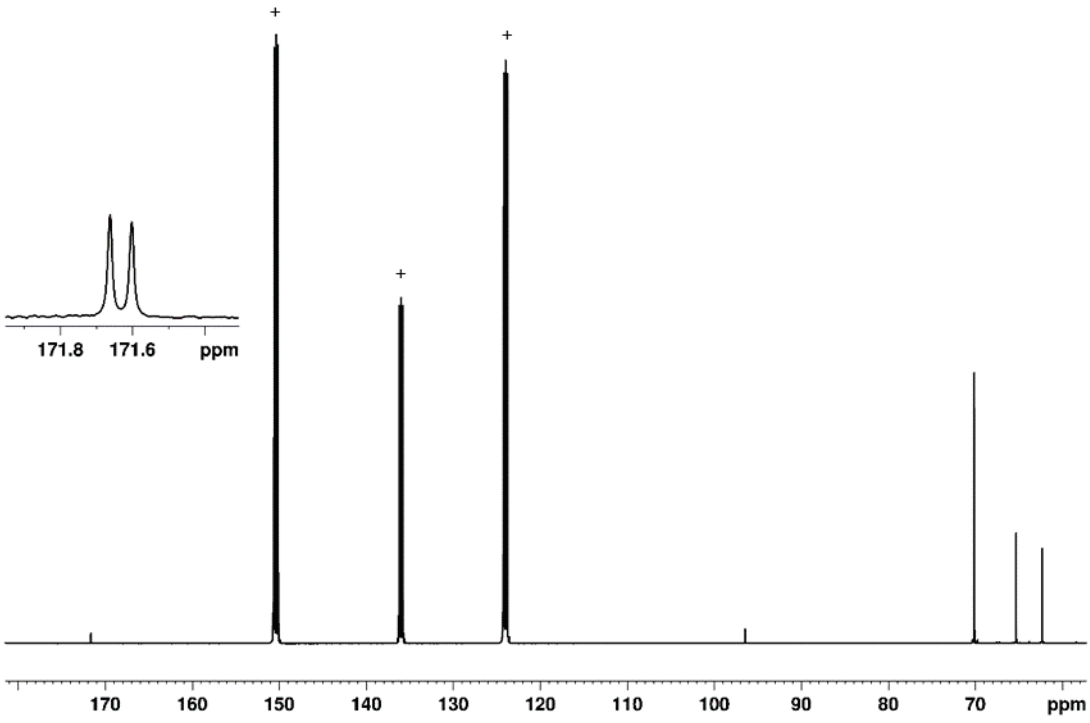

Figure 5.4: $^{13}C\{^{1}H\}$ NMR spectrum of **21** in d_5-pyridine. The doublet corresponding to the carboxamic carbon is shown in the inset. Solvent peaks are highlighted with +.

Due to its similarity with **21**, compound **22** shows analogous set of NMR spectroscopic data, also collected in d_5-pyridine. The ^{31}P NMR spectrum shows a triplet at –132.8 ppm ($^1J_{P–H}$ = 208 Hz) and the ^1H NMR spectrum shows a doublet centred at 3.78 ppm ($^1J_{H–P}$ = 208 Hz), both collapse to singlets upon proton or phosphorus decoupling, respectively, and correspond to the phosphorus and protons of the phosphine moiety. A doublet at 172.3 ppm ($^1J_{C–P}$ = 7 Hz) in the $^{13}C\{^1H\}$ NMR spectrum is assigned to the carbonyl carbon.

Crystals suitable for X-ray crystal structure determination of **21** and **22** were obtained from a concentrated toluene solution layered with hexane and from a concentrated toluene solution at –33 °C, respectively. In both cases, it was confirmed that the phosphine moiety and the proton attached to the nitrogen exhibit a *cis* configuration relative to the C–N bond (Figure 5.5 and Figure 5.6). Bond metric data is consistent with the examples described in the previous chapters, as well as with the parent phosphinecarboxamide species.[12] For compounds **21** and **22**, the P–C bond lengths are 1.859(4) and 1.867(2), respectively, with the corresponding C–N bond distances of 1.343(4) and 1.333(2), suggesting a P–C single bond a C–N bond with multiple bond character. These data are compared to that of the parent phosphinecarboxamide $H_2NC(O)PH_2$ in Table 5.1

Table 5.1: Selected bond lengths for **15a *trans*** and **13a** given in Å.

	P–C	**C–N**
21	1.859(4)	1.343(4)
22	1.867(2)	1.333(2)
$H_2NC(O)PH_2$	1.865(1)	1.329(2)

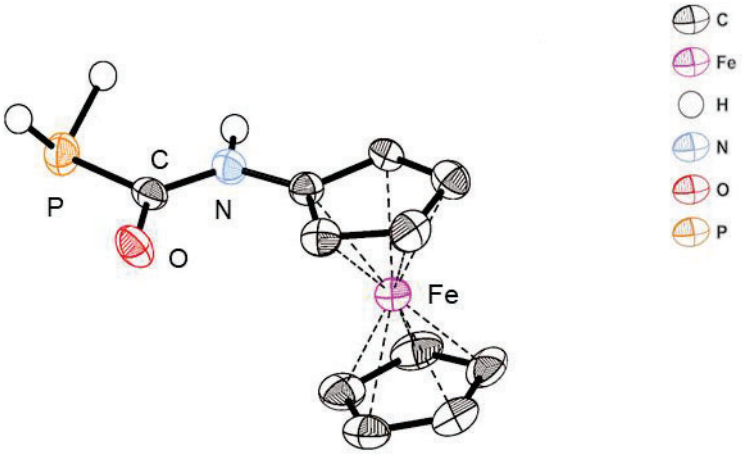

Figure 5.5: Crystal structure of **21**.

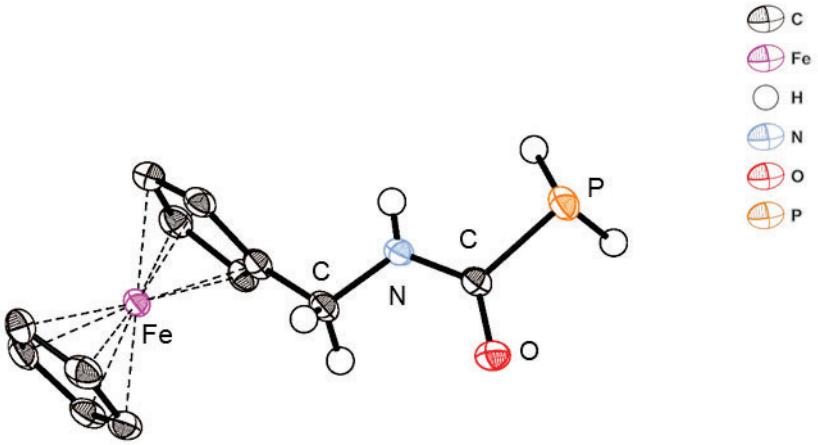

Figure 5.6: Crystal structure of **22**.

5.3.1 Air Stability

To test the air stability of these compounds, **21** and **22** were dissolved in d_5-pyridine and the NMR tubes were opened to air overnight every day for a period of two weeks. The solutions were monitored by ^{1}H and $^{31}P\{^{1}H\}$ NMR spectroscopy.

After a 15 days period, **21** showed no evidence of phosphine or phosphine oxide in the $^{31}P\{^{1}H\}$ NMR, indicating that no oxidation of the phosphinecarboxamide moiety

has occurred. However, it is possible to observe a slight decrease in the intensity of the only peak present over time (Figure 5.7). Additionally, some precipitate started forming at the bottom of the NMR tube after 8 days. These last two observations can be explained by slow hydrolysis of the phosphinecarboxamide moiety by loss of HPCO, which is a very unstable species at room temperature and polymerizes.[13] The ^{1}H NMR is consistent with this assertion as there is no significant change in the spectrum over time other than the decrease in intensity and the appearance of a very broad peak at 5.12 ppm after 3 days which was attributed to the presence of water (Figure 5.8).

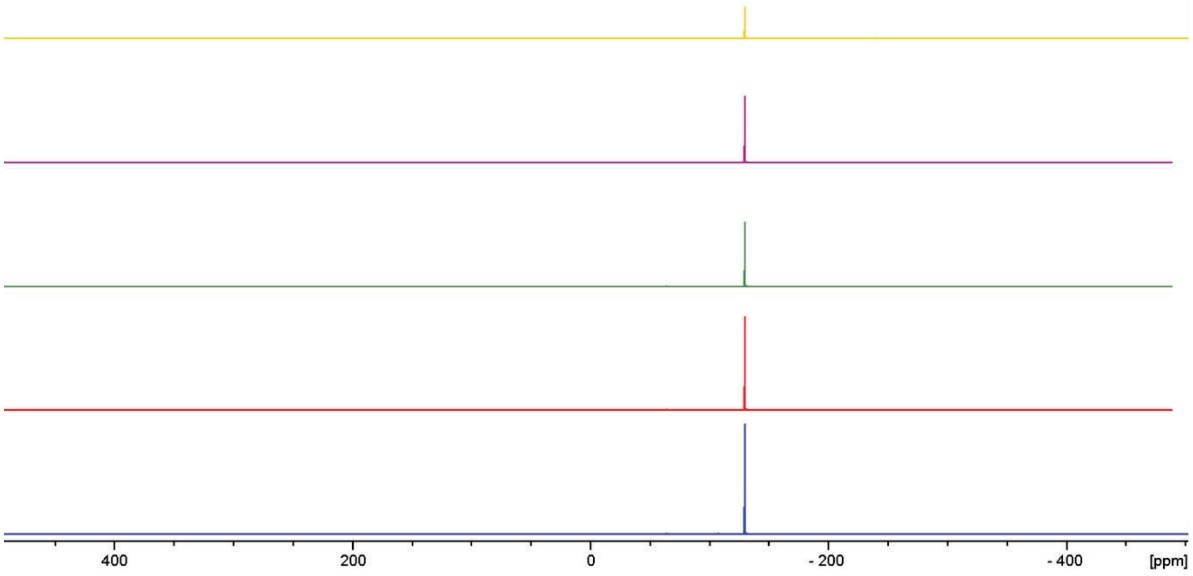

Figure 5.7: $^{31}P\{^{1}H\}$ NMR spectra of a d_5-pyridine solution of **21** after being exposed to air. From the bottom to top: day 1, 2, 3, 9 and 15.

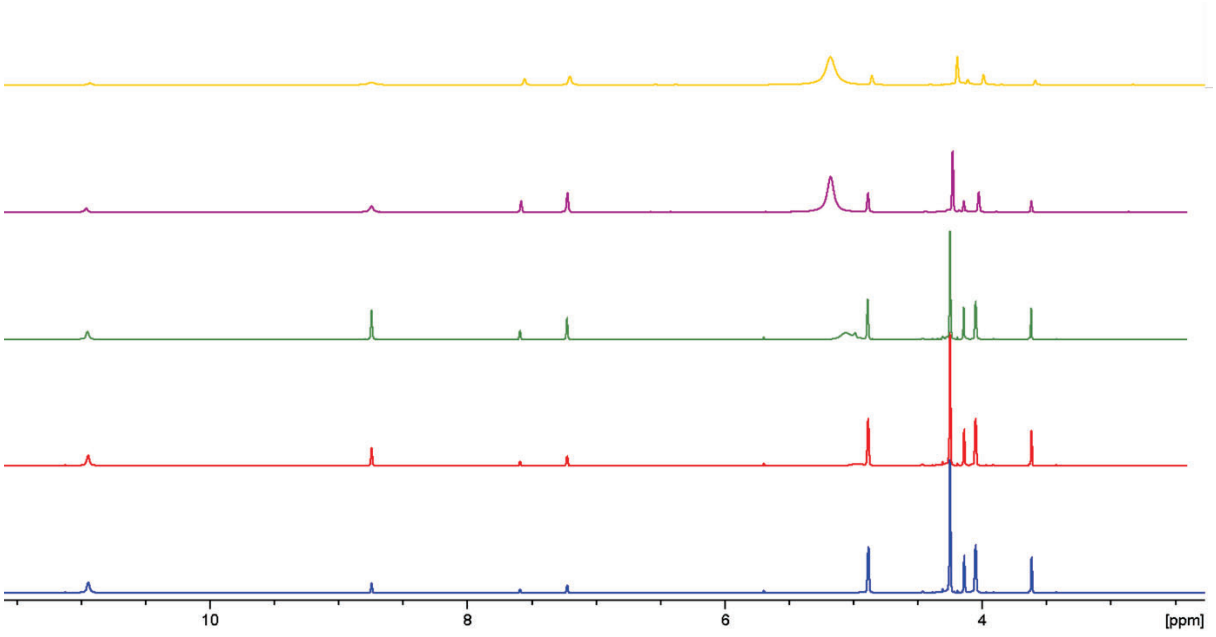

Figure 5.8: ^{1}H NMR spectra of a d_5-pyridine solution of **21** after being exposed to air. From the bottom to top: day 1, 2, 3, 9 and 15.

Similarly, after a two weeks period, **22** showed no evidence of oxidation of the phosphinecarboxamide as evident from the $^{31}P\{^{1}H\}$ NMR spectrum (Figure 5.9). However it was also possible to observe a slight decrease in the intensity of the peak over time. The ^{1}H NMR spectrum also show the appearance of the broad peak at 5.12 ppm after two days (Figure 5.10). These observations are consistent with slow hydrolysis of the phosphinecarboxamide moiety by loss of HPCO, followed by polymerization.

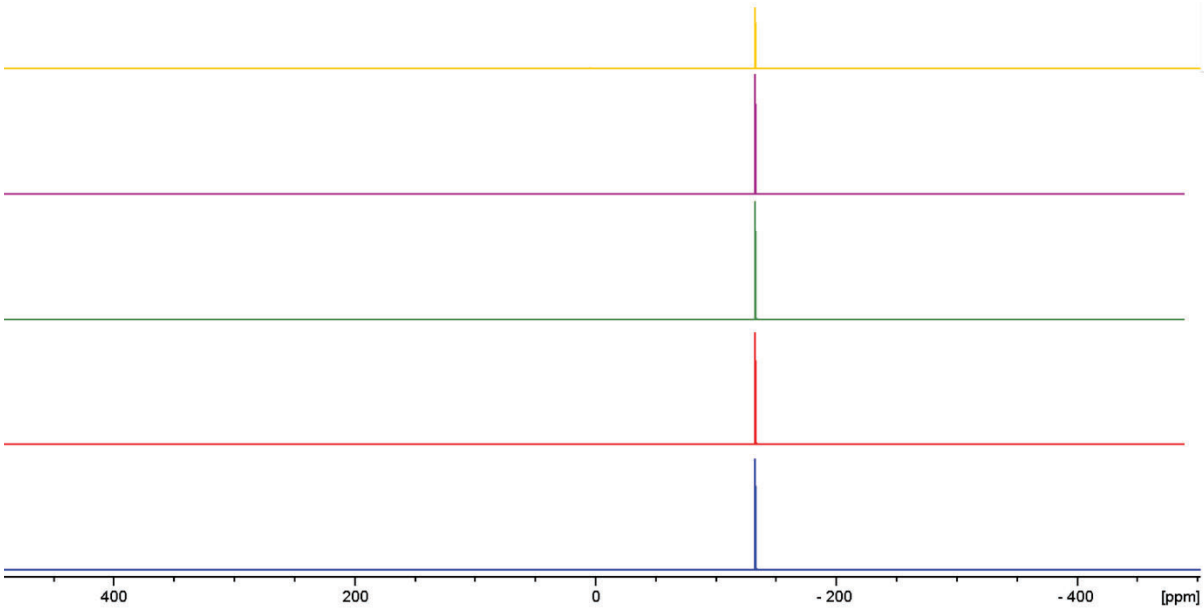

Figure 5.9: $^{31}P\{^{1}H\}$ NMR spectra of a d_5-pyridine solution of **22** after being exposed to air. From the bottom to top: day 1, 2, 3, 6 and 15.

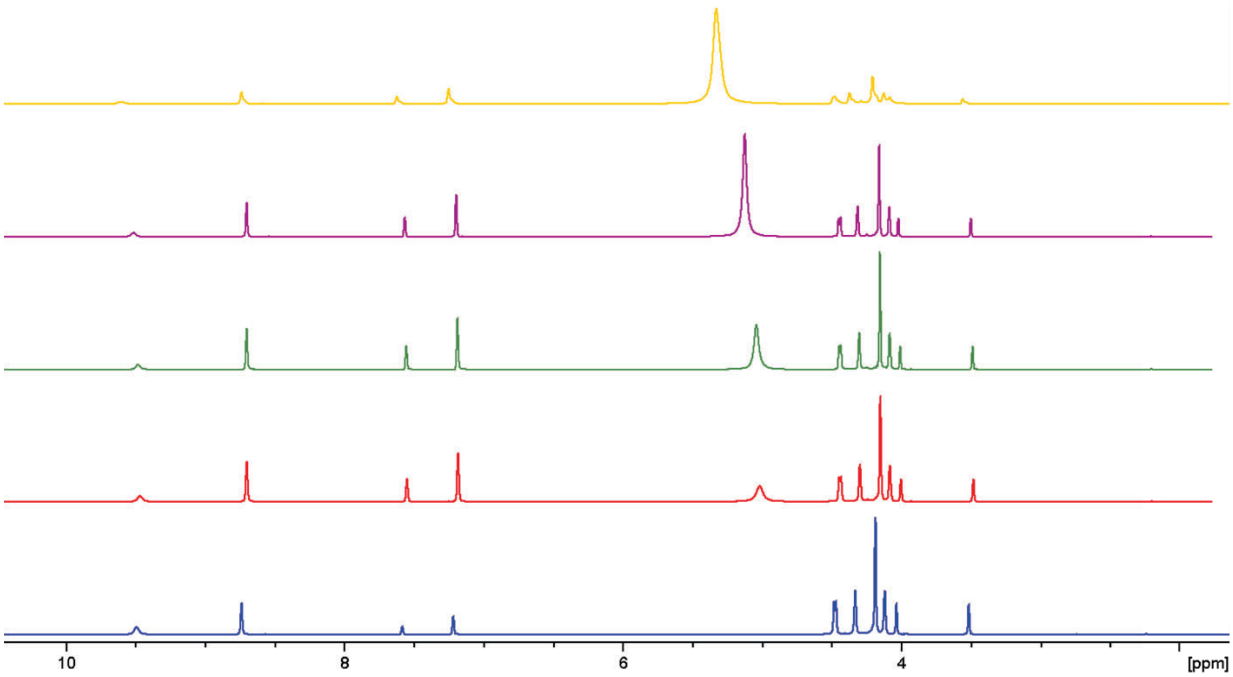

Figure 5.10: ^{1}H NMR spectra of a d_5-pyridine solution of **22** after being exposed to air. From the bottom to top: day 1, 2, 3, 6 and 15.

5.3.2 Electrochemical Studies

All measurements in this section were performed in a THF solution, with $[NBu_4][PF_6]$ used as an electrolyte. Voltammograms were recorded using a glassy

carbon working electrode, a platinum wire counter electrode and a silver wire as a quasi-reference electrode. The reference electrode was calibrated with cobaltocenium hexafluorophosphate, that was added to the solutions after an initial measurement.

$[NBu_4][PF_6]$ (190 mg, 0.5 mmol) was added to THF (5 mL) and stirred until dissolved. A background scan of the solution was performed before the measured compound was added (**21**: 1.3 mg, 5 μmol; **22**: 1.4 mg, 5 μmol). Measurements were taken using a number of different scan rates (1000, 500, 300, 200, 100, 50 (mV/s)). Cobaltocenium hexafluorophosphate (0.5 mg, 1.5 μmol) was then added and another scan of the solution was run. Cyclic voltammetry data was collected on compounds **21** and **22** to assess their redox properties. All measurements have been referenced against the $Co(Cp)^{+/0}$ couple.

Figures 5.11 and 5.12 show one of the cycles recorded for compounds **21** and **22** using a scan rate of 100 mV/s. From this data, it is possible to calculate the half-wave potential, $E_{1/2} = 0.5(E_{pc} + E_{pa})$, of the two compounds relative to $Co(Cp)^{+/0}$, as well as the ratio of the peak cathodic and anodic currents (i_{pc}/i_{pa}) (Table 5.2).

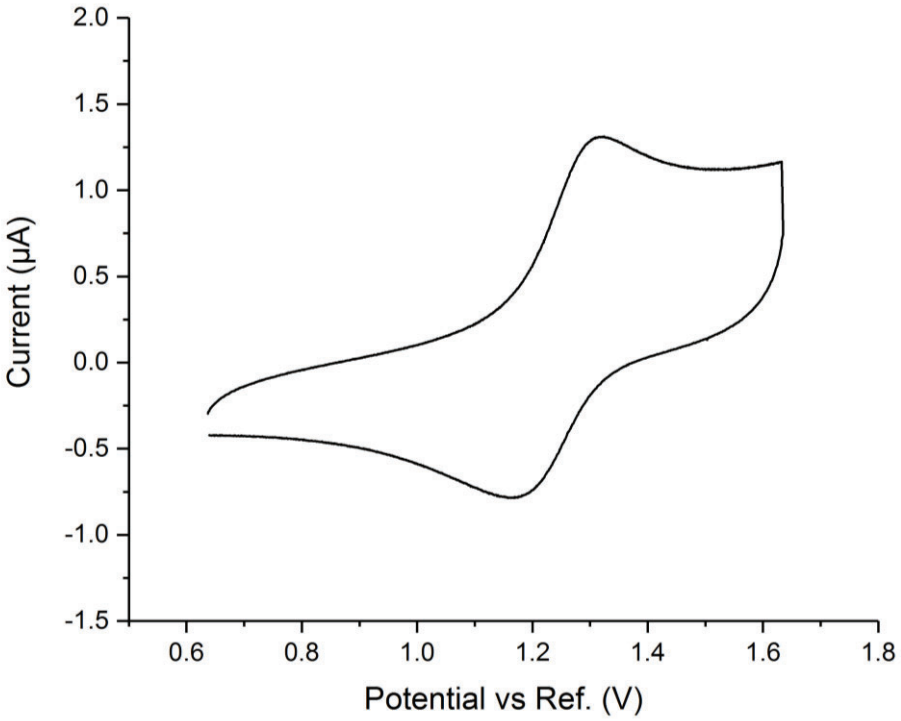

Figure 5.11: Voltammogram of **21** collected with a scan rate of 100 mV/s.

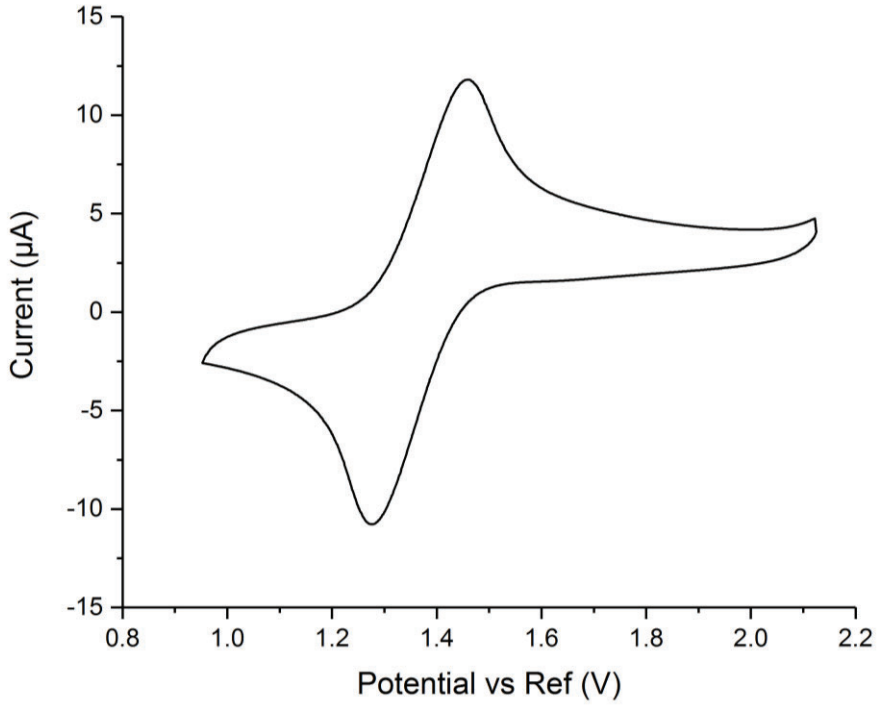

Figure 5.12: Voltammogram of **22** collected with a scan rate of 100 mV/s.

Table 5.2: Ratio of peak anodic and cathodic currents for compounds **21** and **22** at multiple scan rates.

Scan Rate (mV/s)	i_{pc}/i_{pa} (21)	i_{pc}/i_{pa} (22)
1000	1.18	0.96
500	1.26	0.97
300	1.15	0.99
200	0.81	0.96
100	0.94	1.03
50	0.88	1.10

The ratio of the peak cathodic and anodic currents indicates an electrochemical behaviour of **21** is best described as quasi-reversible, whereas **21** is reversible. The $E_{1/2}$ of **21** and **22** were calculated to be 1.320 V and 1.243 V relative to $Co(Cp)^{+/0}$, respectively. The reduction potential of the $Co(Cp)^{+/0}$ couple relative to $Fc^{+/0}$ in DCM is –1.33 V. As $E_{1/2}$ variations tend to be small in larger coordinatively saturated reagents such as [$CoCp_2$], it is reasonable to assume that a similar value would be obtained in THF, indicating that the $E_{1/2}$ of both products exhibit somewhat comparable redox behaviour to ferrocene.[14] The lower $E_{1/2}$ of **21** compared to **22** is perhaps due to an increase in electron density on the ferrocene moiety caused by electron donation from the neighbouring nitrogen lone-pair.

5.4 Reactivity

5.4.1 Deprotonation

In order to obtain the corresponding deprotonated ferrocenyl phosphinecarboxamide species, **21** was reacted with one equivalent of potassium bis(trimethylsilyl)amide (KHMDS). The ^{31}P NMR spectrum of the reaction mixture

revealed two resonances, a broad doublet at –99.2 ppm ($^1J_{P–H}$ =150 Hz) and a triplet centred at –145.1 Hz ($^1J_{P–H}$ = 206 Hz) (Figure 5.13). Both resonances collapse to singlets upon proton decoupling.

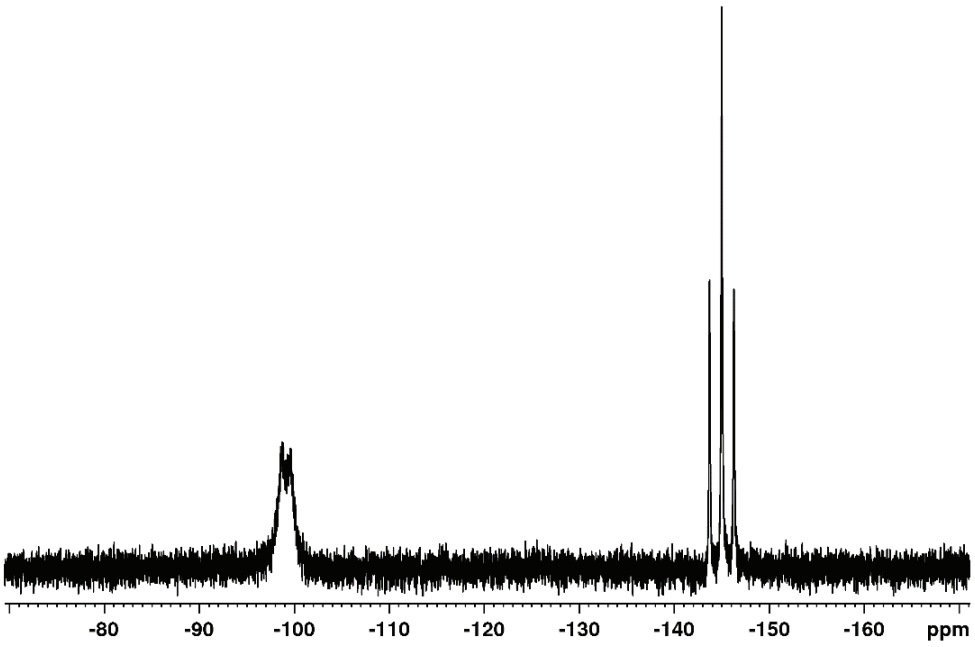

Figure 5.13: ^{31}P NMR spectrum of the reaction between **21** and KHMDS.

Consequently, two doublets can be seen in the ^{1}H NMR spectrum at 2.10 ppm and 3.17 ppm with the same coupling constants found in the ^{31}P NMR spectrum. Upon selective phosphorus decoupling, the doublets collapse to singlets, suggesting that the two products formed correspond to deprotonation at the phosphorus and at the nitrogen respectively. The broad nature of the doublet suggests the presence of a dynamic equilibrium between the products **23a** and **23b** shown in Figure 5.14.

23a **23b**

Figure 5.14: Proposed structures of the deprotonation products of **23**.

In order to facilitate crystallization, one equivalent of 18-crown-6 was added to the solution. Interestingly, the triplet disappeared and the ^{31}P NMR spectrum revealed a much sharper doublet at –93.2 ppm ($^{1}J_{P–H}$ = 148 Hz) which collapses to a singlet upon proton decoupling and is approximately 37 ppm downfield shifted relative to **21**. This result suggests that the sequestering agent favoured exclusive deprotonation at the phosphorus atom, resulting in the targeted compound **23**, which is consistent with other deprotonated phosphinecarboxamides (Figure 5.15). A decrease in the $^{1}J_{P–H}$ coupling constant upon deprotonation is observed when compared to the neutral species (–129.9 ppm; $^{1}J_{P–H}$ = 210 Hz), consistent with reduced phosphorus s orbital participation in the P–H bond.[15]

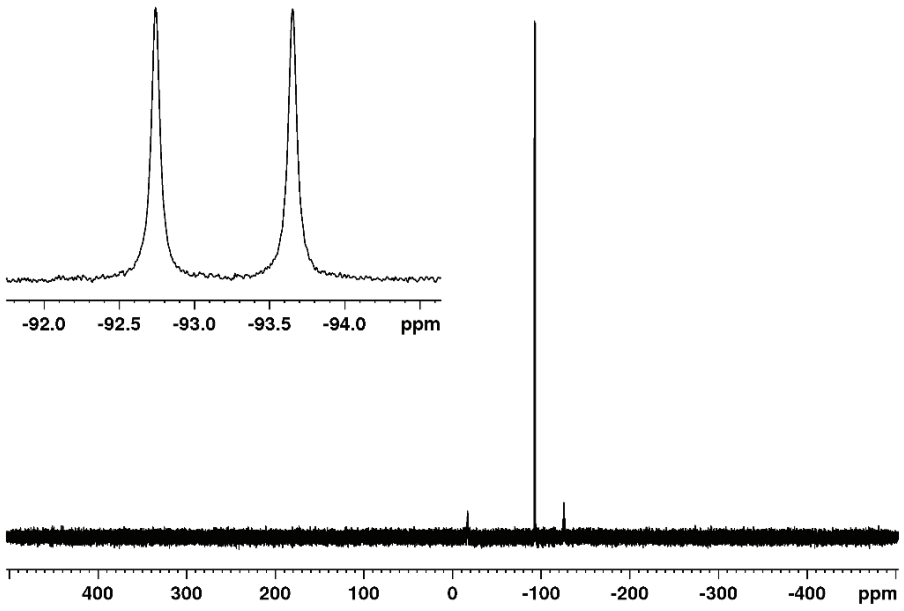

Figure 5.15: ^{31}P NMR spectrum of [(K(18-crown-6)][**23**]

The broad singlet at –16 ppm is attributed to the phosphorus containing analogue of biuret, which results from the nucleophilic attack of **23** on an unreacted molecule of **21** (Scheme 5.2), that can also be seen as a triplet at –126 ppm in the ^{31}P NMR spectrum.[16]

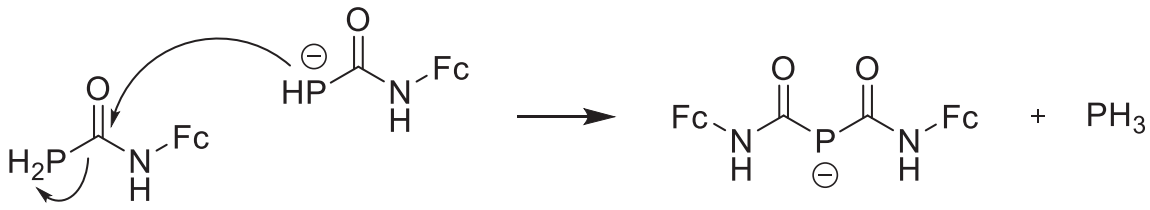

Scheme 5.2: Formation of the product corresponding to the broad singlet at –16 ppm.

The ^{1}H NMR spectrum of **23** shows a doublet at 1.88 Hz ($^{1}J_{H–P}$ = 148 Hz) and the $^{13}C\{^{1}H\}$ NMR spectrum also contains a doublet at 202 ppm ($^{1}J_{C–P}$ = 62 Hz) corresponding to the carbonyl carbon. The noticeable increase in the $^{1}J_{C–P}$ coupling is consistent with an increase in multiple bond character between the phosphorus and the carbon, as was observed in Chapter 4, as well as in other previously reported examples.

In contrast, when **22** was reacted with one equivalent of KHMDS, decomposition took place as the ^{31}P NMR spectrum showed mainly the formation of phosphine (PH_3). In order to tackle this issue, **22** was then reacted with one equivalent of KHMDS in the presence of 18-crown-6. The ^{31}P NMR spectrum is now consistent with exclusive deprotonation at the phosphorus atom, showing a doublet at –104.7 ppm ($^{1}J_{P–H}$ = 146 Hz) which collapses to a singlet upon proton decoupling originating compound **24** (Figure 5.16). The formation of the desired product can also be confirmed by the presence of a doublet centred at 1.78 ppm ($^{1}J_{H–P}$ = 146 Hz) in the ^{1}H NMR spectrum that collapses to a singlet on selective ^{31}P decoupling and corresponds to the phosphide and by the presence of a doublet in the $^{13}C\{^{1}H\}$ NMR spectrum at 203.7 ($^{1}J_{C–P}$ = 61 Hz). The considerable increase in $^{1}J_{C–P}$ is consistent with increase in multiple bond character between carbon and phosphorus after deprotonation.

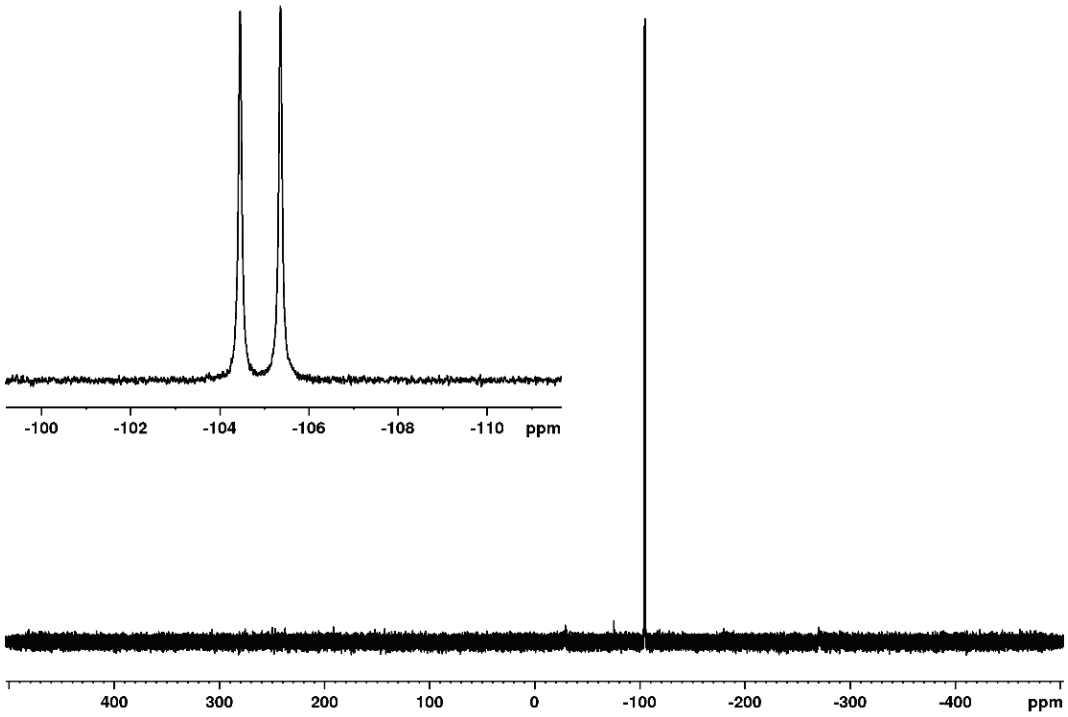

Figure 5.16: ^{31}P NMR spectrum of [(K(18-crown-6)][**24**].

5.4.2 *P*-functionalisation chemistry

Once compounds **23** and **24** were synthesized, the next goal was to asses if the new species can tolerate further functionalization to obtain secondary phosphines. In order to achieve that, iodomethane (MeI) was used as an electrophile as a proof of concept.

Compound **23** was formed *in situ* in THF by the reaction of **21** and KHMDS. Subsequent addition of MeI allowed the formation of the corresponding methylated product **25** (Scheme 5.3). THF was removed under vacuum together with the HMDS formed and toluene was added to separate the product from the potassium iodide by-product.

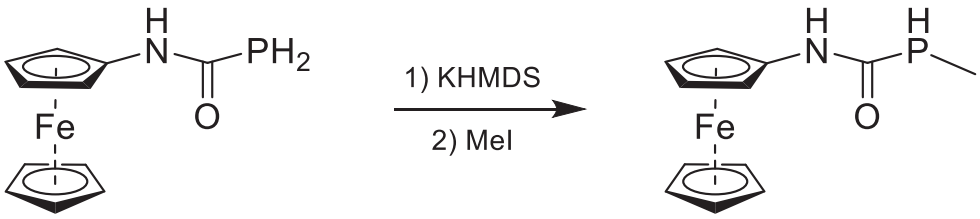

21 **25**

Scheme 5.3: Reaction of **21** with KHMDS and MeI to form **25**.

In the ^{31}P NMR spectrum of **25** it is possible to observe a broad doublet of quartets centred at –78.9 ppm ($^{1}J_{P-H}$ = 207 Hz, $^{2}J_{P-H}$ = 2 Hz) which collapses to a singlet upon proton decoupling (Figure 5.17).

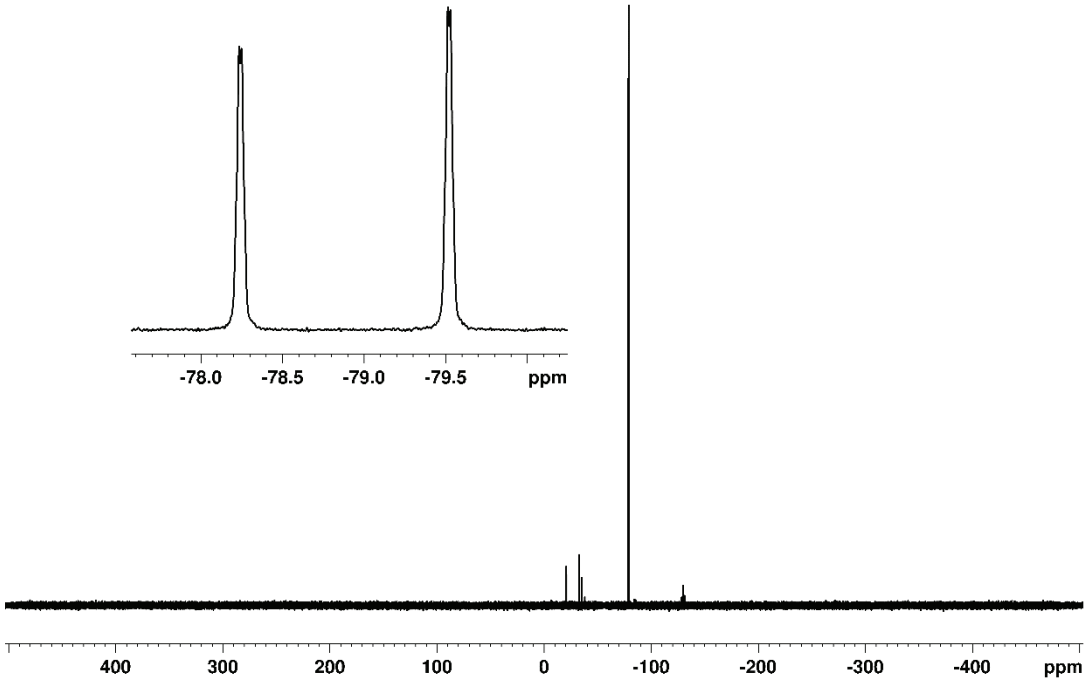

Figure 5.17: ^{31}P NMR spectrum of **25.**

In the ^{1}H NMR spectrum, the corresponding phosphine resonance is now a doublet of quartets centred at 4.14 ppm ($^{1}J_{H-P}$ = 207 Hz, $^{3}J_{H-H}$ = 7 Hz) that collapse to a quartet upon phosphorus decoupling, and the new methyl group is observed as a doublet of doublets at 1.39 ppm ($^{2}J_{H-P}$ = 3 Hz, $^{3}J_{H-H}$ = 8 Hz). The $^{13}C\{^{1}H\}$ NMR

spectrum contains two doublets that indicate the formation of the product, one at 177 ppm ($^1J_{C–P}$ = 12 Hz) and one at 1.72 ppm ($^1J_{C–P}$ = 8 Hz), corresponding to the carbonyl and methyl carbons, respectively. It is worth mentioning that although the reaction of **21** with KHMDS in the absence of 18-crown-6 also shows deprotonation at the nitrogen atom, no evidence of methylation at this position was observed.

Similarly, when iodomethane was added to a THF solution of **22**, KHMDS, and 18-crown-6, the corresponding methylated product, **26**, was isolated using the same method described above. The ^{31}P NMR spectrum reveals a doublet of quartets at –81.5 ppm ($^1J_{P–H}$ = 207 Hz, $^2J_{P–H}$ = 3 Hz) that collapses to a singlet upon proton decoupling. The ^{1}H NMR spectrum also shows a doublet of quartets at 4.06 ppm ($^1J_{H–P}$ = 207 Hz, $^3J_{H–H}$ = 7 Hz), and a doublet of doublets at 1.38 ppm ($^2J_{H–P}$ = 3 Hz, $^3J_{H–H}$ = 8 Hz), which collapse to a quartet and a doublet, respectively, upon ^{31}P decoupling. These resonances correspond to the phosphine and methyl protons of **26** respectively. The ^{13}C{^{1}H} NMR spectrum display a doublet at 177 ppm ($^1J_{C–P}$ = 11 Hz) and 1.76 ppm ($^1J_{C–P}$ = 8 Hz) and belong to the carbonyl and methyl carbons respectively.

5.4.3 Coordination

To assess the ligand behaviour of **21** and **22** towards transition metals, W(CO)$_5$(NCMe) was chosen as a suitable reagent (Scheme 5.4). In this case, coordination through the phosphorus could easily be observed by ^{31}P{^{1}H} NMR spectroscopy due to the presence of ^{183}W satellites.

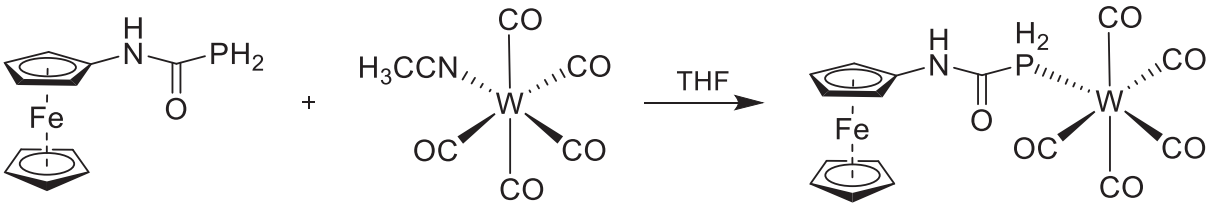

27

Scheme 5.4: Reaction of **21** and $W(CO)_5(NCCH_3)$ to yield **27**.

The reaction of **21** and **22** with $W(CO)_5$(NCMe) in THF resulted in three triplet resonances around – 91 ppm with $^1J_{P-H}$ coupling between 310 Hz and 353 Hz. If we take the case of the reaction involving **21** as an example, in the ^{31}P NMR spectrum we observe triplets centred at –82.3 ppm, –89.9 ppm and –97.5 ppm which integrate in a 0.15 : 1 : 0.12 ratio, with $^1J_{P-H}$ coupling constants of 319 Hz, 350 Hz and 353 Hz, respectively, as well as 1% of the unreacted starting material.

We have assigned the major product of this reaction to the target compound **27**. The fact that the corresponding resonance remained a triplet after coordination but now shows a downfield shift of at least 43 ppm relative to the free ligand accompanied by an increase in the coupling constant is consistent with coordination through the phosphine for the same reasons discussed in the previous chapter on the coordination of phosphinecarboxamides with Ru(II). These findings are corroborated by the presence of ^{183}W satellites in the $^{31}P\{^1H\}$ NMR spectrum (Figure 5.18), with a $^1J_{P-W}$ coupling constant value of 213 Hz. Furthermore, these results are in agreement with the ones obtained when the parent phosphinecarboxamide species was used.[17]

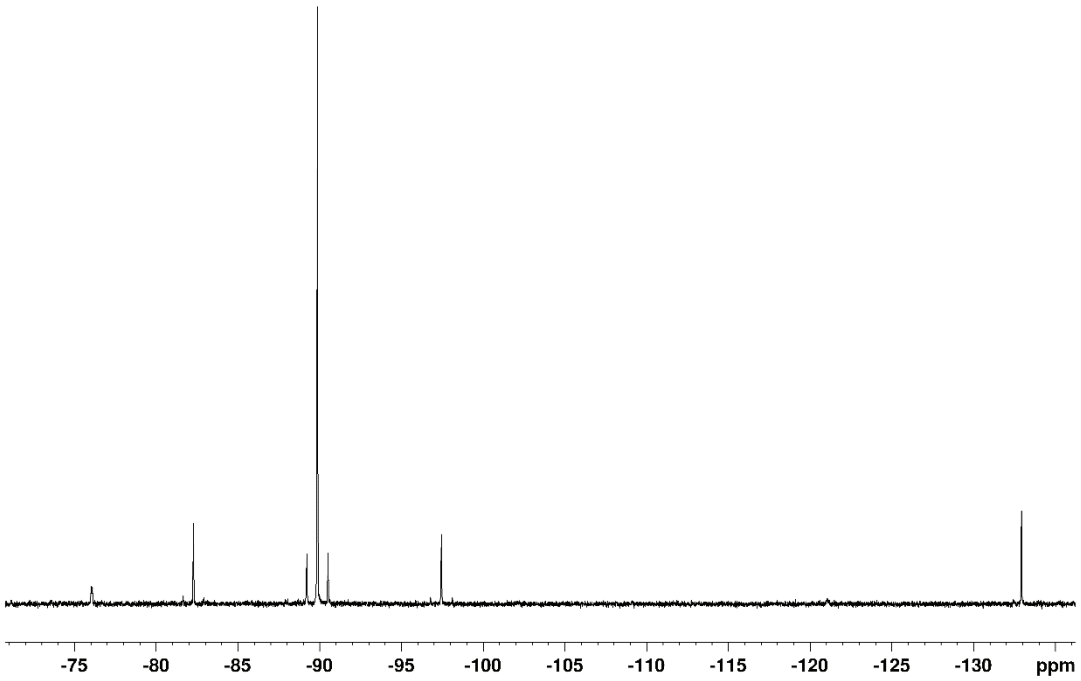

Figure 5.18: $^{31}P\{^{1}H\}$ NMR spectrum of reaction between **21** and $W(CO)_5(NCMe)$ in THF.

We propose that the two minor products formed are four membered phosphametallacycles in which the phosphinecarboxamide moiety acts as a chelating ligand bonding through both nitrogen and phosphorus atoms as shown in Figure 5.19. This educated guess is based on previous reports on this type of complexes.[18,19]

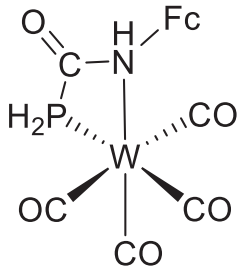

Figure 5.19: Proposed structure of the minor products formed in the reaction between **21** and $W(CO)_5(NCCH_3)$.

5.5 Conclusions

Ferrocene phosphinecarboxamide derivatives, namely *N*-ferrocene and *N*-methylferrocene phosphinecarboxamides were obtained by the reaction of the corresponding primary amines bearing ferrocenyl backbones and the 2-phosphaethynolate anion. These compounds have been fully characterized and their solid-state structures elucidated and were shown to be consistent with those of known phosphinecarboxamides. Both compounds have been studied electrochemically and **21** has been shown to display quasi-reversible redox properties while **22** is reversible. These properties are similar to those of ferrocene. **21** and **22** exhibited reasonable air and moisture stability, showing no signs of oxidation of the phosphinecarboxamide moiety, but slowly hydrolysing after 8 days by loss of HPCO.

Compounds **21** and **22** show similar properties, as would be expected, due to the similarities in their structures. These species can be further *P*-functionalised via addition of a base to form the deprotonated anionic species that can then be reacted with an electrophile to yield a secondary phosphine. Interestingly, even though there was evidence that **23** could also be deprotonated at the nitrogen atom, the phosphide could be exclusively formed with the addition of a sequestering agent. Furthermore, no evidence of methylation at the nitrogen was found. Moreover, **21** and **22** were shown to be able to act as a Lewis bases by using the lone-pair at the phosphorus to bond to form transition metal complexes as was observed from the spectroscopic and crystallographic data.

5.6 References

[1] M. Brynda, *Coord. Chem. Rev.* **2005**, *249*, 2013–2034.

[2] T. Clark, C. Landis, *Tetrahedron: Asymmetry* **2004**, *15*, 2123–2137.

[3] G. Hoge, B. Samas, *Tetrahedron: Asymmetry* **2004**, *15*, 2155–2157.

[4] K. V. Katti, H. Gali, C. J. Smith, D. E. Berning, *Acc. Chem. Res.* **1999**, *32*, 9–17.

[5] T. N. Hooper, M. A. Huertos, T. Jurca, S. D. Pike, A. S. Weller, I. Manners, *Inorg. Chem.* **2014**, *53*, 3716–3729.

[6] H. Dorn, R. A. Singh, J. A. Massey, A. J. Lough, I. Manners, *Angew. Chemie Int. Ed.* **1999**, *38*, 3321–3323.

[7] B. Stewart, A. Harriman, L. J. Higham, *Organometallics* **2011**, *30*, 5338–5343.

[8] J. T. Fleming, L. J. Higham, *Coord. Chem. Rev.* **2015**, *297–298*, 127–145.

[9] N. J. Goodwin, W. Henderson, B. K. Nicholson, *Chem. Commun.* **1997**, 31–32.

[10] N. J. Goodwin, W. Henderson, B. K. Nicholson, J. Fawcett, D. R. Russell, *J. Chem. Soc. Dalt. Trans.* **1999**, *0*, 1785–1794.

[11] W. Henderson, S. R. Alley, *J. Organomet. Chem.* **2002**, *656*, 120–128.

[12] A. R. Jupp, J. M. Goicoechea, *J. Am. Chem. Soc.* **2013**, *135*, 19131–19134.

[13] A. Hinz, R. Labbow, C. Rennick, A. Schulz, J. M. Goicoechea, *Angew. Chemie Int. Ed.* **2017**, *56*, 3911–3915.

[14] N. G. Connelly, W. E. Geiger, *Chem. Rev.* **1996**, *96*, 877–910.

[15] O. Kühl, *Phosphorus-31 NMR Spectroscopy: A Concise Introduction for the Synthetic Organic and Organometallic Chemist*, **2009**.

[16] A. R. Jupp, G. Trott, É. Payen De La Garanderie, J. D. G. Holl, D. Carmichael, J. M. Goicoechea, *Chem. - A Eur. J.* **2015**, *21*, 8015–8018.

[17] M. B. Geeson, A. R. Jupp, J. E. McGrady, J. M. Goicoechea, *Chem. Commun.* **2014**, *50*, 12281–12284.

[18] W. Malisch, C. Hahner, K. Grün, J. Reising, R. Goddard, C. Krüger, *Inorganica Chim. Acta* **1996**, *244*, 147–150.

[19] Z. Chen, H. W. Schmalle, T. Fox, O. Blacque, H. Berke, *J. Organomet. Chem.* **2007**, *692*, 4875–4885.

Chapter 6: Conclusions and Future Work

6.1 Conclusions

The compounds reported in this thesis have contributed to extend and better understand the chemistry of a relatively new and unexplored family of primary phosphines. Inspired by Wöhler's seminal synthesis of urea, the phosphinecarboxamides are obtained by the reaction of the 2-phosphaethynolate anion, PCO^-, a heavier congener of the cyanate anion, with ammonium salts. These species are phosphorus-containing analogues of urea, RHPC(O)NHR'.

Initially, due to their undeniable biological relevance, amino acids were our substrates of choice. Their reaction with PCO^- salts afforded amino acids bearing an *N*-carbamoyl phosphine residue. Amino acids possess inherent amphoteric character and hence, the amino acid derived phosphinecarboxamides or, alternatively, (phosphanyl)carbonyl-amino acid derivatives, could be readily accessed as no side products were formed. Compounds **1**–**6** were found to display unusual air and moisture stability for primary phosphines over a two weeks period. Furthermore, these compounds were shown to undergo deuterium exchange when in the presence of protic solvents. The transformations used to access such systems can be employed for the *N*-labelling of amino acids with an NMR active functional group that can potentially be used to incorporate phosphorus in peptides.

Subsequently, our goal was to establish the reactivity trends of PCO^- with diamines. This investigation started with the smallest diamine available, hydrazine, and progressed by increasing the number of methylene spacers between the two nitrogen atoms. The synthesis and characterization of the *cis* and *trans* isomers of the hydrazine mono-phosphinecarboxamide, **13**, and the ethylenediamine bis-phosphinecarboxamide, **14**, was described. The two isomers of **13**, **13a** and **13b**, could be observed in the ^{31}P NMR spectrum of the products of this reaction and both

could be crystalized, making it possible to elucidate their solid-state structures. The experimental data was supported by calculations that showed that the internal rotation barrier of the amide bond is large enough for the observation of **13a** and **13b** at room temperature. Despite several attempts, the hydrazine bis-phosphinecarboxamide derivative could not be obtained, always leading to the incorporation of only one equivalent of the PCO^- anion. When methylenediamine was used, $H_2NC(O)PH_2$ was the obtained. We propose that the desired methylenediamine mono-phosphinecarboxamide was initially formed, but rapidly eliminates methylene imine, CH_2NH, to form the parent phosphinecarboxamide species. This decomposition pathway continues further to form urotropine and ammonia. We have shown, by theoretical calculations, that these are the most energetically favoured products of this reaction. Compound **14** is exclusively obtained as the *cis* isomer of bis-phosphinecarboxamide. Its solid-state structure was confirmed by single crystal X-ray diffraction.

Compounds **13** and **14** were then used to illustrate how phosphinecarboxamides can be used as chemical reagents to generate a variety of phosphorus-containing compounds. The reaction of **13** with a non-nucleophilic base promotes deprotonation at both the phosphorus and nitrogen atoms, **15**, the latter being the major product. Further investigation of this reaction revealed that there is a chemical exchange between the isomers. Compound **15** has six possible isomers, bearing the negative charge at the phosphorus, α or β nitrogen atoms, **15a**–**15c**, either in their *cis* or *trans* conformations. The energy of each isomer was calculated showing that the *cis* phosphide is the most stable species. Interestingly, only the *trans* phosphide species could be crystallised. The reaction of **14** with a base promoted exclusive deprotonation at the phosphorus atoms. The phosphides obtained were

subsequently functionalised to afford the *P*-functionalised phosphinecarboxamides **17a**, **17b**, **18a** and **18b**. The reaction of **14** with $[Ru(p\text{-cymene})Cl_2]_2$ and $W(CO)_5(NCMe)$ has shown that these compounds can also act as ligands, bonding to the metal centres through the lone-pair at the phosphorus.

Finally, two examples of ferrocenyl functionalised phosphinecarboxamides, **21** and **22**, were described and their reactivity explored. These compounds have been fully characterized and their solid-state structures authenticated. The results obtained are consistent with the other phosphinecarboxamides reported in this thesis. Both compounds have been studied electrochemically. Compound **21** displays quasi-reversible redox properties while **22** is reversible. These compounds exhibit similar electrochemical properties to those of unfunctionalized ferrocene. Compounds **21** and **22** exhibited reasonable air and moisture stability, showing no signs of oxidation of the phosphinecarboxamide moiety, but slowly hydrolysing after eight days by loss of HPCO. These species were further *P*-functionalised via addition of a base to form the corresponding phosphides that were subsequently reacted with an electrophile to yield a secondary phosphine. Moreover, **21** and **22** were shown to act as a Lewis bases by using the lone-pair at the phosphorus to bond with transition metal complexes.

6.2 Future Work

This thesis has described relatively straight forward synthetic procedures to access primary and secondary phosphines bearing one or two carbamoyl groups. For example, ethylenediamine bis-phosphinecarboxamide could find application in catalysis, where it could be used as a chelating ligand. Phosphinecarboxamides display relative air and moisture stability, which is a desirable and quite rare property of primary phosphines. Consequently, these compounds could, in principle, be used

as a safer and more convenient alternative to processes that employ phosphine gas for instance, which is known for being a toxic and pyrophoric reagent.

Simple primary amines containing a carbon–carbon double bond, such as allylamine, should yield novel phosphinecarboxamides. Carbon–carbon double bonds are prone to polymerization and can pave the way to a new family of phosphorus containing polymers. Furthermore, it would be interesting to investigate the possibility to access heavier analogues of phosphinecarboxamides by reacting ammonium salts with heavier analogues of PCO^-, such as $AsCO^-$ and PCS^-.

Chapter 7: Experimental

7.1 General Experimental Details

All reactions and product manipulations were carried out under an inert atmosphere of argon using standard Schlenk-line or glovebox techniques (MBraun UNIlab glovebox maintained at < 0.1 ppm H_2O and < 0.1 ppm O_2) unless otherwise noted.

Tetrahydrofuran (THF; Sigma Aldrich, 99.9%) and 1,4-dioxane (Alfa Aesar, 99+%, stab. 5-10 ppm BHT) were distilled from a sodium/benzophenone mixture. Pyridine (py; Alfa Aesar, 99+%) was distilled over CaH_2. *N*,*N*-dimethylformamide (DMF; Rathburn, peptide synthesis grade), dichloromethane (CH_2Cl_2, DCM; Sigma Aldrich, HPLC grade), 1,2-dimethoxyethane (DME; Sigma Aldrich, anhydrous, 99.5%), hexane (Sigma Aldrich, HPLC grade), and toluene (Sigma Aldrich, HPLC grade) were purified using an MBraun SPS-800 solvent system. d_8-THF (Fluorochem, >99.5%), d_5-pyridine (d_5-py; Cambridge Isotope Laboratories Inc, 99.5%), CD_2Cl_2 (Sigma Aldrich, >99.5%) were dried over CaH_2, vacuum distilled, and degassed before use. D_2O was used as purchased. All solvents were stored under argon in gas-tight ampoules over activated 3 Å molecular sieves and degassed before use. Deionised water was obtained from a Millipore Milli-Q purification system and sparged overnight with nitrogen.

[K(18-crown-6)][PCO],[1] [Na(dioxane)$_x$][PCO] (x = 1.78 – 4.17)[2] and [W(CO)$_5$(NCMe)][3] were synthesized according to literature procedures and stored at ambient temperature in an inert atmosphere glovebox.

The suppliers and purification procedures for commercially available chemicals are detailed in Table 7.1.

Table 7.1: Supplier and purification procedures for commercially available chemicals.

Reagent	Supplier	Purity	Purification
Sodium	Acros Organics	99.8%, oiled sticks	Washed with hexane, dried under vacuum
Red Phosphorus	Sigma Aldrich	99.99%	Used as received
Naphthalene	Sigma Aldrich	99%	Sublimed under vacuum
$[W(CO)_6]$	Strem	99%	Used as received
$Me_3NO{\cdot}2H_2O$	Alfa Aesar	98%	Used as received
D_2O	Apollo	>99.92 atom % D	Used as received
$[Ru(p\text{-cymene})Cl_2]_2$	Sigma Aldrich	97%	Used as received
L-alanine	Alfa Aesar	99%	Dried under vacuum
L-serine	Alfa Aesar	99%	Dried under vacuum
L-cysteine	Sigma Aldrich	97%	Dried under vacuum
L-asparagine hydrate	PanReac AppliChem	99%	Dried under vacuum
L-glutamine	Alfa Aesar	99%	Dried under vacuum
L-proline	MP Biomedicals	99%	Dried under vacuum
L-arginine	Sigma Aldrich	99%	Dried under vacuum
Pyridinium triflate	Alfa Aesar	97%	Used as received
Hydrazine hydrochloride	Sigma Aldrich	97%	Used as received
Hydrazine dihydrochloride	Sigma Aldrich	99.9%	Used as received
Methylenediamine dihydrochloride		>98%	Used as received
Ethylenediamine	Alrich	99%	Refluxed over Na, distilled
HCl (aq. soln.)	Fisher	S.G. 1.18 (37%)	Used as received
18-crown-6	Alfa Aesar	99%	Dried under vacuum with heating
KHMDS	Sigma Aldrich	95%	Used as received
Iodo methane	Sigma Aldrich	99.5%	Used as received

7.2 Synthesis of compounds

7.2.1 Synthesis of compounds described in Chapter 2

7.2.1.1 [Na][$H_2PC(O)NHCHMeCO_2$] ([Na][1])

[Na(dioxane)$_{3.36}$][PCO] (3.00 g, 8.88 mmol) and L-alanine (0.79 g, 8.88 mmol) were weighed out into a Schlenk tube and dissolved in a mixture of pyridine (40 mL) and distilled water (6 mL). The resulting pale orange solution was stirred overnight at room temperature. The solution was pale orange on the next day. Filtration of the solution and removal of volatiles under dynamic vacuum yielded the product as a pale pink solid (1.49 g, 96% yield).

^{1}H NMR (400.2 MHz, d_5-pyridine and a drop of H_2O, 298 K): δ (ppm) 8.89 (bs, 1H; N*H*), 4.93 (q, 1H; NC*H*(CH_3)), 3.93 (m, $^1J_{H–P}$ = 211 Hz, $^2J_{H–H}$ = 12 Hz, 1H; P*H*H), 3.90 (m, $^1J_{H–P}$ = 211 Hz, $^2J_{H–H}$ = 12 Hz, 1H; PH*H*), 1.76 (d, $^3J_{H–H}$ = 7 Hz, 3H; NCH(C*H*$_3$)). **^{1}H{^{31}P} NMR** (400.2 MHz, d_5-pyridine and a drop of H_2O, 298 K): δ (ppm) 3.93 (m, $^2J_{H–H}$ = 12 Hz), 3.90 (m, $^2J_{H–H}$ = 12 Hz), other resonances unchanged. **^{31}P NMR** (162.0 MHz, d_5-pyridine and a drop of H_2O, 298 K): δ (ppm) –131.0 (t, $^1J_{P–H}$ = 211 Hz). **^{31}P{^{1}H} NMR** (162.0 MHz, d_5-pyridine and a drop of H_2O, 298 K): δ (ppm) –131.0 (s). **^{13}C{^{1}H} NMR** (125.8 MHz, d_5-pyridine and a drop of H_2O, 298 K): δ (ppm) 179.7 (s; *C*O_2^-), 175.0 (d, $^1J_{C–P}$ = 8 Hz; P*C*(O)), 53.6 (s; αC), 20.7 (s; βC). **ESI-MS** (–ve ion mode, MeOH): *m/z* = 148.0168.

7.2.1.2 Deuterium exchange experiment with [Na][1]

[Na][**1a**] (16 mg, 0.09 mmol) was dissolved in D_2O. The resulting pale yellow solution was slightly cloudy. The ^{31}P NMR spectrum shows deuterium exchange with the phosphine protons. The ^{1}H NMR spectrum shows no evidence of the broad amide singlet or of the doublet corresponding to the PH_2 moiety.

^{1}H NMR (400.2 MHz, D_2O, 298 K): δ (ppm) 4.22 (q, 1H; NC*H*(CH_3)), 1.35 (d, $^{3}J_{H–H}$ = 7 Hz, 3H; NCH(C*H*$_3$)). **^{31}P NMR** (162.0 MHz, D_2O, 298 K): δ (ppm) –134.1 (q, $^{1}J_{P–D}$ = 33 Hz). **^{31}P{^{1}H} NMR** (162.0 MHz, D_2O, 298 K): δ (ppm) –134.1 (q, $^{1}J_{P–D}$ = 33 Hz). **^{13}C{^{1}H} NMR** (125.8 MHz, D_2O, 298 K): δ (ppm) 179.8 (s; *C*O_2^-), 176.9 (d, $^{1}J_{C–P}$ = 11.7 Hz; P*C*(O)), 51.6 (s; αC), 17.1 (s; βC).

7.2.1.3 [Na][$H_2PC(O)NH(CH_2OH)CO_2$] ([Na][2])

[Na(dioxane)$_{4.17}$][PCO] (4.00 g, 8.90 mmol) and L-serine (0.94 g, 8.90 mmol) were weighed out into a Schlenk tube, dissolved in a mixture of pyridine (50 mL) and distilled water (3 mL) and stirred overnight at room temperature. Addition of extra amino acid (0.14 mg, 0.001 mmol) was necessary for the reaction to reach completion. The mixture was stirred overnight at room temperature. Filtration of the solution and removal of volatiles under dynamic vacuum yielded the product as a pale pink solid (1.62 g, 96% yield).

^{1}H NMR (400.2 MHz, d_5-pyridine and a drop of H_2O, 298 K): δ (ppm) 9.02 (d, 1H; N*H*), 5.10 (s, 1H; αH), 4.46 (m, 2H; βH), 3.84 (m, $^{1}J_{H–P}$ = 210 Hz, $^{2}J_{H–H}$ = 12 Hz, 2H; P*H*$_2$). **^{1}H{^{31}P} NMR** (400.2 MHz, d_5-pyridine and a drop of H_2O, 298 K): δ (ppm) 3.84 (m, $^{2}J_{H–H}$ = 12 Hz, 2H; P*H*$_2$), other resonances unchanged from ^{1}H NMR spectrum. **^{31}P NMR** (161.9 MHz, d_5-pyridine and a drop of H_2O, 298 K): δ (ppm) –131.4 (t, $^{1}J_{P–H}$ = 210 Hz). **^{31}P{^{1}H} NMR** (161.9 MHz, d_5-pyridine and a drop of H_2O, 298 K): δ (ppm) –131.4 (s). **^{13}C{^{1}H} NMR** (100.6 MHz, d_5-pyridine and a drop of H_2O, 298 K): δ (ppm) 177.2 (s, *C*O_2^-), 174.2 (d, $^{1}J_{C–P}$ = 8 Hz, P*C*(O)), 64.6 (s, αC), 59.1 (s, βC). **ESI-MS** (–ve ion mode, MeOH): m/z = 164.0117.

7.2.1.4 [Na][$H_2PC(O)NH(CH_2SH)CO_2$] ([Na][3])

[Na(dioxane)$_{1.78}$][PCO] (4.00 g, 16.75 mmol) and L-cysteine (2.03 g, 16.75 mmol) were dissolved in pyridine (50 mL) at room temperature. Distilled water was added to the resulting pale orange solution, which contained some undissolved amino acid and the mixture was stirred overnight. After this time, the solution was almost clear. Filtration of the solution and removal the volatiles under dynamic vacuum yielded the product as a pale pink solid (3.19 g, 92% yield).

^{1}H NMR (400.2 MHz, d$_5$-pyridine, 298 K): δ (ppm) 9.25 (d, 1H; N*H*), 5.02 (q, 1H; αH), 3.86 (bd, $^1J_{H–P}$ = 210 Hz, 2H; P*H*$_2$), 3.38 (m, 2H; βH), 2.62 (bs, S*H*). **^{1}H{^{31}P} NMR** (400.2 MHz, d$_5$-pyridine, 298 K): δ (ppm) 3.86 (bs, 2H; P*H*$_2$), other resonances unchanged from ^{1}H NMR spectrum. **^{31}P NMR** (161.9 MHz, d$_5$-pyridine, 298 K): δ (ppm) –130.6 (t, $^1J_{P–H}$ = 210 Hz). **^{31}P{^{1}H} NMR** (161.9 MHz, d$_5$-pyridine, 298 K): δ (ppm) –130.6 (s). **^{13}C{^{1}H} NMR** (100.6 MHz, d$_5$-pyridine, 298 K): δ (ppm) 176.8 (s, *C*O_2^-), 174.6 (d, $^1J_{C–P}$ = 8 Hz, P*C*(O)), 59.4 (s, αC), 28.2 (s, βC). **ESI-MS** (–ve ion mode, MeOH): *m/z* = 179.9888.

7.2.1.5 [Na][$H_2PC(O)NH(CH_2C(O)NH_2)CO_2$] ([Na][4])

Pyridine (40 mL) and distilled water (40 mL) were added to a mixture of [Na(dioxane)$_{4.17}$][PCO] (4.00 g, 8.90 mmol) and L-asparagine monohydrate (1.34 g, 8.90 mmol) at room temperature. The resulting pale yellow solution was stirred for 1h at which stage NMR spectroscopy revealed the presence of some PCO^-. Addition of extra 0.001 mmol of the amino acid was necessary for the reaction to reach completion. Filtration of the solution and removal of volatiles under a dynamic vacuum yielded the product as a beige solid (1.89 g, 98% yield).

^{1}H NMR (400.2 MHz, d_5-pyridine and a drop of H_2O, 298 K): δ (ppm) 9.07 (d, 1H; N*H*), 8.54 (s, 1H; N*H*H), 7.59 (s, 1H; NH*H*), 5.38 (q, 1H; αH), 3.92 (m, $^{1}J_{H–P}$ = 211 Hz, $^{2}J_{H–P}$ = 12 Hz 2H; PH_2), 3.35 (m, 2H; βH). **^{1}H{^{31}P}** NMR (400.2 MHz, d_5-pyridine and a drop of H_2O, 298 K): δ (ppm) 3.92 (m, $^{2}J_{H–P}$ = 12 Hz 2H; PH_2), other resonances unchanged from ^{1}H NMR spectrum. **^{31}P NMR** (161.9 MHz, d_5-pyridine and a drop of H_2O, 298 K): δ (ppm) –131.0 (t, $^{1}J_{P–H}$ = 211 Hz). **^{31}P{^{1}H} NMR** (161.9 MHz, d_5-pyridine and a drop of H_2O, 298 K): δ (ppm) –131.0 (s) **^{13}C{^{1}H} NMR** (100.6 MHz, d_5-pyridine and a drop of H_2O, 298 K): δ (ppm) 177.7 (s, *C*O_2^-), 177.0 (s, γC), 175.8 (d, $^{1}J_{C–P}$ = 9 Hz, P*C*(O)), 55.1 (s, αC), 41.0 (s, βC). **ESI-MS** (–ve ion mode, MeOH): *m/z* = 191.0226. **CHN** Calcd. (Found) for $C_5H_8N_2NaO_4P$: 28.05 (28.07), 3.77 (3.84), 13.08 (12.90).

7.2.1.6 [Na][$H_2PC(O)NH(CH_2)_2C(O)NH_2)CO_2$] ([Na][5])

Pyridine (30 mL) and sparged water (30 mL) were added to a mixture of [Na(dioxane)$_{3.36}$][PCO] (3.00 g, 8.88 mmol) and L-glutamine (1.30 g, 8.88 mmol) at room temperature. The resulting pale brown cloudy solution was stirred overnight. Filtration of the solution and removal of the volatiles under dynamic vacuum afforded the product as a beige solid (1.20 g, 59 % yield).

^{1}H NMR (400.2 MHz, d_5-pyridine and a drop of H_2O, 298 K): δ (ppm) 8.85 (d, 1H; N*H*), 8.49 (s, 1H; N*H*H), 7.55 (s, 1H; NH*H*), 5.07 (q, 1H; αH), 3.86 (m, $^{1}J_{H–P}$ = 210 Hz, $^{2}J_{H–P}$ = 12 Hz 2H; PH_2), 2.74 (m, 4H; β, γH). **^{1}H{^{31}P} NMR** (400.2 MHz, d_5-pyridine and a drop of H_2O, 298 K): δ (ppm) 3.86 (m, $^{2}J_{H–P}$ = 12 Hz 2H; P*H*H), other resonances unchanged from ^{1}H NMR spectrum. **^{31}P NMR** (161.9 MHz, d_5-pyridine and a drop of H_2O, 298 K): δ (ppm) –131.3 (t, $^{1}J_{P–H}$ = 210 Hz). **^{31}P{^{1}H} NMR** (161.9 MHz, d_5-pyridine and a drop of H_2O, 298 K): δ (ppm) –131.3 (s). **^{13}C{^{1}H} NMR** (100.6 MHz, d_5-pyridine and a drop of H_2O, 298 K): δ (ppm) 178.6 (s, *C*O_2^-), 177.7 (s, δC), 174.5 (d, $^{1}J_{C–P}$ = 8 Hz, P*C*(O)), 57.3 (s, αC), 34.0 (s, γC), 31.1 (s, βC). **ESI-MS** (–ve ion mode, MeOH):

m/z = 205.0381. **CHN** Calcd. (Found) for $C_6H_{10}N_2NaO_4P$: 31.59(30.69), 4.42(4.37), 12.28 (11.67).

7.2.1.7 [Na][$H_2PC(O)N(CH_2)_3CHCO_2$] ([Na][6])

Pyridine (60 mL) and distilled water (2 mL) were added to a mixture of [Na(dioxane)$_{3.36}$][PCO] (2.00 g, 5.91 mmol) and L-proline (0.68 g, 5.91 mmol) at room temperature. The resulting pale orange solution was stirred overnight. Volatiles were removed under dynamic vacuum to yield the product as a pale yellow solid (1.15 g, 97 % yield).

^{1}H NMR (499.9 MHz, d_5-pyridine, 298 K): δ (ppm) 4.70 (bs, 1H; αH (*cis*)), 4.51 (d, 1H; αH (*trans*)), 4.08 (dd, $^1J_{H–P}$ = 213 Hz, $^2J_{H–H}$ = 11 Hz, 1H; P*H*H (*trans*)), 3.97 (dd, $^1J_{H–P}$ = 213 Hz, $^2J_{H–H}$ = 11 Hz, 1H; PH*H* (*trans*)), 3.87 (m, 1H; δH (*trans*)), 3.85 (bd, $^1J_{H–P}$ = 217 Hz, 2H; PH_2 (*cis*)), 3.72 (m, 1H; δH (*trans*)), 3.59 (bs, 1H; δH(*cis*)), 3.33 (bs, 1H; δH (*cis*)), 2.50 (bs, 1H; βH (*trans*)), 2.34 (bs, 1H; βH (*cis*)), 2.15 (m, 1H; βH (*trans*)), 2.06 (bs, 1H; βH (*cis*)), 1.69 (s, 1H; γH (*cis*)), 1.69 (s, 1H; γH (*trans*)). **^{1}H{^{31}P} NMR** (499.9 MHz, d_5-pyridine, 298 K): δ (ppm) 4.08 (dd, $^2J_{H–H}$ = 11 Hz, 1H; P*H*H (*trans*)), 3.97 (dd, $^2J_{H–H}$ = 11 Hz, 1H; PH*H* (*trans*)), 3.85 (s, 2H; PH_2 (*cis*)); other resonances unchanged from ^{1}H NMR spectrum. **^{31}P NMR** (161.9 MHz, d_5-pyridine, 298 K): δ (ppm) –127.6 (t, $^1J_{P–H}$ = 217 Hz; *cis*), –131.2 (t, $^1J_{P–H}$ = 213 Hz; *trans*). **^{31}P{^{1}H} NMR** (161.9 MHz, d_5-pyridine, 298 K): δ (ppm) –127.6, –131.2. **^{13}C{^{1}H} NMR** (125.8 MHz, d_5-pyridine, 298 K): δ (ppm) 178.7 (s, *C*O_2^- (*cis*)), 178.2 (s, *C*O_2^- (*trans*)), 174.2 (d, $^1J_{C–P}$ = 7 Hz, P*C*(O) (*cis*)), 173.6 (d, $^1J_{C–P}$ = 6 Hz, P*C*(O) (*trans*)), 65.0 (d, $^2J_{C–P}$ = 2 Hz, αC (*trans*)), 63.7 (s, αC (*cis*)), 49.7 (d, $^2J_{C–P}$ = 5 Hz, δC (*cis*)), 47.5 (s, δC (*trans*)), 32.3 (s, βC (*trans*)), 30.6 (s, βC (*cis*)), 25.4 (s, γC (*trans*)), 23.8 (s, βC (*cis*)). **ESI-MS** (–ve ion mode, MeOH): *m/z* = 174.0324.

7.2.1.8 $H_2PC(O)NHCHMeCOOH$ (7)

Pyridinium chloride (67.6 mg, 0.58 mmol) and [Na][**1**] (100 mg, 0.58 mmol) were weighed into a Schlenk and DCM (3 mL) was added. The mixture was stirred overnight. The colorless solution was then filtered to be separated from the pale-yellow precipitate formed. Volatiles were removed under vacuum affording a colorless oil. Freezing with liquid nitrogen and treatment under dynamic vacuum did not yield a solid. Addition of the minimum amount of DCM, just enough to dissolve the oil, and further addition of hexane (2 mL) precipitated the product as a white solid, which was dried under dynamic vacuum. (43.2 mg, 49.96% yield).

^{1}H NMR (400.2 MHz, d_5-pyridine, 298K): δ (ppm) 15.34 (bs, 1H; COO*H*), 9.80 (d, 1H; N*H*), 5.16 (q, $^{3}J_{H-H}$ = 7 Hz, 1H; NC*H*(CH_3)), 3.86 (m, $^{1}J_{H-P}$ = 209 Hz, $^{2}J_{H-H}$ = 12 Hz, 1H; PH_2), 1.60 (d, $^{3}J_{H-H}$ = 7 Hz, 3H; NCH(CH_3)). **^{1}H{^{31}P} NMR** (400.2 MHz, d_5-pyridine, 298K): δ (ppm 3.86 (m, $^{2}J_{H-H}$ = 12 Hz, 1H; PH_2), other resonances unchanged. **^{31}P NMR** (162.0 MHz, d_5-pyridine, 298K): δ (ppm) –132.6 (t, $^{1}J_{P-H}$ = 209 Hz). **^{31}P{^{1}H} NMR** (162.0 MHz, d_5-pyridine, 298K): δ (ppm) –132.6 (s). **^{13}C{^{1}H} NMR** (125.8MHz, d_5-pyridine, 298K): δ (ppm) 175.9 (s; *C*OOH), 173.2 (d, $^{1}J_{C-P}$ = 7.3 Hz; P*C*(O)), 49.9 (s; αC), 18.6 (s; βC). **ESI-MS** (–ve ion mode, DCM): *m/z* = 148.0167. **CHN** Calcd. (Found) for $C_4H_8NO_3P$: 32.23(31.02), 5.41(4.40), 9.40(7.63).

7.2.1.9 $H_2PC(O)NH(CH_2OH)COOH$ (8)

Pyridinium triflate (12 mg, 0.05 mmol) and the previously synthesized [Na][**2**] (10 mg, 0.05 mmol) were weighed into a gas-tight NMR tube and d_5-pyridine (0.5 mL) was added to give a pale yellow solution where the product was formed. Attempts to scale up this reaction were made but the purification step was challenging due to solubility issues.

^{1}H NMR (400.2 MHz, d_5-pyridine, 298 K): δ (ppm) 12.26 (bs, 2H; COO*H*), 9.84 (d, 1H; N*H*), 5.42 (m, 1H; αH), 4.49 (m, 2H; βH), 3.88 (bd, $^{1}J_{H–P}$ = 210 Hz, 2H; PH_2). **^{1}H{^{31}P} NMR** (400.2 MHz, d_5-pyridine, 298 K): δ (ppm) 3.88 (bs, 2H; PH_2), other resonances unchanged from ^{1}H NMR spectrum. **^{31}P NMR** (161.9 MHz, d_5-pyridine, 298 K): δ (ppm) –131.6 (t, $^{1}J_{P–H}$ = 210 Hz). **^{31}P{^{1}H} NMR** (161.9 MHz, d_5-pyridine, 298 K): δ (ppm) –131.6 (s). **^{13}C{^{1}H} NMR** (100.6 MHz, d_5-pyridine, 298 K): δ (ppm) 174.3 (s, *C*OOH), 174.0 (d, $^{1}J_{C–P}$ = 8 Hz, P*C*(O)), 63.5 (s, αC), 57.3 (s, βC).

7.2.1.10 $H_2PC(O)NH(CH_2SH)COOH$ (9)

Pyridinium chloride (113.78 mg, 0.99 mmol) and [Na][**3**] (200 mg, 0.99 mmol) were weighed into a Schlenk tube and dissolved in DCM (5 mL). The mixture was stirred overnight. The colourless solution was then filtered to be separated from the white precipitate formed. Volatiles were removed under vacuum affording a colourless oil. Hexane (5 mL) was added to this oil and the mixture was stirred overnight. Removal of the volatiles under a dynamic vacuum yielded an oily white solid. Several cycles of freeze/pump/thaw degassing ultimately afforded the product as a pale yellow solid. (92.5 mg, 51.84% yield).

^{1}H NMR (500.3 MHz, d_5-pyridine, 298 K): δ (ppm) 16.01 (bs, 1H; COO*H*), 9.95 (d, 1H; N*H*), 5.45 (m, 1H; αH), 3.89 (bd, $^{1}J_{H–P}$ = 210 Hz, 2H; PH_2), 3.35 (m, 2H; βH), 2.58 (bs; S*H*). **^{1}H{^{31}P} NMR** (400.2 MHz, d_5-pyridine, 298 K): δ (ppm) 3.89 (bs, 2H; PH_2), other resonances unchanged from ^{1}H NMR spectrum. **^{31}P NMR** (161.9 MHz, d_5-pyridine, 298 K): δ (ppm) –131.9 (t, $^{1}J_{P–H}$ = 210.2 Hz). **^{31}P{^{1}H} NMR** (161.9 MHz, d_5-pyridine, 298 K): δ (ppm) –131.9 (s). **^{13}C{^{1}H} NMR** (100.6 MHz, d_5-pyridine, 298 K): δ (ppm) 173.8 (d, $^{1}J_{C–P}$ = 8.2 Hz, P*C*(O)), 173.5 (s, *C*OOH), 56.5 (s, αC), 27.7 (s, βC). **ESI-MS** (–ve ion mode, DCM): m/z = 179.9888.

7.2.1.11 $H_2PC(O)NH(CH_2C(O)NH_2)COOH$ (10)

Pyridinium chloride (57.8 mg, 0.50 mmol) and [Na][**4**] (107.2 mg, 0.50 mmol) were weighed into a Schlenk tube and dissolved in DCM (3 mL). The mixture was stirred overnight. The colourless solution was then filtered to be separated from the white precipitate formed. Volatiles were removed under vacuum affording a colourless oil. Extraction of the product into distilled water (0.5 mL), followed by filtration and treatment of the filtrate under a dynamic vacuum yielded the product as a colourless solid. (18.2 mg, 18.95% yield).

^{1}H NMR (400.2 MHz, d_5-pyridine, 298 K): δ (ppm) 15.95 (bs, 1H; COO*H*), 9.86 (d, 1H; N*H*), 8.56 (s, 1H; N*H*H), 7.98 (s, 1H; NH*H*), 5.72 (m, 1H; αH), 3.83 (d, $^1J_{H–P}$ = 209 Hz, 2H; PH_2), 3.40 (d, 2H; βH). **^{1}H{^{31}P} NMR** (400.2 MHz, d_5-pyridine, 298 K): δ (ppm) 3.83 (s, 1H; PH_2), other resonances unchanged from ^{1}H NMR spectrum. **^{31}P NMR** (162.0 MHz, d_5-pyridine, 298 K): δ (ppm) –131.9 (t, $^1J_{P–H}$ = 209 Hz). **^{31}P{^{1}H} NMR** (162.0 MHz, d_5-pyridine, 298 K): δ (ppm) –131.9 (s). **^{13}C{^{1}H} NMR** (100.6 MHz, d_5-pyridine, 298 K): δ (ppm) 174.7 (s, *C*OOH), 173.5 (d, $^1J_{C–P}$ = 7.7 Hz, P*C*(O)), 173.4 (s, γC), 51.5 (s, αC), 38.5 (s, βC). **ESI-MS** (–ve ion mode, DCM): m/z = 191.0224.

7.2.1.12 $H_2PC(O)NH(CH_2)_2C(O)NH_2)COOH$ (11)

Pyridinium triflate (15 mg, 0.07 mmol) and [Na][**5**] (15 mg, 0.07 mmol) were weighed into a gas-tight NMR tube and d_5-pyridine (0.5 mL) was added to give a pale yellow solution where the product was formed. Attempts to scale up this reaction up were made but the purification step was limiting due to solubility issues.

^{1}H NMR (400.2 MHz, d_5-pyridine, 298 K): δ (ppm) 12.42 (bs, H; COO*H*), 9.95 (d, 1H; N*H*), 8.45 (s, 1H; N*H*H), 7.82 (s, 1H; NH*H*), 5.30 (m, 1H; αH), 3.84 (bd, $^1J_{H–P}$ = 210 Hz 2H; PH_2), 2.66 (m, 4H; β, γH). **^{1}H{^{31}P} NMR** (400.2 MHz, d_5-pyridine, 298 K): δ (ppm)

3.84 (m, 2H; PH_2), other resonances unchanged from ^{1}H NMR spectrum. **^{31}P NMR** (162.0 MHz, d_5-pyridine, 298 K): δ (ppm) –132.3 (t, $^1J_{P–H}$ = 210 Hz). **^{31}P{^{1}H} NMR** (162.0 MHz, d_5-pyridine, 298 K): δ (ppm) –132.3 (s). **^{13}C{^{1}H} NMR** (100.6 MHz, d_5-pyridine, 298 K): δ (ppm) 175.9 (s, *C*OOH), 175.3 (s, δC), 174.0 (d, $^1J_{C–P}$ = 8 Hz, P*C*(O)), 54.1 (s, αC), 33.1 (s, γC), 29.1 (s, βC).

7.2.1.13 $H_2PC(O)N(CH_2)_3CHCOOH$ (12)

Pyridinium chloride (58.7 mg, 0.51 mmol) and [Na][**6**] (100 mg, 0.51 mmol) were weighed into a Schlenk and dissolved in DCM (3 mL). The mixture was stirred for 5h. The colourless solution was then filtered to be separated from the white precipitate formed. Volatiles were removed under vacuum give a pale yellow oil. The oil was treated with hexane (3 mL) and stirred overnight. Removal of volatiles under vacuum yielded the product as a pale yellow solid (58.0 mg, 64.9% yield).

^{1}H NMR (499.9 MHz, d_5-pyridine, 298 K): δ (ppm) 15.85 (bs, 1H; COO*H*), 4.87 (t, 1H; αH (*cis*)), 4.72 (dd, 1H; αH (*trans*)), 3.95 (m, $^1J_{H–P}$ = 212 Hz, $^2J_{H–H}$ = 12 Hz, 1H; PH_2 (*trans*)), 3.85 (m, 1H; δH (*trans*)), 3.82 (m, $^1J_{H–P}$ = 216 Hz, $^2J_{H–H}$ = 11 Hz, 1H; PH_2 (*cis*)), 3.68 (m, 1H; δH (*trans*)), 3.62 (m, 1H; δH (*cis*)), 3.39 (q, 1H; δH (*cis*)), 2.31 ((m, 1H; βH (*trans*)), 2.23 (m, 1H; βH (*cis*)), 2.14 (m, 1H; βH (*trans*)), 2.02 (m, 1H; βH (*cis*)), 1.89 (m, 1H; γH (*cis*)), 1.77 (m, 1H; γH (*trans*)). **^{1}H{^{31}P} NMR** (499.9 MHz, d_5-pyridine, 298 K): δ (ppm) 3.95 (d, $^2J_{H-H}$ = 14 Hz, 2H; PH_2 (*trans*)), 3.82 (bs, 2H; PH_2 (*cis*)); other resonances unchanged from ^{1}H NMR spectrum. **^{31}P NMR** (202.4 MHz, d_5-pyridine, 298 K): δ (ppm) –129.4 (t, $^1J_{P–H}$ = 216 Hz), –130.2 (t, $^1J_{P–H}$ = 212 Hz). **^{31}P{^{1}H} NMR** (202.4 MHz, d_5-pyridine, 298 K): δ (ppm) –129.4 (s), –130.2 (s). **^{13}C{^{1}H} NMR** (125.8 MHz, d_5-pyridine, 298 K): δ (ppm) 175.4 (s, *C*OOH (*trans*)), 174.9 (s, *C*OOH (*cis*)), 173.5 (d, $^1J_{C–P}$ = 10.5 Hz, P*C*(O) (*trans*)), 172.9 (d, $^1J_{C–P}$ = 9.8 Hz, P*C*(O) (*cis*)), 62.4 (d, $^2J_{C–P}$ = 3.6 Hz, αC (*trans*)), 60.2 (s, αC (*cis*)), 49.1 (d, $^2J_{C–P}$ = 5.8 Hz δC (*cis*)), 47.5

(s, δC (*trans*)), 31.9 (s, βC (*trans*)), 30.3 (s, βC (*cis*)), 25.2 (s, γC (*cis*)), 23.5 (s, βC (*trans*)). **ESI-MS** (–ve ion mode, DCM): m/z = 174.0323.

7.2.2 Synthesis of compounds described in Chapter 3

7.2.2.1 $H_2NNHC(O)PH_2$ (13)

$[Na(dioxane)_{1.97}][PCO]$ (931.8 mg, 3.65 mmol) and $H_2NNH_2{\cdot}HCl$ (250 mg, 3.65 mmol) were weighed out into a Schlenk tube. THF (20 mL) was added to the solids and the resulting mixture was stirred overnight. On the following day, the pale-yellow solution was filtered into a pre-weighed Schlenk and the solid was washed once with THF (20 mL) and filtered again. The two solutions were combined, and the solvent evaporated at 0˚ under dynamic vacuum to yield the product as an oil (118.1 mg, 35.2% yield).

^{1}H NMR (500.3 MHz, d_5-pyridine): δ (ppm) 10.73 (s br, 2H; N*H* (*cis*)), 10.20 (s br, 1H; N*H* (*trans*)), 5.42 (s br, 2H; NH_2 (*trans*)), 5.18 (s br, 4H; NH_2 (*cis*)), 4.02 (d, 2H, $^1J_{H-P}$ = 218 Hz; PH_2 (*trans*)), 3.72 (d, 4H, $^1J_{H-P}$ = 206 Hz; PH_2 (*cis*)). **^{1}H{^{31}P} NMR** (400.2 MHz, d_5-pyridine): δ (ppm) 4.02 (s, 2H, PH_2 (*trans*)), 3.72 (s, 4H, PH_2 (*cis*)); other resonances unchanged from ^{1}H NMR spectrum. **^{31}P NMR** (162.0 MHz, d_5-pyridine): δ (ppm) −139.90 (t, $^1J_{P-H}$ = 206 Hz; (*cis*)), −128.22 (td, $^1J_{P-H}$ = 218 Hz, $^3J_{P-H}$ = 4.6 Hz (*trans*)). **^{31}P{^{1}H} NMR** (162.0 MHz, d_5-pyridine): δ (ppm) −139.90 (s (*cis*)), −128.22 (s (*trans*)). **^{13}C{^{1}H} NMR** (125.8 MHz, d_5-pyridine): δ (ppm) 172.6 (d, $^1J_{C-P}$ = 8.6 Hz; P*C*(O), (*cis*)), 181.5 (s, P*C*(O), (*trans*)).

7.2.2.2 $PH_2C(O)NH(CH_2)_2NHC(O)PH_2$ (14)

$[Na(dioxane)_{2.08}][PCO]$ (11.3 g, 42.6 mmol) and $H_2N(CH_2)_2NH_2{\cdot}2HCl$ (2.83 g, 21.3 mmol) were weighed into a Schlenk tube. Distilled water (50 mL) was added to the solids resulting in a pale-yellow solution with light brown precipitate (the solid became pale yellow after stirring for 10 minutes). The mixture was stirred overnight. The pale-

yellow solution was filtered and the solvent evaporated. The product was extracted into THF (3 × 15 mL). Volatiles were removed at 0˚ under dynamic vacuum to yield the product as a white solid (854.2 mg, 22.3% yield).

^{1}H NMR (499.9 MHz, d_5-pyridine): δ (ppm) 9.53 (s br, 2H; N*H*), 3.72 (d, 4H, $^{1}J_{H-P}$ = 208 Hz; P*H*$_2$), 3.68 (m; C*H*$_2$). **^{1}H{^{31}P} NMR** (499.9 MHz, d_5-pyridine): δ (ppm) 3.72 (s, 4H, P*H*$_2$); other resonances unchanged from ^{1}H NMR spectrum. **^{31}P NMR** (202.3 MHz, d_5-pyridine): δ (ppm) −132.99 (t, $^{1}J_{P-H}$ = 208 Hz). **^{31}P{^{1}H} NMR** (202.3 MHz, d_5-pyridine): δ (ppm) −132.9 (s). **^{13}C{^{1}H} NMR** (125.7 MHz, d_5-pyridine): δ (ppm) 40.07 (s, *C*H$_2$), 172.8 (d, $^{1}J_{C-P}$ = 6.7 Hz; P*C*(O)). **CHN** Calcd. (Found) for $C_4H_{10}N_2O_2P_2$: 26.68 (26.92), 5.60 (5.56), 15.56 (15.35).

7.2.3 Synthesis of compounds described in Chapter 4

7.2.3.1 Deprotonated hydrazine *mono*-phosphinecarboxamide (15)

[Na(dioxane)$_{1.97}$][PCO] (559.1 mg, 2.19 mmol) and H_2NNH_2·HCl (150 mg, 2.19 mmol) were weighed out into a Schlenk tube. THF (15 mL) was added to the solids and the resulting mixture was stirred overnight. On the next day, the pale-yellow solution was filtered into a pre-weighed Schlenk and the solid was washed once with THF (10 mL) and filtered again. The two fractions were combined. Benzyl potassium (285.1 mg, 2.19 mmol) and 18-crown-6 (578.7 mg, 2.19 mmol) were weighed in another Schlenk and dissolved in THF (15mL). The benzyl potassium/18-crown-6 mixture was added to **13** and stirred for 15 minutes. The solution was kept in the freezer for a day to yield diamond shaped colourless crystals that were filtered and isolated (117.2 mg, 15% crystalline yield).

^{1}H NMR (499.9 MHz, d_5-pyridine): δ (ppm) 7.7 (br s; N*H* (**15a**)), 5.26 (br s; N*H*$_2$ (**15c**)), 4.49 (br s; N*H*$_2$ (**15a**)), 4.08 (d, $^{1}J_{P-H}$ = 190 Hz; P*H*$_2$ (**15c**), 3.51 (s; 18-crown-6), 2.95

(d, $^1J_{P-H}$ = 150 Hz; P*H* (**15a**)). **^{1}H{^{31}P} NMR** (499.9 MHz, d_5-pyridine): δ (ppm) 4.08 (s; PH_2 (**15c**)), 2.95 (s; P*H* (**15a**); other resonances unchanged from ^{1}H NMR spectrum. **^{31}P NMR** (162.0 MHz, d_5-pyridine): δ (ppm) −128.6 (t, $^1J_{P-H}$ = 190 Hz), −109.4 (br d, $^1J_{P-H}$ = 150 Hz). **^{31}P{^{1}H} NMR** (162.0 MHz, d_5-pyridine): δ (ppm) −128.6 (s), −109.4 (br s). **^{13}C{^{1}H} NMR** (100.6 MHz, d_5-pyridine): δ (ppm) 162.2 (br s, P*C*(O), **15a** and **15c**), 70.1 (s, 18-crown-6).

7.2.3.2 [K(18-crown-6)]$_2$[PHC(O)NH(CH$_2$)$_2$NHC(O)PH] (16)

Compound **14** (7 mg, 0.0389 mmol), KHMDS (15.5 mg, 0.0777 mmol) and 18-crown-6 (20.6 mg, 0.0777 mmol) were weighed out into an air-tight NMR tube. d_5-pyridine (0.4 mL) was added to the solids and the resulting bright yellow solution as analysed by multi-elemental NMR spectroscopy.

^{1}H NMR (499.9 MHz, d_5-pyridine): δ (ppm) 6.46 (s br, 2H; N*H*), 3.77 (m; CH_2), 3.55 (s, 18-crown-6), 2.78 (d, 2H, $^1J_{H-P}$ = 150 Hz; P*H*), 0.16 (s, HMDS). **^{1}H{^{31}P} NMR** (499.9 MHz, d_5-pyridine): δ (ppm) 2.78 (s, P*H*); other resonances unchanged from ^{1}H NMR spectrum. **^{31}P NMR** (162.0 MHz, d_5-pyridine): δ (ppm) –98.8 (br d, $^1J_{P-H}$ = 150 Hz, P*H*), –256.5 (br t, $^1J_{P-H}$ = 134 Hz, KPH_2 impurity). **^{31}P{^{1}H} NMR** (162.0 MHz, d_5-pyridine): δ (ppm) –98.8 (br s), –256.5 (br s). **^{13}C{^{1}H} NMR** (100.6 MHz, d_5-pyridine): δ (ppm) 203.8 ($^1J_{C-P}$ = 59 Hz; P*C*(O)), 70.8 (s, 18-crown-6), 43.3 (s, *C*H$_2$), 3.2 (s, HMDS).

7.2.3.3 Methylated hydrazine *mono*-phosphinecarboxamide (17)

[Na(dioxane)$_{1.97}$][PCO] (37.3 mg, 0.1459 mmol) and H_2NNH_2·HCl (10 mg, 0.1459 mmol) were weighed out into a Schlenk tube. THF (4 mL) was added to the solids and the resulting mixture was stirred for two days. The colourless solution was filtered and MeI (9.1 µL, 0.1459 mmol) was added to it and allowed to stir for 15 minutes. KHMDS (29.1 mg, 0.1459 mmol) was weighed into another Schlenk and dissolved it in 3 mL of

THF. The KHMDS solution was added to the **13**/MeI mixture. A white solid precipitated as the addition was taking place. The mixture was stirred for 2 hours and the colourless solutions filtered. Volatiles were removed under vacuum to yield a colourless oil that was subsequently dissolved in d_5-pyridine and analysed by multi-elemental NMR spectroscopy.

^{1}H NMR (400.2 MHz, d_5-pyridine): δ (ppm) 10.65 (br s, N*H*, **17b**), 10.49 (br s, N*H*, **17a**), 5.13 (br s, NH_2, **17a**), 4.99 (br s, NH_2, **17b**), 4.58 (dq, $^1J_{P–H}$ = 227 Hz, $^3J_{H–H}$ = 7 Hz, P*H*CH_3, **17b**), 4.11 (dq, $^1J_{P–H}$ = 206 Hz, $^3J_{H–H}$ = 7 Hz, NCH_3PH_2, methylated product derived from **15b** ***trans*** or **15c** ***cis***), 4.04 (dq, $^1J_{P–H}$ = 207 Hz, $^3J_{H–H}$ = 8 Hz, P*H*CH_3, **17a**), 1.46 (d, $^2J_{P–H}$ = 3 Hz, NC*H*$_3PH_2$, methylated product derived from **15b** ***trans*** or **15c** ***cis***), 1.38 (d, $^2J_{P–H}$ = 3 Hz, PHC*H*$_3$, **17b**), 1.35 (d, $^2J_{P–H}$ = 3 Hz, PHC*H*$_3$, **17a**). **^{1}H{^{31}P} NMR** (400.2 MHz, d_5-pyridine): δ (ppm) 4.58 (q), 4.11 (q), 4.04 (q); other resonances unchanged from ^{1}H NMR spectrum. **^{31}P NMR** (162.0 MHz, d_5-pyridine): δ (ppm) –86.6 ppm (br dq, $^1J_{P–H}$ = 113 Hz; *P*HCH_3, **17b**), –85.3 ppm (dq, $^1J_{P–H}$ = 207 Hz, $^2J_{P–H}$ = 3 Hz; *P*HCH_3, **17a**), –84.2 ppm (br d, $^1J_{P–H}$ = 106; NCH_3PH_2, methylated product derived from **15b** ***trans*** or **15c** ***cis***), –44.2 (sept, $^2J_{P–H}$ = 2.4 Hz; *P*$(CH_3)_2$). **^{31}P{^{1}H} NMR** (162.0 MHz, d_5-pyridine): δ (ppm) –86.6 ppm (s, *P*HCH_3), –85.3 ppm (s, *P*HCH_3), –84.2 ppm (s, NCH_3PH_2), –44.2 (s, *P*$(CH_3)_2$). **^{13}C{^{1}H} NMR** (125.7 MHz, d_5-pyridine): δ (ppm) 181.4 (d, $^1J_{C–P}$ = 18 Hz; P*C*(O), **17a**), 177.8 (d, $^1J_{C–P}$ = 13 Hz; P*C*(O), **17b**), 1.54 (d, $^1J_{C–P}$ = 9 Hz; PH*C*H_3, **17a**), 11.5 (d, $^1J_{C–P}$ = 12 Hz; PH*C*H_3, **17b**).

7.2.3.4 Methylated ethylenediamine bis-phosphinecarboxamide (18)

Compound **14** (10.0 mg, 0.055 mmol) was dissolved in 2 mL of THF in a Schlenk tube. MeI (6.9 µL, 0.111 mmol) was added and the mixture was allowed to stir for 15 minutes. KHMDS (22.1 mg, 0.111 mmol) was weighed into another Schlenk and dissolved it in 2 mL of THF. The KHMDS solution was added to the **14**/MeI mixture. A white solid

precipitated as the addition was taking place. The mixture was stirred for 3 hours and the colourless solutions filtered. Volatiles were removed under vacuum to yield the product as a white solid (4 mg, 34% yield).

^{1}H NMR (400.2 MHz, d_5-pyridine): δ (ppm) 9.38 (br s, N*H*C(O)PHCH$_3$), 9.01 (br s, N*H*C(O)PH(CH$_3$)$_2$), 3.75 (m, C*H*$_2$, **18a**, **18b**), 3.72 (m, C*H*$_2$NHC(O)PH(CH$_3$)$_2$), 1.35 (d, $^{2}J_{H-H}$ = 3 Hz, PC*H*$_3$), 1.34 (d, $^{2}J_{H-H}$ = 3 Hz, PHC*H*$_3$, **18b**),1.32 (d, $^{2}J_{H-H}$ = 3 Hz, PHC*H*$_3$, **18a**). **^{1}H{^{31}P} NMR** (400.2 MHz, d_5-pyridine): δ (ppm) 4.04 (q, $^{3}J_{H-H}$ = 3 Hz), 4.00 (q, $^{3}J_{H-H}$ = 3 Hz); other resonances unchanged from ^{1}H NMR spectrum. **^{31}P NMR** (162.0 MHz, d_5-pyridine): δ (ppm) –81.2 (dq, $^{1}J_{P-H}$ = 208 Hz, $^{3}J_{H-H}$ = 3 Hz; P*H*CH$_3$, **18a**), –81.1 ppm ($^{1}J_{P-H}$ = 208 Hz, $^{3}J_{H-H}$ = 3 Hz, P*H*CH$_3$, **18b**), –41.0 (sept, $^{2}J_{P-H}$ = 2.7 Hz; *P*(CH$_3$)$_2$), –41.1 (sept, $^{2}J_{P-H}$ = 2.7 Hz; *P*(CH$_3$)$_2$). **^{31}P{^{1}H} NMR** (162.0 MHz, d_5-pyridine): δ (ppm) –81.2 (s), –81.1 (s), –41.0 (s), –41.1 (s). **^{13}C{^{1}H} NMR** (100.6 MHz, d_5-pyridine): δ (ppm) 183.1 (d, $^{1}J_{C-P}$ = 16 Hz, (CH$_3$)$_2$P*C*(O)), 182.9 (d, $^{1}J_{C-P}$ = 16 Hz, (CH$_3$)$_2$P*C*(O)), 178.81 (d, $^{1}J_{C-P}$ = 11 Hz, P*C*(O), **18a**), 178.79 (d, $^{1}J_{C-P}$ = 11 Hz, P*C*(O), **18b**), 40.82 (s, *C*H$_2$), 11.6 (d, $^{1}J_{C-P}$ = 8 Hz, P(*C*H$_3$)$_2$), 1.72 (d, $^{1}J_{C-P}$ = 8 Hz, PH*C*H$_3$, **18a**, **18b**).

7.2.3.5 [Ru(*p*-cymene)Cl$_2$][PH$_2$C(O)NH(CH$_2$)$_2$NHC(O)PH$_2$] (19)

Compound **14** (15 mg, 0.083 mmol) and [Ru(*p*-cymene)Cl$_2$]$_2$ (51mg, 0.083 mmol) were weighed into a Schlenk tube. Distilled THF (4 mL) was added to the solids resulting in a slightly cloudy bright orange solution. The mixture was stirred for 40 minutes. At the end of this period, an orange solid has precipitated. Volatiles were removed under dynamic vacuum to yield the product as an orange solid (43.3 mg, 50% yield).

^{1}H NMR (400.2 MHz, CD$_2$Cl$_2$): δ (ppm) 7.77 (br s, 2H; N*H*), 5.67 (d, $^{3}J_{H-H}$ = 6 Hz, 2H; *H*$_{Ar}$), 5.55 (d, $^{3}J_{H-H}$ = 6 Hz, 2H; *H*$_{Ar}$), 5.38 (d, $^{1}J_{H-P}$ = 377 Hz, 4H; P*H*$_2$), 3.40 (m, 2H; (C*H*$_2$)$_2$), 2.81 (sept, $^{3}J_{H-H}$ = 7 Hz, 2H; C*H*(CH$_3$)$_2$), 2.19 (s, 6H; C$_{Ar}$C*H*$_3$), 1.24 (d, $^{3}J_{H-H}$ =

7 Hz, 12H; CH(CH_3)$_2$). **^{1}H{^{31}P} NMR** (400.2 MHz, CD_2Cl_2): δ (ppm) 5.38 (s, 4H, PH_2); other resonances unchanged from ^{1}H NMR spectrum. **^{31}P NMR** (202.3 MHz, CD_2Cl_2): δ (ppm) –38.9 ppm (t, $^1J_{P–H}$ = 377 Hz). **^{31}P{^{1}H} NMR** (202.3 MHz, CD_2Cl_2): δ (ppm) –38.9 ppm (s). **^{13}C{^{1}H} NMR** (125.8 MHz, CD_2Cl_2): δ (ppm) 166.3 (d, $^1J_{C–P}$ = 54 Hz; P*C*(O)), 107.5 (d, $^1J_{C–P}$ = 2 Hz; *C*$_{ar}$CH(CH$_3$)$_2$)), 103.2 (d, $^1J_{C–P}$ = 2 Hz; *C*$_{Ar}$CH$_3$), 87.2 (d, $^1J_{C–P}$ = 4.3 Hz; H*C*$_{Ar}$), 87.0 (d, $^1J_{C–P}$ = 3.3 Hz; H*C*$_{Ar}$), 39.9 (d, $^3J_{C–P}$ = 3.8 Hz; N*C*H$_2$), 31.5 (s; *C*H(CH$_3$)$_2$), 22.5 (s; CH(*C*H$_3$)$_2$), 18.9 (s; *C*H$_3$).

7.2.3.6 [W(CO)$_5$]$_2$[PH$_2$C(O)NH(CH$_2$)$_2$NHC(O)PH$_2$] (20)

Compound **14** (5 mg, 0.0278 mmol) and W(CO)$_5$(NCMe) (20.3 mg, 0.0555 mmol) were weighted into an air-tight NMR tube. d$_8$-THF (0.4 mL) was added to the solids and the resulting dark green/brown solution as analysed by multi-elemental NMR spectroscopy.

^{1}H NMR (499.9 MHz, d$_8$-THF): δ (ppm) 8.34 (br s, N*H*, proposed chelating product), 7.92 (br s, N*H*, **20**) 5.27 (d, $^1J_{P–H}$ = 349Hz, P*H*$_2$, proposed chelating product), 5.19 (d, $^1J_{P–H}$ = 348Hz, P*H*$_2$, **20**), 3.46 (m, C*H*$_2$, **20**), 3.44 (m, C*H*$_2$, proposed chelating product). **^{1}H{^{31}P} NMR** (499.9 MHz, d$_8$-THF): δ (ppm) 5.27 (s), 5.19 (s); other resonances unchanged from ^{1}H NMR spectrum. **^{31}P NMR** (202.3 MHz, d$_8$-THF): δ (ppm) –96.7 (t, $^1J_{P–H}$ = 348 Hz, **20**), –91.2 (t, $^1J_{P–H}$ = 349 Hz, proposed chelating product). **^{31}P{^{1}H} NMR** (202.3 MHz, d$_8$-THF): δ (ppm) –96.7 (s, $^1J_{P–W}$ = 211 Hz), –91.2 (s, $^1J_{P–W}$ = 211 Hz). **^{13}C{^{1}H} NMR** (125.7 MHz, d$_8$-THF): δ (ppm) 172.9 (d, $^1J_{C–P}$ = 52 Hz; P*C*(O), **20**), 36.2 (s, *C*H$_2$, **20**).

7.2.4 Synthesis of compounds described in Chapter 5

7.2.4.1 Fe(η^5-C_5H_5)(η^5-$C_5H_4NHC(O)PH_2$) (21)

DCM (30mL) was added to a mixture of aminoferrocene (15 g, 7.46 mmol), pyridinium triflate (1.71 mg, 7.46 mmol) and [Na(dioxane)$_{0.62}$][PCO] (1.1g, 7.46 mmol) and the resulting orange suspension stirred overnight. The orange solution was filtered and concentrated under vacuum. Hexane was added at –78° C to precipitate the product as an orange-red solid (1.35 g, 69% yield). Crystals were grown from a concentrated toluene solution layered with hexane.

^{1}H NMR (400.2 MHz, d_5-pyridine, 298 K): δ (ppm) 10.94 (s, 1H, N*H*), 4.88 (t, $J_{H–H}$ = 1.76 Hz, 2H, βC*H*), 4.24 (s, 5H, η^5-Cp), 4.05 (t, $^3J_{H–H}$ = 1.8 Hz, 2H, γC*H*), 3.87 (d, $^1J_{H–P}$ = 210 Hz, 2H, PH_2). **^{1}H{^{31}P} NMR** (400.2 MHz, d_5-pyridine, 298 K): δ (ppm) 3.87 (s, 2H, PH_2), other resonances remain unchanged. **^{31}P NMR** (162.0 MHz, d_5-pyridine, 298 K): δ (ppm) –129.84 (t, $^1J_{P–H}$ = 210 Hz). **^{31}P{^{1}H} NMR** (162.0 MHz, d_5-pyridine, 298 K): δ (ppm) –129.84 (s). **^{13}C{^{1}H} NMR** (125.8 MHz, d_5-pyridine, 298 K): δ (ppm) 171.62 (d, $^1J_{C–P}$ = 7.50 Hz, (O)*C*P), 96.45 (d, $^3J_{C–P}$ = 3 Hz, α*C*), 70.31 (s, η^5-Cp), 65.30 (s, β*C*), 62.31 (s, γ*C*). **EI-MS:** Calc. $C_{11}H_{12}FeNOP$ *m/z* = 261.0006. Found *m/z* = 260.9999. **CHN:** Calc. (Found) for $C_{11}H_{12}FeNOP$: 50.61 (50.88), 4.63 (4.80), 5.37 (5.58).

7.2.4.2 Fe(η^5-C_5H_5)(η^5-$C_5H_4CH_2NHC(O)PH_2$) (22)

DCM (200mL) was added to a mixture of aminomethylferrocene hydrochloric salt (3.68 g, 14.6 mmol) and [Na(dioxane)$_{3.94}$][PCO] (6.28 g, 14.6 mmol) at room temperature. The resulting orange-yellow suspension was stirred for 4 h. The orange solution was filtered and concentrated under vacuum. Hexane was added at –78° C to precipitate the product as a light orange powder, that was dried under vacuum. The new filtrate was concentrated, and the precipitation process repeated to increase the yield (2.96g, 74%).

^{1}H NMR (400.2 MHz, d_5-pyridine, 298 K): δ (ppm) 9.50 (s, 1H, N*H*), 4.49 (s, 1H, CH*H*), 4.47 (s, 1H, C*H*H), 4.33 (t, $^{3}J_{H–H}$ = 1.8 Hz, 2H, βC*H*), 4.19 (s, 5H, η^5-Cp), 4.12 (t, $^{3}J_{H–H}$ = 1.8 Hz, 2H, γC*H*), 3.78 (d, , $^{1}J_{H–P}$ = 208 Hz, 2H, PH_2). **^{1}H{^{31}P} NMR** (400.2 MHz, d_5-pyridine, 298 K): δ (ppm) 3.78 (s, 2H, PH_2), other resonances remain unchanged. **^{31}P NMR** (162.0 MHz, d_5-pyridine, 298 K): δ (ppm) –132.83 (t, $^{1}J_{P–H}$ = 208 Hz). **^{31}P{^{1}H} NMR** (162.0 MHz, d_5-pyridine, 298 K): δ (ppm) –132.83 (s). **^{13}C{^{1}H} NMR** (125.8 MHz, d_5-pyridine, 298 K): δ (ppm) 172.30 (d, $^{1}J_{C–P}$ = 67 Hz, (O)*C*P), 86.35 (s, α*C*), 69.69 (s, β*C*), 69.55 (s, η^5-Cp), 68.90 (s, γ*C*), 40.03 (s, *C*H$_2$). **EI-MS:** Calc. $C_{12}H_{14}FeNOP$ *m/z* = 275.0163. Found *m/z* = 275.0159. **CHN:** Calc. (Found) for $C_{12}H_{14}FeNOP$: 52.40 (52.88), 5.13 (4.94), 5.09 (5.16).

7.2.4.3 [K(18-crown-6][Fe(η^5-C$_5$H$_5$)(η^5-C$_5$H$_4$NHC(O)PH] (23)

d_8-THF (0.5 mL) was added to a mixture of KHMDS (15.3 mg, 0.0766 mmol), and **21** (20 mg, 0.0766 mmol) at room temperature to give a bright red solution. The solution was allowed to stir for 5 minutes. 18-crown-6 (20.4 mg, 0.0766 mmol) was subsequently added to the solution.

^{1}H NMR (500.3 MHz, d_8-THF, 298 K): δ (ppm) 6.73 (s, 1H, N*H*),4.65 (t, $^{3}J_{H–H}$ = 1.8 Hz, 2H, βC*H*), 4.49 (t, impurity), 4.07 (s, η^5-Cp, overlap impurity), 3.70 (t, $^{3}J_{H–H}$ = 1.8 Hz, 2H, γC*H*), 1.88 (d, $^{1}J_{H–P}$ = 147.9 Hz, 1H, P*H*). **^{1}H{^{31}P} NMR** (400.2 MHz, d_8-THF, 298 K): δ (ppm) 1.88 (s, 1H, P*H*), other resonances remain unchanged. **^{31}P NMR** (162.0 MHz, d_8-THF, 298 K): δ (ppm) –16.01 (s, impurity), –92.92 (d, $^{1}J_{P–H}$ = 147.9 Hz, *P*H), –245.28 (s, PH_3). **^{31}P{^{1}H} NMR** (162.0 MHz, d_8-THF, 298 K): δ (ppm) –92.92 (s, *P*H), other resonances remain unchanged. **^{13}C{^{1}H} NMR** (125.8 MHz, d_8-THF, 298 K): δ (ppm) 202.4 (d, $^{1}J_{C–P}$ = 62.0 Hz, (O)*C*P), 197.0 (d, impurity), 104.4 (s, impurity), 102.4 (s, α*C*), 68.9 (s, impurity), 68.6 (s, η^5-Cp), 62.8 (s, impurity), 62.5 (β*C*), 60.7 (s, impurity), 59.2 (s, γ*C*).

7.2.4.4 [K(18-crown-6][Fe(η^5-C$_5$H$_5$)(η^5-C$_5$H$_4$CH$_2$NHC(O)PH] (24)

d_8-THF (0.5 mL) was added to a mixture of KHMDS (14.5 mg, 0.0727 mmol), 18-crown-6 (19.2 mg, 0.0727 mmol) and **22** (20 mg, 0.0727 mmol) at room temperature to give an orange solution.

^{1}H NMR (400.2 MHz, d_8-THF, 298 K): δ (ppm) 5.40 (s, 1H, N*H*), 4.19 (s, 2H, β*H*), 4.16 (s, 2H, γ*H*), 4.14 (s, 5H, η^5-Cp), 3.96 (s, 1H, CH*H*), 3.94 (s, 1H, C*H*H), 1.78 (d, $^1J_{H–P}$ = 146.4 Hz, 1H, P*H*). **^{1}H{^{31}P} NMR** (400.2 MHz, d_8-THF, 298 K): δ (ppm) 1.78 (s, 1H, P*H*) other resonances remain unchanged. **^{31}P NMR** (162.0 MHz, d_8-THF, 298 K): δ (ppm) –29.4 (s, impurity), –104.7 (d, $^1J_{P–H}$ = 146.4 Hz, *P*H), –245.3 (q, $^1J_{P–H}$ = 187.7 Hz, phosphine). **^{31}P{^{1}H} NMR** (162.0 MHz, d_8-THF, 298 K): δ (ppm) –104.7 (s, *P*H), –245.3 (s, phosphine), other resonances remain unchanged. **^{13}C{^{1}H} NMR** (100.6 MHz, d_8-THF, 298 K): δ (ppm) 203.7 (d, $^1J_{C–P}$ = 60.8 Hz, (O)*C*P), 91.8 (s, α*C*), 90.63 (s, impurity), 69.1 (s, impurity), 68.8 (s, η^5-Cp), 68.1 (s, β*C*), 68.0 (s, impurity), 67.4 (s, impurity), 67.3 (s, γ*C*), 39.2 (s, *C*H$_2$), 37.9 (s, impurity).

7.2.4.5 Fe(η^5-C$_5$H$_5$)(η^5-C$_5$H$_4$NHC(O)PHMe (25)

THF (10 mL) was added to a mixture of KHMDS (57.3 mg, 0.287 mmol) and (**21**) (75 mg, 0.287 mmol), at room temperature. The resulting red solution was stirred for 10 minutes before iodomethane (17.9 µL, 0.287 mmol) was added, causing a white precipitate to immediately form. The mixture was stirred for 1 h. Volatiles were removed under vacuum to afford an orange solid. Toluene (15 mL) was added to the solid and the mixture was stirred for 1 h. The orange solution was filtered and pumped to dryness to yield the product as an orange solid (35.2 mg, 44.3%).

^{1}H NMR (500.3 MHz, d_5-pyridine, 298 K): δ (ppm) 10.85 (s, 1H, N*H*), 4.99 (s, 1H, βC*H*), 4.89 (s, 1H, βC*H*), 4.25 (s, 5H, η^5-Cp), 4.14 (dq, $^1J_{H–P}$ = 207.5 Hz, $^3J_{H–H}$ = 7.6 Hz, 1H,

P*H*), 4.05 (s, 2H, γC*H*), 1.39 (dd, $^{3}J_{H-H}$ = 7.6 Hz, $^{2}J_{H-P}$ = 2.6 Hz, 3H, C*H*$_3$). **^{1}H{^{31}P} NMR** (400.2 MHz, d$_5$-pyridine, 298 K): δ (ppm) 4.14 (q, $^{3}J_{H-H}$ = 7.6 Hz, 1H, P*H*), 1.39 (d, $^{3}J_{H-H}$ = 7.6 Hz, 3H, C*H*$_3$). **^{31}P NMR** (162.0 MHz, d$_5$-pyridine, 298 K): δ (ppm) –78.87 (d, $^{1}J_{P-H}$ = 208.0 Hz). **^{31}P{^{1}H} NMR** (162.0 MHz, d$_5$-pyridine, 298 K): δ (ppm) –78.87 (s). **^{13}C{^{1}H} NMR** (125.8 MHz, d$_5$-pyridine, 298 K): δ (ppm) 177.05 Hz (d, $^{1}J_{C-P}$ = 11.7 Hz, (O)*C*P), 96.76 (d, $^{3}J_{C-P}$ = 4.6 Hz, α*C*), 70.10 (s, η^5-Cp), 65.28 (s, γ*C*), 65.18 (s, γ*C*), 62.43 (s, β*C*), 62.08 (s, β*C*), 1.72 (d, $^{1}J_{C-P}$ = 7.71 Hz, *C*H$_3$).

7.2.4.6 Fe(η^5-C$_5$H$_5$)(η^5-C$_5$H$_4$CH$_2$NHC(O)PHMe (26)

THF (10 mL) was added to a mixture of KHMDS (72.5 mg, 0.364 mmol), 18-crown-6 (96.1 mg, 0.364 mmol), and (**22**) (100 mg, 0.364 mmol). The resulting orange solution was stirred for 10 minutes before iodomethane (22.6 µL, 0.364 mmol) was added, causing a gelatinous clear solid to quickly form. The mixture was stirred for 1 h, then all volatiles were removed under vacuum leaving an orange solid. Toluene (15 mL) was added to the solid and the mixture stirred for 1 h. The orange solution was separated from the white solid by filtration and pumped to dryness leaving an oily orange solid. Hexane (10 mL) was added to purify the compound before being removed by filtration. The solid was dried and weighed (48.5 mg, 46.1%).

^{1}H NMR (400.2 MHz, d$_5$-pyridine, 298 K): δ (ppm) 9.33 (s, 1H, N*H*), 4.53 (s, 1H, CH*H*), 4.52 (s, 1H, C*H*H), 4.34 (m, 2H, βC*H*), 4.20 (s, 5H, η^5-Cp), 4.13 (s, 2H, γC*H*), 4.06 (dq, $^{1}J_{H-P}$ = 207.3 Hz, $^{3}J_{H-H}$ = 7.5 Hz, 1H, P*H*), 3.53 (s) (18-crown-6), 1.38 (dd, $^{3}J_{H-H}$ = 7.5 Hz, $^{2}J_{H-P}$ = 2.8 Hz, 3H, C*H*$_3$). **^{1}H{^{31}P} NMR** (400.2 MHz, d$_5$-pyridine, 298 K): δ (ppm) 4.06 (q, $^{3}J_{H-H}$ = 7.5 Hz, 1H, P*H*), 1.38 (d, $^{3}J_{H-H}$ = 7.5 Hz, 3H, C*H*$_3$), other resonances remain unchanged. **^{31}P NMR** (162.0 MHz, d$_5$-pyridine, 298 K): δ (ppm) –31.0 (s) (impurity), –41.2 (s) (impurity), –81.5 (dq, $^{1}J_{P-H}$ = 207.3 Hz, $^{2}J_{P-H}$ = 2.8 Hz). **^{31}P{^{1}H} NMR** (162.0 MHz, d$_5$-pyridine, 298 K): δ (ppm) –81.5 (s), other resonances remain

unchanged. **$^{13}C\{^{1}H\}$ NMR** (100.6 MHz, d_5-pyridine, 298 K): δ (ppm) 177.49 (d, $^{1}J_{C–P}$ = 10.8 Hz, (O)*C*P), 86.76 (s, α*C*), 69.63 (s, β*C*), 69.61 (s, β*C*), 69.55 (s, η^5-Cp), 68.83 (s, γ*C*), 39.84 (d, $^{3}J_{C–P}$ = 1.59 Hz, *C*H_2), 1.76 (d, $^{1}J_{C–P}$ = 8.2 Hz, *C*H_3).

7.3 Characterization techniques

7.3.1 NMR spectroscopy

NMR samples were prepared inside an inert atmosphere glovebox in NMR tubes fitted with a gas-tight valve. ^{1}H NMR spectra were recorded at either 499.9 MHz or 400.1 MHz on a Bruker AVIII 500 or a Bruker AVIII 400 NMR spectrometer, respectively. $^{13}C\{^{1}H\}$ NMR spectra were recorded at either 125.8 MHz or 100.6 MHz on a Bruker AVII 500 fitted with a cryoprobe or a Bruker AVIII 400 NMR spectrometer, respectively. ^{31}P NMR spectra were recorded on 202.4 MHz or 162.0 MHz on a Bruker AVIII 500 or a Bruker AVIII 400 NMR spectrometer, respectively. ^{1}H and ^{13}C NMR spectra are reported relative to tetramethylsilane (TMS) and referenced to the most downfield residual solvent resonance were possible (d_5-pyridine: δH = 8.74 ppm, δC = 150.35 ppm; d_8-THF: δ_H = 3.58 ppm, δ_C = 67.57 ppm; CD_2Cl_2: δ_H = 5.32 ppm, δ_C = 54.00 ppm). ^{31}P NMR spectra were externally referenced to an 85% solution of H_3PO_4 in H_2O (δ = 0 ppm). Data analysis was performed using Bruker TopSpin 4.0.7 software.

7.3.2 Single X-ray diffraction

Single-crystal X-ray diffraction data were collected using an Oxford Diffraction Supernova dual-source diffractometer equipped with a 135 mm Atlas CCD area detector. Crystals were selected under Paratone-N oil, mounted on micromount loops, and quench-cooled using an Oxford Cryosystems open flow N_2 cooling device. Data were collected at 150 K using mirror monochromated Cu Kα radiation (λ = 1.5418 Å; Oxford Diffraction Supernova) or graphite-monochromated Mo Kα radiation (λ =

0.71073 Å; Enraf-Nonius kappa-CCD). Data collected on the Oxford Diffraction Supernova diffractometer were processed using the CrysAlisPro package, including unit cell parameter refinement and interframe scaling (which was carried out using SCALE3 ABSPACK within CrysAlisPro). Equivalent reflections were merged, and diffraction patterns processed with the CrysAlisPro suite. Structures were solved using direct methods or using the charge flipping algorithm as implemented in the program SUPERFLIP and refined on F^2 using the SHELXL 97-2 package.

7.3.3 Mass spectrometry

Analyses were performed using a Thermo Exactive mass spectrometer equipped with Waters Acquity liquid chromatography system. Instrument control and data processing were performed using Thermo Xcalibur Software. The system was calibrated on the day of the analysis and its mass accuracy with external calibration (as used for these experiments) is better than 5 ppm for 24 hours following calibration. The mass spectrometer was operated using the heated electrospray (HESIII) probe and resolution was set to 50,000. Electrospray source conditions were adjusted to maximise sensitivity. A mixture of 10% water, 89.9% methanol and 0.1% formic acid was used to transport samples to the mass spectrometer at a flow rate of 0.2 mL/min.

7.3.4 Elemental Analysis

CHN elemental microanalyses were carried out by Elemental Microanalysis Ltd., Devon. Samples were submitted in Pyrex ampoules sealed under vacuum. All values are given as percentages.

7.3.5 Cyclic Voltammetry

All measurements were performed in a THF solution, with $[NBu_4][PF_6]$ used as an electrolyte. Voltammograms were recorded using a glassy carbon working

electrode, a platinum wire counter electrode and a silver wire as a quasi-reference electrode. The reference electrode was calibrated with cobaltocenium hexafluorophosphate, that was added to the solutions after an initial measurement.

7.3.6 Computational details

All calculations were performed the Gaussian09 software package. Geometries were fully optimised without imposing any symmetry constraints. Stationary points were characterised by analysis of their vibrational frequencies, with minima and transition states having exactly zero and one imaginary frequencies, respectively. All quantum chemical results were visualised using the GaussView 5.0.9 software.

7.4 References

[1] A. R. Jupp, J. M. Goicoechea, *Angew. Chemie Int. Ed.* **2013**, *52*, 10064–10067.

[2] D. Heift, Z. Benko, H. Grützmacher, *Dalt. Trans.* **2014**, *43*, 831–840.

[3] F. Nief, F. Mercier, F. Mathey, *J. Organomet. Chem.* **1987**, *328*, 349–355.

Appendix:
Single crystal X-ray diffraction data

Compound	K[(18-crown-6)][**1**]	**13a**
Formula	$C_{16}H_{31}KNO_9P$	$C_{1.25}H_{7.5}N_{2.5}O_{1.25}P_{1.25}$
Fw (g mol^{-1})	451.49	116.31
T(K)	150(2)	150(2)
crystal system	monoclinic	monoclinic
space group	$P2_1$	$P2_1/c$
a (Å)	8.6146(2)	25.026(2)
b (Å)	29.8779(5)	4.8946(4)
c (Å)	17.5654(3)	6.9706(10)
α (°)	90	90
β (°)	99.466(2)	93.901(10)
γ (°)	90	90
V (Å^3)	4459.53(15)	851.85(16)
Z	8	8
ρ_{calc} (g/cm^3)	1.345	1.814
μ (mm^{-1})	3.166	5.428
F(000)	1920	490
Radiation	CuKα (λ = 1.54178)	CuKα (λ = 1.54184)
2Θ range for data collection/°	7.814 to 152.19	7.08 to 153.968
Index ranges	-10 ≤ h ≤ 10, -22 ≤ k ≤ 37, -21 ≤ l ≤ 21	-31 ≤ h ≤ 29, -6 ≤ k ≤ 6, -8 ≤ l ≤ 6
reflections collected	26764	5710
independent reflections	13248 [R_{int} = 0.0463, R_{sigma} = 0.0474]	1765 [R_{int} = 0.0663, R_{sigma} = 0.0676]
Data/restraints/parameters	13248/20/1036	1765/0/131
Goodness-of-fit on F^2	1.017	1.121
Final R indexes [I>=2σ (I)]	R_1 = 0.0421, wR_2 = 0.1104	R_1 = 0.0815, wR_2 = 0.2160
Final R indexes [all data]	R_1 = 0.0469, wR_2 = 0.1137	R_1 = 0.1143, wR_2 = 0.2310
Largest diff. peak/hole / e Å^{-3}	0.29/-0.61	1.05/-0.77

Compound	(18-crown-6)**13b**	**14**
Formula	$C_7H_{17}N_2O_4P$	$C_4H_{10}N_2O_2P_2$
Fw (g mol^{-1})	224.19	180.08
T(K)	150(2)	150(2)
crystal system	monoclinic	monoclinic
space group	$P2_1/c$	$P2_1/n$
a (Å)	13.9885(2)	7.1091(2)
b (Å)	11.78140(10)	4.91330(10)
c (Å)	14.7581(2)	12.5171(3)
α (°)	90	90
β (°)	109.5020(10)	92.067(2)
γ (°)	90	90
V (Å^3)	2292.66(5)	436.927(18)
Z	8	2
ρ_{calc} (g/cm^3)	1.299	1.369
μ (mm^{-1})	2.122	4.156
F(000)	960	188
Radiation	CuKα (λ = 1.54184)	CuKα (λ = 1.54178)
2Θ range for data collection/°	9.838 to 152.034	14.112 to 151.83
Index ranges	-17 ≤ h ≤ 17, -14 ≤ k ≤ 14, -18 ≤ l ≤ 14	-8 ≤ h ≤ 8, -6 ≤ k ≤ 5, -15 ≤ l ≤ 15
reflections collected	22090	3760
independent reflections	4757 [R_{int} = 0.0152, R_{sigma} = 0.0110]	896 [R_{int} = 0.0148, R_{sigma} = 0.0093]
Data/restraints/parameters	4757/6/293	896/0/66
Goodness-of-fit on F^2	1.038	1.134
Final R indexes [I>=2σ (I)]	R_1 = 0.0551, wR_2 = 0.1317	R_1 = 0.0238, wR_2 = 0.0617
Final R indexes [all data]	R_1 = 0.0566, wR_2 = 0.1329	R_1 = 0.0242, wR_2 = 0.0620
Largest diff. peak/hole / e Å^{-3}	2.06/-1.11	0.28/-0.25

Compound	**15a *trans***	**21**
Formula	$C_{13}H_{28}KN_2O_7P$	$C_{11}H_{12}FeNOP$
Fw (g mol^{-1})	394.44	261.04
T(K)	150(2)	150(2)
crystal system	orthorhombic	monoclinic
space group	$Pna2_1$	$P2_1/c$
a (Å)	16.5692(3)	15.9398(5)
b (Å)	8.8974(2)	7.9962(3)
c (Å)	12.9189(3)	17.9686(5)
α (°)	90	90
β (°)	90	103.758(3)
γ (°)	90	90
V (Å^3)	1904.54(7)	2224.53(13)
Z	4	8
ρ_{calc} (g/cm^3)	1.376	1.559
μ (mm^{-1})	0.398	11.995
F(000)	840	1072
Radiation	MoKα (λ = 0.71073)	CuKα (λ = 1.54178)
2Θ range for data collection/°	4.916 to 57.72	10.136 to 152.306
Index ranges	-21 ≤ h ≤ 22, -11 ≤ k ≤ 11, -17 ≤ l ≤ 16	-17 ≤ h ≤ 19, -8 ≤ k ≤ 9, -22 ≤ l ≤ 20
reflections collected	25455	11907
independent reflections	4693 [R_{int} = 0.0351, R_{sigma} = 0.0272]	4582 [R_{int} = 0.0514, R_{sigma} = 0.0571]
Data/restraints/parameters	4693/1/233	4582/1/295
Goodness-of-fit on F^2	1.059	1.02
Final R indexes [I>=2σ (I)]	R_1 = 0.0292, wR_2 = 0.0587	R_1 = 0.0442, wR_2 = 0.1016
Final R indexes [all data]	R_1 = 0.0349, wR_2 = 0.0620	R_1 = 0.0650, wR_2 = 0.1134
Largest diff. peak/hole / e Å^{-3}	0.26/-0.23	0.67/-0.92

Compound	**22**
Formula	$C_{12}H_{14}FeNOP$
Fw (g mol^{-1})	275.06
T(K)	150(2)
crystal system	orthorhombic
space group	Pbca
a (Å)	9.6692(2)
b (Å)	9.2447(2)
c (Å)	25.8542(6)
α (°)	90
β (°)	90
γ (°)	90
V (Å^3)	2311.08(9)
Z	8
ρ_{calc} (g/cm^3)	1.581
μ (mm^{-1})	11.577
F(000)	1136
Radiation	CuKα (λ = 1.54178)
2Θ range for data collection/°	11.428 to 152.744
Index ranges	-12 ≤ h ≤ 10, -11 ≤ k ≤ 8, -32 ≤ l ≤ 30
reflections collected	11413
independent reflections	2400 [R_{int} = 0.0339, R_{sigma} = 0.0244]
Data/restraints/parameters	2400/0/165
Goodness-of-fit on F^2	1.058
Final R indexes [I>=2σ (I)]	R_1 = 0.0278, wR_2 = 0.0661
Final R indexes [all data]	R_1 = 0.0336, wR_2 = 0.0699
Largest diff. peak/hole / e Å^{-3}	0.29/-0.42